Studies in frictionally damped waves. December 1973.

Author:
Pite, H. D.

Publication details:
Report No. UNSW Water Research Laboratory Report No. 138

Publication Date:
1973

DOI:
https://doi.org/10.4225/53/579ad6c9d0731

License:
https://creativecommons.org/licenses/by-nc-nd/3.0/au/
Link to license to see what you are allowed to do with this resource.

THE UNIVERSITY OF NEW SOUTH WALES

water
research
laboratory

Manly Vale N.S.W. Australia

STUDIES IN FRICTIONALLY DAMPED WAVES

By
H.D. Pite

December 1973

The University of New South Wales

School of Civil Engineering

STUDIES IN FRICTIONALLY DAMPED WAVES

by

H. D. Pite

8. ABSTRACT This investigation deals with some aspects of surface waves subject to a linear frictional force originating from horizontal bottom stresses. The wave properties for this model are deduced. Theoretical reflection and transmission coefficients were found for these waves when incident to a depth discontinuity positioned normal to the wave crests. These results were compared with experimental ones and agreement was generally good although there was some evidence of extraneous energy losses by turbulence at the discontinuity.

A circular shelf model was considered with the theoretical results showing a large reduction in the "Q" of the resonance peaks when compared to the frictionless case. It was also found that, except at the lower frequencies, a large number of overlapping resonance peaks which were out of phase with one another occupied relatively narrow frequency band. Experiments using several frequencies carried out for the circular sill model and the results were in very good agreement with the theoretical ones.

9. DISTRIBUTION STATEMENT
Unlimited

10. KEY WORDS Waves (water); Ocean Waves; Energy Dissipation; Velocity.

11. CLASSIFICATION	12. NUMBER OF PAGES	13. PRICE $8.00

SUMMARY

This thesis examines some aspects of frictionally damped
surface waves. The frictional term is assumed, for simplicity, to be
proportional to the near bottom velocity and effects of finite
amplitude and of surface tension are neglected. The equations of
motion are solved for a constant depth and a number of properties of
the waves including the velocities and energy flux are deduced from
them.

Two models with frictionally damped waves incident to a depth
discontinuity are considered, the first being an infinite shelf
whose edge is parallel to the wave crests and the second being a
circular sill. The matching of the solutions in the two regions
separated by the depth discontinuity was accomplished by assuming,
at any instant, a continuous surface streamline and a continuous
energy flux at the discontinuity. The theoretical results for the
shelf model showed a reflection and transmission coefficient which
differed only by a small amount from the frictionless results when
realistic amounts of friction are introduced. The results for the
circular sill model shows large reductions in the "Q" of the
resonant peaks brought about by frictional damping. It is also
found that, except at low frequencies, a large number of overlapping
resonance peaks which were out phase with one another occupied a

relatively narrow frequency band.

Experiments with the depth everywhere uniform are carried
out to determine values for the linear friction constant, the
effective depth with reference to a bottom boundary layer and to
investigate particle phases in comparison to the surface profile
phase. Experimental results are presented for the shelf model
showing the reflection and transmission coefficients, an estimate
of the energy loss and some features of the local surface
disturbances at the discontinuity. The experimental verification
of the effects of frictional damping derived in the circular sill
model is presented.

ACKNOWLEDGEMENTS

TABLE OF CONTENTS

Page No.

TABLE OF CONTENTS   (Cont's.)

LIST OF APPENDICES

LIST OF FIGURES

LIST OF FIGURES   (Cont'd.)

LIST OF FIGURES   (Cont'd.)

LIST OF FIGURES   (Cont'd.)

LIST OF FIGURES IN APPENDICES

LIST OF FIGURES IN APPENDICES (Cont'd.)

LIST OF FIGURES IN APPENDICES   (Cont'd.)

LIST OF TABLES

LIST OF TABLES (Cont'd.)

LIST OF PHOTOGRAPHS

LIST OF MAIN SYMBOLS

A	Wave Amplitude
A_n	Wave Amplitude over the Sill
B_n	Scattered Wave Amplitude
C	Linear Friction Constant
$\mathcal{C}$	General Cylindrical Function
$E_{AVG.}$	Wave Energy averaged over 1 Wave Period
F	Friction Force
H	Wave Height
$H_n^{(1),(2)}$	Bessel Functions of the third kind
$I\{x\}$	Imaginary part of X
J_n	Bessel Functions of the first kind
K	Complex Wave Number $(k + i\mathcal{l})$
L	Wave Length
P	Instantaneous Energy Flux or Power
$P_{AVG.}$	Average of P over 1 Wave Period
Q	Quality Factor in a Resonating System
R	Radius of Circular Sill
$\mathcal{R}\{x\}$	Real part of X
T	Wave Period
U	Two-dimensional Horizontal Particle Velocity
u	Radial Particle Velocity
X	A General Argument for a Function

Y_n Bessel Functions of the second kind

z Translated Vertical Co-ordinate $= \zeta + h$

a_n Modulus of A_n

b_n Modulus of B_n

e Base of the Natural Logarithm

$\left.\begin{array}{c} E \\ E_{AVG} \end{array}\right\}$ Average Energy of the Wave

f or F The ζ Dependant Term in the Potential Function

f_{ζ} See Equation (7-9)

f^* Quadratic Bottom Friction Constant

g Acceleration of Gravity

h $\left\{\begin{array}{l} \text{Fluid Depth} \\ \\ \text{Effective Fluid depth in Experimental Context} \end{array}\right.$

h' Measured Fluid Depth

h_n Modulus of the $H_n^{(1)}$ Bessel Function

Δh Difference between the effective and measured Fluid Depth

i $\sqrt{-1}$

$\hat{i}$ Unit Vector in x Direction

j_n Modulus of the J_n Bessel Function

$\hat{j}$ Unit Vector in y Direction

k Real part of the Wave Number K

$\hat{k}$ Unit Vector in ζ Direction

n An Integer

p Fluid Pressure

p_v Variable or Dynamic part of p

r Radial Polar co-ordinate

$\hat{r}$ Unit Vector in r Direction

t Time Variable

u x Component of the Particle Velocity

v y Component of the Particle Velocity

v_e Energy Velocity

v_g Group Velocity

v_p Phase Velocity

w z Component of the Particle Velocity

x Cartesian Co-ordinate

y Cartesian Co-ordinate

z Cartesian Co-ordinate

α Decay Coefficient (imaginary part of K)

δ See Equation (3-1)

Δ See Equation (3-1); May also be used to denote an increment in a function

γ Euler's Constant $= 0.5772....$

γ_j Phase Angle associated with A_r or A_t

LIST OF MAIN SYMBOLS   (Cont'd.)

$\gamma_{n,j}$ Phase Angle associated with A_n or B_n

ϵ See Equation (3-1)

ϵ_n $\epsilon_0 = 1$; $\epsilon_n = 2$ for $n \geq 1$

η Surface Configuration

Θ Angular Polar Co-ordinate

$\hat{\Theta}$ Unit Vector corresponding to Θ

K See Equation (3-1)

ν Kinematic Viscosity

$\nu_{n,j}$ Phase Angle associated with $H_n^{(1)}(K, r)$

ξ Spatial Position of a Fluid Particle

$O(X)$ The Order of X

π 3.141592....

ρ Density of the Fluid

σ Radian Frequency

τ_ℓ Linear Bottom Shear Stress

τ_q Quadratic Bottom Shear Stress

Υ Surface Tension

ϕ Potential Function

Φ Horizontal Dependance on the Potential Function

ψ Stream Function

ω_j See Equation (5-10); $\left(= f_j \right)$

Ω See Equation (3-1)

Ω_{ν_2} Phase Angle associated with $J_\nu (\kappa_2 r)$

Subscripts

b   Indicates the Function is evaluated at $z = -h$

c   Indicated the Quantity is complex valued

        (May also be used as a superscript)

i Refers to the Incident Wave

j Takes either value of 1 or 2

ν Order of a Function

r   Refers to the Reflected Wave

s   Refers to the Scattered Wave

t   Refers to the Transmitted Wave

1   Refers to the Region in which the Incident Wave travels

        or to the Upwave Region

2   Refers to the Region in which the Transmitted Wave travels

        to the region over the Sill or to the Downwave Region

$\vec{X}$ or $\bar{X}$ Is the Directed Quantity with Magnitude $|X|$

Other symbols are defined where they are used in the text.

Chapter 1 - Introduction

The knowledge of the interaction of surface waves with
irregular bathymetry on the ocean floor is of considerable
importance in the design of harbours and waterways as well as
in defence against damage by tsunami and by storm surge. A
striking example of wave-bottom interaction is depicted in Photo
1, which is an aerial photograph of Botany Bay (N.S.W.) taken in
1971. Surface waves were incident from the bottom left hand
corner and totally reflected along a dredged channel. This
reflection created an area of calm waters between the land spit,
the shore and the dredged channel; in effect protection from
ocean waves without a conventional breakwater. Unfortunately,
the calm area was not required for the project and the reflected
waves created strong longshore currents which eroded the beach
in the foreground. As a consequence, the dredged channel was
refilled.

This thesis investigates the reflection and transmission
of damped rectilinear surface waves incident across a straight
depth discontinuity and their resonance and amplification over a
submerged circular sill.

The effects of friction are included using a linear friction
model. Experiments were carried out to investigate the validity
of the models.

1.1   The Linear Friction Term

An approach to modelling the bottom friction whilst still retaining linear equations is to assume that the bottom friction may be replaced by a distributed body force proportional to the near bottom velocity. This approach must, however, be regarded as a first approximation. In the literature there appear to be two general methods of approach to the problem of damping of small amplitude water waves by bottom friction. The first of these are laminar boundary layer techniques whereas the second is to ignore the details of motion near the bottom and to assume a frictional force proportional to some power of the near bottom velocity.

Viscous dissipation in boundary layers have been investigated classically by Hough, (1897) Biesel (1949), and Hunt (1952), who develop a linear set of boundary layer equations. More recently, Iwagaki, Tsuchoya and Chen (1967) have used perturbation methods on the non-linear boundary layer equations and Hunt (1964) has solved the linearized Navier-Stokes equations together with the resulting characteristic equation. All these solutions give, with varying degrees of approximation, a description of the motion, both inside and outside the boundary layer.

Experimentally, it has been found that the value for the amplitude attenuation coefficient is at least 30 percent greater than that predicted by the above theories. This discrepancy has been investigated by Van Doran (1966) who obtained good experimental

PHOTOGRAPH 1   Aerial photograph of Botany
                Bay showing wave reflection
                along a dredged channel.

agreement with his theory for the attenuation coefficient by

considering energy losses in a boundary layer at the free surface

as well as in one at the channel bottom. The energy loss term for

the surface was found to be much less than that for the bottom

when reasonably long waves were considered. But, according to

Iwagaki, Tsuchiya and Chen (1967), his derivation for the dissipation

of energy at the free surface by assuming a horizontally immobile

free surface appears questionable. This boundary layer at the air-

water interface has been more thoroughly investigated by Dore

(1968), using an extension of Johns's (1968) work on the damping

of interfacial waves by viscous stresses at the density discontinuity.

The second method, which is generally employed in oceanographic

work, is to assume that the frictional force exerted on the fluid is

proportional to the square of the near bottom particle velocity.

These solutions ignore any details of the fluid motion in the generally

turbulent dissipative layer near the bottom. It is considered that

the height of roughness of the channel bottom is much greater than

the boundary layer developed through oscillatory motions. Thus,

according to Putnam and Johnson (1949) in their study of waves on

sloping beaches, "The bottom may behave as a hydraulically rough

surface in the sense that the friction coefficient depends only on

the roughness and not directly on the viscosity of the water."

The equations of motion incorporating the quadratic resistance

term may be linearized by the replacement of the quadratic term with

a constant multiplied by the near bottom velocity. This constant
is then evaluated to make the linear term compatible with the
quadratic by equating the frictional work done over a quarter
wave period by the quadratic resistance term to the work done
over the same period by the linearized resistance term.
(See, for example, A.T. Ippen and D.E.R. Harleman (1961)).
This method has been used by Defant (1961), Fjeldstat (1925),
Einstein and Fuchs (1954), Neumann (1944), Ippen and Harleman
(1961) and Proudman (1952), among others in the study of tidal
attenuation in canals and estuaries. The difficulty in using the
linear theory is to obtain on a priora value for the roughness
constant. To date, this problem has not been successfully resolved,
although values for roughness constants when the quadratic term is
retained have been obtained by Iwagaki and Kakinuma (1967) with
results considerably larger than those found by Bretschneider (1954).
With the exception of Proudman, all the above authors consider the
frictional force to be uniformly distributed from the bottom to the
free surface. Proudman assumed the frictional force to greater near
the bottom than at intermediate depths and, as a consequence,
obtained phase differences between the bottom currents and inter-
mediate currents.

In this investigation, the details of motion in the boundary
layer or near a hydraulically rough bottom are not examined and no
concern is taken with an a priore value for the roughness constant.

The aim is to investigate the gross effects of bottom friction on
wave motion, to this end any dissipation at the free surface or in
the body of the fluid is neglected and a linear frictional force
proportional to the near bottom velocity is assumed. It is further
assumed that this force is distributed evenly throughout a vertical
column of fluid. This latter assumption is perhaps the most
questionable, and is for the most part indefensible although
experimental for very long period waves (Ippen and Harleman (1961))
lend support to its validity. It is thus important to determine if
this model for frictional wave damping is in agreement with the
experimental results. In Chapter 2 the equations of motion for
the model are solved and various characteristics of the waves are
illustrated in Chapter 3. Experimental verification is carried
out and presented in Chapter 4.

1.2   The Reflection of damped Surface Waves Incident Normally to a
Sudden Change in Depth.

The partial reflection of inviscid surface waves incident
normally to a depth discontinuity has been investigated by Lamb (1932),
Bartholomeusz (1958), Le Me haute (1960) Newman (1965) and Ippen
(1966), among others. For the special case of long waves they
obtain the same results for the reflection and transmission
coefficient. However, in laboratory experiments it is difficult to
obtain very long progressive waves due to the limiting length of
the wave flume causing unwanted reflections. Hence, some attempts

have been made to verify results obtained using long wave theory

using wave length to depth ratios which are considerably smaller

than desired. (Williams and Krishna Kartha (1969)). It is

important to know the errors involved in using the long wave

approximations; also, in the majority of engineering problems

involving surface waves, the waves involved do not fall into this

long wave class. It is therefore important to investigate the

interaction of bottom topography on inviscid surface waves of all

wavelength to depth ratios. It is also desirable to gain some

understanding of the effects of bottom friction on the wave-bottom

topography interaction. For inviscid surface waves approaching

normally to a sudden change in depth, Bartholomeusz investigated

the complete problem with the boundary conditions as set out below

in Figure (1). The free surface ABC is considered a continuous

streamline and the horizontal and vertical velocity components,

designated by u and w respectively, are continuous across BB'.

The small amplitude assumption was made and a complete solution,

in integral form, was obtained for all wave lengths. The solution

showed a reflected and transmitted wave as well as a standing wave in the

vicinity of the step. Asymptotic values for reflection and

transmission coefficients were evaluated for long waves at large

distances from both sides of the discontinuity. Newman, using similar

boundary conditions, obtained a solution when one of the depths was

considered infinite and the other finite. Thus there are two solutions
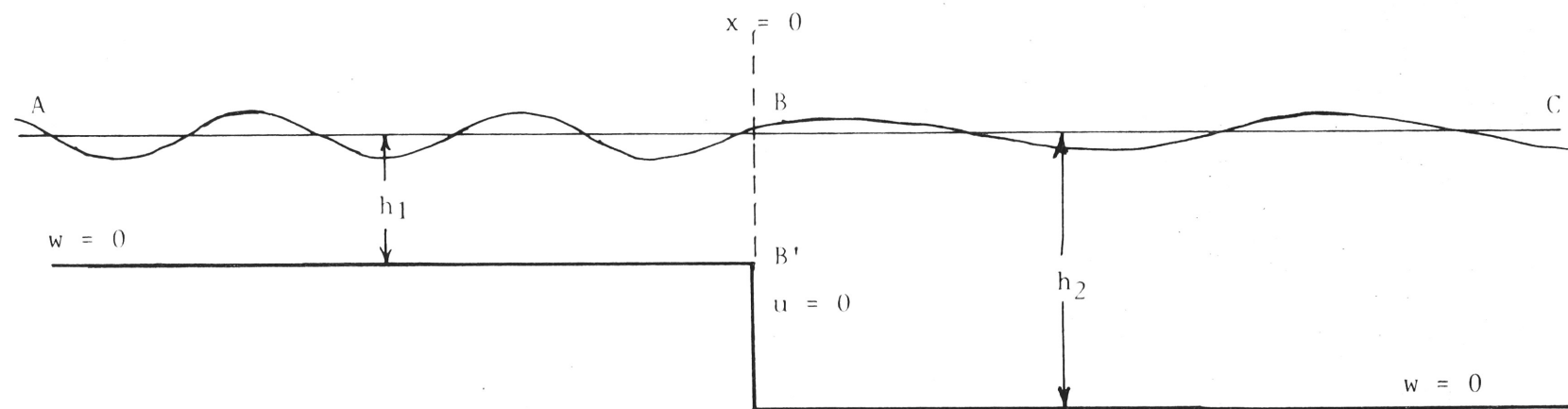
FIGURE 1.   SCHEMATIC DIAGRAM OF THE DEPTH DISCONTINUITY

for the complete inviscid boundary value problem, and these are
standards against which any approximate solution may be judged.
Lamb (1932), Le Me haute (1960) and Ippen (1966) amongst others
have obtained approximate solutions to the problem by ignoring
the details of the flow near the step and assuming that a solution
can be obtained by matching, at the step, two of the following
conditions:

> 1.)   the flux of mass
>
> 2.)   the flux of energy
>
> 3.)   the surface elevation

The solutions are then stated to be satisfactory at a distance
from the step. That is, where the local disturbances caused by the
standing waves are negligible.

Considering the region near the step where Bartholomeusz
standing wave solution is important it is evident that during any
portion of a wave period this region could act as a storage for mass
and energy as well as being the necessary mechanism to produce a
continuous surface. But, over one wave period there can be no net
transport of mass, or storage of energy, and the surface must
return to the state it was at the start of the period.

Hence, any evaluation of the reflection and transmission
coefficients by matching the flux of mass and the surface elevation
leads to difficulties because of storage in the standing wave region
during any portion of a wave period and a trivial result when an
integral number of wave periods are considered. The same remarks
are true for the time dependant parts of the energy flux. Assuming

no energy losses in a region near to the step, the only condition
that must necessarily be fulfilled is that, over an integral number
of wave periods, the flux of energy entering this region must equal
that leaving. This, since we are dealing with progressive waves,
will give a non-trivial result but leads to only one equation with
four unknown parameters.

The approximate solution to be used must satisfy, as nearly
as possible, the results of Bartholomeusz and those of Newman as
well as the balance of energy condition stated above. The formulation
of the problem will be to assume a discontinuity in the particle
velocity at the step and to disregard the standing wave disturbance.
Sufficient equations can then be found to evaluate the unknown
parameters when two of the three matching conditions, as listed
above, are evaluated at the discontinuity for any instant in time.
For long waves, any two of the three conditions satisfy the
Bartholomeusz solution and the energy condition. The instantaneous
flux of mass and continuous surface elevation conditions give
solutions which produce an energy imbalance and give poor
agreement with Newman's results. The conditions of continuous
instantaneous energy and mass fluxes yields a solution which,
while satisfying the energy requirement, gives results that are
not in accord with Newman. The final two possibilities, of a
continuous instantaneous energy flux and a continuous surface
elevation, satisfy the energy condition and agree reasonably well
with Newman's solution for the transmitted and reflected amplitudes.
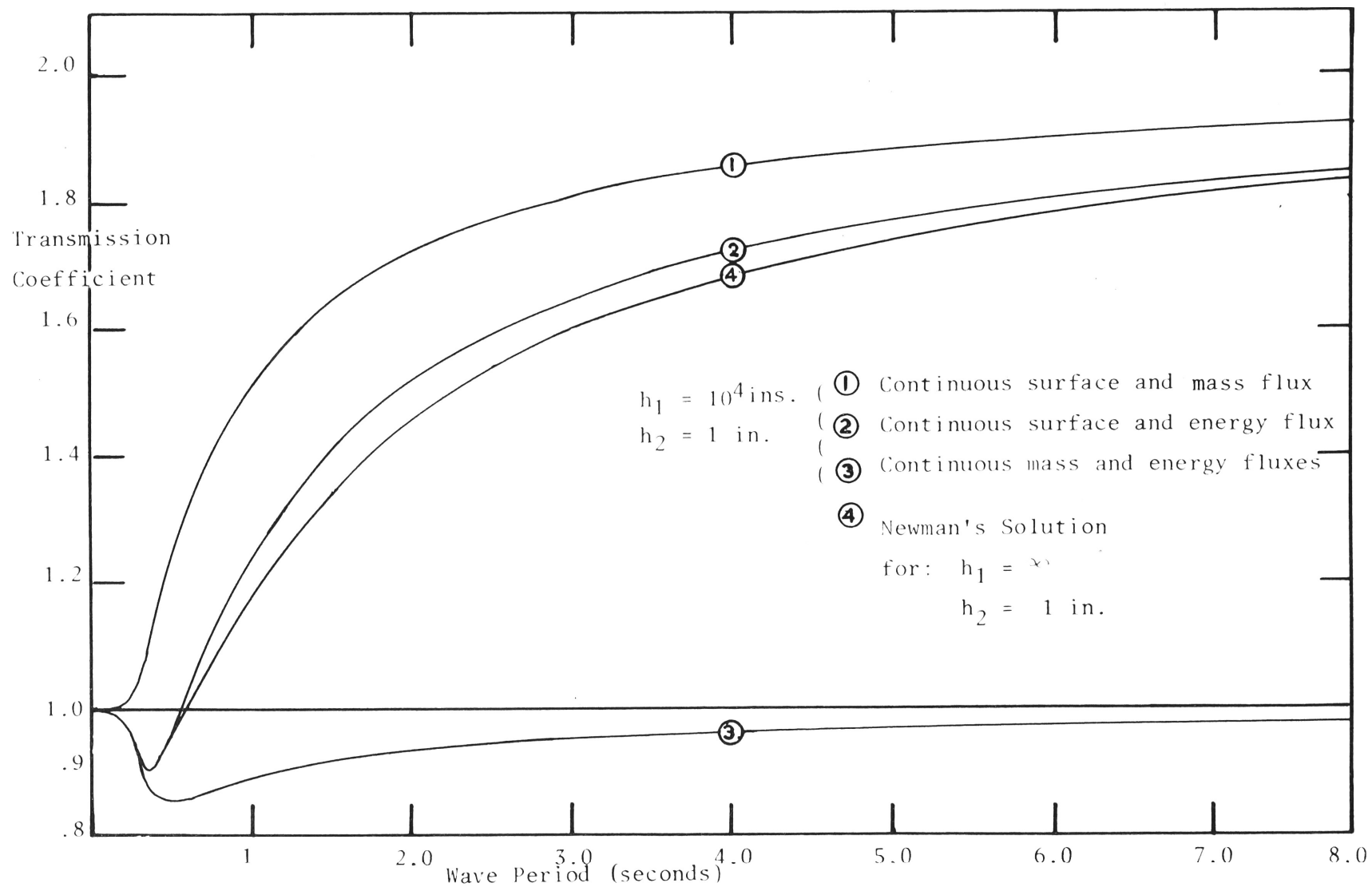
FIGURE 2.   TRANSMISSION COEFFICIENTS USING THREE DIFFERENT MATCHING CONDITIONS
            AT THE STEP IN COMPARISON TO NEWMAN'S SOLUTION.
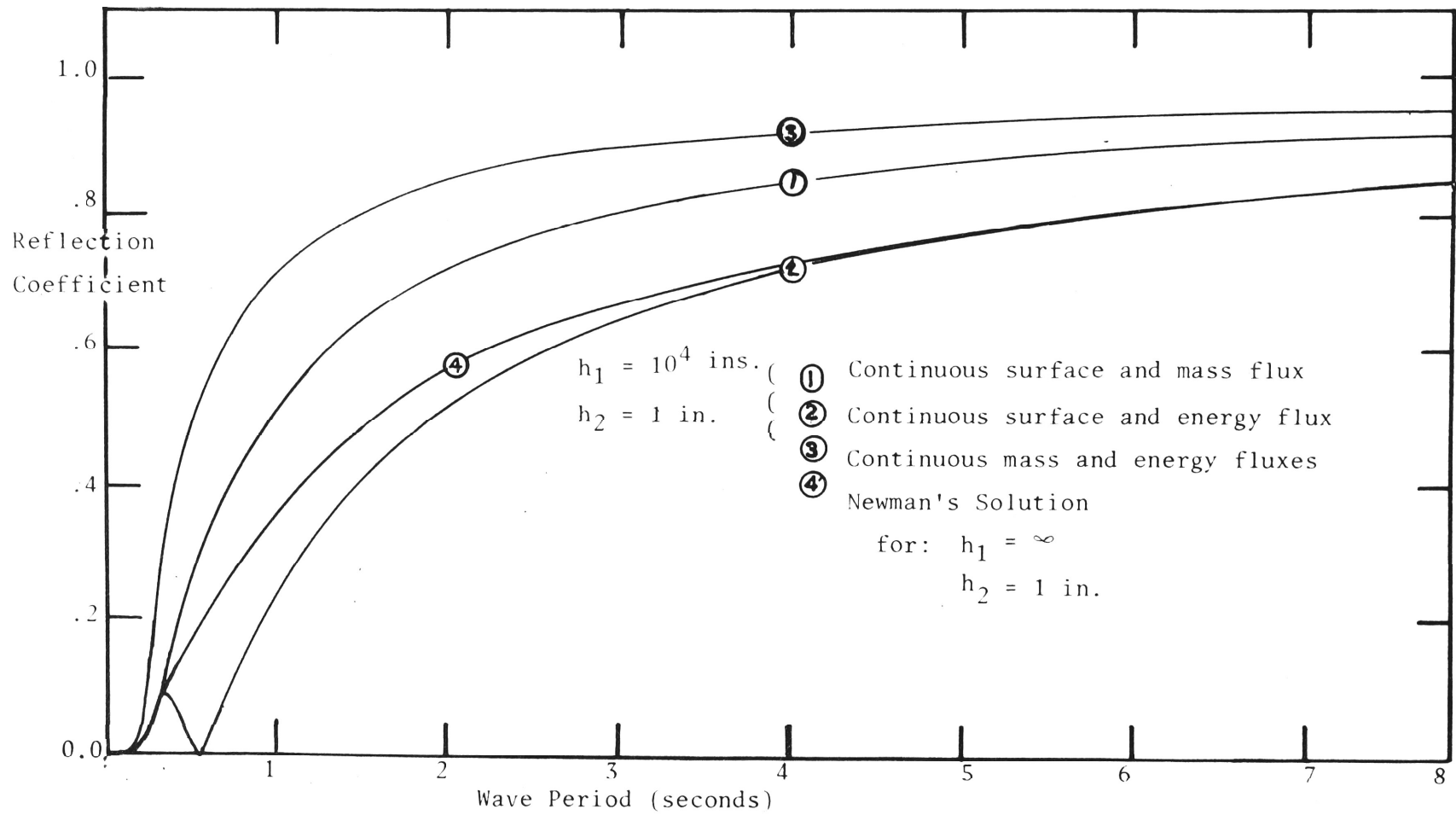
FIGURE 3. REFLECTION COEFFICIENTS USING THREE DIFFERENT MATCHING CONDITIONS
AT THE STEP IN COMPARISON TO NEWMAN'S SOLUTION.

$$\Delta P = \left/ \frac{(\text{Incident} + \text{Reflected} - \text{Transmitted}) \text{ Energy Fluxes}}{(\text{Incident} + \text{Reflected} + \text{Transmitted}) \text{ Energy Fluxes}} \right/ \times 100\%$$

$h_1 = 1$ in.

(① $h_2 = 10^4$ ins.
(② $h_2 = 10$ ins.
(③ $h_2 = 5$ ins.

Wave Period (seconds)
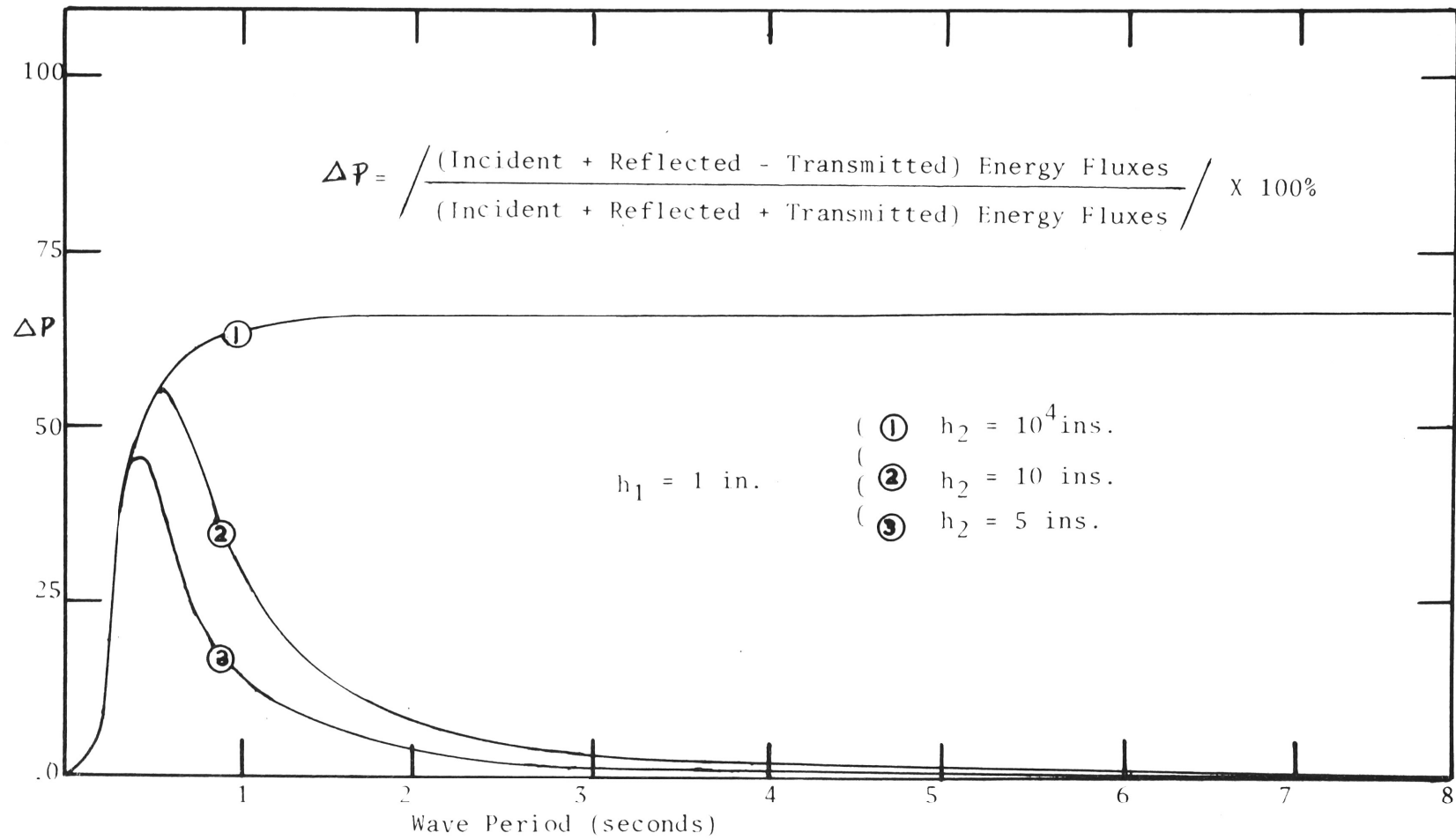
FIGURE 4.   ENERGY FLUX IMBALANCE USING THE CONDITION OF A
CONTINUOUS SURFACE AND MASS FLUX AT THE STEP.

The main discrepancy being the inability of this approximate

solution (or any of the others) to predict the phase shifts, these

lead to some error in the magnitude of the reflected and transmitted

waves. Comparisons between the three frictionless approximate

solutions are shown in Fig. (2), Fig. (3) and Fig. (4). This

solution will depart further from reality because of viscous effects

which will cause the generation of an eddy of oscillating size

at the step. These effects are also of considerable importance in

the interpretation of model results. Chapter 5 presents the

theoretical reflection and transmission coefficients and Chapter 6

the experimental verification.

1.3 Excitation of Waves over a Circular Seamount by Forced Oscillations

Longuet-Higgins (1967) made extensive investigations into the

excitation of waves over a submerged circular sill, or sea mount,

when the driving force was an infinite train of rectilinear

progressive long waves. Subsequent work by Summerfield (1969)

was carried out using a circular island-shelf model and an elliptical

sill model. Many others have investigated the amplitude

response due to irregular bathymetry in the ocean, an extensive

survey on the literature of this subject is made by Summerfield

(1969). In almost all cases of theoretical work in this field the

waves were considered to be in the long-wave region and friction

was neglected from the equations of motion. Thus with these two

assumptions it was permissible to match the conditions of a

continuous mass flux and a continuous surface elevation. But,

where the waves are not necessarily long-waves and/or friction is important, then these conditions give erroneous results. Chapter 7 of this thesis presents a theory of the forced excitation of frictionally damped surface waves over a circular sea mount. Again, a simple linear friction term is introduced into the equations of motion and the amplitude response coefficients over the sea mount and in the ocean are calculated using the matching conditions as applied in the case of the straight shelf. The experimental verification of the theory is presented in Chapter 8.

Chapter 2 - Formulation of the Mathematical Model

This chapter deals with the formulation and solution of the equations of motion for surface waves having a frictional term as described previously. The solution is carried out in rectilinear and polar co-ordinates.

2.1 Co-ordinate System

We will consider a non-rotating co-ordinate system in which the vertical direction, labelled by γ, will be directed positive upward and have its origin on the still water surface.

The horizontal co-ordinates will be defined as $\bar{x} = (x, y)$ in right handed or cartesian co-ordinates or $\bar{x} = (r, \theta)$ in the polar co-ordinates. Departure form the undisturbed surface at $\gamma = 0$ will be designated " $\eta (x, t)$ " and we will require that these departures are very much less than the fluid depth h or, more correctly, that the second order term in the Stokes expansion is much less than the first order term, such that the small amplitude approximations may be used. In order to retain the linear equations, the frictional force will be defined as a body force per unit mass of

$\dfrac{c u_b}{h}$ where c is a constant and u_b is the horizontal velocity at $\gamma = -h$. It is to be expected that this frictional constant will vary with wave period since the period determines the thickness of the boundary layer (Li(1945)) and hence the amount of dissipation per unit time. This dependence on the frequency of oscillation does not appear in the equations of motion but will be determined experimentally.

To eliminate the added complication of a boundary layer thickness
we will define an "effective depth" h as being: that distance below
the undisturbed surface which is required to produce a theoretical
phase velocity that is equal to the measured phase velocity of the
actual fluid. That is, in Figure (5-a) we have the situation that
could exist in the actual fluid and in Figure (5-b) the modelled
situation.

Phase velocities of waves (v_p) are the same in both cases. The
difference $(h'-h)$ will be defined as Δh, the displacement
thickness.

2.2 The Equations of Motion for the model over a horizontal bed are:

$$\frac{\partial \bar{u}}{\partial t} = -\frac{1}{\rho} \bar{\nabla} p - \bar{F}(\bar{x}, t) - \bar{g} \qquad (2\text{-}1)$$

ρ is the fluid density

$\bar{g}$ is the acceleration of gravity

p is the pressure

$\bar{u}$ is the particle velocity

$\bar{x}$ is the horizontal co-ordinate

and $\bar{F} = \dfrac{c\bar{u}_b}{h}$ is the frictional force

We will assume the existence of a velocity potential such that:

1) $\quad \nabla^2 \phi_c = 0$ (Laplace's equation) $(2\text{-}2)$

and 2) $\quad \bar{\nabla} \phi_c = -\bar{u}$ $(2\text{-}3)$
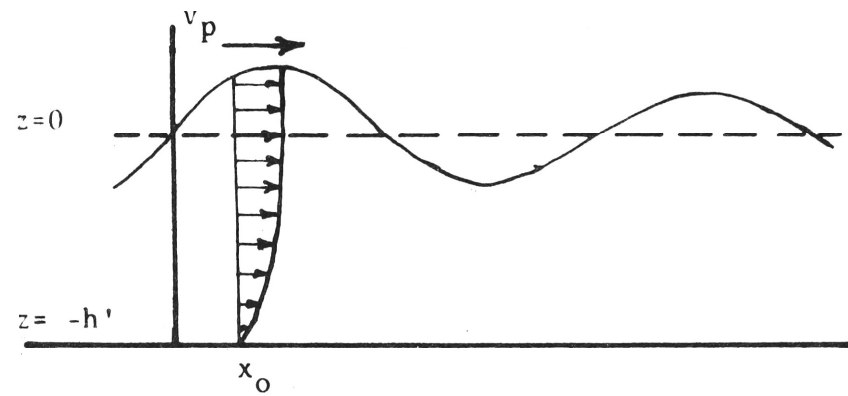
FIGURE 5-a.   FLOW WITH BOUNDARY LAYER
EXTENDING TO BOTTOM.
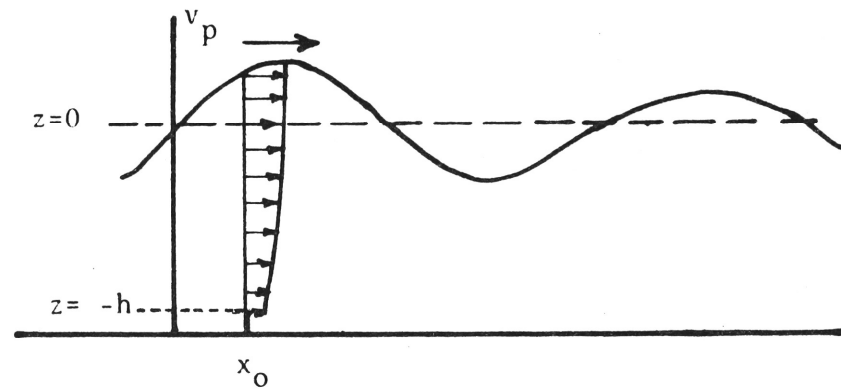
FIGURE 5-b.   MODELLED FLOW WITH BOUNDARY
LAYER ELIMINATED.

Substituting (2-3) in (2-1) gives:

$$\frac{\partial}{\partial t}(-\bar{\nabla}\phi_c) = -\frac{1}{\rho}\bar{\nabla}p - \bar{F} - \bar{g}$$

or, interchanging the order of differentiation

$$\bar{\nabla}\frac{\partial\phi_c}{\partial t} = -\frac{1}{\rho}\bar{\nabla}p + \bar{F} + \bar{g}$$

or since $\bar{F} = \frac{c\bar{u}_b}{h} = \frac{c\bar{U}_b}{h}$ by virtue of no vertical

velocity component " $\overline{w}$ " at the bottom.

thus $\bar{F} = -\frac{c}{h}\bar{\nabla}(\phi_c)_b$

where $(\phi_c)_b$ is the velocity potential evaluated at the bottom$(z=-h)$.

Thus (2-1) becomes

$$\bar{\nabla}(\frac{\partial\phi_c}{\partial t} - \frac{1}{\rho}p + \frac{c}{h}(\phi_c)_b) = \bar{g}$$

Assuming a constant fluid density.

Integrating and absorbing the constant of integration into the

potential function to arrive at the integrated Bernoulli equation:

$$\frac{\partial\phi_c}{\partial t} - \frac{p}{\rho} + \frac{c}{h}(\phi_c)_b = g z \qquad (2\text{-}4)$$

2.3 Solution of $\nabla^2\phi_c = 0$

The Boundary Conditions:

(a) The kinematic boundary condition states that a fluid particle once

on the surface remains on the surface.

At the surface the vertical displacement is

so $\quad \dfrac{dz}{dt}\Big|_{z=\eta} = w\big/_{z=\eta} = \left(u\,\dfrac{\partial \eta}{\partial x}\right)\Big/_{z=\eta} + \dfrac{\partial \eta}{\partial t}\Big/_{z=\eta}$

The assumption of small motions and amplitudes has been made and the surface slope $\dfrac{\partial \eta}{\partial x}$ is then small.

therefore: $\quad w\big/_{z=\eta} \simeq \dfrac{\partial \eta}{\partial t}$

but since $\quad \bar{\nabla} \phi_c = -\bar{U}$

it follows $\quad \bar{\nabla}_2\,\phi_c + \hat{k}\,\dfrac{\partial \phi_c}{\partial z} = -\bar{u}\,(\bar{x},t) - \hat{k}\,w\,(\bar{z},t)$

where $\bar{\nabla}_2$ is the differential operator for the horizontal parameters and $\hat{k}$ is a unit vector in the z direction

thus $\quad \dfrac{\partial \phi_c}{\partial z} = -w$

and. $\quad -\dfrac{\partial \phi_c}{\partial z}\Big/_{z=\eta} \simeq \dfrac{\partial \eta}{\partial t}$ $\qquad$ (2-5)

(b) The condition that there is no flow across the solid boundary on the bottom requires that:

$$w\big/_{z=-h} = 0$$

or $\quad \dfrac{\partial \phi_c}{\partial z}\Big/_{z=-h} = 0$ $\qquad$ (2-6)

Assuming that the potential function can be written as a product of the form:

$$\phi_c = f(\mathfrak{z}) \; \Phi(\bar{x}) \; e^{-i\sigma t}$$

which is harmonic with time.

gives

$$\nabla^2 \phi_c = \frac{1}{\Phi} \nabla_2^2 \Phi + \frac{1}{f} \frac{\partial^2 f}{\partial \mathfrak{z}^2} = 0$$

and since each term is independent of the other they each must equal a constant.

Letting

$$\frac{1}{f} \frac{\partial^2 f}{\partial \mathfrak{z}^2} = K^2$$

then

$$f = a e^{K \mathfrak{z}} + b e^{-K \mathfrak{z}}$$

where "a" and "b" are constants to be determined from the boundary conditions.

From condition (A) and invoking the small amplitude assumption:

$$- \Phi e^{-i\sigma t} K (a-b) = \frac{\partial \eta}{\partial t}$$

The value for the surface profile $\eta(x,t)$ is obtained from equation (2-4). At the surface this Bernoulli equation is:

$$\left(\frac{\partial \phi_c}{\partial t} + \frac{c}{h} (\phi_c)_b \right)_{\mathfrak{z} \simeq 0} = g\eta \qquad (2\text{-}7a)$$

so

$$\Phi e^{-i\sigma t} \left\{ \left(\frac{-i\sigma f(\mathfrak{z}) + \frac{c}{h} f(-h)}{g} \right)_{\mathfrak{z} \simeq 0} \right\} = \eta \qquad (2\text{-}7b)$$

the term inside the curly brackets is a constant so $\eta = A' \Phi e^{-i\sigma t}$

and $\quad \dfrac{\partial \eta}{\partial t} = -i\sigma A \Phi e^{-i\sigma t} = -K \Phi e^{-i\sigma t} \quad (a-b)$

thus $\quad a - b = \dfrac{i\sigma A'}{K}$

using boundary condition (B) gives:

$$K\left(a e^{-kh} - b e^{kh}\right) = 0$$

in general $\quad K \neq 0 \quad$ so $\quad a = \dfrac{b e^{Kh}}{e^{-Kh}}$

and $\quad f(\mathfrak{z}) = b\left\{\dfrac{e^{Kh}}{e^{-Kh}} e^{K\mathfrak{z}} + e^{-K\mathfrak{z}}\right\}$

$$= b\left\{\dfrac{e^{K(\mathfrak{z}+h)} + e^{-K(\mathfrak{z}+h)}}{e^{-Kh}}\right\}$$

but from condition (A)

$$b = \dfrac{i\sigma A' e^{-Kh}}{K\left(e^{Kh} - e^{-Kh}\right)}$$

thus $\hspace{8cm}$ (2-8)

$$f(\mathfrak{z}) = \dfrac{i\sigma A'}{K} \dfrac{\cosh K(\mathfrak{z}+h)}{\sinh Kh}$$

So the potential function becomes (the real part of):

$$\phi_c = \dfrac{i\sigma A' \cosh K(\mathfrak{z}+h)}{K \sinh Kh} \cdot \Phi(\bar{x}) e^{-i\sigma t} \hspace{2cm} (2\text{-}9)$$

and are left with the equation

$$\dfrac{1}{\Phi} \nabla_2^2 \Phi(\bar{x}) = -K^2 \hspace{3cm} (2\text{-}10)$$

<u>Case 1.</u> Rectilinear co-ordinates: If the wave crests move in a line parallel to the y axis then $\quad \bar{x} = \hat{i} x \quad$ where $\quad \hat{i}$. is a unit normal in the x direction.

Equation (2-8) becomes simply $\dfrac{\partial^2 \Phi}{\partial x^2} + K^2 \Phi = 0$

which has a solution as: $\Phi = a' e^{-i(Kx+\sigma t)} + b' e^{i(Kx-\sigma t)}$

or, since it is required that the wave to travel from left to right

$a' = 0$;

and $\Phi = b' e^{i(Kx-\sigma t)}$

thus $\phi_c = \dfrac{i\sigma A \cosh K(\mathfrak{z}+h)}{K \sinh Kh} e^{i(Kx-\sigma t)}$ (2-11)

Case 2. Polar co-ordinates: If the physical problem is most easily expressed in polar co-ordinates the solution (2-10) is expected to be in terms of circular functions.

In this case $\bar{x} = \hat{r}\, r + \hat{\Theta}\, \Theta$

where $\hat{r}$ is a unit vector in the (outward) radial direction and $\hat{\Theta}$ is a unit vector perpendicular to $\hat{r}$ and directed in a positive sense.

In polar co-ordinates $\nabla_2^2 = \dfrac{\partial^2}{\partial r^2} + \dfrac{1}{r}\dfrac{\partial}{\partial r} + \dfrac{1}{r^2}\dfrac{\partial^2}{\partial r^2}$

so that (2-10) becomes:

$$\dfrac{\partial^2 \Phi}{\partial r^2} + \dfrac{1}{r}\dfrac{\partial \Phi}{\partial r} + \dfrac{1}{r^2}\dfrac{\partial^2 \Phi}{\partial \Theta^2} + K^2 \Phi = 0$$

Assuming that $\Phi = R(r)\,\Theta(\Theta)$; separating variables gives:

$$\left\{ \dfrac{1}{R}\left(r^2 \dfrac{\partial^2 R}{\partial r^2} + r \dfrac{\partial R}{\partial r}\right) + K^2 r^2 \right\} + \left\{ \dfrac{1}{\Theta} \dfrac{\partial^2 \Theta}{\partial \Theta^2} \right\} = 0$$

As before, each term is dependent on only one variable so each must be a constant.

Let $\dfrac{1}{\Theta}\dfrac{\partial^2 \Theta}{\partial \theta^2} = -m^2$

then $\Theta = c'_m \sin m\theta + d'_m \cos m\theta$

or $\Theta = E'_m \cos(m\theta - \beta_m)$

Thus arriving at Bessel's equation of order "m" for R

$$r^2 \frac{\partial^2 R}{\partial r^2} + r \frac{\partial R}{\partial r} + (k^2 \cdot r^2 - m^2) R = 0$$

which has solutions of the form

$$R_m = A'_m J_m(K_r) + B'_m Y_m(K_r)$$

or

$$R_m = A''_m H_m^{(1)}(K_r) + B''_m H_m^{(2)}(K_r)$$

Where J_m are Bessel Functions of the first kind

Y_m are Bessel Functions of the second kind

$H_m^{(1,2)}$ are Bessel Functions of the third kind

(or Hankel Functions) $H_m^{(1,2)} = J_m \pm i Y_m$

Therefore $\phi_{cm} = \dfrac{i\sigma \cosh K(z+h)}{K \sinh Kh} \left\{ A_m J_m + B_m Y_m \right\} \cos(m\theta - \beta_m) e^{-i\sigma t}$

$$(2-12)$$

It is required that ϕ_{cm} is periodic in θ, that is

$$\phi_{cm}(z, r, \theta, t) = \phi_{cm}(z, r, \theta + 2m\pi, t); \quad m = 0, 1, 2 \cdots$$

Hence m is a positive integer or zero.

The special case for $m = 0$ produces lines of equal ϕ_{cm} forming concentric circles with the origin as centre. For convenience, the

phase angle β_n is taken to be zero.

Since a sum of solutions is also a solution to the differential equation (2-2), the potential function can be written in the more general form:

$$\phi_c = \sum_{n=0}^{\infty} \phi_{cn} = \frac{i\sigma \cosh K(z+h)}{K \sinh Kh} \sum_{n=0}^{\infty} (A_n J_n + B_n Y_n) \cos n\theta\, e^{-i\sigma t}$$

provided the series converges.

For any physical probelm that includes the origin, solutions involving Bessel functions of the second kind must be excluded because of their logarithmic behaviour near this point, hence $B_n = 0$

and $\phi_c = \dfrac{i\sigma \cosh K(z+h)}{K \sinh Kh} \displaystyle\sum_{n=0}^{\infty} A_n J_n \cos n\theta\, e^{-i\sigma t}$ \hfill (2-13)

For problems where the origin is excluded the solution can be written as:

$$\phi_c = \frac{i\sigma \cosh K(z+h)}{K \sinh Kh} \sum_{n=0}^{\infty} ('A_n H_n^{(1)} + 'B_n H_n^{(2)}) \cos n\theta\, e^{-i\sigma t} \qquad (2-14)$$

Chapter 3 - Plane Waves in Constant Depth

In this chapter the theoretical properties of the waves with a distributed body force as modelled in the previous section is investigated. We consider plane, rectilinear, waves propagated in the x direction with the still water depth everywhere being constant.

3.1 The Potential Function

The potential function for this model is expressed by equation (2-10) as:

$$\phi_c (x, \zeta, t) = \frac{\iota \sigma A \cosh \mathcal{K} (\zeta + h)}{\mathcal{K} \sinh \mathcal{K} h} e^{\iota (\mathcal{K} x - \sigma t)}$$

where, in general, $\mathcal{K}$ is complex. This representation of the potential function satisfies the Laplace Equation and the appropriate boundary conditions on the surface and at the bottom of the fluid. However, in any physical problem only the real part of the above expression may be retained. This is evaluated in Appendix 1 and is found to be

$$R(\phi_c) = \phi = \frac{-\sigma A e^{-\alpha x}}{\Delta \mathcal{K}} \left\{ \cosh kZ \cos \alpha Z \sin (kx - \sigma t - \epsilon) \right.$$
$$\left. + \sinh kZ \sin \alpha Z \cos (kx - \sigma t - \epsilon) \right\} \qquad (3-1)$$

where
$$\Delta = (\sinh^2 kh + \sin^2 \alpha h)^{1/2}$$
$$\mathcal{K} = (k^2 + \alpha^2)^{1/2}$$
$$\epsilon = \Omega + \delta = \tan^{-1} \frac{\alpha}{k} + \tan^{-1} \left(\frac{\cosh kh \sin \alpha h}{\sinh kh \cos \alpha h} \right)$$
$$Z = \zeta + h$$

and
$$k + \iota \alpha = \mathcal{K}$$

3.2   The Wave Number and Decay Coefficient

The two unknown parameters in the above expression, namely,

k , the wave number and α , the decay coefficient: are

evaluated from the free surface Bernoulli Equation. (Equation (2-7a))

$$\left\{ \frac{\partial \phi_c}{\partial t} + \frac{c}{h} \left(\phi_c \right)_b \right\}_{\xi \,\cong\, 0} = g\eta$$

Using the value for $\phi = \mathcal{R} \left\{ \phi_c \right\}$ as found above, the

dispersion relation is obtained:

$$\frac{\sigma^2}{\Delta k} \left\{ \begin{array}{l} \cosh kh \cos \alpha h \cos (kx - \sigma t - \epsilon) \\ - \sinh kh \sin \alpha h \sin (kx - \sigma t - \epsilon) \\ - \frac{c}{\sigma h} \sin (kx - \sigma t - \epsilon) \end{array} \right\} = \cos (kx - \sigma t) \qquad (3\text{-}2)$$

It was found more expedient to solve equation (2-7a) and

then equate real and imaginary parts of the expression to obtain

equations for k and α than it was to solve equation (3-2).

Two transcendental equations defining (implicitly) k

and α are determined (see Appendix 2)

$$k = \frac{\sigma^2}{2g} \left\{ \frac{\sinh 2kh + \frac{2c}{\sigma h} \cosh kh \sin \alpha h}{\sinh^2 kh + \sin^2 \alpha h} \right\} \qquad (3\text{-}3a)$$

$$\alpha = \frac{\sigma^2}{2g} \left\{ \frac{- \sin 2\alpha h + \frac{2c}{\sigma h} \sinh kh \cos \alpha h}{\sinh^2 kh + \sin^2 \alpha h} \right\} \qquad (3\text{-}4a)$$

These equations were solved numerically and the results are presented in Figure 6.

Special Cases:

1) Long Waves

For this class of waves $kh \ll 1$ and it follows from equation (3-3a) and equation (3-4a) that αh is also much less than unity. (See Appendix 2). With this restriction on kh the hyperbolic and trigonometric functions having kh or αh as arguments can be approximated with the first term in their Taylor's series expansion.

Thus obtaining:
$$k \simeq \frac{\sigma}{\sqrt{2gh}} \left\{ 1 + \sqrt{1 + \left(\frac{c}{\sigma h}\right)^2} \right\}^{1/2} \qquad (3\text{-}3b)$$

and
$$\alpha \simeq \frac{\sigma}{\sqrt{2gh}} \left\{ -1 + \sqrt{1 + \left(\frac{c}{\sigma h}\right)^2} \right\}^{1/2} \qquad (3\text{-}4b)$$

If also $\dfrac{c}{\sigma h} \ll 1$, then
$$k \simeq \frac{\sigma}{\sqrt{gh}} \left(1 + O\left(\frac{\theta'}{2}\right)^2 \right) \qquad (3\text{-}3c)$$

and
$$\alpha \simeq \frac{\sigma}{\sqrt{gh}} \left(\frac{c}{2\sigma h} + O\left(\frac{\theta'}{2}\right)^3 \right) \qquad (3\text{-}4c)$$

where $\theta' = \sinh^{-1}\left(\frac{c}{\sigma h}\right)$

In this case the wave number k is changed by only a small amount from its frictionless value and the decay coefficient varies as $h^{-3/2}$. This variation with h is in agreement with viscous damping theories for long-waves (See, for example, Hunt (1952)). It
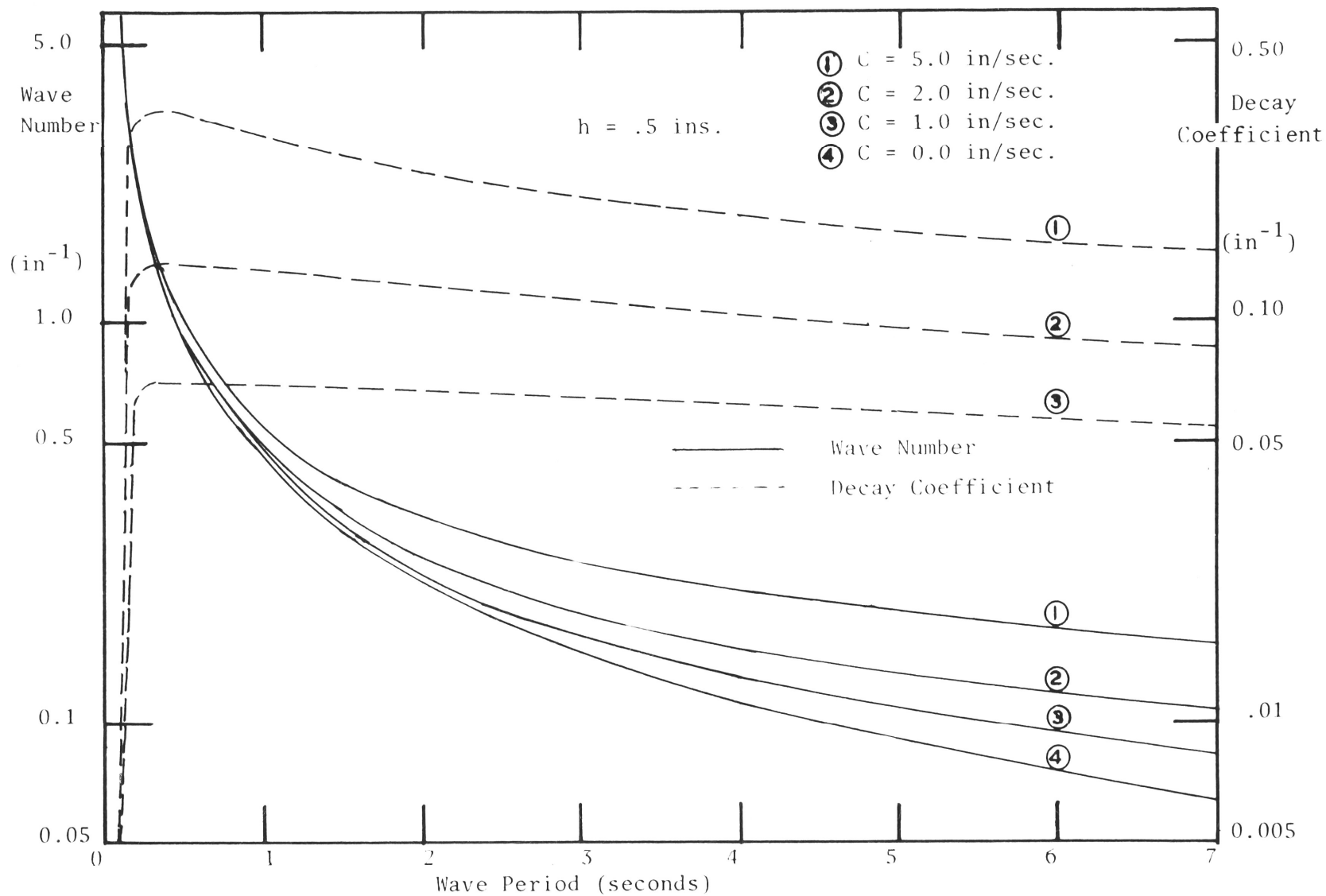
FIGURE 6.   WAVE NUMBER AND DECAY COEFFICIENT AS A FUNCTION OF THE
WAVE PERIOD FOR VARIOUS FRICTION CONSTANTS

should be noted that long-waves with a small damping coefficient do not necessarily imply a small $\left(\dfrac{c}{\sigma h}\right)$ term.

Equation (3-3b) is the same solution as obtained by Voigt (1899) in his study of the well known Telegraphist's equation:

$$\frac{\partial^2 \psi}{\partial t^2} = c^2 \frac{\partial^2 \psi}{\partial x^2} - \kappa' \frac{\partial \psi}{\partial t}$$

where c and κ' are constants.

To show that equation (2-1) reduces to the above in the case of long-waves it is noted that the contribution to the pressure through vertical accelerations is negligible and the only pressure variations are hydrostatic.-

viz: $\quad \bar{\nabla} p = \dfrac{\partial}{\partial x} (\zeta + \eta) \rho \bar{g} = \rho \bar{g} \dfrac{\partial \eta}{\partial x}$

Using the equation of continuity $\bar{\nabla} \cdot \bar{u} = 0$ gives (See Lamb (1932)): $\quad \dfrac{\partial \eta}{\partial t} \underset{\sim}{} -h \dfrac{\partial u}{\partial x}$

where small terms have been neglected.

Thus $\quad \dfrac{\partial}{\partial t} \bar{\nabla} p = \rho g \dfrac{\partial}{\partial x} \dfrac{\partial \eta}{\partial t} = -\rho g h \dfrac{\partial^2 u}{\partial x^2}$

Differentiation of equation (2-1) with respect to time yields:

$$\frac{\partial^2 u}{\partial t^2} = gh \frac{\partial^2 u}{\partial x^2} - \frac{\partial F}{\partial t}$$

letting $\sqrt{gh} = v_{op}$, the frictionless long-wave celerity, and noting $u = u_b$ thus arriving at:

$$\frac{\partial^2 u}{\partial t^2} = v_{op}^2 \frac{\partial^2 u}{\partial x^2} - \frac{c}{h} \frac{\partial u}{\partial t} \qquad\qquad (3\text{-}5)$$

Telegraphist's equation.

2) Deep-water Waves

For these waves where $h \rightarrow \infty$ there is no wave motion at the bottom and the decay is expected to be zero in the limit. This is shown using the dispersion relation for α :

$$\lim_{h \to \infty} \alpha = \lim_{h \to \infty} \left\{ \frac{-\sin 2\alpha h + \frac{2c}{\sigma h} \sinh kh \cos \alpha h}{\sinh^2 kh + \sin^2 \alpha h} \right\}$$

the sine terms will be much smaller than the hyperbolic terms for large kh

so

$$\lim_{h \to \infty} \alpha = \lim_{h \to \infty} \frac{\frac{2c}{\sigma h} \cos \alpha h}{\sinh kh}$$

$$\leqslant \frac{2c}{\sigma} \lim_{h \to \infty} \frac{1}{h \sinh kh} \longrightarrow 0$$

Thus, as was expected, the decay is zero in deep water for this model. Similarly, the wave number approaches the frictionless deep water value. i.e.:

$$\lim_{h \to \infty} k \longrightarrow \frac{\sigma^2}{2g}$$

3.3 The Particle Velocities and Stream Function

The velocities of the fluid particles are evaluated from the relation (2-3)

$$\bar{\nabla} \phi_c = -\bar{U}$$

or more correctly $\bar{\nabla} (\mathcal{R} \{\phi_c\}) = -\bar{U}$

or $\mathcal{R} \{\bar{\nabla} \phi_c\} = -\bar{U}$

3.3a The Horizontal Particle Velocity

$$\omega = -\mathcal{R} \left\{ \frac{\partial \phi_c}{\partial x} \right\}$$

and using (2-11) gives:

$$u = \mathcal{R}\left\{ \frac{\sigma A \cosh k(z+h)}{\sinh kh} \, e^{i(kx-\sigma t)} \right\}$$

$$= \mathcal{R}\left\{ \frac{\sigma A (\cosh kz \cos \alpha z + i \sinh kz \sin \alpha z)}{\Delta \, e^{i\delta}} \, e^{i(k+i\alpha)x} \, e^{-i\sigma t} \right.$$

$$= \frac{\sigma A e^{-\alpha x}}{\Delta} \left[\cosh kz \cos \alpha z \cos(kx - \sigma t - \delta) \right.$$

$$\left. - \sinh kz \sin \alpha z \sin(kx - \sigma t - \delta) \right] \qquad (3\text{-}6)$$

Letting $Q(z) = \left[(\cosh kz \cos \alpha z)^2 + (\sinh kz \sin \alpha z)^2 \right]^{1/2}$

$$= \frac{1}{\sqrt{2}} (\cosh 2kz + \cos 2\alpha z)^{1/2}$$

and $\quad p'(z) = \tan^{-1} \left(\dfrac{\sinh kz \sin \alpha z}{\cosh kz \cos \alpha z} \right)$

Then equation (3-6) becomes:

$$u = \frac{\sigma A e^{-\alpha x}}{\Delta} \, Q(z) \cos(kx - \sigma t - \delta + p'(z)) \qquad (3\text{-}6a)$$

Comparing this with the frictionless horizontal velocity:

$$u_0 = \frac{\sigma A_0}{\sinh k h} \cosh k_0 z \cos(k_0 x - \sigma t)$$

Therefore, the presence of friction reduces the horizontal amplitude
of motion (for a given surface wave amplitude $A e^{-\alpha x} = A_0$)
by a factor:

$$\frac{u}{u_0} = \frac{\sinh k_0 h}{\sqrt{2} \cosh k_0 h} \sqrt{\frac{\cosh 2kz + \cos 2\alpha z}{\sinh^2 kh + \sin^2 \alpha h}}$$

which, for long-waves, reduces

to:
$$\frac{u}{u_o} \simeq \frac{k_o}{\sqrt{k^2 + \alpha^2}}$$

this, since $\alpha > 0$ AND $k > k_o$ is always less than unity. Which is the same result as found by Ippen (1966) (Equation 10.39).

Comparison of the surface profile described as
$$\eta = A e^{-\alpha x} \cos (kx - \sigma t)$$

with equation (3-6a) show that a phase shift of $(p(z)-\delta)$ exists between the surface wave motion and the horizontal particle velocity. It is now demonstrated that this phase shift is always negative indicating that the horizontal currents follow the surface wave motion.

Firstly, it is noted that the arguments for both the inverse tangent functions and hence the functions themselves are positive. This can be seen from the description of the model where k, α, h and z are taken positive, so the hyperbolic functions are all positive and αz and αh are positive. That $\alpha h \leq \frac{\pi}{2}$ is seen by examining equation (3-4a): Suppose $\frac{\pi}{2} < \alpha h < \frac{3\pi}{2}$ then, in general, the numerator becomes negative and a negative decay coefficient results contrary to the model, so $0 \leq \alpha h < \frac{\pi}{2}$ and the trigonometric functions are always positive.

at $z = 0$; $\left(p'(0) - \delta\right) = -\delta$

at $z = h$; $\left(p'(h) - \delta\right) = \tan^{-1}\left(\frac{\sinh kh \sin \alpha h}{\cosh kh \cos \alpha h}\right) - \tan^{-1}\left(\frac{\cosh kh \sin \alpha h}{\sinh kh \cos \alpha h}\right)$

which is negative since $\sinh kh \leq \cosh kh$ for $0 \leq kh < \infty$ and since the inverse tangent function is positive

and increasing in this region.

Because the magnitude of the phase is greater at the bottom $z = 0$ than at the top $z = h$ then, if there are no turning points between $z = 0$ and $z = h$ the magnitude of the phase must decrease monotonically from the bottom to the surface. This is easily shown since:

$$\frac{\partial}{\partial z}\left(p(z) - \delta\right) = \frac{\partial}{\partial z}\tan^{-1}\left(\tanh kz \tan \alpha z\right) = \frac{k \operatorname{sech}^2 kz \tan \alpha z + \alpha \sec^2 \alpha z \tanh kz}{1 + (\tanh kz + \tan \alpha z)^2}$$

For a turning point this must equal zero, but all the terms are positive or, in the trivial case, zero, so the equation is positive and there are no turning points in $0 < z \leqslant h$ The trivial cases of k and/or α equalling zero are those that designate infinitely long waves or no friction respectively and obviously exhibit a zero phase shift throughout the fluid column.

For reasonably "long waves" the phase $p'(z)$ is much smaller than δ ; for in this case:

$$p(z) - \delta \simeq \tan^{-1}(k\alpha h^2) - \tan^{-1}\frac{\alpha}{k}$$
$$\text{AND} \qquad k\alpha h^2 \ll \frac{\alpha}{k}$$

so $p(z) - \delta \simeq -\tan^{-1}\frac{\alpha}{k}$ which is constant throughout a fluid column. Similar remarks can be made for the phase shifts found in the other wave properties.

3.3b The Vertical Particle Velocity

$$w = -\mathcal{R}\left\{\frac{\partial \phi_c}{\partial \zeta}\right\}$$
$$= -\mathcal{R}\left\{\frac{i\sigma A \sinh k(\zeta + h)}{\sinh kh} e^{i(kx - \sigma t)}\right\}$$
$$w = \frac{\sigma A e^{-\alpha x}}{\Delta}\left\{\sinh kz \cos \alpha z \sin(kx - \sigma t - \delta)\right.$$
$$\left. + \cosh kz \sin \alpha z \cos(kx - \sigma t - \delta)\right\} \tag{3-7}$$

3.3c   The Stream-Function

The stream-function ψ is defined such that

$$u = -\frac{\partial \psi}{\partial y}$$

and

$$w = \frac{\partial \psi}{\partial x}$$

Thus
$$\psi = -\int u \, \partial y$$

$$= \int R\left\{\frac{\partial \phi_c}{\partial x}\right\} \partial y$$

$$= R\left\{\frac{-\sigma A \sinh K(y+h)}{K \sinh Kh} e^{i(kx-\sigma t)}\right\} + C_1(x)$$

where C_1 is a constant of integration.

Similarly :-

$$\psi = \int w \, \partial x$$

$$= R\left\{\frac{-\sigma A \sinh K(y+h)}{K \sinh Kh} e^{i(kx-\sigma t)}\right\} + C_2(y)$$

From these two relations it follows that:

$$C_1 = C_2 = \text{constant.}$$

Taking the origin for the stream function such that $C_1 = 0$ gives:

$$\psi = \frac{\sigma A e^{-\alpha x}}{\Delta K}\left\{\begin{array}{l} -\sinh kz \cos \alpha z \cos(kx-\sigma t-\epsilon) \\ + \cosh kz \sin \alpha z \sin(kx-\sigma t-\epsilon)\end{array}\right\} \qquad (3\text{-}8)$$

The form of the lines $\psi = $ constant are shown in Figure 7.

3.4   The Energy and Energy Flux

3.4a   The Average Energy

Consider a section of width dx and 1 unit in the y direction extending from the bottom to the surface. The average (over 1 wave
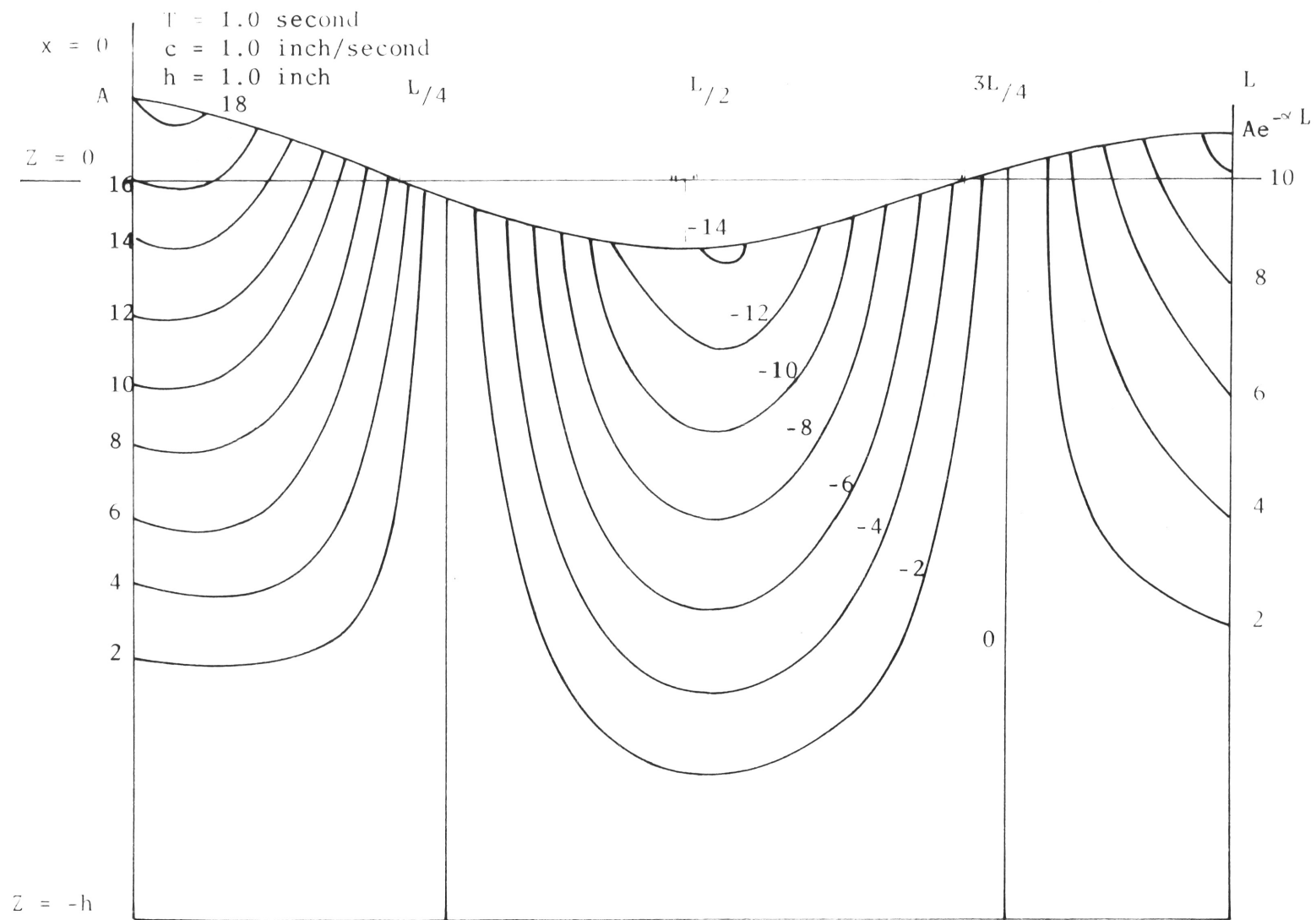
FIGURE 7. THE STREAM FUNCTION

period) potential and kinetic energy contained in this section is calculated as follows.

With the assumption that dx is small enough so that the wave amplitude may be considered constant across the section, then the potential energy contained in the section at any time t will be:

$$d(PE) = \frac{\rho g}{2} \eta^2 dx$$

$$= \frac{\rho g}{2} A^2 e^{-2\alpha x'} \cos^2(kx' - \sigma t) dx \qquad \text{(Kinsman (1965))}$$

and taking the time average yields:

$$d(PE)_{AVG.} = \frac{1}{T} \int_{t}^{t+T} \left(\left(\frac{\rho g}{2} \eta^2 \right) dx \right) dt \qquad (3\text{-}9)$$

$$= \frac{\rho g A^2 e^{-2\alpha x'}}{4} dx$$

Similarly, the kinetic energy contained in the section at any time t, will be:

$$d(KE) = \left\{ \rho \int_{-h}^{\eta \simeq 0} (u^2 + w^2) \, dz \right\} dx \qquad \text{(Kinsman (1965))}$$

And the average over 1 wave period is:

$$d(KE)_{AVG.} = \frac{\rho g A^2 e^{-2\alpha x'}}{4 \left(1 + \frac{c}{\sigma h} \frac{\sin \alpha h}{\sinh kh} \right)} dx \qquad (3\text{-}10)$$

The time average energy in this section is the sum of the kinetic and potential energy averages thus:

$$d(E)_{AVG} = \frac{\rho g A e^{-2\alpha x'}}{4} \left\{ 1 + \frac{1}{1 + \frac{c}{\sigma h} \frac{\sin \alpha h}{\sinh kh}} \right\} dx \qquad (3\text{-}11a)$$

alternately

$$d(E)_{AVG.} = \frac{\rho \sigma^2 A^2 e^{-2\alpha x'}}{4 \Delta K} \left\{ \frac{\sinh 2kh}{\Delta} + \frac{c}{\sigma h} \sin \delta \right\} dx \qquad (3-11b)$$

by use of equation (3 - 3a).

Examination of equations (3-9) and (3-10) reveal that there is not the usual condition of equipartition of energy (i.e.: $PE = KE$). The average kinetic energy in the section from x' to $x' + dx$ is less than the average potential energy by an amount:

$$d(\Delta E_{AVG.}) = \frac{\rho g A^2 e^{-2\alpha x'}}{4} \left\{ 1 - \frac{1}{1 + \frac{c}{\sigma h} \frac{\sin \alpha h}{\sinh kh}} \right\} dx$$

which reduces (with the help of equation (3-3a)) to:

$$d(\Delta E_{AVG.}) = \left\{ \frac{c \rho \sigma}{4 \Delta kh} \sin \delta \, A^2 e^{-2\alpha x'} \right\} dx$$

This energy difference is a consequence of the particle velocities u and w being reduced by friction over and above that caused by the amplitude decay directly (See (3-3a), (3-3b)). Thus since the potential energy is dependant only on the surface elevation it is not surprising that $d(PE)_{AVG.} > d(KE)_{AVG.}$.

During one wave period the phase of the wave has moved from x' to $(x' + L)$. The total energy in this region will be made up of the energy of the decaying wave and that lost from the wave through dissipation. Thus the total energy contained in the region from x' to $(x' + L)$ can be considered to be that which would result from a hypothetical non-decaying wave of amplitude $A e^{-\alpha x'}$ travelling

between x' and $x'+L$. The average energy of the hypothetical wave in this region will be:

$$E(x')_{AVG.} = \frac{1}{L} \int_{x'}^{x'+L} d\,(E)_{AVG.}$$

$$= \frac{1}{L} \int_{x'}^{x'+L} \frac{\rho g A^2 e^{-2\alpha x'}}{4} \left(1 + \frac{1}{1 + \frac{c}{\sigma h} \frac{\sin \alpha h}{\sinh kh}} \right) dx$$

$$= \frac{\rho g A^2 e^{-2\alpha x'}}{4} \left\{ 1 + \frac{1}{1 + \frac{c}{\sigma h} \frac{\sin \alpha h}{\sinh kh}} \right\} \qquad (3\text{-}12a)$$

or, using equation (3-11b):

$$E(x')_{AVG.} = \frac{\rho \sigma^2 A^2 e^{-2\alpha x'}}{4 \Delta K} \left\{ \frac{\sinh 2kh}{\Delta} + \frac{c}{\sigma h} \sin \delta \right\} \qquad (3\text{-}12b)$$

3.4b   The Average Energy Flux or Average Power

The time average rate of transmission of energy across a plane of unit width set in the fluid at a position x' is given by (Lord Raleigh (1877)):

$$P_{AVG.} = \frac{1}{T} \int_{-h}^{\eta} \int_{t}^{t+T} p_v \, u \, dy \, dt \qquad (3\text{-}13)$$

where p_v is the variable part of the pressure found from the integrated Bernoulli equation and the average is taken over one complete wave period ($T = \frac{2\pi}{\sigma}$) .

From equation (2-4) the total pressure is:

$$p = \rho \left\{ \frac{\partial \phi}{\partial t} + \frac{c}{h} \phi_b - gy \right\}$$

of which the variable part is:

$$p_v = \rho \left\{ \frac{\partial \phi}{\partial t} + \frac{c}{h} \phi_b \right\}$$

The energy flux integral becomes:

$$P_{AVG.} \simeq \frac{\rho}{T} \int_{-h}^{0} \int_{t}^{t+T} \left\{ \frac{\partial \phi}{\partial t} + \frac{c}{h} \phi_b \right\} \mu \, dz \, dt \qquad (3\text{-}14)$$

where the small amplitude assumption is used.

The evaluation of the products in the integrand must be carried out using the real parts of the horizontal velocity and the potential function due to the fact that, in general,

$$R\left\{ z_1 z_2 \right\} \neq R\left\{ z_1 \right\} \cdot R\left\{ z_2 \right\}$$

where z_1 and z_2 are complex numbers. Writing the power expression explicitly:

$$P_{AVG.} = \frac{\rho \sigma^3 A^2 e^{-2\alpha x'}}{\Delta^2 KT} \int_{t}^{t+T} dt \int_{0}^{h} \left\{ \left[\cosh k z \cos \alpha z \cos X_\epsilon - \sinh k z \sin \alpha z \sin X_\epsilon \right] \right.$$

$$\cdot \left[\cosh k z \cos \alpha z \cos X_\delta - \sinh k z \sin \alpha z \sin X_\delta \right] \right\} dz$$

$$(3\text{-}15)$$

$$+ \frac{c}{h} \frac{A \sigma e^{-\alpha x'}}{\Delta KT} \int_{t}^{t+T} \left\{ \sin X_\epsilon \left[\psi \right]_0^h \right\} dt$$

where $X_\epsilon = kx' - \sigma t - \epsilon$

and $X_\delta = kx' - \sigma t - \delta$

The second integral in this expression is obtained by noting that $\frac{c}{h} w_b$ is independant of the depth and then using the definition of the stream function:

viz: $\psi = \int \mu \, dz$; so $\int_{0}^{h} \mu \, dz = {}_0^h\left[\psi \right]$

Evaluation of this integral over the fluid depth and averaging over one wave period yields:

$$P_{AVG.} = \frac{\rho \sigma^3 A^2 e^{-2\alpha x'}}{8 \Delta^2 K^2} \left\{ \sinh 2kh + \frac{\alpha}{k} \sin 2\alpha h \right.$$

$$\left. + \frac{4c}{\sigma h} \cosh kh \sin \alpha h \right\} \qquad (3\text{-}16)$$

(See Appendix 3 for details)

That this equation reduces to the usual frictionless model can be seen by taking the limit $\alpha \to 0$

$$P_{0\ AVG.} = \lim_{\alpha \to 0} P_{AVG.} = \frac{\rho \sigma^3 A^2}{8 k_o^2 \sinh^2 k_o h} \left\{ \sinh 2k_o h + k_o \lim_{\alpha \to 0} \frac{\sin 2\alpha h}{\alpha} \right\}$$

and by use of L'Hospital's rule it follows that:

$$P_{0\ AVG.} = \frac{\rho \sigma^3 A^2}{8 k_o^2 \sinh^2 k_o h} \left\{ 2 k_o h + \sinh 2 k_o h \right\}.$$

3.5 The Wave Velocities

In this section of the thesis three different wave velocities are investigated, namely:

a) The Phase Velocity: $\upsilon_p = \sigma/k$

b) The Energy Velocity: $\upsilon_e = P_{AVG.}/E_{AVG.}$

c) The Group Velocity: $\upsilon_g = \frac{\partial \sigma}{\partial k}$

It will be shown that, in general, these three velocities are different.

3.5a The Phase Velocity

The usual definition of the phase velocity is given by (Brillouin (1960)) $\upsilon_p = \sigma/k$ for wave described as $\eta = A \cos (kx - \sigma t)$

In the model the phase velocity is then: (from equation (3-3a)):

$$v_p = \frac{2g}{\sigma} \frac{\sinh^2 kh + \sin^2 \alpha h}{\sinh^2 kh + \frac{2c}{\sigma h} \cosh kh \sin \alpha h} \qquad (3\text{-}17)$$

or for "long-waves" (From equation (3-3b)):

$$v_p \simeq \left\{ \frac{2gh}{1 + \sqrt{1 + (\frac{c}{\sigma h})^2}} \right\}^{1/2} \qquad (3\text{-}17a)$$

which is a function of the frequency (provided the frictional constant is not directly proportional to the frequency). Therefore, with friction introduced, long-waves no longer exhibit a non-dispersive nature.

3.5b The Energy Velocity

Following Lord Raleigh (1877) the energy velocity is defined as the ratio of the energy propagated across a fixed plane in unit time $\frac{2\pi}{\sigma}$ to that existing in the unit length $\frac{2\pi}{k}$. From this definition the equation for the energy velocity is:

$$v_e = P_{AVG} / E_{AVG.}$$

Where $P_{AVG.}$ and $E_{AVG.}$ are given by equations (3-17) and (3-12) respectively.

or, more explicitly:

$$v_e = \frac{\sigma^3}{2\Delta^2 Kg} \left(\frac{\sinh 2kh + \frac{k}{\alpha} \sin 2\alpha h + \frac{4c}{\sigma h} \cosh kh \sin \alpha h}{1 + \frac{1}{1 + \frac{c}{\sigma h} \frac{\sin \alpha h}{\sinh kh}}} \right) \qquad (3\text{-}18a)$$

alternately, using the form of the energy equation as in equation (3-12b), the result is:

$$\upsilon_e = \frac{\sigma k}{2 K^2} \left(\frac{1 + \frac{k}{\measuredangle}\frac{\sin 2\measuredangle h}{\sinh 2kh} + \frac{2c}{\sigma h}\frac{\sin \measuredangle h}{\sinh kh}}{1 + \frac{c}{2\sigma h}\frac{\sin \measuredangle h}{\sinh kh}} \right) \qquad (3\text{-}18b)$$

In the frictionless case

$$\upsilon_{oe} = \lim_{\measuredangle \to o} \upsilon_e = \frac{\sigma}{2k_o} \left(1 + \frac{2 k_o h}{\sinh 2 k_o h} \right)$$

which is the usual representation for the group velocity (Lamb (1932)). In this case , $\measuredangle \to o$, the group velocity and the energy velocity are identical, but when there is frictional damping the equality of these two velocities is not longer true as will be shown in 3.5c.

For long-waves the result is:

$$\upsilon_e \simeq \frac{\sigma k}{2 K^2} \left\{ 1 + \frac{\frac{c}{2\sigma h}\cdot\frac{\measuredangle}{k}}{1 + \frac{c}{2\sigma h}\frac{\measuredangle}{k}} \right\} \qquad (3\text{-}18c)$$

which is not equal to the phase velocity as in the case for frictionless waves.

3.5c The Group Velocity

The group velocity is defined (Sommerfeld (1914)) as the maximum velocity of propagation of beats, or $\upsilon_g = \dfrac{\partial \sigma}{\partial k}$

Differentiation of the dispersion equation (3-3a) for k results in:

$$v_g = \frac{\frac{g}{\sigma}(kh \sinh 2kh + \Delta^2) - \sigma h(\cosh 2kh + \frac{c}{\sigma h}\sinh kh \sin \lambda h)}{\frac{2kg}{\sigma^2}\Delta^2 - \frac{c}{\sigma h}\cosh kh \sin \lambda h} \quad (3\text{-}19)$$

Comparison of equation (3-18a) and the above reveal that the energy velocity and the group velocity are no longer the same. This is in accord with the theory of electromagnetic waves passing through an absorbing media: "The energy velocity thus decreases greatly in this anomalous region (absorption band) and passes through a minimum. It is quite different from the group velocity." (Brillouin (1960)).

Comparisons between the three velocities are presented in Figure 8, Figure 9 and Figure 10.
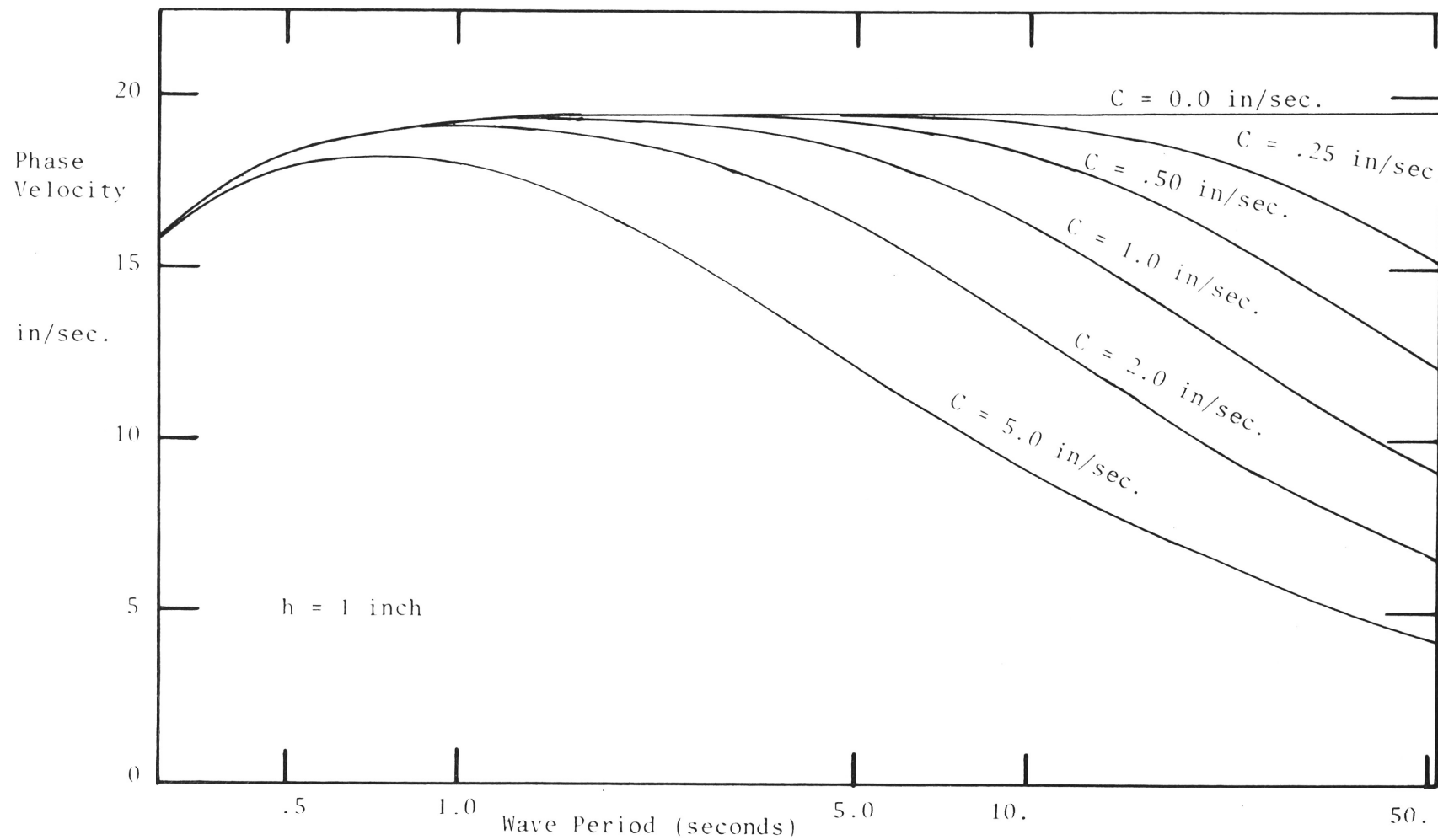
FIGURE 8. THE PHASE VELOCITY AS A FUNCTION OF THE WAVE PERIOD FOR VARIOUS FRICTION CONSTANTS.
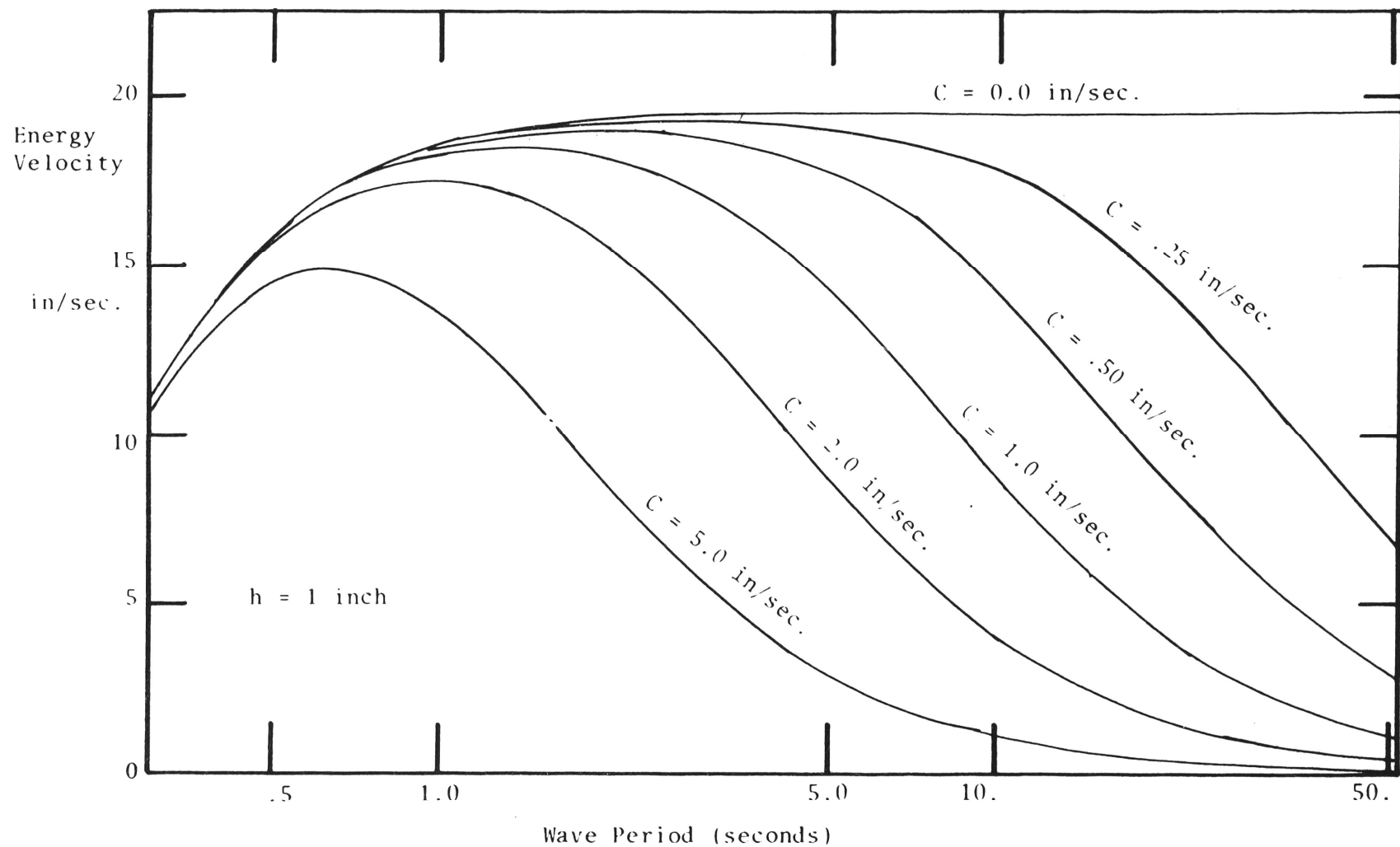
FIGURE 9. THE ENERGY VELOCITY AS A FUNCTION OF THE WAVE PERIOD FOR VARIOUS FRICTION CONSTANTS.
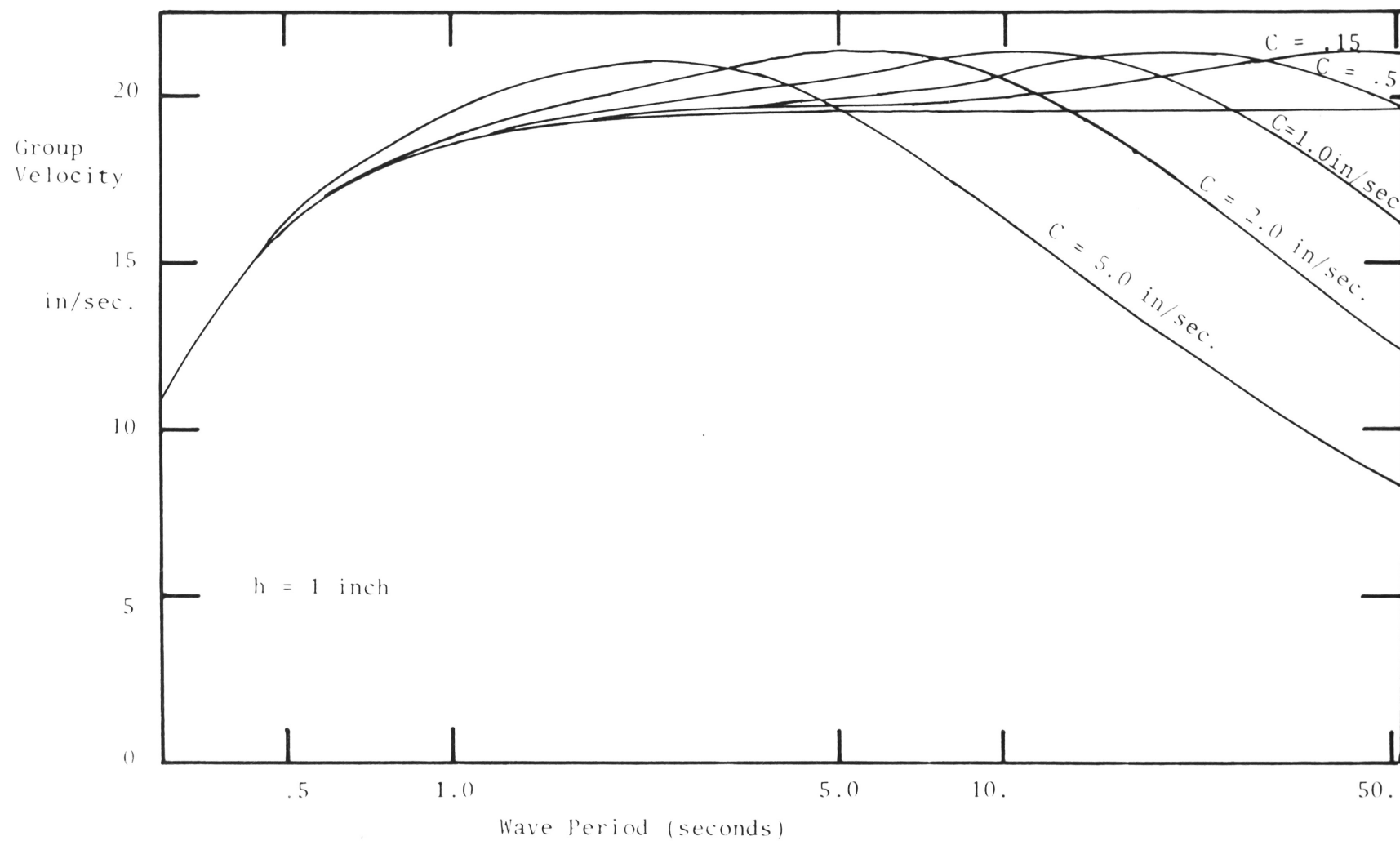
FIGURE 10. THE GROUP VELOCITY AS A FUNCTION OF THE WAVE PERIOD FOR VARIOUS FRICTION CONSTANTS.

Chapter 4 - Experiments Pertaining to Waves in a Uniform Depth

Experiments were carried out with a uniform fluid depth to determine:

1) the "effective" fluid depth "h"

2) the decay coefficient α and the frictional constant C

and to investigate

3) the frictional induced phase "δ"

The equipment used in these experiments has been described in detail in the Appendices 6,7,8 and 9. Since a frictional model was being investigated a moderately viscous fluid was used for many of the tests. This fluid was a glycerol and water mixture; two mixtures were used, the first 55% and the second 77% glycerol by volume. A small amount of NaCl was added to increase the electrical conductivity necessary for the wave profile and particle position measurements. There were several disadvantages in using this type of mixture, namely:

1) it tended to become temperature stratified

2) it absorbed water vapour from the atmosphere

3) it was moderately expensive

The temperature stratification, which was quite stable due to the high viscosity, was overcome by removing the fluid into a large drum and thoroughly mixing with a high speed impellor. After the fluid had cleared itself of air bubbles, it was poured back into the flume and an

experimental run was immediately carried out. The experiments were carried

out in an insulated room and the air temperature was brought as near

as possible to that of the fluid to prevent any re-stratification.

Fluid temperatures were measured at about 1/10 inch below the surface

and variations were kept to less than ±.2 degrees C during a run.

The water vapour absorbed through the surface could not be

eliminated, but its effect was kept to a minimum by the mixing and by

keeping the time for each run as short as possible. In fact, there

appeared to be no significant change of the decay due to surface

contamination over periods of up to an hour. (See Section (4.2)).

Since the glycerol was quite costly, the same fluid was used over a

period of about one year and the water absorbed through the surface would

have changed the viscosity. This did not effect the experiments since

the value for C which would depend on the viscosity was determined for

each run.

Tap water was used in a few of the tests in the small flume and

all of the tests in the large tank. Its conductivity was sufficiently

high so that no salt needed to be added and, since new water was used for

each experiment, there were no problems of stratification.

For some of the experiments it was necessary to use two wave probes

or one wave probe and the particle follower. This gave a complication

since the carrier signal was not of precisely the same frequency for

both bridges, a "beat" was picked up by the probe and displayed on the

output thus masking the fluid wave form. This beat frequency was

eliminated by changing the carrier frequency of one of the bridges from 2000 H_z to 1500 H_z.

Because of the large range of wave amplitudes measured in a single run, it was not always possible to obtain the complete set of measurements using one setting of the bridge attenuation switch. Table (1) shows the different measured wave heights for a standard simulated wave, it is seen that there is no common ratio between the different attenuation settings for either of the probes. This adds no complication provided the standard and experimental wave can be recorded using the same attenuation setting but, in some cases, this is only possible if the height of the standard is changed. This proved too time consuming, so wave heights were kept as near as possible to the two standards of 5.8×10^{-3} inches and 6.3×10^{-3} inches; in cases where the waves became too large to fit on the chart or too small for good resolution corrections were made using Table (1).

There was always some high frequency background noise which increased the line thickness slightly, account was taken of this by measuring the thickness of the line when no waves were present and subtracting this value from the extremes of the peak to peak wave height. In the cases where a rapid chart speed was used as in the phase velocity determination and the frictional phase estimation, it proved more convenient to redraw the wave form using a thin pencil line.

4.1   The Effective Fluid Depth

The effective fluid depth "h" has been determined in terms of the phase velocity "v_p" of the wave. Two experiments were carried out. The first, to determine the change in the effective depth with change in the actual (measured) depth for a fixed wave period. The second, to determine the influence of the wave period on the effective depth for a constant measured depth. The error in the velocity measurements was less than about 1% which gave at most a 2% error in the determination of the effective depth.

The measured phase velocity was determined by using two identical wave probes a known distance apart situated along a line parallel to the direction of wave propagation. The wave profiles were recorded simultaneously and the time difference between corresponding points of phase were measured. In all cases these points of phase were taken as being those that lay midway between crest and trough. These were used since the slope of the trace was greatest at these points and allowed for the greatest accuracy in determining positions of equal phase.

Instead of using the rather inaccurate inbuilt timer on the recorder, use was made of the highly consistent wave period from the 50 cycle commercial power lines to determine the time intervals. This 50 cycle current was suitably attenuated and connected to a third galvanometer in the recorder thus giving a trace on the recorder paper of a sine wave with about a 4mm wave length (at a chart speed of $\simeq$ 200mm/sec.). The

TABLE 1

THE MEASURED AMPLITUDE OF THE STANDARD WAVE
FOR DIFFERENT BRIDGE ATTENUATION POSITIONS

Bridge Attenuation Scale Position	Measured Standard Wave Height	
	Probe #1 H = .0058 inches	Probe #2 H = .0063 inches
.3 mm	1.8 scale units	1.2 scale units
.1 mm	5.8	3.4
30 μ	20.0	11.6
10 μ	60.5	37.4

distance between a peak on the timing trace and an experimental point
from the water wave trace could be estimated to within a confidence limit
of ± 1/500 second and, since the time for a point of phase of the water
wave to travel between probes was usually greater than 1 second, this gave
a corresponding error of at most .4% for the velocity determination.
Figure (11) shows a typical experimental trace used to determine the
phase velocity.

The distance between the two probes was determined using a 1/100
foot scale mounted on the flume, since the hair lines were set on a
scale division the error in the distance measurement was less than 2/10
of a scale division. Thus for a probe separation of 1 foot a maximum
error of .2% in the distance measurement was encountered; in fact, the
probe separation was often two or three times this amount, so the error
was correspondingly less.

Due to the limiting length of the flume and the difficulty in
eliminating reflections from the end wall it was necessary to use the
quick start mechanism and then determine the phase velocity from the
first few waves of the train. It was found that the wave form changed
shape slightly as the wave travelled down the flume and this was more
pronounced in the deeper water than for the shallower water. This change
of form gave different results for the phase velocity when measurements
were taken on the back and on the front of the wave. However, the
average of these velocities was found to be fairly constant for

successive waves in the train and this average was essentially the
same for different positions of the downstream probe keeping the
upstream probe at a fixed position. The phase velocity was taken to be
the mean of back and front velocities for several of the waves in the
train using measurements at several downstream probe positions. Table
(2) shows a typical set of phase velocity measurements using a number
of different fluid depths and a nearly constant wave period.

The phase velocity was calculated from equation (3-17) using the
measurements of fluid depth and period along with the value for C
determined by the decay of the wave between the two probes (See Section
4.2). The effect of surface tension and of finite amplitude on the
phase velocity was calculated by assuming that, since both these effects
were small, they could be calculated exclusive of one another using the
inviscid form of the correction term with the wave number increased by
friction according to Equation (3-3a). The surface tension correction
for the square of the phase velocity is given by: (Milne-Thompson (1962)
p.408) $\left\{ \dfrac{\gamma k^2}{\rho g} \right\}$

where γ is the surface tension.

The finite amplitude correction for the square of the phase velocity
was taken to be the third order term in the Stokes expansion:

$$H^2 \left\{ k^2 \frac{(8+\cosh 4kh)}{8 \sinh^4 kh} \right\} = H^2 f(kh)$$

50 cycle/sec. timing trace

upstream profile

downstream profile

H = .0077"

upstream profile

downstream profile

H = .0033"

Note: An interval of 24 cycles on the timing trace has been omitted between the upper and lower chart.
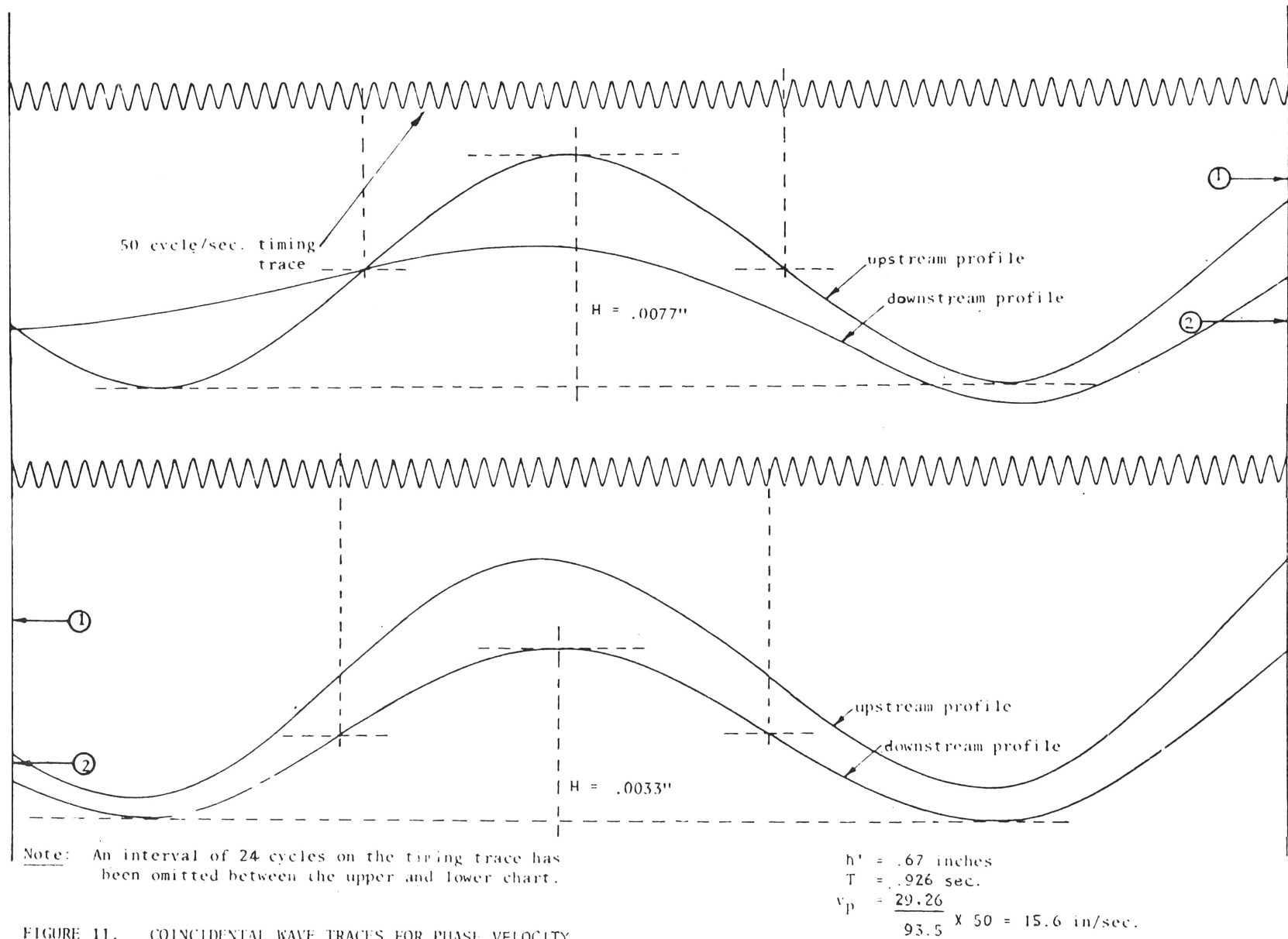
FIGURE 11. COINCIDENTAL WAVE TRACES FOR PHASE VELOCITY MEASUREMENTS.

h' = .67 inches
T = .926 sec.
$v_p = \dfrac{29.26}{93.5} \times 50 = 15.6$ in/sec.

probe separation = 29.26 inches

average number of timing cycles = 93.5

TABLE 2

SAMPLE OF RESULTS

USED TO DETERMINE THE CALCULATED AND MEASURED PHASE VELOCITIES

Wave Period 1	Measured Depth 2	Probe Separation 3	No. of cycles on Timer		Phase Velocity			Difference of 7 & 8 9
			Front of Wave 4	Back of Wave 5	Experimental Average of 4 & 5 6	Average of 6 7	Calculated from 1 & 2 8	
±.005sec	±.01ins	±.02ins	±.2	±.2	in/sec	in/sec	in/sec	in/se.
.935	1.86	12.46	25.0	23.5	25.7±.3	25.7±.2	25.8	.1±.2
			33.9	33.4	25.7±.2			
		17.26	34.6	32.8	25.7±.2			
		23.26	45.7	44.6	25.6±.1			
			57.8	55.8	25.8±.1			
		29.26	58.5	56.0	25.5±.1			
.935	1.52	12.46	27.1	26.4	23.3±.3	23.3±.2	23.5..1	.2±.3
			27.8	26.0	23.2±.3			
		17.26	37.3	26.2	23.5±.2			
			38.1	36.6	23.1±.2			
		23.26	50.4	49.i	23.3±.1			
			50.9	49.0	23.3±.1			
		29.26	63.1	60.9	23.6±.1			
.944	1.31	12.46	29.1	28.2	21.8±.2	21.6±.2	21.9±.1	.3±.3
			29.2	28.6	21.6±.2			
		17.26	40.1	39.1	21.8±.2			
			40.6	39.8	21.5±.2			
		29.26	68.9	66.8	21.6±.1			
			69.8	66.3	21.5±.1			
.921	1.06	17.26	45.0	44.4	19.3±.1	19.4±.1	19.8±.1	.4±.2
			45.1	44.4	19.3±.1			
			60.2	59.4	19.4±.1			
		23.26	60.2	59.3	19.4±.1			
		29.26	75.7	74.4	19.5±.1			
			75.7	74.4	19.5±.1			
		35.26	91.2	89.5	19.5±.1			
			91.8	89.9	19.6±.1			
.923	.86	17.26	49.6	49.4	17.4±.1	17.5±.1	17.9±.1	.4±.2
			49.7	49.6	17.4±.1			
		29.26	83.8	83.0	17.5±.1			
			83.7	83.8	17.5±.1			
		35.26	100.9	99.8	17.6			
			100.8	100.8	17.5			
		41.26	117.2	116.2	17.6			
.926	.67	17.6	55.7	56.6	15.4±.1	15.6	15.8±.1	.2±.1
			55.3	56.1	15.5±.1			
		29.26	95.9	93.1	15.7			
			93.6	93.7	15.6			
		35 26	113.0	113.9	15.7			
			112.6	113.7	15.7	0		
		41 26	132.2	130.4	15.7			
			130.7	131.3	15.7			
.921	.52	17.26	62.9	63.1	13.7±.1	13.8±.1	14.0±.1	.2±.2
			62.1	62.9	13.8±.2			
		29.26	105.4	104.9	13.9			
		35.26	127.4	127.4	13.8			
.927	.40	12.46	53.1	53.1	11.8±.1	12.0±.2	12.2±.1	.2±.2
			52.1	52.8	12.1±.1			

where H is the wave height. See, for example, Wiegel (1964) Equation (2.127).

Since the wave was decaying between the two points of measurement, H was not constant and an average finite amplitude correction term was defined as:

$$\frac{1}{d} \int_{x=0}^{x=d} H^2(x) \, f(kh) \, dx = H_o \frac{1-e^{-2\alpha d}}{2\alpha d} f(kh)$$

where d is the distance between the probes and $H(x) = H_o d^{-\alpha x}$; H_o being the wave height at the upstream probe, x = 0.

The theoretical average phase velocity between x = 0 and x = d is then:

$$v_p = \frac{\sigma}{k} \left\{ 1 + \frac{\gamma k^2}{\rho g} + H_o \frac{1-e^{-2\alpha d}}{2\alpha d} \left(\frac{k^2(8+\cosh 4kh)}{8 \sinh^4 kh} \right) \right\}^{1/2}$$

These combined corrections were small as the following numerical example will show.

Using:

ρ	=	.043 lbs/in.^{3}
h	=	.51 inches
T	=	.924 seconds
γ	=	9.6×10^{-4} lbs/in.^{2}
α	=	.044 inches^{-1}
H	=	.0163 inches
d	=	24.5 inches

These figures (from a run on 4/1/72) give a phase velocity of 13.88 ins/sec. with the correction terms and of 13.82 ins/sec. without the correction terms or a difference of .4%. This example was used since it gave a rather large correction term in comparison with other experiments and so .4% can be taken as an outer bound for the percentage corrections. This was negligible in comparison with the error encountered in the measurement of the physical parameters used to calculate the phase velocity.

The Effective Depth as a Function of the Measured Depth

Table (3) lists the measured and calculated phase velocities and their differences. A second order least-squares polynomial was fitted to these differences as a function of the measured depth. The average error or the average distance from this curve to the experimental points was ±.2 inches/second. A phase velocity curve was calculated using a constant wave period of .930 seconds. Differences obtained from the least-squares polynomial were subtracted from this phase velocity curve, thus giving a least-square fit to the measured phase velocity.

It would have been more direct to calculate a least-squares fit to the measured phase velocity directly but this led to difficulties because of the slight variations in wave period from run to run giving different phase velocities for the same depth. Using the adopted procedure the assumption was made that boundary layer had a constant effect on the phase velocity within the range of periods obtained (i.e. .930 ± .020 seconds) and in effect the experimental results were set to a fixed period.

TABLE 3

SUMMARY OF THE CALCULATED AND MEASURED PHASE VELOCITIES
AND THEIR DIFFERENCES FOR VARIOUS DEPTHS

Run	Depth inches	Period seconds	Temperature degrees C.	v_p calc. in/sec.	v_p meas. in/sec.	v_p calc.$-v_p$ meas. in/sec.
1	.30	.926	24.8	10.6	10.1	.5
	.47	.934	24.7	13.3	12.7	.6
	.55	.930	24.2	14.4	13.7	.7
	.70	.932	24.2	16.2	15.3	.9
	1.13	.920	24.?	20.4	19.8	.6
	1.15	.914	24.2	20.6	20.3	.3
2	.40	.927	23.7	12.2	12.0	.2
	.67	.926	23.7	15.8	15.6	.2
	.87	.923	23.7	17.9	17.5	.4
	1.06	.921	23.7	19.8	19.4	.4
	1.?1	.944	23.7	21.9	21.6	.3
	1.??	.935	23.7	23.5	23.3	.2
	1.86	.935	23.5	25.8	25.7	.1
3	.40	.941	21.9	12.3	11.9	.4
	.60	.941	21.9	15.0	14.5	.5
	.60	.946	22.1	15.0	14.5	.5
	1.60	.941	22.1	24.1	24.0	.1
4	.75	.940	12.8	16.8	16.1	.7
5	.75	.930	13.?	16.8	16.3	.5
6	.52	.928	16.6	14.0	13.1	.9
	1.02	.928	16.6	19.4	19.2	.2
7	.51	.946	12.5	13.9	13.0	.9
	.51	.936	12.3	13.9	13.2	.7
8	.50	.932	18.0	13.7	12.7	1.0
	1.00	.910	17.3	19.2	18.7	.5
9	1.02	.946	17.0	19.5	18.6	.9
10	.52	.946	17.3	14.0	13.0	1.0
	.56	.928	17.3	14.5	14.0	.5
11	.51	.924	24.2	13.9	13.9	.0
	.60	.941	22.3	15.0	14.6	.4
	.73	.917	24.2	16.5	16.4	.1
	.98	.914	24.2	19.1	19.0	.1

55% Glycerol used in Run 1

77% Glycerol used in Run 2 - 11

This measured phase velocity was plotted on the same graph as the calculated one. (Figure (12)). The effective depth corresponding to a measured depth could then be read off the graph. For example, suppose a fluid depth of .60 inches is measured, this corresponds to an experimental phase velocity of 14.5 inches/second. From the calculated phase velocity curve, it is found that 14.5 inches/second corresponds to a depth of .57 inches which is taken to be the effective depth.

The Variation of Effective Depth with Wave Period

Using a fixed measured depth h', phase velocities were measured for a range of wave periods between about .45 and .93 seconds. These, and the corresponding calculated phase velocities, are listed in Table (4) and shown graphically in Figure (13). Using Figure (13), curves of experimental and calculated phase velocities as a function of depth were drawn for various (constant) wave periods. Figure (14) shows a typical graph for a period of .7 seconds, the effective depth could then be read directly from this plot. This procedure would necessitate the drawing of a graph for each wave period tested: instead, a table was constructed of $\Delta h = h'-h$ for various depths and periods, and, since Δh was slowly varying for the range of parameters used, the value of h could be read directly from this table (Table (5)).

In all subsequent experiments using the glycerol and water fluid, the actual depth was measured and the effective depth determined using Figure (12) or Table (5). The variation in effective depth using the 55% and the 77% glycerol mixtures did not give any appreciable difference in

the displacement depth, nor did the variations in temperature of the fluid. Although the uncertainties in the values found for Δh are quite large, there does appear to be a definite trend to these values and it was therefore believed that an improved value for the depth measurement could be obtained by this method.

Phase velocities measured in the large tank using tap water were found to agree within 1% of those calculated using the fluid depth and period, hence no correction to the depth for the boundary layer thickness was found necessary for water.

In all subsequent work the depths quoted will refer to the effective depth, h, unless otherwise stated.

4.2   The Decay Coefficient and the Frictional Constant

Experiments were carried out to find the decay coefficient and the frictional constant C for various depths keeping the wave period constant and for various periods keeping the depth constant. The former of these checked the validity of the assumption made in Section 2.1 that C is invariant with depth whereas the latter gave an experimental determination of the change of C with frequency; this had not been included in the mathematical development.

Two methods were used to determine the decay coefficient. The first was to use a single wave probe and to measure wave heights at various
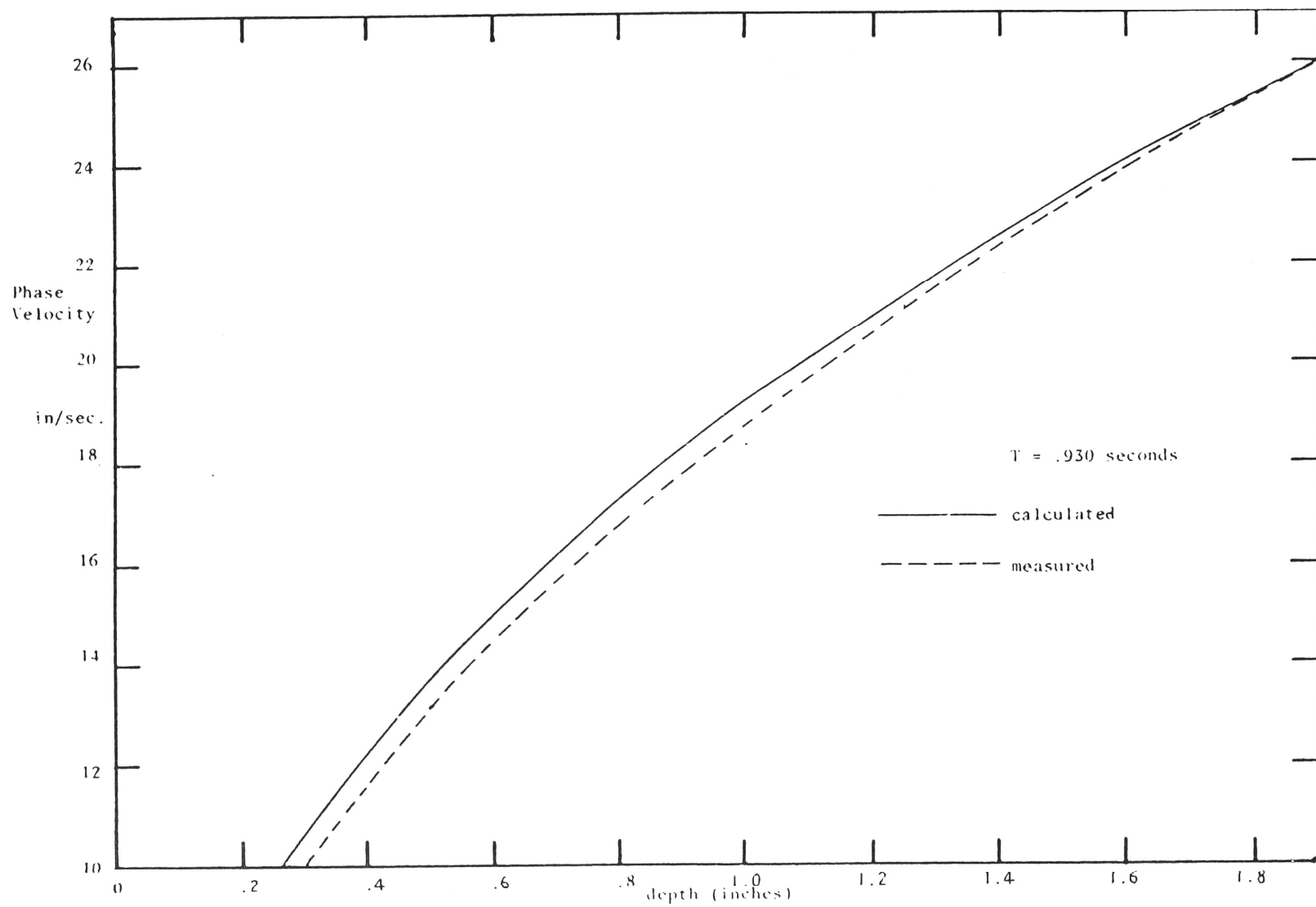
FIGURE 12. THE CALCULATED AND MEASURED (LEAST SQUARES) PHASE VELOCITIES
AS A FUNCTION OF THE DEPTH.

TABLE 4

SUMMARY OF CALCULATED AND MEASURED PHASE VELOCITIES

FOR VARIOUS DEPTHS AND PERIODS

Fluid: 81% Glycerol at 21.2 degrees C

Measured Depth	Wave Period	Phase Velocity	
		Calculated	Measured
inches	seconds	in/sec.	in/sec.
1.02	.914	19.4	19.0
	.758	19.2(S)	18.8
	.614	19.0(S)	18.7
	.531	18.6	18.4
	.485	18.3(S)	18.2(S)
	.458	18.2	18.0
0.76	.917	16.8	16.4
	.775	16.7	16.3
	.775	16.7	16.3
	.640	16.5(S)	16.2
	.530	16.3	16.1
	.478	16.1	15.9
0.55	.934	14.4	13.8
	.781	14.3	13.9
Trial 1	.635	14.2	13.9
	.535	14.0(S)	13.7
	.470	13.8(S)	13.5
	.926	14.4	13.8
	.766	14.3	13.8
Trial 2	.633	14.2	13.7(S)
	.536	14.0(S)	13.5(S)
	.924	14.4	13.9
Trial 3	.787	14.3	13.9(S)
	.641	14.2	13.9
	.530	14.0	13.7
0.42	.926	12.4(S)	11.9
	.758	12.4	12.0
	.635	12.3(S)	11.9
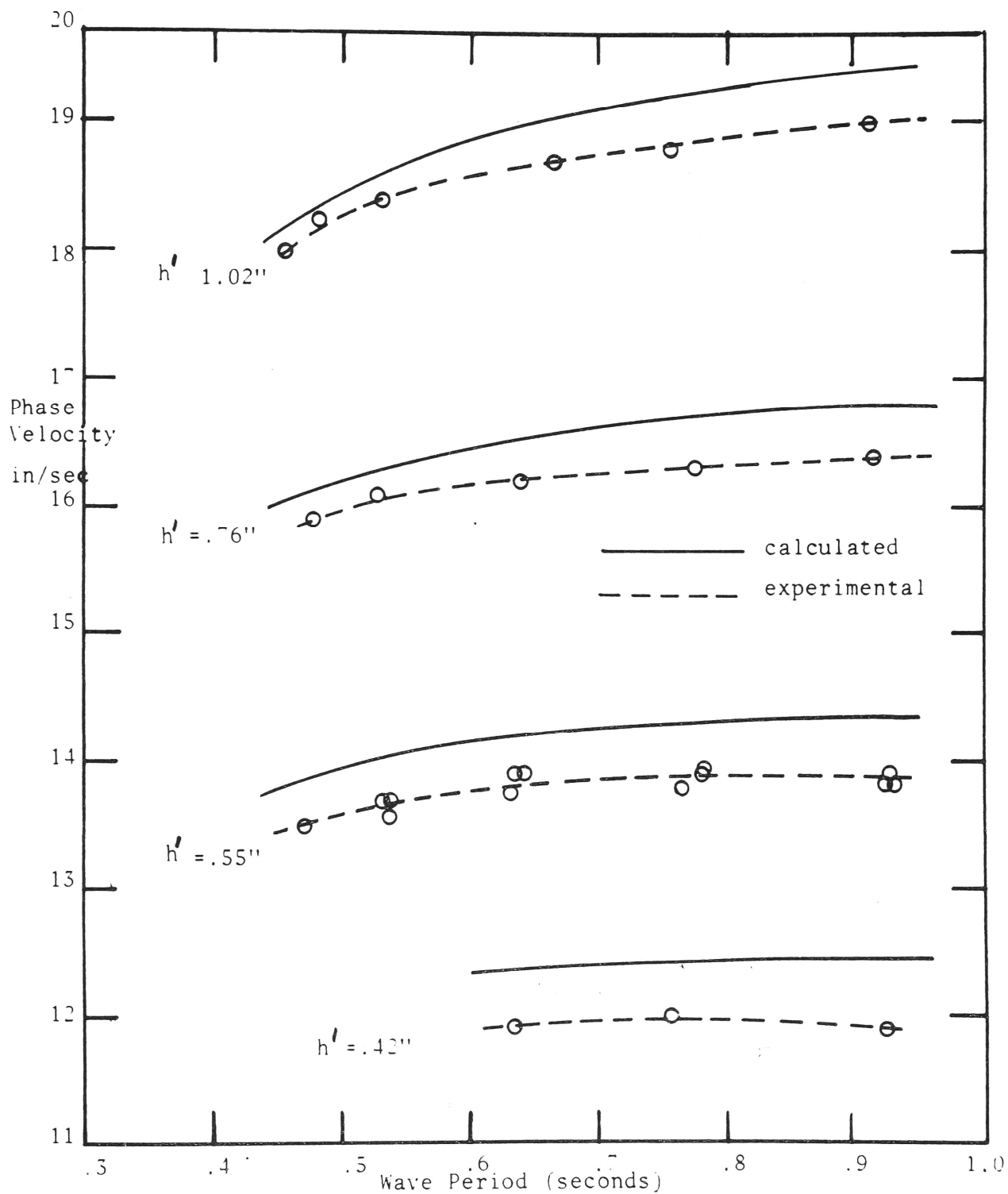
FIGURE 13. MEASURED AND CALCULATED PHASE VELOCITIES AS A FUNCTION OF WAVE PERIOD FOR VARIOUS DEPTHS.

FIGURE 14.   MEASURED (FROM FIG. (13)) AND CALCULATED
              PHASE VELOCITIES AS A FUNCTION OF THE DEPTH
              FOR T = .⁻ SECONDS.
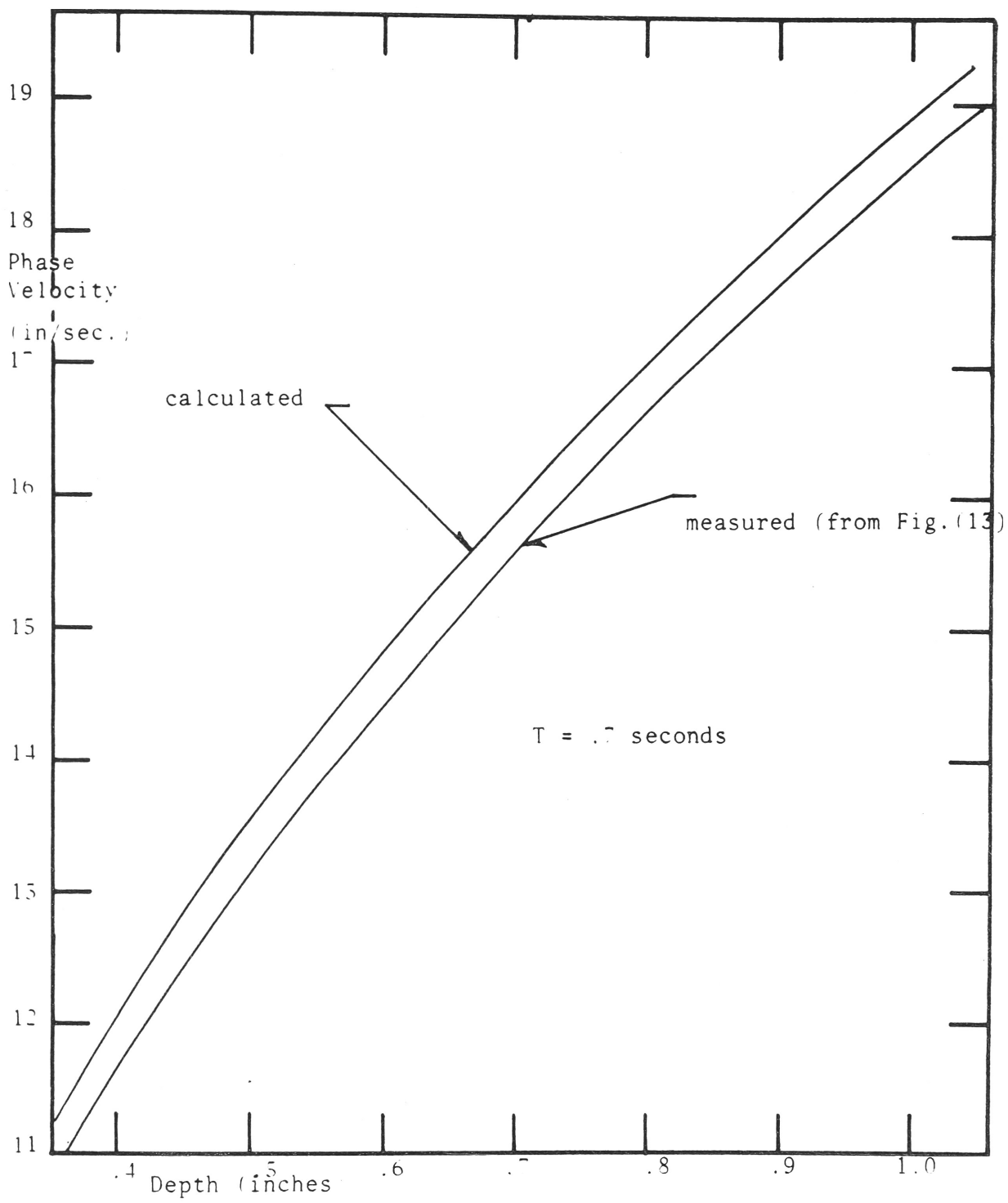
TABLE 5

Δh FOR VARIOUS MEASURED DEPTHS AND WAVE PERIODS

	Wave Period				
	.5sec	.6sec	.7sec	.8sec	.9sec
Measured Depth	Δh	Δh	Δh	Δh	Δh
inches	inches	inches	inches	inches	inches
.40	.03	.03	.03	.03	.03
.50	.03	.03	.03	.03	.04
.60	.03	.03	.03	.03	.04
.70	.03	.03	.04	.04	.04
.80	.02	.03	.04	.04	.04
.90	.02	.03	.04	.04	.04
1.00	.02	.03	.04	.04	.04

positions along the flume. These heights and distances were put on a
semi-log plot and a straight line fitted through the points. The value
for α could then be deduced from the slope of the line.

The second method, which was more direct, was to measure the wave
height at two positions along the tank and directly calculate the decay
coefficient from:

$$\alpha = \frac{1}{(x_2 - x_1)} \quad \text{LOG}_e \quad \frac{H_1}{H_2}$$

where the subscripts 1 and 2 refer to the upstream and downstream
positions respectively. A series of measurements using different down-
stream probe positions were taken and an average value for α calculated.
This second method had the advantage of compensating for changing
incident wave heights during a run since each measurement gave a specific
value for α . The first had the advantage of using the same probe for
all measurements which eliminated the small error involved in determining
the calibration (standard) wave height; in other words it was unnecessary
in this case to obtain an absolute experimental wave height. It was
found that the incident wave amplitude was very nearly constant for each
test thus the choice between the two methods was only one of convenience.

As in the phase velocity determinations, wave measurements were
taken near the front of a train to eliminate the complications of end
wall reflections. Relatively long wave periods and shallow depths were
used such that, although all the waves did not fall into the long-wave

category, the dispersion at the wave front caused by the inequality of the phase and energy velocities was kept reasonably small. Wave height measurements were taken far enough behind the front such that the reduction in height by dispersion was negligible and the waves had reached a constant height. Typical wave traces for the experimental and standard profiles using the one and two probe methods are shown in Figure (15-a) and (15-b) respectively; sample calculations of the relative and absolute wave heights are given below.

Data Applicable to Figure (15-a)

Location: ⁻Large Tank

Fluid: Tap Water

Fluid Depth = .33±.01 inches

Position of Probe: 12 inch position

Probe Used: #1

Experimental Wave Measurement:

Period   = .902 seconds

Measured Height   = 24.5 ± .2 units

Bridge Attenuation Switch   = 10u position

Standard Wave Measurement:

Period   = 1.00 seconds

Measured Height   = 26.2 ± .2 units

Standard Wave Trace

Experimental Wave Trace
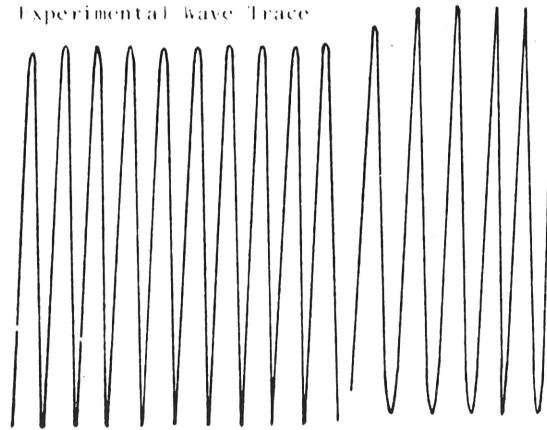
FIGURE 15-a SINGLE PROBE TRACE
FOR ∝ DETERMINATION

STANDARD WAVE TRACE

Experimental Wave Trace

Upstream

Downstream

DOWNSTREAM

UPSTREAM
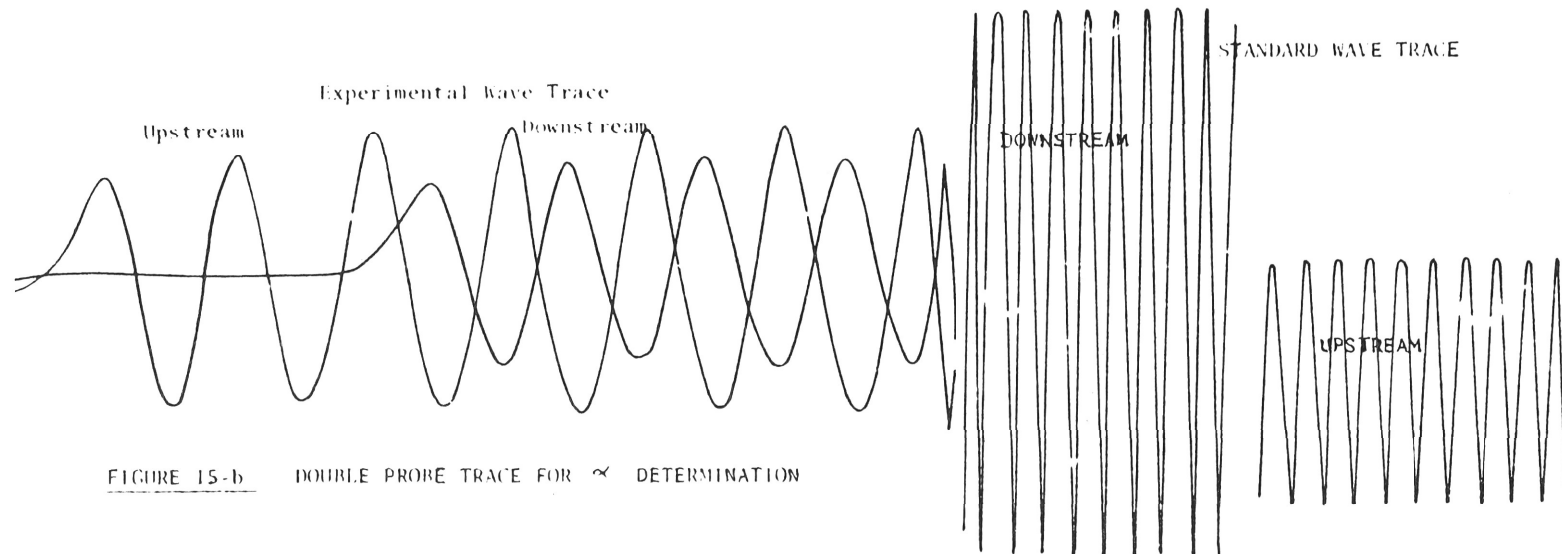
FIGURE 15-b   DOUBLE PROBE TRACE FOR ∝ DETERMINATION

Corrected for difference

in bridge attenuation between   Nil

experimental and standard

Adjusted Measured Height = $\dfrac{26.2\pm.2}{.94}$ =   27.9±.2 units

(to T = .63 seconds)

Experimental Relative Wave Height = $\dfrac{24.5\pm.2}{27.9\pm.2}$ =   .878±.016

The correction for the change in recorded amplitude caused by the bridge circuit (See Figure (A8:4)) was only carried out for the standard wave since this changed slightly at each experimental point whereas the experimental wave period was kept constant for each run. The correction of the standard heights was in reference to the maximum point on the calibration curve which in effect set these heights to a constant period of .63 seconds. Several other wave heights using this depth and period were measured. These, along with those obtained for other wave periods, are plotted on (Figure (16)).

Data Applicable to (Figure (15-b))

Location: Small Flume

Fluid: 77% Glycerol

Fluid depth   =   .48±.01 inches

Distance between Probes   =   29.2 inches

Upstream

Probe used: #1

Experimental Wave Height:

Period   =   .93±.10 secs.

Measured Height   =   16.5±.2 units

Bridge Attenuation   =   10u position

Standard Wave Measurement:

Period   =   .83±.1 secs.

Actual Height   =   .0058 ± .0001 inches

Measured Height   =   15.2±.2 units

Bridge Attenuation   =   10u position

Corrected for difference ⎫
in Bridge Attenuation   ⎬   Nil
between Experimental and ⎪
Standard   ⎭

Corrected to period of ⎫
Experimental Wave   ⎬   = $\dfrac{.95}{.97}$ x 15.2 = 14.9±.2 units

Absolute Wave Height   = $\dfrac{16.5±.2}{14.9±.2}$ x (5.8±.1) x 10^{-3}ins.

                          =   (6.4 ± .3) x 10^{-3}inches

Downstream

Probe used: #2
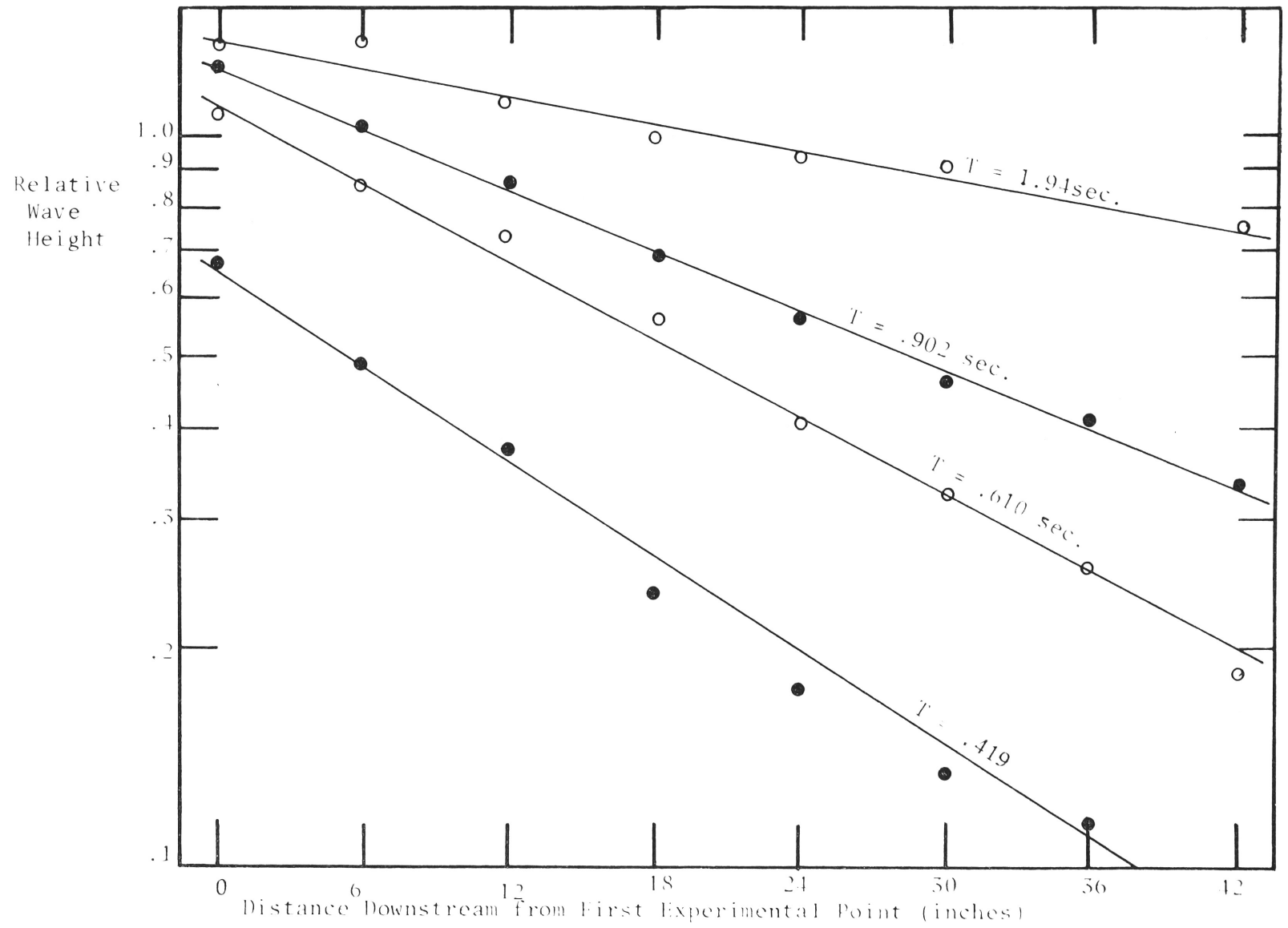
FIGURE 16.   RELATIVE WAVE HEIGHTS AS A FUNCTION OF DISTANCE
FOR VARIOUS WAVE PERIODS.

Experimental Wave Measurement:

Period   =   .93 ± .1 sec.

Measurement Height   =   13.0 ± .2 units

Bridge Attenuation   =   10u position

Standard Wave Measurement:

Period   =   .86±.01 sec.

Actual Height   =   .0063± .0001 inches

Measured Height   =   35.2± .2 units

Bridge Attenuation   =   10u position

Corrected for difference ⎫
in Bridge Attenuation   ⎪
between Experimental   ⎬   Nil
and Standard   ⎭

Corrected to Period of   ⎫
                                      ⎬   = $\dfrac{.95}{.97}$ x 35.2±.2 = 34.4±.2 units
Experimental Wave   ⎭

Absolute Wave Height   = $\dfrac{13.0 \pm .2}{34.4 \pm .2}$ x (6.3±.1) x 10^{-3} inches

                                      =   (2.4 ± .1) x 10^{-3} inches

Calculation of α : α = $\dfrac{1}{29.2}$ $\log_e$ ($\dfrac{6.4 \pm .3}{2.4 \pm .1}$) inches $^{-1}$

                                      =   (.034±.003) inches $^{-1}$

Using two other probe separations of 36.4 inches and 24.4 inches

values for α of $(.033\pm.003)$ inches^{-1} and $(.035\pm.002)$ inches^{-1} were

found respectively with an average of the three positions giving

$\alpha_{AVG.}$ = $(.034\pm.003)$ inches. The weighted average was calculated

using:

$$\alpha_{AVG.} = \frac{\sum_{i=1}^{n} \frac{\alpha_i}{\Delta\alpha_i}}{\sum_{i=1}^{n} \frac{1}{\Delta\alpha_i}}$$

and

$$\Delta\alpha_{AVG.} = \frac{\alpha_{AVG}}{n} \sum_{i=1}^{n} \frac{\Delta\alpha_i}{\alpha_i}$$

where α_i is the decay coefficient for the ith run and $\Delta\alpha_i$ is the

estimated error for the ith value of α_i .

A check was run to see if surface contamination and stratification

had a significant effect on the damping coefficient. The temperature of

the fluid was set about 2 degrees C lower than the surrounding air, so it

was expected that a stratified layer near the surface would form during

the experiment. This stratification would be more severe than that for

any of the other experiments where the air and fluid temperature were

nearly equal.

The "two probe" method was used and the time origin was at the

point when the mixed fluid was poured into the flume; measurements of

wave height were taken at various times during the next 50 minutes.

The results are summarized in Table (6) and there appear to be no

trends in either the incident wave heights or in the decay coefficient;

in addition, the phase velocity was found to be very consistent during

TABLE 6

THE PHASE VELOCITIES, WAVE HEIGHTS AND DECAY COEFFICIENTS
FOR DIFFERENT TIME INTERVALS AFTER MIXING THE FLUID

Elapsed Time minutes	Phase Velocity in/sec.	Wave Height		Decay Coefficient in $^{-1}$
		Upstream x 10^{-2}ins	Downstream x 10^{-2}ins	
2.0	16.3(5)	.91	.54	.016
9.0	16.3	.87	.50	.017
11.5	16.3	.87	.52	.015
15.0	16.3(5)	.88	.49	.018
17.5	16.3(5)	.90	.49	.018
21.0	16.3(5)	.82	.47	.017
26.0	16.3(5)	.88	.49	.018
30.0	16.3	.91	.49	.019
40.0	16.3	.90	.46	.020
50.0	16.3	.84	.48	.017

t_{air} = 16.4 degrees C   h = .71 inches

t_{fluid} = 14.4 degrees C   T = .93 seconds

the time interval. Thus, for the physical parameters used, the changing boundary layer at the surface did not appreciably affect the decay coefficient or the phase velocity. This finding is in agreement with the theoretical result found by Van Doran (1966) that the surface dissipation is much less than the bottom dissipation when reasonably "long waves" are used. A second test with the air temperature and the fluid temperature being equal was run and results similar to the above were found. (Table (7)).

The decay coefficient was found for a range of depths from about .3 inches to 2.2 inches using a wave period of approximately .93 seconds. This experiment was carried out in the small flume using the 77% glycerol mixture. A second experiment was run using the 55% glycerol mixture using the same wave period and a range of depths from .3 to 1.1 inches. From these results values of C (and k) were calculated by solving Equation (3-3a) and Equation (3-4a) simultaneously. These results are tabulated in Table (8); the rather large uncertainty in the value of C for the deeper fluids is a result of the smallness of the decay coefficient. That is, due to the limiting length of the flume it was not possible to situate the probes far enough apart so that large differences in wave heights could be recorded. Therefore, the experimental uncertainty in the wave height gave a considerable relative uncertainty in the value for α and thus an even larger absolute uncertainty for the value for C. From Table (8) it can be seen that the frictional constant is (within the experimental error) constant with depth (for a

fixed wave period). The values for the decay coefficient are plotted
against the depth in Figure (17), the solid curve in this figure was
calculated using a weighted average for the frictional constant in
Equation (3-4a). It can be seen that this curve varies closely as $h^{-3/2}$
as predicted for long waves in Equation (3-4c) and thus with linear
viscous boundary layer theory.

With a fixed fluid depth the decay coefficient was found for a
range of wave periods. A depth of .33 inches was used in the large wave
tank with periods ranging from about .4 seconds to 2.5 seconds. The
fluid used was tap water. A similar set of experiments was run in the
small flume using the 77% glycerol mixture. Again, values for C were
calculated for each experimental value of α . These are shown in Figures
(18), (19) and (20) for the two fluids. The frictional constant can be
seen to vary with the wave period, an increase in wave period giving a
general decrease in C except for the very long periods where there appears
to be a slight increase of the frictional constant. In subsequent
experiments in the large tank it was required to know the variation of C
for a large number of wave periods with a fixed water depth of .33 inches.
To this end a second order lease squares polynomial was fitted to the
values for the frictional constant, this is shown by the solid curve in
Figure (18). The polynomial obtained had the form C = $(.10T^2 - .41T + .52)$
(in/sec.) valid between periods of .4 seconds and 2.6 seconds for water.

Iwagaki, Yoshito and Chen (1966), using perturbation methods, found
the decay coefficient to be:

TABLE 7

THE PHASE VELOCITIES, WAVE HEIGHTS AND DECAY COEFFICIENTS
FOR DIFFERENT TIME INTERVALS AFTER MIXING THE FLUID

| Elapsed Time minutes | Phase Velocity in/sec. | Wave Height | | Decay Coefficient in^{-1} |
		Upstream x 10^{-2} ins	Downstream x 10^{-2} ins	
1.0	16.2	.87	.45	.020
7.0	16.1(5)	.86	.47	.018
16.0	16.0	.85	.47	.018
21.0	16.1(5)	.84	.44	.019
31.0	16.1	.87	.48	.018
41.0	16.1	.87	.47	.018
56.0	16.1(5)	.87	.48	.018

t_{air} = 12.8 degrees C.   h = .70 inches

t_{fluid} = 12.8 degrees C.   T = .94 seconds

TABLE 8.

THE DECAY COEFFICIENT AND FRICTION COEFFICIENT
FOR VARIOUS DEPTHS WITH A CONSTANT WAVE PERIOD (.93 SECONDS)

Depth (inches)	Decay Coefficient (inches) $^{-1}$	Friction Constant inches/second	
2.22	.0049±.0035	.640±.465	
1.86	.0067±.0031	.670±.381	
1.50	.0072±.0031	.521±.231	
1.27	.0088±.0021	.496±.125	
1.01	.0143±.0016	.571±.073	77% Glycerol
0.82	.0194±.0013	.567±.049	
0.63	.0323±.0024	.636±.064	
0.48	.0431±.0027	.565±.054	
0.36	.0689±.0046	.589±.066	
		.580	= Weighted average
1.11	.0112±.0018	.515±.091	
1.09	.0082±.0012	.367±.060	
0.66	.0224±.0011	.473±.034	
0.51	.0316±.0010	.453±.028	55% Glycerol
0.43	.0417±.0013	.463±.031	
0.26	.0867±.0029	.455±.043	
		.464	= Weighted average
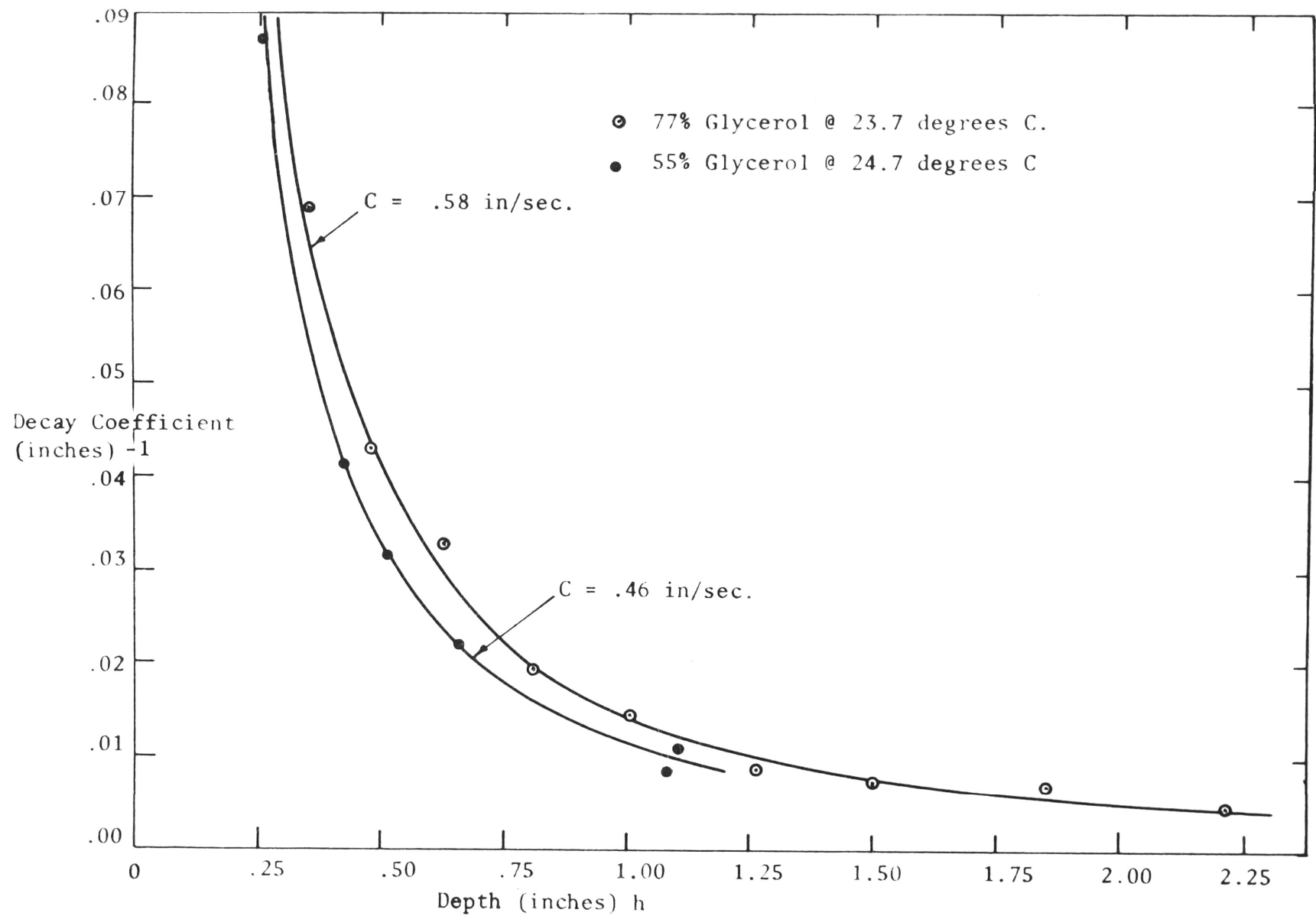
FIGURE 17. THE DECAY COEFFICIENT AS A FUNCTION OF THE DEPTH "h"
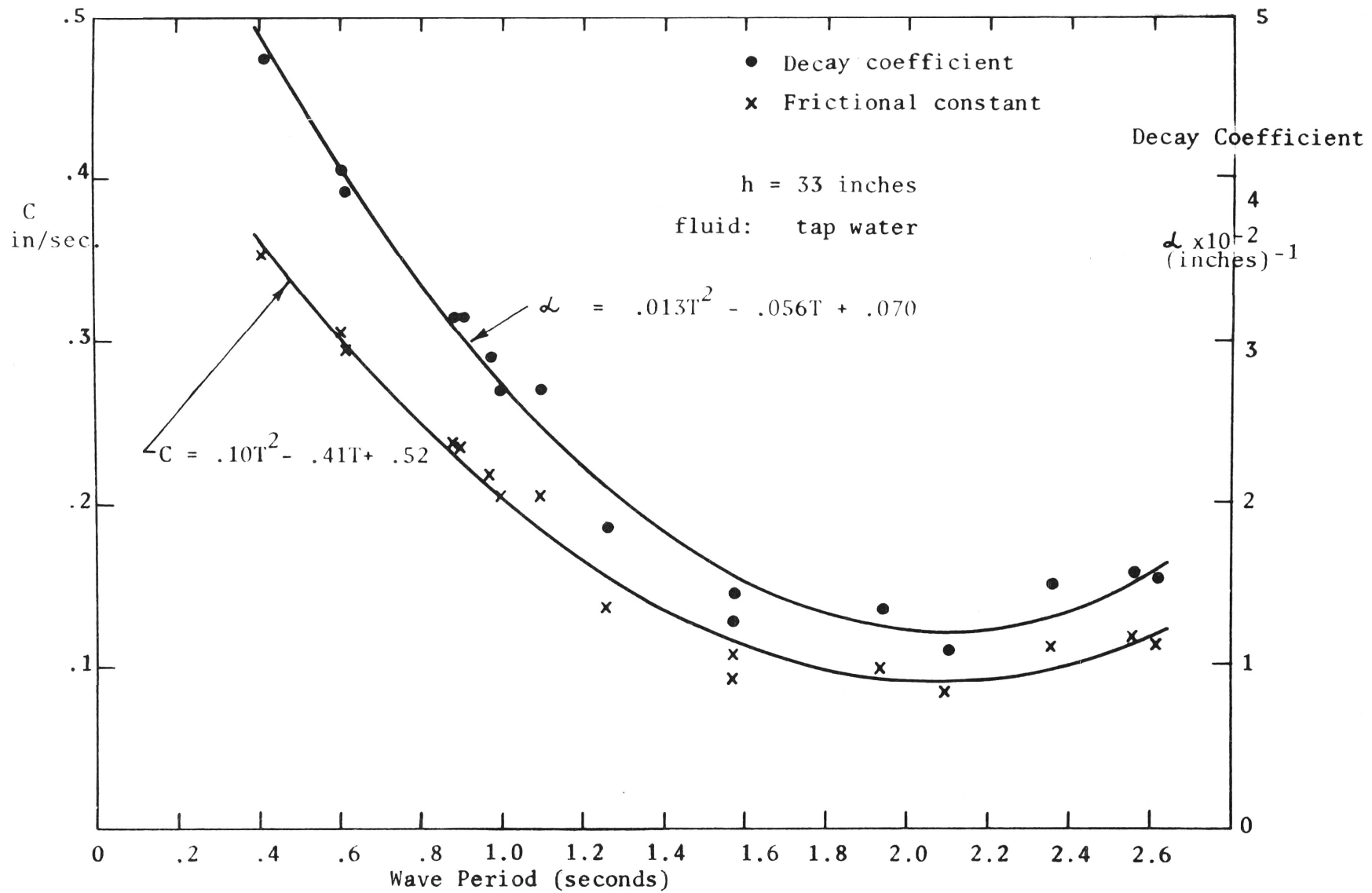
FIGURE 18. THE DECAY COEFFICIENT AND FRICTIONAL CONSTANT FOR TAP WATER WITH h=.33inches
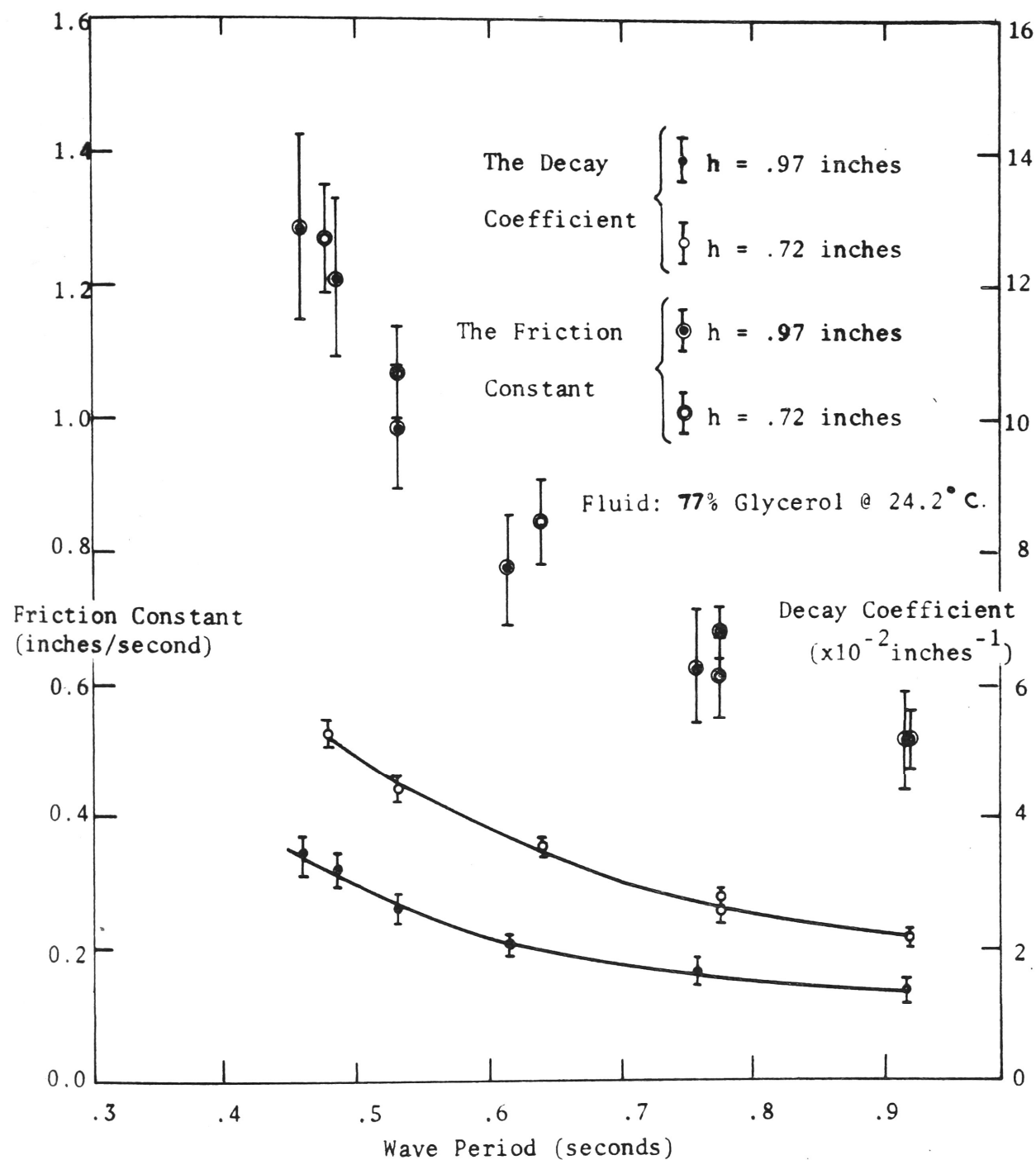
FIGURE 19. THE DECAY COEFFICIENT AND FRICTION CONSTANT AS A
FUNCTION OF THE WAVE PERIOD.
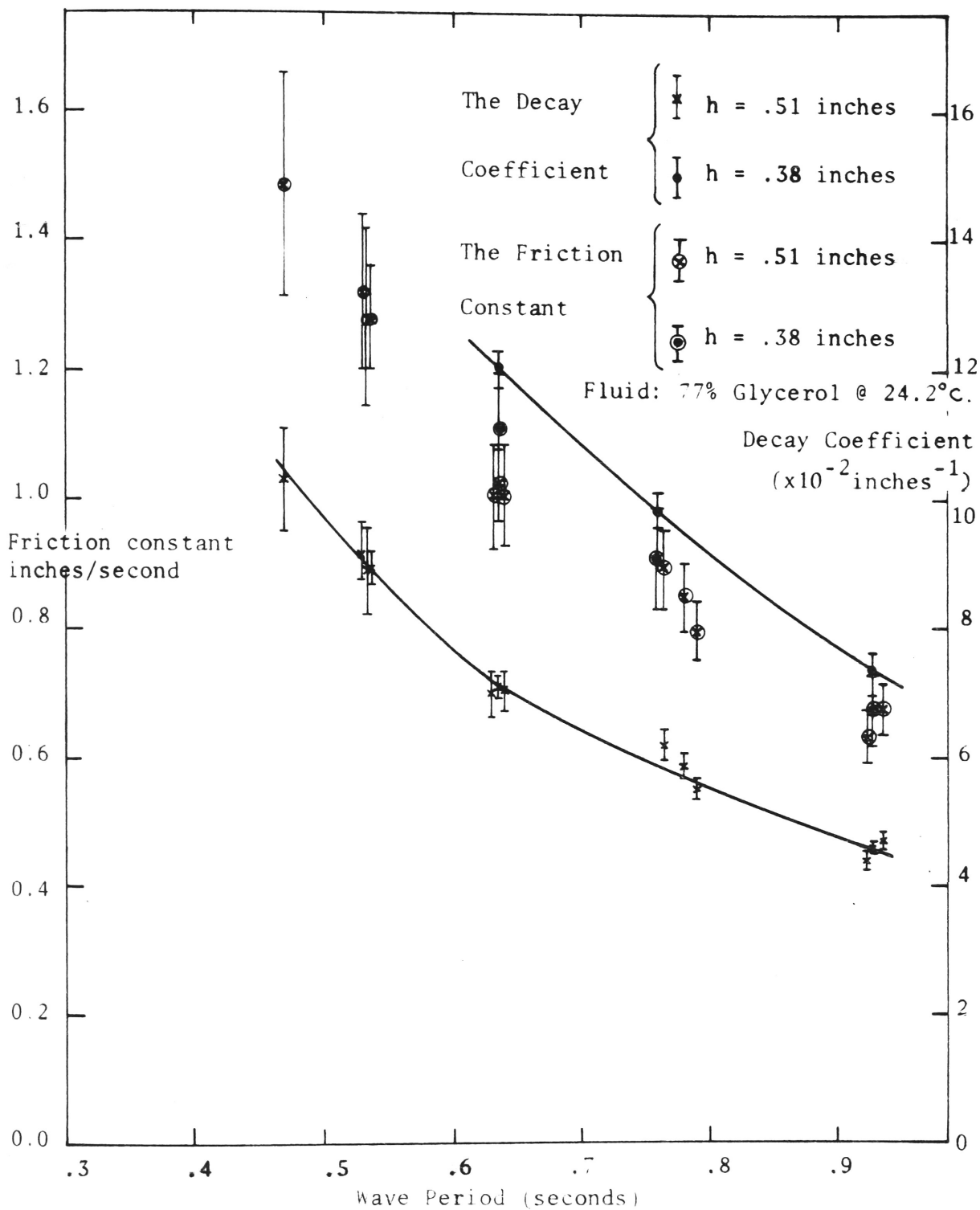
FIGURE 20. THE DECAY COEFFICIENT AND FRICTION CONSTANT AS A FUNCTION OF THE WAVE PERIOD

$$\alpha \simeq \sqrt{\frac{\nu T}{\pi} \frac{k^2}{\sinh 2kh + 2kh}} \left\{ 1 - \frac{.197\, kH}{2 \sinh kh} \right\}$$

which, for $\dfrac{.197kH}{2\sinh kh}$ $\ll 1$, is the same as the linear theory.

For long waves this solution reduces to:

$$\sqrt{\frac{\nu \pi}{4 T g h^3}} \left\{ 1 - \frac{.197}{2} \frac{H}{h} \right\}$$

In all the experiments carried out in this thesis

$$H < .02 \text{ inches}$$

$$h \geqslant .02 \text{ inches}$$

so $\dfrac{.197}{2} \dfrac{H}{h}$ $< .01$ which is insignificant compared with unity. Thus the linear boundary layer theory should provide an adequate description of the decay coefficient. In particular is is expected that the decay coefficient should vary as $T^{-\frac{1}{2}}$.

A log-log graph of vs. T was plotted to check if the experimental results agreed with the above prediction. From Figure (21) it can be seen that for the tests using glycerol the decay coefficient varies closely as $T^{-5/4}$ and for the test using tap water there appears to be no variation for α as T^X. In all cases the variation of the decay coefficient showed a stronger dependence on T than that predicted by the

theory.

Using Hunt's (1964) theory for the decay coefficient it was again found that there was no agreement between his results (shown by the solid line on Figure (21)) and the experimental variation of α with T. An explanation for this discrepancy is that since small fluid depths are used the boundary layer thickness as defined by $\delta^* = 6.5 \sqrt{\frac{\nu}{\sigma}}$ (ft.) (See, Li (1954)), extends through a significant portion of the fluid depth and thus the above theories do not adequately describe the damping in this region. As found by other authors (for example Iwagaki, Yoshito and Chen (1966)) the predicted values for α were considerably lower than the experimental ones.

4.3 The Frictional Induced Phase Shift for the Horizontal Particle Position

Experiments were carried out to determine the difference in phase between the surface profile $\eta = Ae^{-\alpha x} \cos(kx - \sigma t)$ and the horizontal position of a fluid particle. Integrating the horizontal velocity expression (Equation (3-6a)) with respect to time and setting the constant of integration to zero gives:

$$\xi = \frac{Ae^{-\alpha x}}{\Delta} Q(z) \cos\left(kx - \sigma t - \left(\delta - p'(z) + \frac{\pi}{2}\right)\right) \qquad (4-1)$$
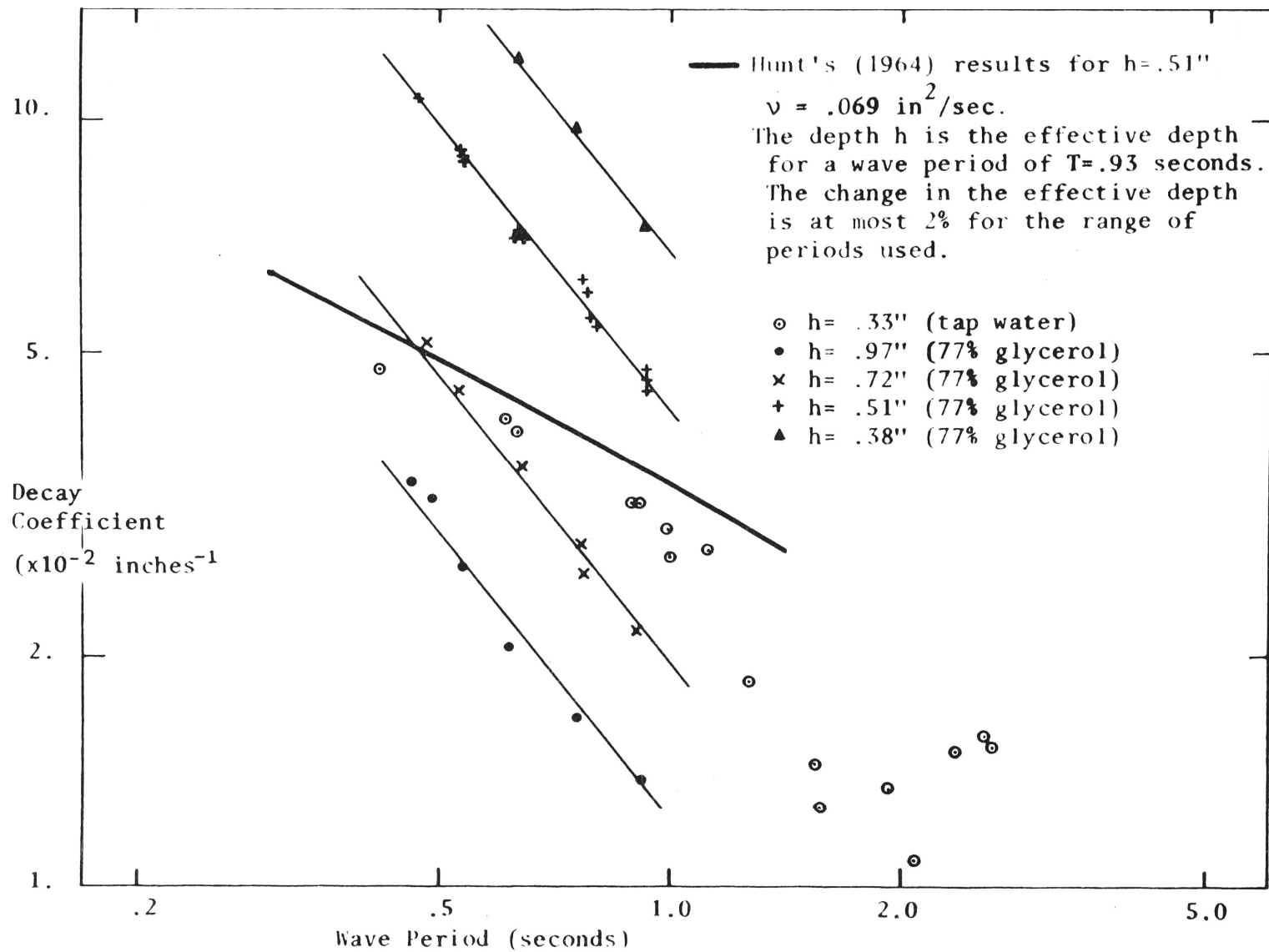
FIGURE 21. THE DECAY COEFFICIENT AS A FUNCTION OF THE WAVE PERIOD FOR VARIOUS FLUIDS AND DEPTHS.

for the position of a fluid particle. To be more correct, the value

for x in Equation (4-1) should be replaced by (x-ξ) so that the measure-

ment of ξ refers to a co-ordinate system moving horizontally with the

fluid. That is, when the fluid particle is at a position (x+ξ) it is

influenced by the fluid properties at this point and not those at x.

Taking the equilibrium position of the particle as:

$$x = 0 \quad \text{gives:}$$

$$\eta = A \cos \sigma t \qquad (4-2)$$

for the surface profile

and:

$$\xi = \frac{-A}{\Delta} Q(z) \cos\left(\sigma t + \left(\delta - p^{1}(z) + k\xi + \frac{\pi}{2}\right)\right) \qquad (4-3)$$

where it has been assumed that $e^{-\xi \mathcal{L}} \simeq 1$

Therefore the surface profile and the particle position are out

of phase by an angle of $(\delta - p^{1} + k\xi + \frac{\pi}{2})$ radians which corresponds to

a time interval of $\frac{1}{\sigma}(\delta - p^{1} + k\xi + \frac{\pi}{2})$ time units. The calculation

of the numerical value for this phase was carried out by evaluating,

for a given depth and time, the constants on the R.H.S. of Equation

(4-3) and then solving numerically the resulting equation:

$$\xi = B_{1} \cos (B_{2} + k\xi)$$

A typical set of results using the following parameters:

T = .94 seconds

h = .70 inches

α = .0186 (inches)$^{-1}$

z = .44 inches

A = .0043 inches

gives the results:

δ = .045 radians

p^1 = .0023 radians

$k\xi$ = ± .0060 radians at the maximum displacements

= 0.0 at the equilibrium position

The phase difference between when the surface displacement is zero and when the particle position is zero (ξ = 0) is then:

$$(\frac{\pi}{2} + .045 - .0023) \quad radian$$

$$= 1.613 \ radians$$

The value at the bottom was 1.616 radians and at the surface 1.612 radians, these give the maximum and minimum values for the phase difference.

An attempt at measuring this phase difference was carried out using the surface probe described in Appendix 8 and the particle follower described in Appendix 9.

These instruments did not measure the surface and the particle position exactly, but had a phase difference between the actual and measured event

The measured surface profile lagged the actual profile, this phase difference is shown on Figures (A8-8) and (A8-9), a result of .025 radians is given using the above parameters. The equation of motion describing the pendulum motion is developed in Appendix 8 and for the pendulum and the fluid used (77% glycerol at 12.8 degrees C) it is (Equation (A9: 11)):

$$\ddot{x} = -79x + 460 (u-\dot{x}) \mid u-x \mid^{.61}$$

where $x,\dot{x}$ and $\ddot{x}$ are the position, velocity and acceleration of the pendulum respectively and u is the horizontal fluid velocity. This equation was integrated numerically using a time step of T/500 seconds.

Using a starting point for the numerical solution of:

$$t_o = 0$$
$$x_o = 0$$
$$\dot{x}_o = u \max.$$

It was found that the phase between the actual fluid position, ξ , and the pendulum position, x, was dependent on time. But after a time of $\frac{3T}{2}$, the phase difference was within 5% of the value for the steady state solution (time $= \infty$). This phase difference was found to be .157 radians with the pendulum preceding the particle.

The total phase difference between the actual and measured results should then be .157 + .025 = .182 radians.

Thus the situation for the various wave motions is as depicted in Figure (22) where the various phases have been exaggerated and all the amplitudes have been normalized to unity. From this Figure it is clear that the optimum times to measure the phase difference is when the curves cross the zero or equilibrium position. The phase difference between the measured surface profile and the pendulum position is then:

$$p_t^+ = \frac{\pi}{2} + p_1 + p_2 + p_3 \qquad (4-4)$$

where the various symbols are shown on Figure (22).

To obtain this phase difference simultaneous measurements of the surface profile and the particle position were taken. To avoid problems with small variations in the time response between various types of bridges, identical bridges and recording circuits were used. A thin line parallel to the wave crests was marked on the bottom of the small flume. The wave probe was set directly above this line by running the micrometer down so that the probes sensing wires were nearly touching bottom and then moving the instrument carriage such that both wires were directly above the line. The probe wires were then brought back to the near surface position required for wave measurements. The particle follower position was set by moving the paddle to a near bottom location and adjusting the horizontal position of the paddle so that it was co-linear with the line. The construction of the particle follower allowed for horizontal movement of the pendulum without moving the instrument carriage. Parallel setting of the paddle with the line was accomplished by rotating the pendulum mounting block slightly

Particle position in the absence of friction

Particle position with friction

Pendulum position

P_3

P_2

$\frac{\pi}{2}$

P_1

p^+

p^-

Actual surface profile

Measured surface profile

P_1 refers to the surface probe phase lag

P_2 refers to the friction phase advance

P_3 refers to the pendulum phase advance
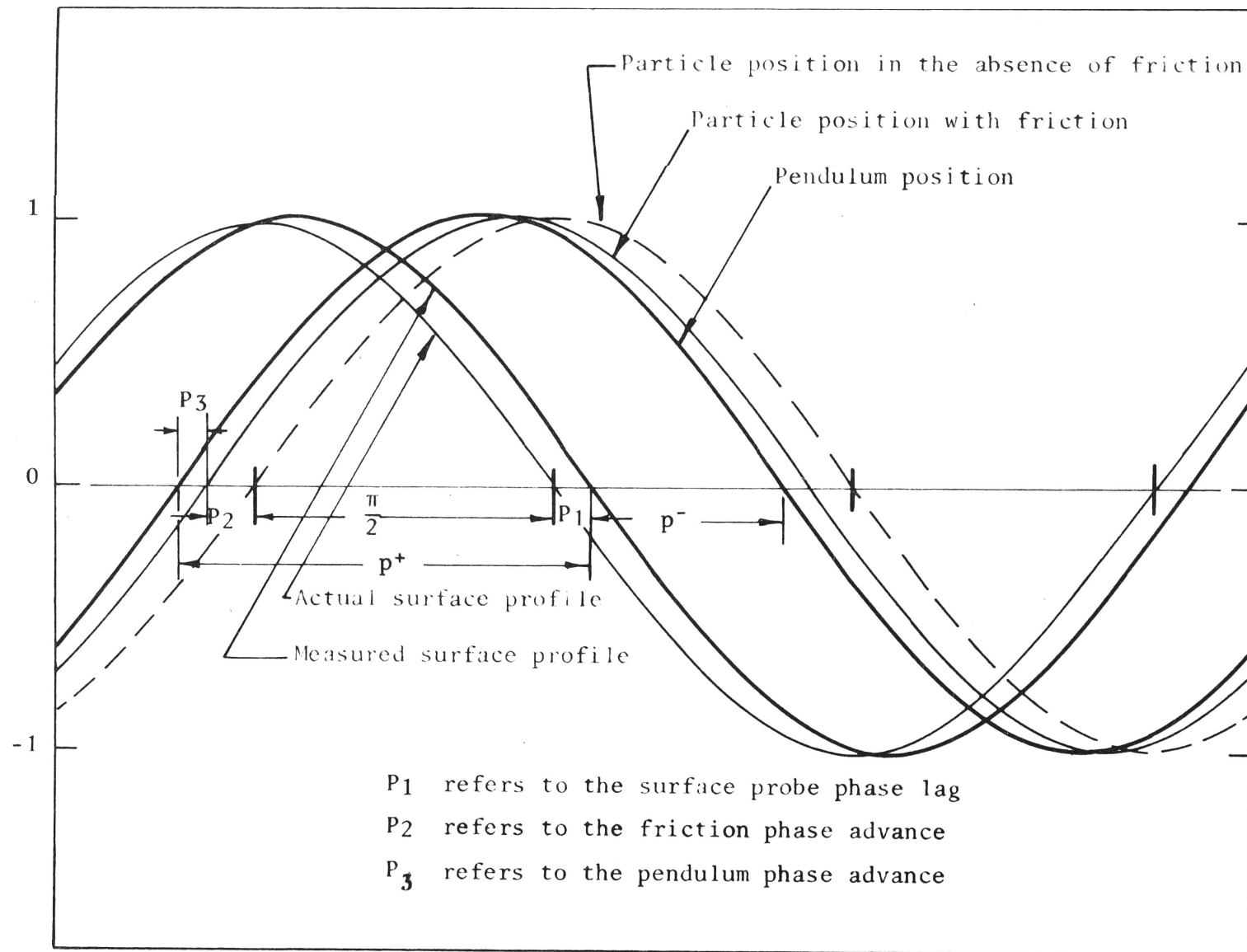
FIGURE 22. SCHEMATIC DIAGRAM OF PHASES FOR THE MEASURED SURFACE PROFILE
AND THE PARTICLE FOLLOWER.

until the desired position was found. The paddle was then taken to the required depth for the particle position measurements. The wave maker was started and measurements of the surface profile and the particle position were recorded as a function of time.

The measured distance between the zero positions recorded on the chart paper when compared to the measured distance on the chart corresponding to a wave period gave the measured phase difference. The chart speed was considered to be constant over a time interval corresponding to two or three wave periods.

Referring to Figure (22) it can be seen that either p_t^+ or
$p_t^- = \frac{\pi}{2} - (p_1 + p_2 + p_3)$ may be measured to arrive at the frictional phase p_2.

An experiment investigating the phase difference was carried out concurrently with the one investigating the change of decay coefficient with time using an equal fluid and air temperature. The results are summarized in Table (9) where p_t^+ and p_t^- are the average of several measurements of phase. There appears to be a decrease of about .07 radians between the phase measured at time t = 0 minutes and time t = 55 minutes. Since the temperature of the air and that of the fluid were kept at a constant value of 12.8 degrees C this change in phase was not attributed to temperature effects but to a changing boundary layer at the surface.

The fluid was again mixed and measurements of phase differences were taken at various depths. This run took approximately ten minutes and, since the first of the series of measurements were those near the surface it was expected that these results would apply to a relatively uncontaminated surface layer. The results are tabulated in Table (10) where the depth, d, refers to the actual (measured) position of the paddle centre below the undisturbed surface. There is a general decrease in the phase between the deeper and the shallower regions except for the near surface result which shows a large phase lag. The predicted result of .047 radians is exceeded in all except one paddle position. The reason for this discrepancy is probably again due to the relatively shallow fluid depth used and the high fluid viscosity. Thus the influence of the bottom boundary layer is expected to extend through a significant portion of the fluid depth. (See Lamb (1932) pp 622-3)). Using dye streaks it was noted that the motion of the thin surface layer was much less than that of the rest of the fluid (exclusive of the motionless thin layer at the bottom). In fact, the surface appeared to be immobile after a time interval after mixing of about one hour, thus this surface boundary layer would impart phase differences to the rest of the fluid column. It is therefore concluded that the phase difference between the surface profile and the particle position as predicted by the theory in this thesis was not resolveable from phase differences caused by the actual surface and bottom boundary layers.

TABLE 9.

THE CHANGE IN PHASE BETWEEN THE SURFACE PROFILE AND THE PARTICLE
POSITION WITH ELAPSED TIME AFTER THE FLUID WAS MIXED

Elapsed Time minutes	Total Measured p_t^+ radians	Phase Difference p_t^- radians	Average Frictional Phase Difference, "p_2", radians
0	1.88	1.27	.12(5)
15	1.87	1.33	.09
20	1.86	1.33	.08(5)
30	1.81	1.34	.05(5)
40	1.82	1.34	.06(0)
55	1.81	1.35	.05(0)

TABLE 10.

THE PHASE BETWEEN THE SURFACE PROFILE AND
THE PARTICLE POSITION FOR VARIOUS DEPTHS

Mean Paddle Depth d inches	Total Measured p_t^+ radians	Phase Difference p_t^- radians	Average Frictional Phase Difference, "p_2" radians
.63	2.11	1.11	.32
.56	1.98	1.16	.23
.46	1.98	1.19	.21(5)
.36	1.96	1.20	.20
.26	1.88	1.27	.12(5)
.16	1.76	1.38	.01
.06	2.13	1.01	.38

CHAPTER 5

TRANSMISSION AND REFLECTION OF SURFACE WAVES INCIDENT

NORMALLY TO A DEPTH DISCONTINUITY

5.1 The Matching Conditions at the Discontinuity

The problem dealt with in this chapter was the reflection and

transmission coefficients for rectilinear surface waves incident normally

to a discontinuity in depth. As pointed out in the Introduction, the

inviscid problem has been tackled by a variety of authors using a number

of different matching conditions at the discontinuity. In this model the

equations developed in Chapter 2 using the linear friction are employed

and the reflected and transmitted amplitudes and phases calculated by

matching the instantaneous energy flux and surface elevation at the

discontinuity.

The assumptions made across BB' (Figure (1)) were that at any time:

1)   the flux of energy incident equalled the sum of

the reflected and transmitted energy fluxes.

and   2)   the sum of the incident and reflected waves

surface elevations equalled the transmitted

waves surface elevation.

The energy flux and the surface elevation at the step are deduced

from the wave properties on both sides of the discontinuity without

regard to any local disturbances generated here.

Both these assumptions are approximations to the real situation

where a standing wave has been shown to exist (Bartholomew (1958)) in

the vicinity of BB'. Thus it is easily seen that the surface ABC may

be a continuous streamline without implying condition (2), the standing

wave "connecting" the two regions A and C. Whereas conservation of

energy requires condition 1) be satisfied when the fluxes are averaged

over an integral number of wave periods it by no means necessitates

their equality at any instant. However, results from experiments carried

out to determine the reflection and transmission coefficients agree

reasonably well with an inviscid model using the conditions as stated

above. (See, for example, Ippen (1966) page 75).

5.2 Evaluation of the Reflection and Transmission Coefficients

Following the definition of the average energy flux as set out in

Section 3.4B an instantaneous energy flux or power will be defined as:

$$P = \lim_{\tau \to 0} \frac{1}{\tau} \int_{-h}^{\eta \simeq 0} \int_{t}^{t+\tau} p_v \, u \, dz \, dt \cdot$$

Taking the discontinuity in depth at x = 0, matching condition 1)

becomes $P_1 \big]_{x=0^+} = P_2 \big]_{x=0^-}$ where subscripts 1 and 2 refer to the

left hand and right hand side respectively of the discontinuity.

or:

$$\underset{\tau \to 0}{\text{Lim}} \frac{1}{\tau} \int_{-h_1}^{\eta_1 \approx 0} \int_{t}^{t+\tau} (p_v)_1 \, u_1 \, dz \, dt \Bigg]_{x=0^-}$$

$$= \underset{\tau \to 0}{\text{Lim}} \frac{1}{\tau} \int_{-h_2}^{\eta_2 \approx 0} \int_{t}^{t+\tau} (p_v)_2 \, u_2 \, dz \, dt \Bigg]_{x=0^+} \qquad (5-1)$$

where $u_1 = u_i + u_r$

$$(p_v)_1 = \rho \left\{ \frac{\partial}{\partial t} (\phi_i + \phi_r) + \frac{c}{h_1} (\phi_i + \phi_r)_{z=-h_1} \right\}$$

$$u_2 = u_t$$

$$(p_v)_2 = \rho \left\{ \frac{\partial}{\partial t} \phi_t + \frac{c}{h_2} (\phi_t)_{z=-h_2} \right\}$$

the subscripts i,r,t referring to incident, reflected and transmitted respectively.

Due to the presence of friction, it is expected that there will be a phase shift between the incident and transmitted waves and hence between the incident and reflected waves. This is a consequence of the phase differences between the surface profile, the particle velocity and the potential function not being the same in both regions.

Taking the arbitrary phase of the incident waves surface elevation as being zero, then the surface elevation of the reflected wave is described as:

$$\eta_r = A_r e^{\alpha_1 x} \cos(-k_1 x - \sigma t + \gamma_r)$$

and that of the transmitted wave as:

$$\eta_t = A_t e^{-\alpha_2 x} \cos(k_2 x - \sigma t + \gamma_t)$$

where γ_r and γ_t are the phases induced at the step, and A_r and A_t are the reflected and transmitted amplitudes at $x = 0$.

Upon integrating and rearranging the L.H.S. of (5-1) becomes: (after taking the limit of $\tau \to 0$)

$$L.H.S = \frac{\rho\sigma^3}{8\Delta_1^2 k_1} \left\{ \left[(A_i^2 - A_r^2)(d_1 \cos \Omega_1 + \frac{\Delta_1}{k_1} \frac{4c}{\sigma h_1} \sin \delta_1) + 2A_i A_r \sin \gamma_r (d_1 \sin \Omega_1 - \frac{\Delta_1}{k_1} \frac{4c}{\sigma h_1} \cos \delta_1) \right] \right.$$

$$+ \cos 2\sigma t \left[(A_i^2 - A_r^2 \cos 2\gamma_r)(a_1 \cos \Theta_1 + b_1 \sin \Theta_1 + \frac{\Delta_1}{k_1} \frac{4c}{\sigma h_1} \sin \beta_1) \right.$$

$$\left. - A_r^2 \sin 2\gamma_r (a_1 \sin \Theta_1 - b_1 \cos \Theta_1 - \frac{\Delta_1}{k_1} \frac{4c}{\sigma h_1} \cos \beta_1) \right]$$

$$- \sin 2\sigma t \left[(A_i^2 - A_r^2 \cos 2\gamma_r)(a_1 \sin \Theta_1 - b_1 \cos \Theta_1 - \frac{\Delta_1}{k_1} \frac{4c}{\sigma h_1} \cos \beta_1) \right.$$

$$\left. \left. + A_r^2 \sin 2\gamma_r (a_1 \cos \Theta_1 + b_1 \sin \Theta_1 + \frac{\Delta_1}{k_1} \frac{4c}{\sigma h_1} \sin \beta_1) \right] \right\}$$

and the R.H.S. becomes:

$$R.H.S = \frac{\rho\sigma^3 A_t^2}{8\Delta_2^2 k_2} \left\{ \left[d_2 \cos \Omega_2 + \frac{\Delta_2}{k_2} \frac{4c}{\sigma h_2} \sin \delta_2 \right] \right.$$

$$+ \cos 2\sigma t \left[\cos 2\gamma_t (a_2 \cos \Theta_2 + b_2 \sin \Theta_2 + \frac{\Delta_2}{k_2} \frac{4c}{\sigma h_2} \sin \beta_2) \right.$$

$$\left. + \sin 2\gamma_t (a_2 \sin \Theta_2 - b_2 \cos \Theta_2 - \frac{\Delta_2}{k_2} \frac{4c}{\sigma h_2} \cos \beta_2) \right]$$

$$- \sin 2\sigma t \left[\cos 2\gamma_t (a_2 \sin \Theta_2 - b_2 \cos \Theta_2 - \frac{\Delta_2}{k_2} \frac{4c}{\sigma h_2} \cos \beta_2) \right.$$

$$\left. \left. - \sin 2\gamma_t (a_2 \cos \Theta_2 + b_2 \sin \Theta_2 + \frac{\Delta_2}{k_2} \frac{4c}{\sigma h_2} \sin \beta_2) \right] \right\}$$

where:

$$a_j = 2h_j + \frac{1}{k_j^2}\left[k_j \sinh 2k_j h_j \cos 2\alpha_j h_j + \alpha_j \cosh 2k_j h_j \sin 2\alpha_j h_j\right]$$

$$b_j = \frac{1}{k_j^2}\left[k_j \cosh 2k_j h_j \sin 2\alpha_j h_j - \alpha_j \sinh 2k_j h_j \cos 2\alpha_j h_j\right]$$

$$d_j = \frac{\sinh 2k_j h_j}{k_j} + \frac{\sin 2\alpha_j h_j}{\alpha_j}$$

$$\beta_j = \epsilon_j + \Omega_j$$

$$\Theta_j = \epsilon_j + \delta_j$$

$$j = 1, 2$$

(See Appendix 10 for details)

Since these equations must be equal for any time t it follows that:
the coefficients of the $\sin \sigma t$ terms must be equal, the coefficients
of the $\cos \sigma t$ terms must be equal and the terms independent of time
must be equal. Therefore arriving at the three equations:

$$\frac{\Delta_2^2 k_2}{\Delta_1^2 k_1}\left[(A_i^2 - A_r^2)(d_1 \cos \Omega_1 + \frac{\Delta_1}{k_1}\frac{4c}{\sigma h_1} \sin \delta_1) + 2A_i A_r \sin \gamma_r (d_1 \sin \Omega_1 - \frac{\Delta_1}{k_1}\frac{4c}{\sigma h_1} \cos \delta_1)\right]$$

$$= A_t^2 (d_2 \cos \Omega_2 + \frac{\Delta_2}{k_2}\frac{4c}{\sigma h_2} \sin \delta_2) \qquad (5\text{-}2)$$

$$\frac{\Delta_2^2 k_2}{\Delta_1^2 k_1}\Bigg\{(A_i^2 - A_r^2 \cos 2\gamma_r)(a_1 \cos \Theta_1 + b_1 \sin \Theta_1 + \frac{\Delta_1}{k_1}\frac{4c}{\sigma h_1} \sin \beta_1)$$

$$- A_r^2 \sin 2\gamma_r \quad (a_1 \sin \Theta_1 - b_1 \cos \Theta_1 - \frac{\Delta_1}{k_1}\frac{4c}{\sigma h_1} \cos \beta_1)\Bigg\}$$

$$= A_t^2\Bigg\{\cos 2\gamma_t \quad (a_2 \cos \Theta_2 + b_2 \sin \Theta_2 + \frac{\Delta_2}{k_2}\frac{4c}{\sigma h_2} \sin \beta_2)$$

$$+ \sin 2\gamma_t (a_2 \sin \Theta_2 - b_2 \cos \Theta_2 - \frac{\Delta_2}{k_2}\frac{4c}{\sigma h_2} \cos \beta_2)\Bigg\}$$

$$(5\text{-}3)$$

$$\frac{\Delta_2{}^2 K_2}{\Delta_1{}^2 K_1} \left\{ (A_i{}^2 - A_r{}^2 \cos 2\gamma_r)(a_1 \sin \Theta_1 - b_1 \cos \Theta_1 - \frac{\Delta_1}{K_1} \frac{4c}{\sigma h_1} \cos \beta_1) \right.$$

$$\left. + A_r{}^2 \sin 2\gamma_r (a_1 \cos \Theta_1 + b_1 \sin \Theta_1 + \frac{\Delta_1}{K_1} \frac{4c}{\sigma h_1} \sin \beta_1) \right\}$$

$$= A_t{}^2 \left\{ \cos 2\gamma_t (a_2 \sin \Theta_2 - b_2 \cos \Theta_2 - \frac{\Delta_2}{K_2} \frac{4c}{\sigma h_2} \cos \beta_2) \right.$$

$$\left. - \sin 2\gamma_t (a_2 \cos \Theta_2 + b_2 \sin \Theta_2 + \frac{\Delta_2}{K_2} \frac{4c}{\sigma h_2} \sin \beta_2) \right\}.$$

$$(5\text{-}4)$$

The second condition that the sum of the surface elevation produced by the incident and reflected waves is equal to the elevation of the transmitted wave gives:

$$\eta_1 \Big]_{x=0^-} = \eta_2 \Big]_{x=0^+}$$

or:

$$(\eta_i + \eta_r) \Big]_{x=0^-} = \eta_t \Big]_{x=0^+}$$

or, more explicitly:

$$\left\{ A_i e^{-\alpha_1 x} \cos (k_1 x - \sigma t) + A_r e^{\alpha_1 x} \cos (-k_1 x - \sigma t + \gamma_r) \right\} \Big|_{x=0^-}$$

$$= A_t e^{-\alpha_2 x} \cos (k_2 x - \sigma t + \gamma_t) \Big|_{x=0^+} \qquad (5\text{-}5)$$

Expanding the trigonometric functions and equating the coefficients of $\cos \sigma t$ and $\sin \sigma t$ yields:

$$A_i + A_r \cos \gamma_r = A_t \cos \gamma_t \qquad (5\text{-}6)$$

and
$$A_r \sin \gamma_r = A_t \sin \gamma_t \tag{5-7}$$

Equations (5-2), (5-3), (5-4), (5-6) and (5-7) form a system of five

equations in the four unknowns, namely A_r, A_t, γ_r and γ_t.

Hence, for this to be a satisfactory solution the values obtained for

the four unknowns when any four of the equations are used must be the

same as when any other set of equations are used. Or, more simply,

using the physically acceptable results from four of the equations, they

must satisfy the equality of the fifth.

Since the equations relating to the energy flux were rather

cumbersome, no attempt was made to find an analytical proof that the

five equations were consistent. Instead, values for the unknowns were

calculated on a computer using the latter four equations which pertain

to the instantaneous conditions and, using these values, both sides of

Equation (5-2) were evaluated and checked for consistency. It should be

noted that Equation (5-2) is the energy flux condition that would result

if, instead of an instantaneous evaluation, the energy flux had been

averaged over an integral number of wave periods; and this is the

equation that must be satisfied if the conservation of energy condition

as set out in Section (1-2) is to be fulfilled. A cross-product term

appears in this equation and is a consequence of the potential function

and the horizontal velocity being out of phase. This term indicates

that there is frictional coupling between waves travelling in opposite

directions to one another.

An exact solution of Equations (5-3), (5-4), (5-6) and (5-7) can be obtained by re-writing the equations in terms of complex exponentials.

For convenience, letting:

$$\alpha_r = \frac{A_r}{A_\iota}$$

and

$$\alpha_t = \frac{A_t}{A_\iota}$$

and re-writing Equations (5-3) and (5-4) respectively as:

$$\frac{S_2}{S_1}\left\{(1-\alpha_r^2 \cos 2\gamma_r)\, T_1^{+} - (\alpha_r^2 \sin 2\gamma_r)\, T_1^{-}\right\}$$

$$= \alpha_t^2 \left\{(\cos 2\gamma_t)\, T_2^{+} + (\sin 2\gamma_t)\, T_2^{-}\right\} \qquad (5\text{-}3A)$$

$$\frac{S_2}{S_1}\left\{(1-\alpha_r^2 \cos 2\gamma_r)\, T_1^{-} + (\alpha_r^2 \sin 2\gamma_r)\, T_1^{+}\right\}$$

$$= \alpha_t^2 \left\{(\cos 2\gamma_t)\, T_2^{-} - (\sin 2\gamma_t)\, T_2^{+}\right\} \qquad (5\text{-}4A)$$

where the coefficients S_j, T_γ^{+}, T_γ^{-} $(\gamma = 1, 2)$ correspond directly to those in (5-3) and (5-4). Multiplying (5-4A) by $\iota = \sqrt{-1}$ and subtracting from (5-3A) gives:

$$\frac{S_2}{S_1}\left\{(T_1^{+} - \iota T_1^{-}) - \alpha_r^2\, e^{\iota 2\gamma_r}\, (T_1^{+} - \iota T_1^{-})\right\}$$

$$= \alpha_t^2\, e^{\iota 2\gamma_t}\, (T_2^{+} - \iota T_2^{-}) \qquad (5\text{-}8)$$

Similarly, Equations (5-6) and (5-7) can be combined as:

$$1 + a_r e^{i \gamma_r} = a_t e^{i \gamma_t} \qquad (5\text{-}9)$$

Letting $\quad a_r^c = a_r e^{i \gamma_r}$

$$a_t^c = a_t e^{i \gamma_t}$$

and $\quad W_j = (T_j^+ - i\, T_j^-) \quad ; \quad j = 1, 2$

Then Equation (5-8) becomes:

$$\frac{S_2}{S_1} \frac{W_1}{W_2} \left(1 - (a_r^c)^2 \right) = (a_t^c)^2 \qquad (5\text{-}8A)$$

and Equation (5-9) becomes:

$$1 + a_r^c = a_t^c \qquad (5\text{-}9A)$$

Solving Equation (5-8A) and Equation (5-9A) simultaneously gives:

$$a_r^c = \frac{-1 \pm \frac{\omega_1}{\omega_2}}{1 + \frac{\omega_1}{\omega_2}} \qquad \text{where:} \quad \omega_j = \frac{W_j}{S_j}$$

taking the positive sign to give a physically acceptable solution
when $\omega_1 \to \omega_2$ gives:

$$\alpha_r^c = \frac{\omega_1 - \omega_2}{\omega_1 + \omega_2} = \alpha_r e^{i\gamma_r}$$

$$= \alpha_r (\cos \gamma_r + i \sin \gamma_r)$$

$$= R(\alpha_r^c) + i I(\alpha_r^c) \qquad (5\text{-}10)$$

hence:

$$\alpha_r = \sqrt{(R(\alpha_r^c))^2 + (I(\alpha_r^c))^2} \qquad (5\text{-}11)$$

and

$$\gamma_r = \tan^{-1} \left\{ \frac{I(\alpha_r^c)}{R(\alpha_r^c)} \right\} \qquad (5\text{-}12)$$

A similar result is found for α_t^c viz:

$$\alpha_t^c = \frac{2\omega_1}{\omega_1 + \omega_2} = \alpha_t e^{i\gamma_t} \qquad (5\text{-}13)$$

so

$$\alpha_t = \sqrt{(R(\alpha_t^c))^2 + (I(\alpha_t^c))^2} \qquad (5\text{-}14)$$

and

$$\gamma_t = \tan^{-1} \left\{ \frac{I(\alpha_t^c)}{R(\alpha_t^c)} \right\} \qquad (5\text{-}15)$$

where $R(x)$ and $I(x)$ represent the real and imaginary parts of x,

respectively.

In the above development the waves have been incident from region (1) and transmitted into region (2). Re-writing Equation (5-10) as:

$$\left(\alpha_r^c\right)^{①} = \frac{\omega_1 - \omega_2}{\omega_1 + \omega_2} = \alpha_r^{①} e^{i \gamma_r^{①}} \tag{5-16}$$

and Equation (5-13) as:

$$\left(\alpha_t^c\right)^{①} = \frac{2\omega_1}{\omega_1 + \omega_2} = \alpha_t^{①} e^{i \gamma_t^{①}} \tag{5-17}$$

where the subscript (1) has been used to differentiate these parameters from the ones obtained for waves incident from region (2) and transmitted into region (1). In this case:

$$\left(\alpha_r^c\right)^{②} = \frac{\omega_2 - \omega_1}{\omega_1 + \omega_2} = \alpha_r^{②} e^{i \gamma_r^{②}} \tag{5-18}$$

and

$$\left(\alpha_t^c\right)^{②} = \frac{2\omega_2}{\omega_1 + \omega_2} = \alpha_r^{②} e^{i \gamma_t^{②}} \tag{5-19}$$

where it is understood that all parameters except the direction of propagation of the incident wave are unchanged.

Equation (5-18) may be re-written as:

$$\alpha_r^{(2)} e^{i(\gamma_r^{(2)}+\pi)} = - \frac{\omega_2 - \omega_1}{\omega_1 + \omega_2} = \alpha_r^{(1)} e^{i\gamma_r^{(1)}}$$

which implies that

$$\alpha_r^{(1)} = \alpha_r^{(2)} \quad \text{AND} \quad \gamma_r^{(1)} = (\gamma_r^{(2)} + \pi) + n\pi$$

n is taken to be zero to agree with the solution to be given later for frictionless waves.

Simple symmetry relations like the above were not found for the transmitted wave, but adding Equations (5-17) and (5-19) gives:

$$\left(\alpha_t^{c}\right)^{(1)} + \left(\alpha_t^{c}\right)^{(2)} = 2$$

or:

$$\alpha_t^{(1)} e^{i\gamma_t^{(1)}} + \alpha_t^{(2)} e^{i\gamma_t^{(2)}} = 2$$

Equating imaginary parts yields the relation that:

$$\frac{\alpha_t^{(1)}}{\alpha_t^{(2)}} = - \frac{\sin \gamma_t^{(2)}}{\sin \gamma_t^{(1)}}$$

The R.H.S. is positive so $\sin \gamma_t^{(2)}$ and $\sin \gamma_t^{(1)}$ must be of opposite signs, therefore if $\gamma_t^{(1)}$ is in the first quadrant then $\gamma_t^{(2)}$ must be in the fourth. These quadrants are chosen since for frictionless waves it will be shown that $\gamma_t = 0$ and it is expected that the transmitted phase induced by friction will not be greatly different from this; that is not in the second or third quadrant.

5.3 The Solution when Friction is Neglected

It is instructive to look at these equations in the less cumbersome form when friction is neglected.

Then:

$$K_\gamma = k_\gamma$$

$$\Delta_\gamma = \sinh k_\gamma h_\gamma$$

$$\Omega_\gamma = 0$$

$$\delta_\gamma = 0$$

$$\beta_\gamma = 0$$

$$\Theta_\gamma = 0$$

$$a_\gamma = \frac{2k_\gamma h_\gamma + \sinh 2k_\gamma h_\gamma}{k_\gamma}$$

$$b_\gamma = 0$$

and

$$d_\gamma = a_\gamma$$

Therefore:

$$\frac{\omega_1}{\omega_2} = \frac{k_2 \sinh^2 k_2 h_2}{k_1 \sinh^2 k_1 h_1} \cdot \frac{\dfrac{2k_1 h_1 + \sinh 2k_1 h_1}{k_1}}{\dfrac{2k_2 h_2 + \sinh 2k_2 h_2}{k_2}}$$

$$= \frac{2k_1 h_1 + \sinh 2k_1 h_1}{k_1^2 \sinh^2 k_1 h_1} \cdot \frac{k_2^2 \sinh^2 k_2 h_2}{2k_2 h_2 + \sinh 2k_2 h_2}$$

That this is the ratio of the undirected energy velocities for the two depths can be seen from:

$$v_e = \frac{\sigma}{2k} \left(1 + \frac{2kh}{\sinh 2kh} \right)$$

$$= \frac{\sigma^3}{4g} \left(\frac{2kh + \sinh 2kh}{k^2 \sinh kh} \right)$$

Hence

$$\frac{\omega_1}{\omega_2} = \frac{v_{e1}}{v_{e2}}$$

Thus α_r^c in Equation (5-10) is real and $\gamma_r = 0$ or π.

From Equation (5-10) it follows, since α_r is positive, that if $v_{e1} < v_{e2}$ then $\gamma_r = \pi$ and if $v_{e1} \geqslant v_{e2}$ then $\gamma_r = 0$

Similarly $\gamma_t = 0$ or π in Equation (5-15) but, since α_t and $\frac{v_{e1}}{v_{e2}}$ are always positive, it follows from Equation (5-13) that $\gamma_t = 0$.

The reflection coefficient is now:

$$\alpha_r = \left| \frac{v_{e1} - v_{e2}}{v_{e1} + v_{e2}} \right| \qquad (5-16)$$

with a corresponding phase:

$$\gamma_r = 0 \quad ; \quad v_{e1} \geqslant v_{e2}$$

$$\gamma_r = \pi \quad ; \quad v_{e1} < v_{e2} \qquad (5-17)$$

and the transmission coefficient is:

$$\alpha_t^c = \alpha_t = \frac{2 v_{e1}}{v_{e1} + v_{e2}} \qquad (5-18)$$

From Equation (5-16) a zero reflection coefficient is indicated when the energy velocities in the two depths are equal and this does not only occur for $h_1 = h_2$.

The condition of equal energy velocities can be visualized from a plot of v_e vs. h where the energy velocity increases from zero to a maximum and then decreases to the asymptotic value of $\frac{g}{2\sigma}$. Thus for any value of $v_e \leq \frac{g}{2\sigma}$ the curve is single valued and for any value of $v_e > \frac{g}{2\sigma}$ there corresponds two values of h. Theoretical and experimental results presented by Newman (1965) and experimental results shown by Sagnon and Bocco (1962) indicate a non zero reflection at the point where $v_{e_1} = v_{e_2}$. Thus the solution for a_r given above is not valid near this point; the solution for α_t at this point is in close agreement with the theoretical and experimental results obtained by the above authors.

Several limiting cases are of interest:

Case 1. $v_{e_1} \gg v_{e_2}$

a)   Region (1) and (2) are such that "long waves" are propagated on both sides of the discontinuity,

then: $v_{e_1} \simeq \sqrt{gh_1}$

and $\qquad v_{e_2} \cong \sqrt{gh_2}$

This gives Lamb's (1932) solution:

$$\alpha_t = \frac{2\sqrt{h_1}}{\sqrt{h_1} + \sqrt{h_2}} \qquad (15\text{-}19)$$

and:

$$\alpha_r = \frac{\sqrt{h_1} - \sqrt{h_2}}{\sqrt{h_1} + \sqrt{h_2}}$$

$$(15\text{-}20)$$

For $\sqrt{h_1} \gg \sqrt{h_2}$ the limiting case of $\alpha_t \Rightarrow 2$ and $\alpha_r \Rightarrow 1$ are arrived at. This limit implies that there is complete reflection at the discontinuity and that no energy is transmitted into region (2); that $\alpha_t \Rightarrow 2$ is a consequence of the surface being a continuous streamline.

If $h_1 = 10^2$ feet and $h_2 = 1$ foot then $a_t = 1.818$ and $\alpha_r = .818$. If $h_1 = 10^4$ feet and $h_2 = 1$ foot then $\alpha_t = 1.980$ and $\alpha_r = .980$. The power, in this long-wave limit, is proportional to $A^2 \sqrt{h}$ For a unit amplitude, the incident energy flux is, in the first instance, ~ 10 and, in the second, $\sim 10^2$. The corresponding reflected energy fluxes are ~ 6.694 and ~ 96.08 whereas the transmitted powers are ~ 3.306 and ~ 3.921. Thus it is easily seen that

a large increase in the incident power produces a large increase in the reflected power whereas the power transmitted into the shallower region is increased only slightly. As a consequence of the incident and reflected power, and thus their wave amplitudes, becoming more and more nearly equal as h_1 becomes large (for a fixed h_2) the transmitted amplitude coefficient must increase to the limiting value of 2 as h_1 and thus the incident energy $\Rightarrow \infty$.

b)   Region (1) is such that "deep water" waves are propagated and region (2) is such that "long waves" are propagated, then:

$$v_{e_1} \simeq \frac{1}{2} \frac{\sigma}{k_1} \simeq \frac{1}{2} \sqrt{\frac{g}{k_1}}$$

$$\simeq \frac{g}{2\sigma}$$

and:

$$v_{e_2} \simeq \sqrt{gh_2}$$

The transmission coefficient is:

$$\alpha_t = 2 \; \frac{\frac{\sqrt{g}}{2\sigma}}{\frac{\sqrt{g}}{2\sigma} + \sqrt{h_2}} \tag{15-21}$$

and the reflection coefficient is:

$$\alpha_r = \frac{\frac{\sqrt{g}}{2\sigma} - \sqrt{h_2}}{\frac{\sqrt{g}}{2\sigma} + \sqrt{h_2}} \tag{15-22}$$

Therefore, if $\dfrac{\sqrt{g}}{2\sigma} \gg \sqrt{h_2}$

then $\alpha_t \Rightarrow 2$

and $\alpha_r \Rightarrow 1$.

That this limit is reached very slowly can be seen by considering very long ocean swell with a period of 8π seconds, (this gives a relatively large value for $\dfrac{\sqrt{g}}{2\sigma}$) then:

$$\alpha_t \simeq 2\ \frac{11\cdot3}{11\cdot3 + \sqrt{h_2}}$$

and:

$$\alpha_r \simeq \frac{11\cdot3 - \sqrt{h_2}}{11\cdot3 + \sqrt{h_2}}$$

Which, for the very shallow depths for h_2 of:

       1 foot gives $\alpha_t \simeq 1.837$

       ¼ foot gives $\alpha_t \simeq 1.915$

       and 1/100 foot gives $\alpha_t \simeq 1.982$

That the transmission coefficient increases more slowly in this example than in the one where long-waves existed in both depths is a result of the greater energy flux for long-waves than for deep water waves when the same water depths are considered. Thus a greater percentage of the energy is transmitted across the discontinuity in this instance of deep water waves in region (1) and a lower percent is reflected, implying a smaller transmission coefficient than would occur for long-

waves using the same depths.

c)   The other possibility for $\upsilon_{\ell_1} \gg \upsilon_{\ell_2}$ occurs when the waves in region (1) are intermediate between long-waves and deep water waves. Again, the limits of $\alpha_t \Rightarrow 2$ and $\alpha_r \Rightarrow 1$ may be obtained (theoretically) by making $\sqrt{h_2}$ sufficiently small. This set of reflection and transmission coefficients would lie between cases a) and b)

Case 2. $\upsilon_{\ell_1} \ll \upsilon_{\ell_2}$

a)   Long-waves-propagated on both sides of the discontinuity. As before

$$\alpha_t = \frac{2\sqrt{h_1}}{\sqrt{h_1} + \sqrt{h_2}} \tag{15-22}$$

and

$$\alpha_r = \frac{-\sqrt{h_1} + \sqrt{h_2}}{\sqrt{h_1} + \sqrt{h_2}} \tag{15-23}$$

with the change in sign occurring from Equation (5-17) for $\upsilon_{\ell_1} < \upsilon_{\ell_2}$

For $\sqrt{h_1} \ll \cdot \sqrt{h_2}$

and $\alpha_t \Rightarrow 0$

             $\alpha_r \Rightarrow 1$

Since the power is proportional to $A^2 \sqrt{h}$ then, it follows from Equations (15-22) and (15-23) that the transmitted power $\sim \alpha_t{}^2 \sqrt{h_1}$ and the reflected power $\sim \alpha_r \sqrt{h_1}$ for a unit incident amplitude and $\sqrt{h_1} \ll \sqrt{h_2}$. The energy is being carried away at a large energy velocity $\sim \sqrt{h_2}$ and since there is only a certain amount available $\sim \alpha_t{}^2 \sqrt{h_1}$ it follows that the transmitted amplitude must be small.

b) Shallow-water waves propagated in region (1) and deep-water waves propagated in region (2); then:

$$\alpha_t \doteq 2 \frac{\sqrt{h_1}}{\frac{\sqrt{g}}{2\sigma} + \sqrt{h_1}} \tag{15-24}$$

and

$$\alpha_r = \frac{\frac{\sqrt{g}}{2\sigma} - \sqrt{h_1}}{\frac{\sqrt{g}}{2\sigma} + \sqrt{h_1}} \tag{15-25}$$

If $\sqrt{h_1} \ll \frac{\sqrt{g}}{2\sigma}$

then $\alpha_t \Rightarrow 0$ and $\alpha_r \Rightarrow 1$

This limit is approached more slowly than for the case of long waves on both sides of the discontinuity. Again this is a consequence of the greater energy velocity for long waves and thus for equal amounts of power being transmitted into region (2) a larger transmission coefficient is arrived at for the deep-water waves. The energy flux

transmitted into region (2) is proportional to $\alpha_t \, 2 \sqrt{h_1}$ and

that reflected back into region (1) $\sim \alpha_r \sqrt{h_1}$ for $h_1 \ll \dfrac{\sqrt{g}}{2\sigma}$

which is the same result as for the case of long waves on both sides of

the discontinuity.

c) Shallow-water waves propagated in region (1) and waves intermediate

between deep and shallow water waves propagated in region (2). The

theoretical limits of $\alpha_t \to 0$ and $\alpha_r \to 1$ may be obtained

for $\sqrt{h_1}$ sufficiently small. As before the transmitted energy flux

is regulated by the shallower depth as $\sim \alpha_t \, 2 \sqrt{h_1}$ and the reflected

power by the same parameter as $\alpha_r \sqrt{h_1}$.

It is worth noting that for frictionless long-waves the commonly

used matching condition at the discontinuity of a continuous mass flux

is implied using the conditions of a continuous surface streamline and

a continuous energy flux. Looking at these two latter conditions:

Continuous surface:

$$\eta_i + \eta_r \Big|_{x=0^-} = \eta_t \Big|_{x=0^+}$$

Continuous energy flux:

$$\int_0^{h_1} p_{v_1} \, \mu_1 \, dz \Big|_{x=0^-} = \int_0^{h_2} p_{v_2} \, \mu_2 \, dz \Big|_{x=0^+}$$

which, in the hydrostatic or long-wave approximation p_v (AND μ) is constant

throughout the depth and $p_v \simeq \eta$ thus the energy condition gives:

$$(\eta_i + \eta_r) \int_0^{h_1} \mu_1 \, dz \Big|_{x=0^-} = \eta_t \int_0^{h_2} \mu_2 \, dz \Big|_{x=0^+}$$

Using the continuous surface condition gives the result that:

$$\int_0^{h_1} \mu_1 \, dz \Big|_{x=0^-} = \int_0^{h_2} \mu_2 \, dz \Big|_{x=0^+}$$

which is the continuous mass flux condition. Therefore, using two of

the three matching conditions as listed above implies the third provided

the variable part of the pressure is independent of the depth.

For frictionless long-waves, whose energy velocity is proportional

to $\sqrt{h}$, it is seen from Equations (15-19) and (15-20) that the

reflection and transmission coefficients depend only on ratio of the

depths, for any other class of waves this simplification does not hold.

5.4   Comparison between the Frictional and Frictionless Models

The Equations (5-10) to (5-15) defining the reflection and trans-

mission coefficients and phases were solved for a large number of cases

using a computer. The results were then put into the time averaged

power equation (Equation (5-2)) to check for consistency of this equation.

It was found that there was an imbalance between the L.H.S. and R.H.S.

of this equation of a magnitude of at most $(10^{-3})\%$, this was most

probably due to machine round-off error. The cross term was found to be

small even for moderately large values of the frictional coefficient

(C = 2 inches/sec. with T = 1 second and h $\leqslant$ 1 inch) and contributed

at most 2 or 3 percent to the L.H.S. of Equation (5-2). If this cross

term is neglected then:

$$\left(A_i^2 - A_r^2\right) \frac{\left(d_1 \cos \Omega_1 + \frac{\Delta_1}{K_1} \frac{4c}{\sigma h_1} \sin \delta_1\right)}{\Delta_1 K_1} \simeq A_t^2 \frac{d_2 \cos \Omega_2 + \frac{\Delta_2}{K_2} \frac{4c}{\sigma h_2} \sin \delta_2}{\Delta_2 K_2}$$

which by comparison with Equation (3-18b) is obviously:

$$(E_i - E_r)\, v_{e_1} \cong E_t\, v_{e_2}$$

When friction is included and for a given amplitude the energy E is reduced (See Equation (3-11A)) and the energy velocity is reduced (See Figure (9)) below the frictionless case. These reductions, for a constant frictional coefficient, are greatest for shallow water and long period waves.

Therefore, an increase from the frictionless model of the transmission coefficient is predicted when region (2) is shallower than region (1). This can easily be seen by considering the extreme conditions when region (1) is deep enough such that essentially frictionless waves are propagated and when region (2) is moderately shallow such that the effects of friction are important. Therefore, the energy incident to the discontinuity is approximately the same as in the frictionless case, but less energy for the same geometry can be transmitted across the discontinuity because of the decrease of energy flux. This would be analogous to considering frictionless waves on both sides of discontinuity and then reducing the shallower depth to reduce the energy flux which in turn would imply an increase in the transmitted amplitude. There is a corresponding increase in the reflection coefficient. The limiting cases of $\alpha_t = 2$ and $\alpha_r = 1$ are found as in the frictionless model, and these limits are approached more rapidly because of the greater reduction

of the energy flux in the shallower than the deeper region.

On the other hand, a reduction in the transmitted coefficient is found for $h_1 < h_2$. This again is a consequence of the greater reduction of the energy flux in the shallower water than in the deeper. The following example illustrates the point. If the amplitude of the incident wave is adjusted such that the incident energy flux at the discontinuity is the same as for the frictionless case, then the incident wave amplitude for the frictional model must be larger than for the frictionless. If region (2) is deep enough so that the energy flux is essentially the same as the frictionless case then the frictionless and friction transmitted amplitudes are the same. From these two statements it follows that $\left(\frac{A_t}{A_i} = \alpha_t \right)_{c=0}$ is less than $\left(\frac{A_t}{A_i} = \alpha_t \right)_{c \neq 0}$ and a corresponding increase in α_t results. The limiting cases of $\alpha_t = 0$ and $\alpha_r = 1$ are again approached more rapidly in the frictional than the frictionless case.

The complex reflection and transmission coefficients $(\alpha_r^c$ and $\alpha_t^c)$ were plotted in a polar co-ordinate system for various depth ratios. Figures (23) and (24) for α_r^c and α_t^c show that, for even comparatively large friction resulting from C = 2 inches/sec. with T = 1 sec. and h = 1 inch, the reflected phase is less than 20 degrees from the principle axis and the transmitted phase is less than 6 degrees.
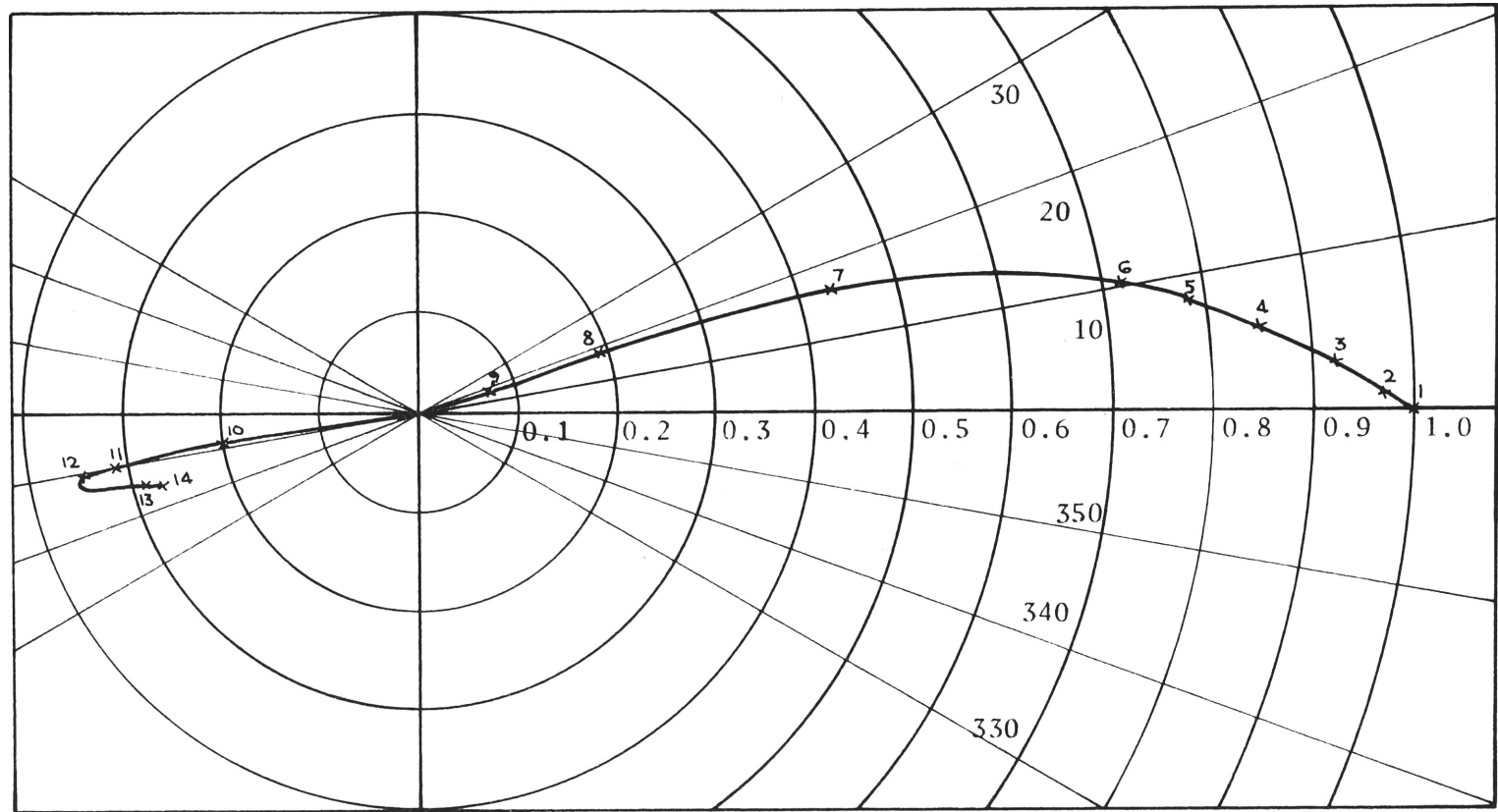
FIGURE 23: THE COMPLEX REFLECTION COEFFICIENT $\left(a_r^c = a_r e^{i \gamma_r} \right)$

		Points	h_2 (inches)	Points	h_2 (inches)	Points	h_2 (inches)
h_1	= 1.0 inches						
T	= 1.0 seconds	1	~ 0	6	.10	11	5.0
		2	.010	7	.25	12	10.0
C	= 2.0 inches/sec.	3	.025	8	.50	13	25.0
		4	.050	9	.75	14	∞
		5	.075	10	2.5		
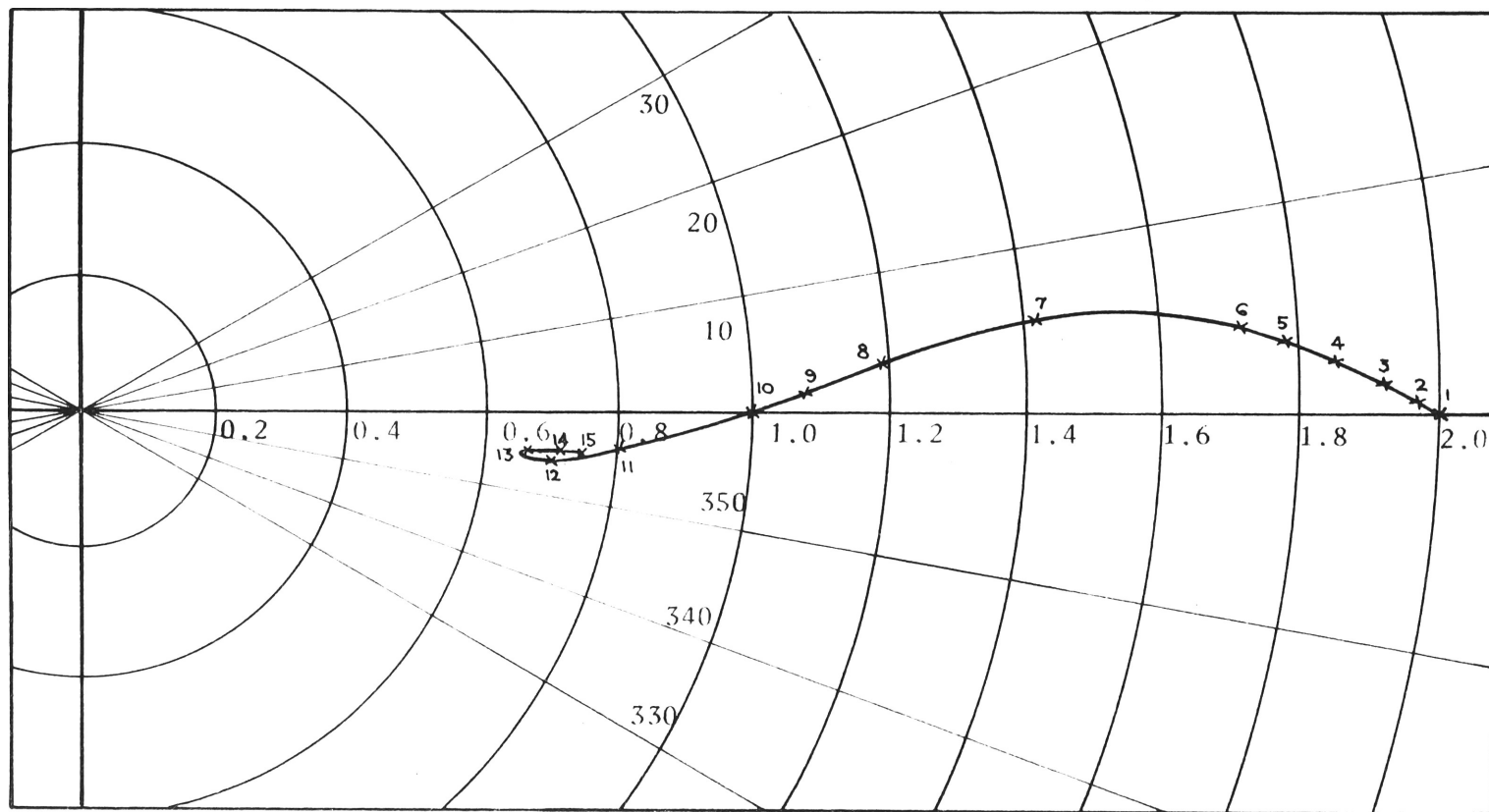
FIGURE 24: THE COMPLEX TRANSMISSION COEFFICIENT $(a_t^c = a_t e^{i\gamma_t})$

h_1 = 1.0 inches	Point	h_2 (inches)	Point	h_2 (inches)	Point	h_2 (inches)
T = 1.0 seconds	1	~ 0	6	.10	11	5.0
C = 2.0 inches/sec.	2	.010	7	.25	12	10.0
	3	.025	8	.50	13	25.0
	4	.050	9	.75	14	50.0
	5	.075	10	2.5	15	∞

For long-waves Equation (3-16) defining the average energy flux becomes (AT $x = 0$):

$$P_{AVG.} = \frac{\rho A^2 g}{\sqrt{2}} \sqrt{gh} \left\{ \frac{(1 + \sqrt{H'})^{1/2} + \frac{c}{\sigma h}(-1 + \sqrt{H'})^{1/2}}{H'} \right\}$$

where

$$H' = 1 + \left(\frac{c}{\sigma h}\right)^2$$

Therefore the transmission and reflection coefficients are no longer the same for constant depth ratios as was found in the frictionless long-wave model.

The reflection and transmission coefficients were plotted on Figures (25) and (26) for the frictionless model and on Figures (27) and (28) using a frictional constant of 2 inches/sec. A scale on the abscissa of $\sqrt[3]{h_2/h_1}$ was used to give an expanded scale for $h_2/h_1 < 1$ and a contracted scale for $h_2/h_1 > 1$. The asymptotic values of the coefficients ($h_2 \Rightarrow \infty$) is shown on the far right hand sides of the diagrams.

Some comparisons between the frictionless and the frictionless models brought out by these diagrams are:

(i) For $h_1 > h_2$

    (a) $(\alpha_t)_o \leqslant (\alpha_t)_f$ subscript o refers to the frictionless case and subscript f to the frictional.

(b)   the limiting values of $\alpha_t \to 2$ and

$\alpha_r \to 1$ are approached more nearly by

the frictional than the frictionless model.

(c)   for shallow depths in h_1 and thus in h_2 the

$(\alpha_t)_f$ and $(\alpha_r)_f$ values are not

constant for the same depth ratio as are

the $(\alpha_t)_o$ and $(\alpha_r)_o$ values (except

in the extreme cases of h_1 $\Rightarrow 0$).

(d) $(\alpha_r)_o \leq (\alpha_r)_f$

(e) $(\alpha_r)_f \neq 0$ for any h_1 and $\dfrac{h_2}{h_1}$,

whereas $(\alpha_r)_o$ can vanish for particular

h_1 and h_2/h_1

(ii) For $h_1 < h_2$

(a) $(\alpha_t)_o \geq (\alpha_t)_f$

(b)   the limiting values of $\alpha_t \to 0$ and

$\alpha_r \to 0$ are approached more

nearly by the frictional model than the

frictionless.

(c) $(\alpha_r)_o \leq (\alpha_r)_f$

(d) $(\alpha_r)_f \neq 0$ for any h_1 and h_2/h_1 whereas $(\alpha_r)_o$

can equal zero for particular depth combinations.

These findings have been explained in detail previously in the text.
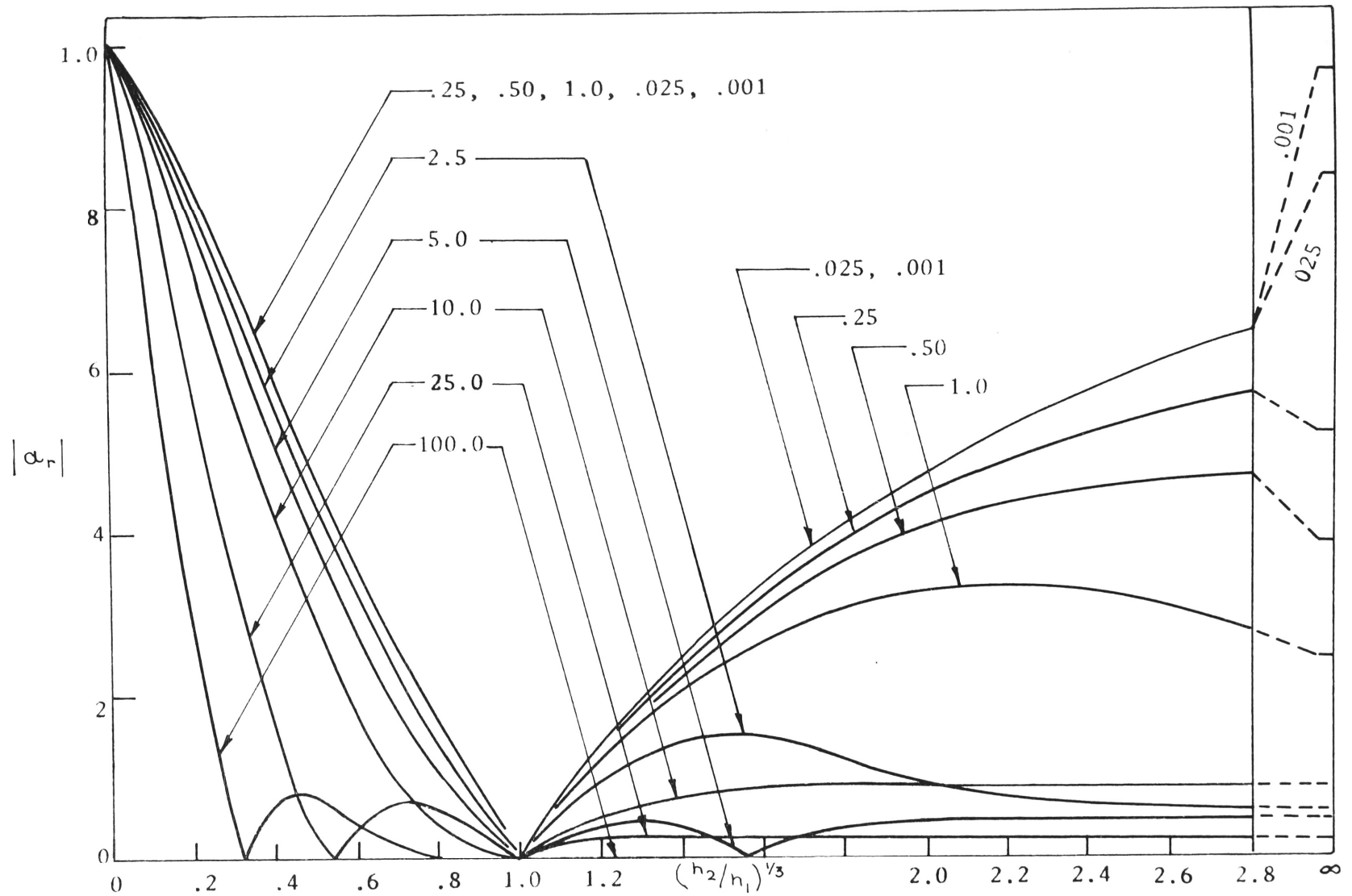
FIGURE 25: THE REFLECTION COEFFICIENTS FOR C = 0 in/sec. AND T = 1 sec.

(The numbers on the figure refer to the depth h_1)
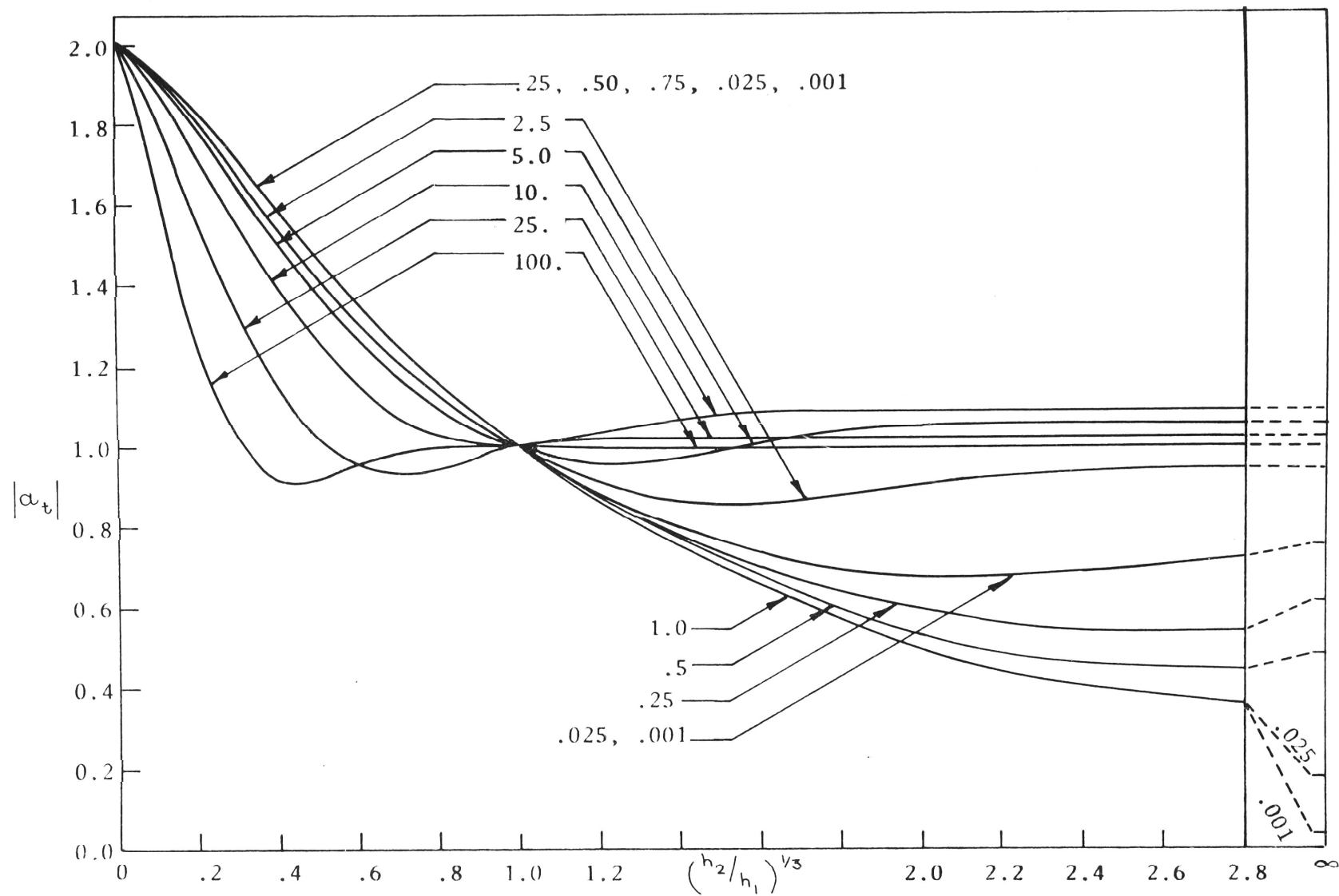
FIGURE 26: THE TRANSMISSION COEFFICIENTS FOR C = 0 in/sec. AND T = 1 sec.

(The numbers on the figure refer to the depth h_1)
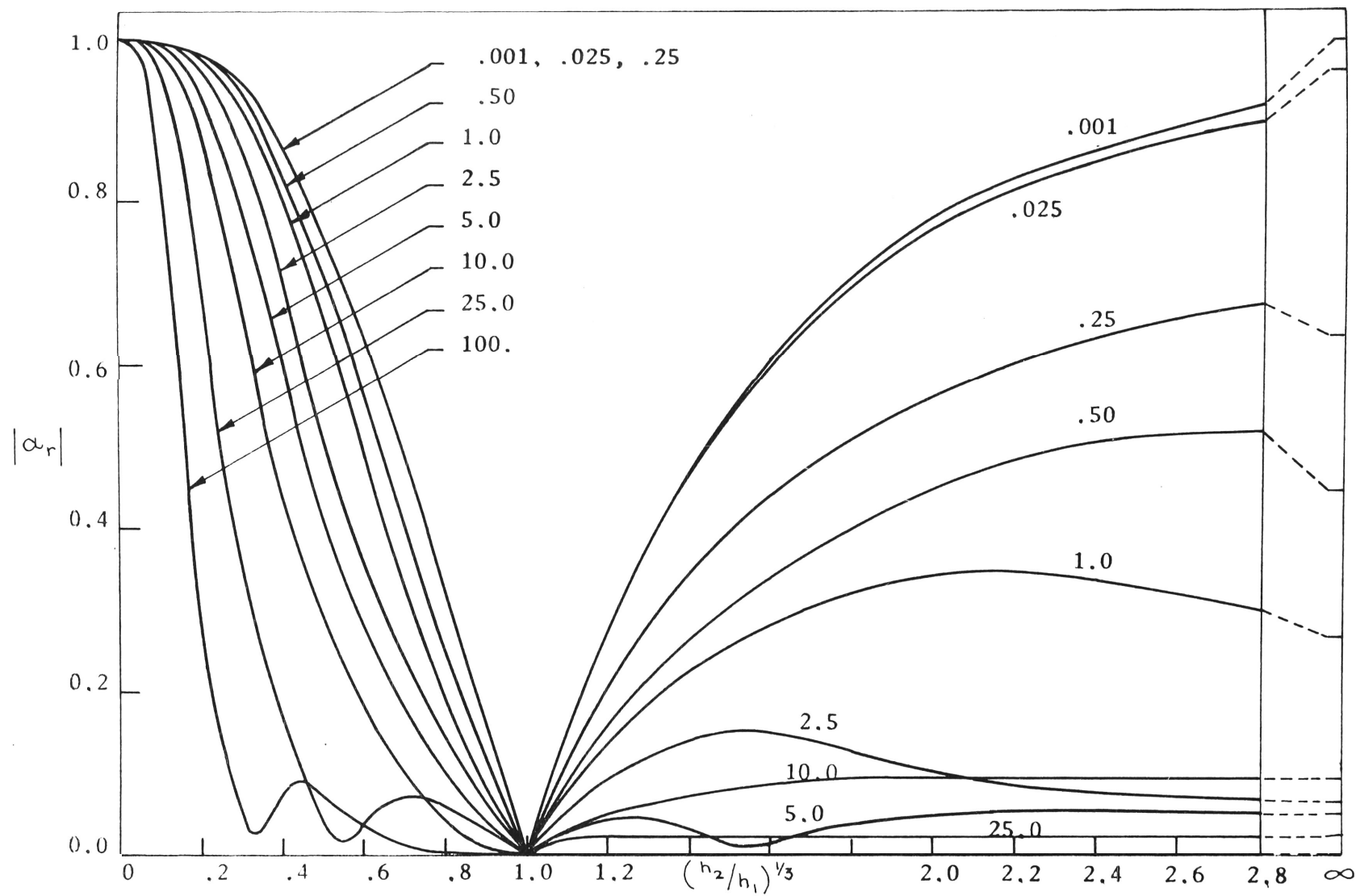
FIGURE: 27   THE REFLECTION COEFFICIENTS FOR C = 2in/sec. AND T = 1 sec.

(The numbers on the figure refer to the depth h_1)

FIGURE 28: THE TRANSMISSION COEFFICIENTS FOR C = 2in/sec. AND T = 1 sec.
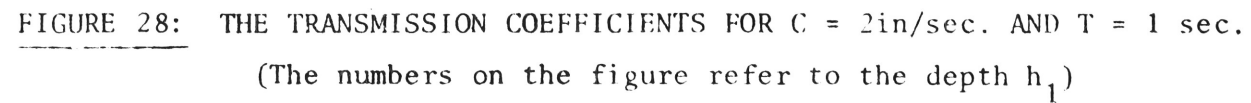
(The numbers on the figure refer to the depth h_1)

5.5 The Reflection and Transmission Coefficients for Oceanographic Situations

Two examples of the reflection and transmission coefficients for oceanographic situations will be given. The first corresponds to the case of tidal waves with periods greater than a few hours being incident from oceanic depth onto a flat shelf of uniform depth. The second corresponds to ocean swell incident form deep water onto a level, shallow reef or ledge. In both cases the assumption is made that the transmission zone from the deeper to the shallower depths is short enough so that it may be considered a vertical wall.

In the first case a value for the frictional coefficient of 094 inches/sec. was used. This is the value found by Weenink (1958) for the southern North Sea and was used by Heaps (1969) in his numerical sea model. With h_1 = 12,000 feet and values for h_2 of 400 feet and 40 feet the transmission and reflection parameters were calculated and compared with the frictionless model.

Table (11) lists the results from which it can be seen that the presence of friction has only a very small effect on the reflection and transmission coefficients.

A value for the linear frictional constant for ocean swell was found by using a quadratic friction coefficient. Following the procedure given by Ippen (1966) the work done over a quarter-period for

the quadratic and the linear friction effects were equated and the
linear friction coefficient C was evaluated.

The bottom shear stress is defined as:

$$\tau_q = f^* \rho \mu_b^2 \qquad \text{(Putnam and Johnson (1949))}$$

for the quadratic friction where f^* is the bottom friction
factor and $\tau_L = C \rho \mu_b$ for the linear friction.

The work done per unit area in a quarter wave period is:

$$W = \int_0^{\pi/2\sigma} \tau \mu_b \, dt$$

Letting $\mu_b = \mu_{MAX}(x) \cos \sigma t$ and equating the work done by
the quadratic and linear friction terms gives:

$$\int_0^{\pi/2\sigma} f^* \rho \mu_b^3 \, dt = \int_0^{\pi/2\sigma} C \rho \mu_b^2 \, dt$$

or:

$$\mu_{MAX} \int_0^{\pi/2\sigma} \cos^3 \sigma t \, dt = C \int_0^{\pi/2\sigma} \cos^2 \sigma t \, dt$$

yields:

$$C = \frac{8}{3\pi} \mu_{MAX} f^*$$

Since μ_{MAX} is dependant on the wave height, H, it is expected
that C will change as the wave decays, therefore in using the linear
friction term a representative value of μ_{MAX} must be used.

TABLE 11

REFLECTION AND TRANSMISSION COEFFICIENTS

AND PHASES CORRESPONDING TO TIDAL PERIODS

Wave Period hours	C = .094in/sec.				C = 0.0in/sec.	
	α_r	γ_r radians	α_t	γ_t radians	α_r	α_t
2	.893	.013	1.893	.006	.891	1.891
6	.904	.031	1.904	.014	.891	1.891
12	.923	.040	1.923	.019	.891	1.891
24	.945	.039	1.945	.019	.891	1.891
2	.691	.004	1.691	.002	.691	1.691
6	.692	.012	1.692	.005	.691	1.691
12	.693	.024	1.693	.010	.691	1.691
24	.698	.047	1.698	.019	.691	1.691

$h_1 = 12,000$ ft.

$h_2 = 40$ ft.

$h_1 = 12,000$ ft.

$h_2 = 400$ ft.

Iwagaki and Kakinuma (1967) found experimentally that f^* varied between .027 and .091 using a method based onsignificant wave heights. In particular they found a value of $f^* = .06$ using the following data at two stations:

Station 1.

H = 7.6 feet

T = 13.0 seconds

h = 44.4 feet

Station 2.

H = 7.1 feet

T = 14.0 seconds

h = 32.2 feet

It is sufficient for the purposes here to take average values for these parameters to calculate C. Since the wavelength is $>$ 400 feet for these periods and depths the long-wave representation of u_{MAX} may be used, then:

$$C \simeq \frac{4}{3\pi} f^* H_{AVG.} \sqrt{\frac{g}{h_{AVG.}}}$$

The frictionless form of u_{MAX} was used for convenience and the error introduced by doing so is very small compared with the uncertainty in the other parameters. The value for C is then found to be:
$$C \simeq 2.0 \text{ inches/sec.}$$
Using this value and equations (3-3b) and (3-4b) results in:

$$k \simeq .0133 \text{ feet}^{-1}$$
$$\text{and} \quad \alpha \simeq 6.2 \times 10^{-5} \text{feet}^{-1}$$

Thus, it takes in the order of 3 miles for the waves to decay by a factor of $1/e$, and the value for k is essentially unchanged from its frictionless size.

Using values for h_1 of 100 feet and 400 feet with h_2 = 7.5 feet and 12.5 feet and C = 2.0 inches/sec. values for the transmission and reflection parameters were found and compared with the frictionless results. The results in Table (12) show that the presence of friction produces only a very small change in these parameters.

TABLE 12

REFLECTION AND TRANSMISSION COEFFICIENTS AND PHASES

CORRESPONDING TO OCEAN SWELL PERIODS

Wave Period seconds	C = 2.0 inches/sec.				C = 0.0 inches/sec.		
	α_r	γ_r radians	α_t	γ_t radians	α_r	α_t	
10	.345	.021	1.345	.005	.345	1.345	h_1 = 100 ft.
15	.477	.020	1.477	.006	.476	1.476	h_2 = 7.5 ft.
20	.520	.023	1.520	.008	.519	1.519	
10	.160	.031	1.160	.004	.160	1.160	h_1 = 400 ft.
15	.362	.019	1.362	.005	.362	1.362	
20	.512	.015	1.512	.005	.511	1.511	h_2 = 12.5 ft.

CHAPTER 6

EXPERIMENTS INVOLVING WAVES INCIDENT NORMALLY

TO A DEPTH DISCONTINUITY

Theoretical results developed in Chapter 5 indicate that the presence of a reasonable amount of friction is unlikely to have an appreciable effect on the magnitude of the transmission and reflection coefficients. The effect it will have is, by frictional damping, to reduce the heights of the waves arriving at the step from a generation region and similarly to reduce the heights of the transmitted and reflected waves at any distance from their generation region (that is, at the step). Experiments were carried out to determine the transmission and reflection coefficients using a moderately viscous fluid. These results were compared with the theoretical coefficients to determine if the presence of friction produced a marked loss of energy at the step. No energy loss term at the step was included in the theoretical development in Chapter 5. The horizontal extent of the local disturbance in the vicinity of the step was also investigated.

6.1 The Reflection and Transmission Coefficient

To obtain values for the reflection and transmission coefficients it was necessary to measure the heights of the reflected and transmitted waves at some distance from the step (situated at x = o) and then deduce the wave heights at the step as if no local disturbances were present. Then, knowing the incident wave height at the step, the reflection and

and transmission coefficients could be found.

Each experiment was run in two parts, the first with the movable bottom of the flume level with the fixed bottom and the second part with the movable bottom at a level above or below the fixed bottom.

Measurements of wave heights along the flume in the first part determined the incident wave height at the step and the decay coefficient. From measurements with $h_1 \neq h_2$ the transmitted wave height could be found directly and the reflected wave height deduced from the composite wave existing in region (1).

In region (1) the combined surface profile is given by the sum of the incident and reflected waves. That is:

$$\eta_1 = H_i e^{-\alpha_1 x} \cos(k_1 x - \sigma t) + H_r e^{\alpha_1 x} \cos(k_1 x + \sigma t - \gamma_r)$$

expanding and collecting terms in the time dependance gives:

$$\eta_1 = \cos \sigma t \left\{ H_i e^{-\alpha_1 x} \cos k_1 x + H_r e^{\alpha_1 x} \cos(k_1 x - \gamma_r) \right\}$$

$$+ \sin \sigma t \left\{ H_i e^{-\alpha_1 x} \sin k_1 x - H_r e^{\alpha_1 x} \sin(k_1 x - \gamma_r) \right\}$$

$$= a(x) \cos \sigma t + b(x) \sin \sigma t$$

$$= \sqrt{a^2 + b^2} \cos(\sigma t - \theta)$$

so:

$$\eta_1 = H(x) \cos(\sigma t - \theta)$$

The square of the "height" of the composite wave at a position x is then:

$$H^2(x) = H_i^2 e^{-2\alpha_1 x} + H_r^2 e^{2\alpha_1 x} + 2 H_i H_r \cos(2k_1 x - \gamma_r)$$

Solving for H_r gives:

$$H_r = \frac{- H_i e^{-\alpha_1 x} \cos(2k_1 x - \gamma_r) \pm \sqrt{H^2 - (H_i e^{-\alpha_1 x} \sin(2k_1 x - \gamma_r))^2}}{e^{\alpha_1 x}}$$

$$(6-1)$$

That the plus sign in front of the radicle must be used when $\cos(2k_1 x - \gamma_r)$ is positive and the minus sign when $\cos(2k_1 x - \gamma_r)$ is negative can be seen from the following example. Consider friction-less waves incident to a permeable barrier set at x = o (with a constant fluid depth everywhere) then $H_r < H_i$. It is also assumed that $\gamma_r = 0$ which is the value which would result from complete reflection at a solid barrier. Then it follows that a physically acceptable solution -

at $2kx_1 = 0$ is $H_r = - H_i + H$

and at $2k_1 x = \pi$ is $H_r = H_i - H$

Thus in the first instance the sign in front of the radicle must be $+$ and in the second $-$.

This ambiguity in sign may be overcome by rewriting (6-1) as:

$$H_r = \frac{- H_i e^{-\alpha_1 x} \cos^2(2k_1 x - \gamma_r) + \sqrt{[H^2 - (H_i e^{-\alpha_1 x} \sin(2k_1 x - \gamma_r))^2] \cos^2(2k_1 x - \gamma_r)}}{e^{\alpha_1 x} \cos(2k_1 x - \gamma_r)}$$

$$(6-2A)$$

for $\cos(2k_1 x - \gamma_r) \neq 0.$

and as:

$$H_r = \frac{\sqrt{H^2 - (H_i e^{-\alpha_1 x})^2}}{e^{\alpha_1 x}} \qquad (6\text{-}2B)$$

for $\cos(2k_1 x - \gamma_r) = 0$

The reflection coefficient is then: $\quad \alpha_r = \dfrac{H_r}{H_i}$

By measuring H and $H_i e^{-\alpha_1 x}$ at two locations, $x^{(1)}$ and $x^{(2)}$, H_r may be eliminated from Equation (6-1) to give:

$$-H_i e^{-\alpha_1 x^{(1)}} \cos(2k_1 x^{(1)} - \gamma_r) \pm \sqrt{(H^{(1)})^2 - (H_i e^{-\alpha_1 x^{(1)}} \sin(2k_1 x^{(1)} - \gamma_r))^2}$$

$$= e^{\alpha_1 (x^{(1)} - x^{(2)})} \left\{ -H_i e^{-\alpha_1 x^{(2)}} \cos(2k_1 x^{(2)} - \gamma_r) \right. \qquad (6\text{-}3)$$

$$\left. \pm \sqrt{(H^{(2)})^2 - (H_i e^{-\alpha_1 x^{(2)}} \sin(2k_1 x^{(2)} - \gamma_r))^2} \right.$$

Thus, in theory, it is possible to deduce the value for γ_r and use this value in Equation (6-2) to determine A_r. But, in actual fact, the uncertainty in determining $2k_1 x$ is generally at least as great as the value for the phase γ_r. The following numerical example illustrates this point. Suppose the uncertainties in the wave period, distance and fluid depth have the rather optimistic values of .5%, .2% and 1.5% respectively; then for frictionless long-waves:

$$2k_1 x \simeq \frac{4\pi x}{T\sqrt{gh_1}} \pm 1.45\%$$

Using   x = 10 inches

         T = 1 second

and h_1 = 1 inch

gives $2 k_1 x \simeq$ 6.44 ± .10, thus the uncertainty in $2 k_1 x$ is

approximately the same as the phase angle γ_r . Therefore, in view of

the added uncertainties in the measurement of the wave heights $H_i e^{-\alpha_1 x}$

and H it is not expected that this phase will be measureable with the

experimental equipment in use.

The fixed flume bottom was set level by adjustment of the set

screws supporting the flume. The brass rails supporting the instruments

were set to a level position over the whole flume as outlined in

Appendix 5 by using the still fluid surface as datum. The movable

bottom was levelled by use of a vernier point gauge mounted on the

instrument carriage. The point gauge (with the tip blunted so as not to

penetrate into the flume bottom) was moved to a position above the fixed

bottom and the vernier scale set to a convenient scale mark. The

instrument was then moved to one corner of the movable bottom and the

tip of the point gauge set on the bottom so that it moved vertically as

the bottom was moved. Adjustments of the set screws supporting the

movable bottom were made until the vernier scale gave the desired

position for this portion of the bottom with respect to the fixed

bottom. The bottom was set in this manner for the other three corners;

the process was then repeated until all four corners gave the same reading on the vernier scale. Since the movable bottom was always completely submerged, moving it from level to level did not change the depth over the fixed portion of the bottom thus making it unnecessary to add or subtract fluid while the experiment was in progress.

The experimental conditions were similar to those used for the runs described in Chapter 4. That is, 77% and 55% glycerol mixtures were used for the most part, the fluid was thoroughly mixed before each run and the fluid and air temperatures were kept to within ±.2 degrees C. The wave period was kept constant at T = .93 seconds for all the runs.

A detailed account of a typical experiment to determine the transmission and reflection coefficients will be given.

The fluid (55% glycerol) was thoroughly mixed and then poured into the flume. The fluid depth over the fixed bottom was measured (.57 inches) with a vernier point gauge and the movable bottom set at the same level as the fixed. Waves were generated using the quick start mechanism with the paddle at the same initial position for each wave train. This latter point was useful when comparing these wave forms with those produced when a reflected component from the step was present. The wave heights were measured at various points along the central axis of the flume. In this run a single probe method as described in Section (4.2) was used. It was unnecessary to obtain absolute wave heights since

only the ratios of the reflected and of the transmitted heights relative
to the incident height was required. The wave heights were plotted as
a function of distance along the flume on semi-log paper (Figure (29)).
The position of the step (x=o) corresponding to the measured distance
along the flume was found be setting the probe wires directly above
the position of the step and reading the lateral scale, in this case
8.88 feet. This position was not the same for the two probes used
interchangeably throughout the runs as the probes were of slightly
different construction. From Figure (29) it can be seen that H_i at
the step is 25.9 scale units and that the decay coefficient is .0151
$(inches)^{-1}$.

The movable bottom was set 0.30 inches above the fixed one so
that the measured depth in region (2) was 0.27 inches. Finite wave
trains were generated as for the incident wave determination and wave
heights were measured at various points along the flume. The measure-
ments on the side of the step toward the wave generator (region (1))
were taken at the same points at those taken when $h_1 = h_2$ so that the
wave forms could be compared.

The Reflection Coefficient: The wave heights, H, were measured at
various locations in region (1) with $h_1 \neq h_2$ and compared with the
heights, $H_i e^{-\alpha_1 x}$, measured at the same position without the step.
Figure (30) shows the two wave traces obtained with and without the step,
the traces have been redrawn such that they are coincident with one
another at the start of the wave train. The standard wave height measure-
ment was the same, in this case, for both experimental wave measurements,

thus no correction to these wave heights was necessary when comparing them. This figure also shows that a constant wave height is reached after 2 or 3 cycles of the wave generator. The reflection coefficient was calculated using Equation (6-2A,B) and the decay coefficient previously obtained. Using the theoretical value of γ_r = .09 radians results in α_r = .20.

Several other sets of measurements of wave heights were taken and the reflection coefficient calculated for each set. These results are listed in Table (13), the average value of 0.21 compares favourably with the calculated result of 0.19. The latter result was found using Equation (5-11) with the effective depths of h_1 = 0.53 inches and h_2 = 0.24 inches and a value for C = 0.21 inches/second which had previously been determined from the decay coefficient. If C is taken as zero the calculated reflection coefficient is within 1.5% of the value calculated when C = 0.21 inches/second. The estimated uncertainty in the experimental value for α_r is about ±20%; this rather large value is a consequence of the relatively small difference between the wave heights found with and without the step as well as the uncertainties in the parameters used in the determination of the wave number.

Transmission Coefficient: The presence of local disturbances near the step did not allow the transmitted height to be determined by direct measurements at this point. It was assumed that this height could be deduced by knowing the transmitted wave heights at some distances away

$$h_1 = h_2 = .53 \text{ inches}$$

$$H_i = 25.9 \text{ scale units}$$
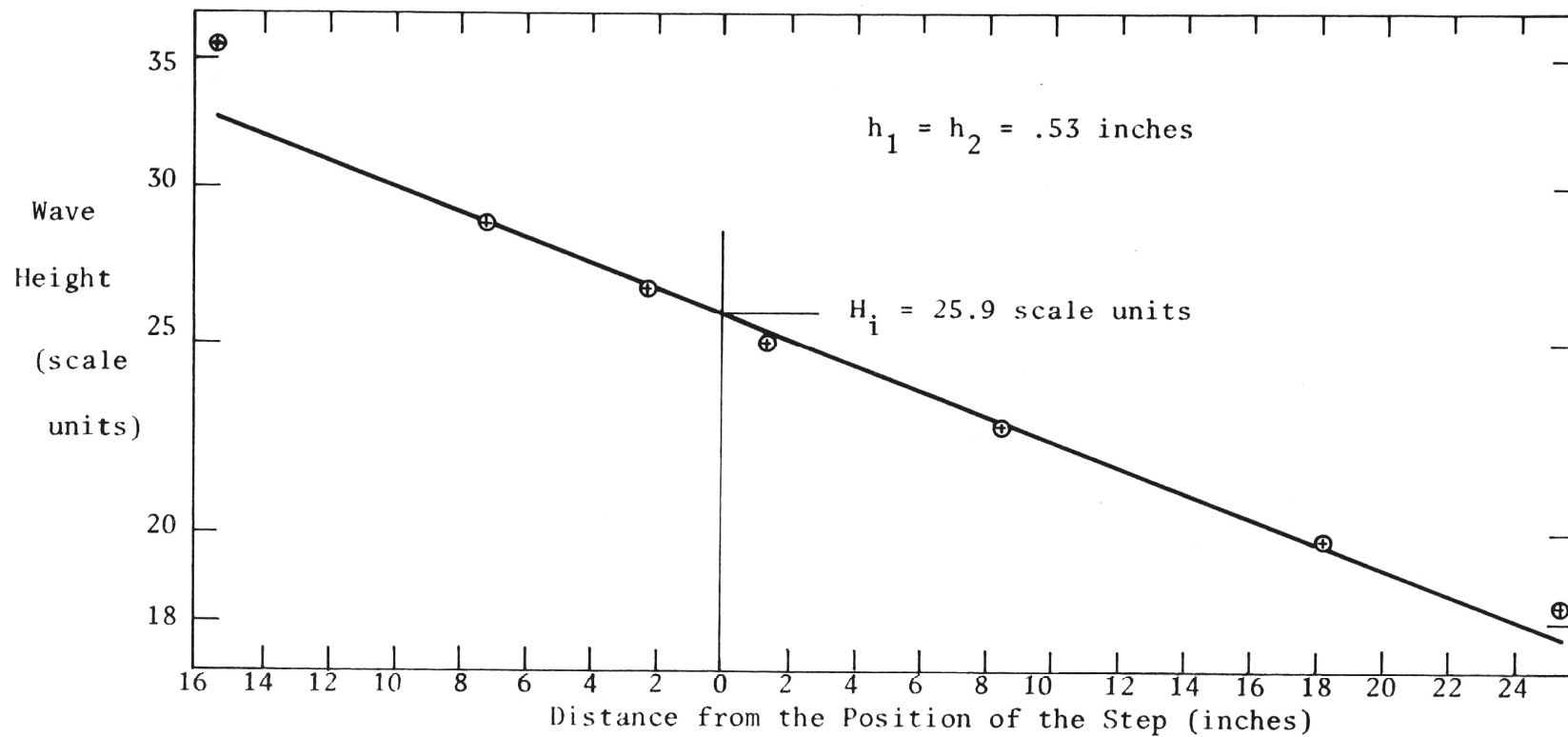
FIGURE 29: VARIATION IN THE INCIDENT WAVE HEIGHT AS A FUNCTION OF THE
DISTANCE FROM THE POSITION OF THE STEP.
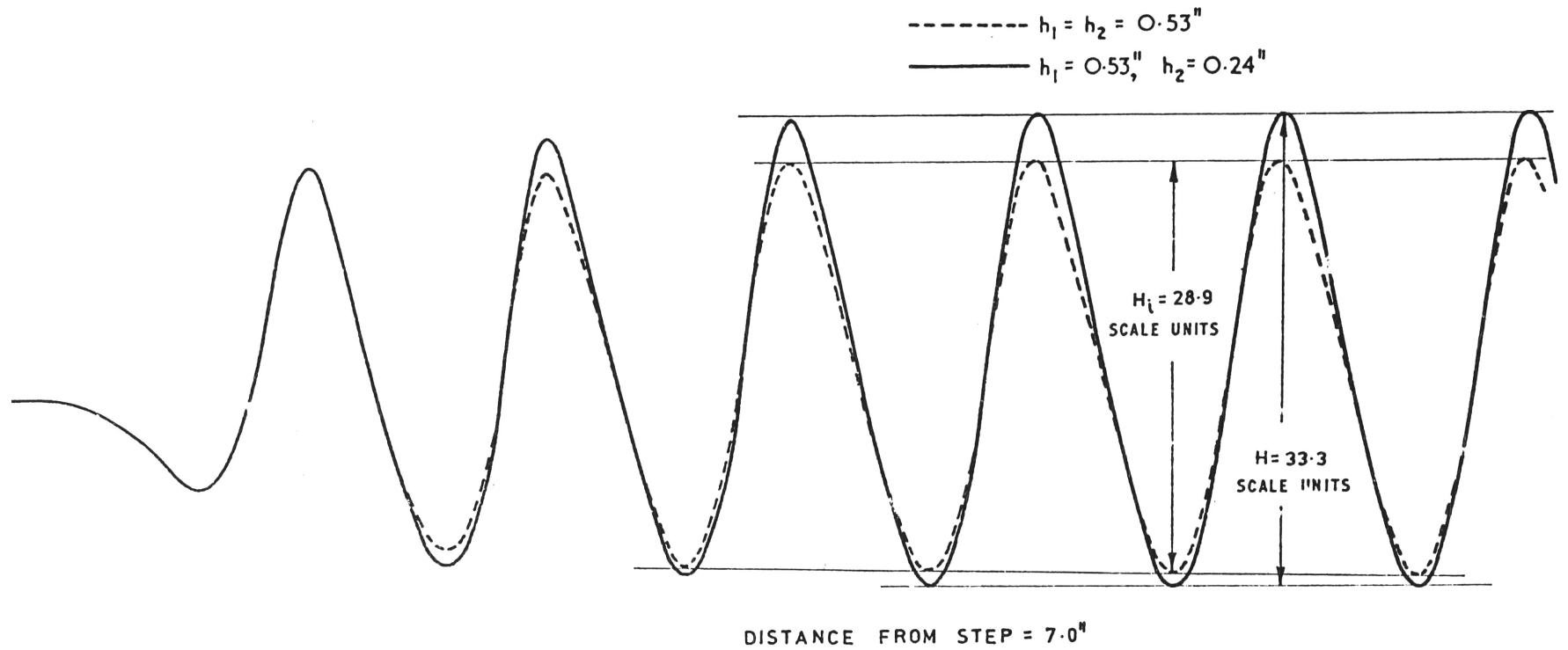
FIGURE 30: COMPARISON OF THE WAVE PROFILES IN REGION ①
WITH AND WITHOUT THE STEP.

TABLE 13

THE MEASURED WAVE HEIGHTS AT VARIOUS POSITIONS IN

REGION (1) AND THE CORRESPONDING REFLECTION COEFFICIENTS

Position on Tank feet	Wave Height with $h_1 = h_2$ scale units	Wave Height $h_1 \neq h_2$ scale units	Reflection Coefficient α_r	
8.70	27.6	24.8	.24	⎫ Trial
8.30	28.9	33.3	.20	⎬ 1
7.60	35.8	32.8	.24	⎭
8.70	27.1	24.7	.20	⎫ Trial
8.30	29.2	33.4	.18	⎬ 2
7.60	35.2	32.8	.20	⎭

Average: .21

Position of Step: 8.88 foot mark

h_1 = .53 inches

h_2 = .24 inches

from the step. Plotting the measured heights against the distance from the step on semi-log paper (Figure (31)) and extrapolating the resulting straight line backwards gives the transmitted height as 31.0 scale units. The transmission coefficient is then:

$$\alpha_t = \frac{31.0 \text{ scale units}}{25.9 \text{ scale units}} = 1.20$$

Using Equation (5-14) with effective depths of h_1 = .53 inches and h_2 = .24 inches and a frictional constant of C = 0.21 inches/second results in a compatible value of α_t = 1.19. With C = 0.0 inches/second the result is within .15% of that using the value for C given above. The uncertainty in the measured value for α_t is less than about ±4%, this relatively small value is a consequence of the coefficient being determined directly from the intercepts of two straight lines fitted to a number of experimental points. Suppose H_i is decreased and H_t is increased by .5 scale units (which is a pessimistic value of the uncertainty in each) then α_t =1.16 which differs from the earlier result by only about 3%.

A number of other depth ratios and other fluids were used and the reflection and transmission coefficients obtained as described above. These results are shown in Figure (32) where the coefficients have been plotted against the ratio $\left| \frac{\omega_1}{\omega_2} \right|$ defined following Equation (5-9A). As pointed out previously this ratio is the ratio of the energy (or group) velocities when friction is neglected. There is generally fair

agreement between these results and the results predicted from
Equations (5-11) and 5-14). The large variation in the value for the
frictional coefficient for the same fluid is a consequence of the
different temperatures of the fluid from run to run; the range was
from about 25 degrees C. to 10 degrees C. which over this range,
produces a change in the kinematic viscosity from .064 in.^{2}/sec. to
.168 in.^{2}/sec. (Rubber Handbook of Chemistry and Physics (1962)).

The experimental results are tabulated in Table (14) and compared
with theoretical results found for the coefficients using a value for
$C \neq 0$ and for $C = 0$. For most cases the difference between these two
calculated values is small and less than the expected uncertainty in
the experimental results. The cases where friction does significantly
change the predicted value for the reflection and transmission
coefficients are listed at the bottom of the table. From these results
it can be seen that there is an increase in the experimental trans-
mission coefficient as predicted by the theory but this increase is
larger than expected; due to the large errors in determining the
reflection coefficient ($\sim$ 20%) the results are inconclusive as to the
effects of friction.

6.2   Estimation of the Energy Loss in the Vicinity of the Step

It is expected that there will be some loss of energy in the
vicinity of the step caused by secondary effects in this region. To
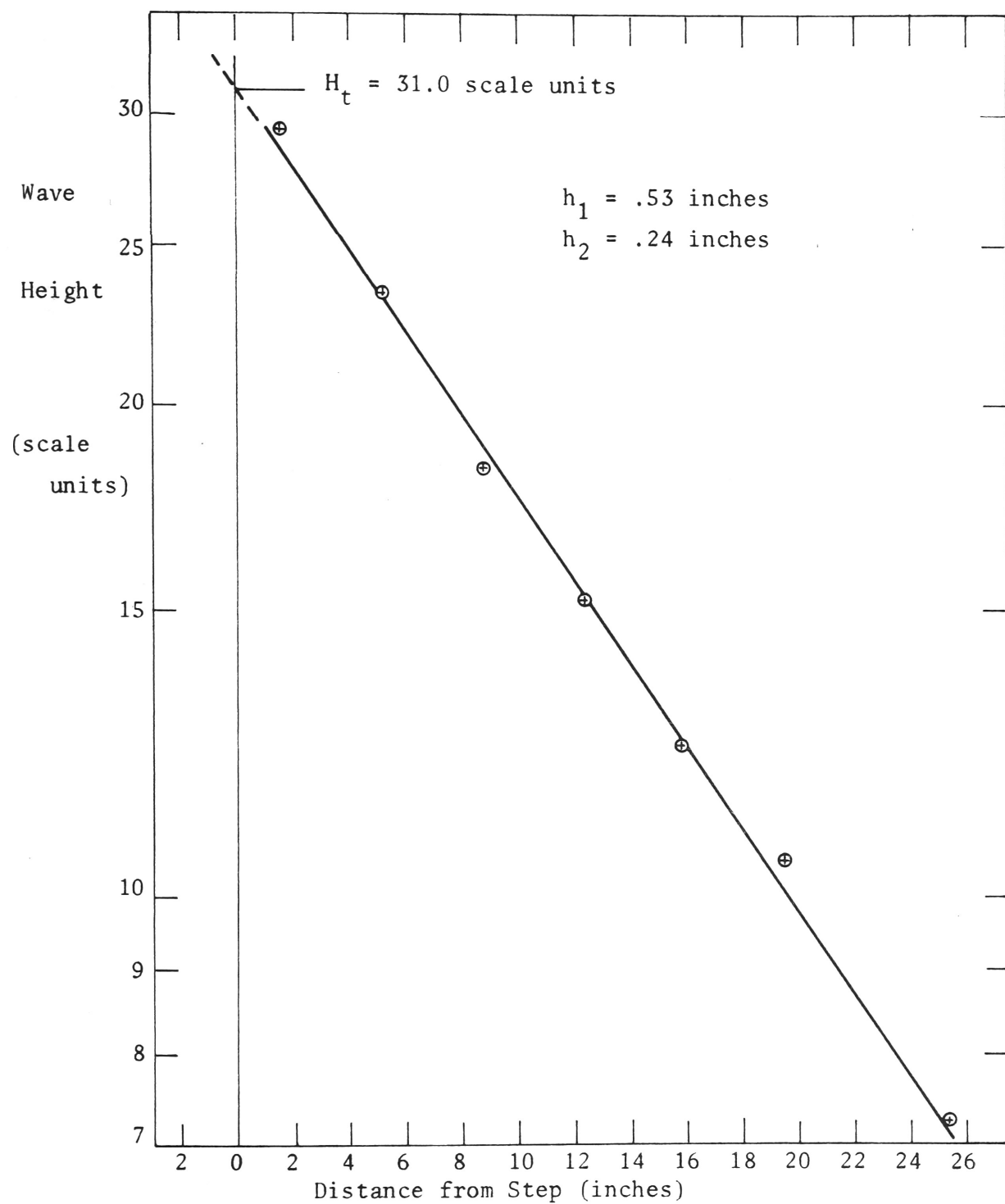
FIGURE 31:   VARIATION IN THE TRANSMITTED WAVE HEIGHT AS A
FUNCTION OF THE DISTANCE FROM THE STEP
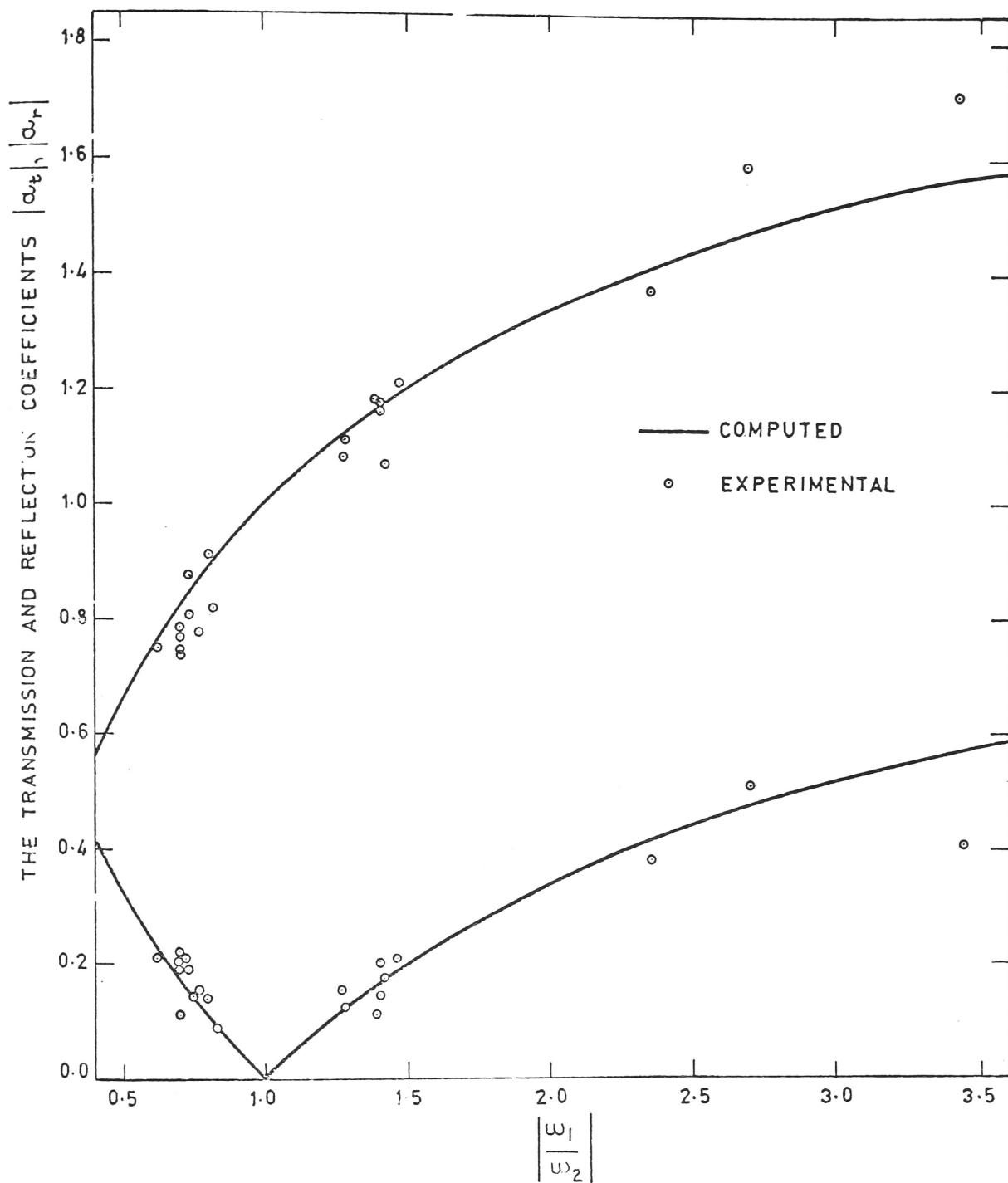
FIGURE 32: THE TRANSMISSION AND REFLECTION COEFFICIENTS
VERSUS THE FUNCTION $\left|\frac{\omega_1}{\omega_2}\right|$

TABLE 14 SUMMARY CALCULATED AND EXPERIMENTAL RESULTS FOR THE TRANSMISSION AND REFLECTION COEFFICIENTS

Fluid *	C Friction Constant in/sec.	h_1 L.H. Depth inches	h_2 R.H. Depth inches	a_t Transmission Coefficient Measured	Calculated C≠0	C=0	a_r Reflection Coefficient Measured	Calculated C≠0	C=0	Reflected Phase Calculated	$\left\|\frac{\omega_i}{\omega_2}\right\|$ Calc.	Energy Deficit %
1	0.17	0.47	1.01	0.788	0.835	0.835	0.22	0.17	0.17	-3.10	0.70	6.9
1	0.17	0.28	0.47	1.18	1.17	1.17	0.14	0.17	0.17	0.04	1.40	-1.6
2	0.36	0.36	0.76	0.735	0.831	0.833	0.19	0.17	0.17	-3.04	0.70	21.7
2	0.29	0.36	0.76	0.744	0.832	0.833	0.19	0.17	0.17	-3.05	0.70	17.7
2	0.26	0.51	1.01	0.806	0.845	0.845	0.19	0.16	0.16	-3.08	0.73	7.4
2	0.34	0.56	1.06	0.880	0.856	0.856	0.14	0.14	0.14	-3.07	0.75	-4.3
2	0.22	0.51	0.89	0.772	0.868	0.868	0.15	0.13	0.13	0.10	0.77	20.6
2	0.40	0.71	1.21	0.912	0.882	0.881	0.14	0.12	0.12	-3.07	0.80	-5.0
2	0.32	0.55	0.80	0.815	0.907	0.908	0.09	0.09	0.09	-3.06	0.84	20.6
2	0.36	0.36	0.22	1.12	1.13	1.12	0.10	0.13	0.12	0.18	1.28	0.1
2	0.29	0.36	0.22	1.08	1.13	1.12	0.15	0.13	0.12	0.15	1.28	6.1
2	0.40	0.71	0.35	1.16	1.17	1.16	0.20	0.17	0.16	0.12	1.40	0.0
2	0.34	0.56	0.27	1.07	1.18	1.17	0.17	0.18	0.17	0.13	1.42	16.9
2	0.21	0.53	0.24	1.21	1.19	1.19	0.21	0.19	0.19	0.09	1.47	-5.1
3	0.38	0.56	1.65	0.750	0.752	0.753	0.21	0.25	0.25	-3.07	0.62	4.9
3	0.44	0.46	1.00	0.768	0.836	0.838	0.11	0.16	0.16	-3.04	0.70	14.0
3	0.32	0.93	0.46	1.18	1.16	1.16	0.11	0.16	0.16	0.07	1.39	-1.7
3	1.30	2.09	0.35	1.37	1.40	1.38	0.38	0.41	0.38	0.21	2.35	5.6
3	1.30	2.09	0.28	1.59	1.47	1.42	0.51	0.47	0.42	0.21	2.69	-19.6
3	1.38	2.09	0.20	1.73	1.56	1.49	0.41	0.57	0.49	0.21	3.44	-3.1

*   1 refers to tap water
    2   "   "   55% glycerol
    3   "   "   77% glycerol

Wave Period = 0.93 seconds

determine if this loss was significant, the incident energy flux was

compared to the sum of the transmitted and reflected energy flux.

Strictly, the coupling term between the incident and reflected energy

fluxes (Equation (5-2)) should be included but for all cases in these

experiments this term was much less than the uncertainties in

determining the energy fluxes and was thus considered insignificant.

The percentage energy flux loss was taken as:

$$\Delta P = \frac{P_i - (P_t + P_r)}{P_i} \times 100\%$$

where P_i, r, t are calculated from Equation (3-16).

For the example given previously this energy loss was

$$\Delta P = \frac{114 \cdot 8 - (114 \cdot 7 + 5 \cdot 0)}{114 \cdot 8} \times 100\% = -4 \cdot 3\%$$

and thus, within the experimental error there appears to be in this case

a balance between the energy flux incident energy to the step with that

carried away. It should be pointed out that an uncertainty of, say, 4%

in the determination of α_t results in an uncertainty of 8% for P_t .

With the added experimental errors found in α_r (which gives a small

contribution since $P_r \ll P_t$) and in the wave parameters used to

calculate P_i, P_r and P_t , the uncertainty in ΔP will be approx-

imately ±10%. The energy losses for the runs involving other fluids

and depths are listed in the final column of Table (14) and for $h_1 > h_2$

there is only a small energy imbalance whereas for $h_1 < h_2$ there

appears to be a general loss of energy. This is probably due to the

formation of an eddy of oscillating size generated in the lee of the

step. Using dye streaks it was found for $h_1 < h_2$ that, just to the

right of the step (in region (2)), the fluid was essentially motionless

below the level of the step whereas above the level of the step the

motion of the dye streaks was approximately the same as that in region

(1). Further to the right sinusoidal motion of the lower portion was

noticeable and in the upper portion the dye streaks were moving with

about the same amplitude as those far to the right of the discontinuity.

At a distance of about 1 to 1½ inches from the step, for $h_1 \simeq .5$

inches and $h_2 \simeq 1.0$ inches, the motion of the dye streaks throughout

the fluid column was the same (visually) as that far from the step.

With $h_1 > h_2$ dye streaks showed that the motion was essentially the

same at all positions in region (2) whereas in region (1) an anagalous

situation existed to the one described previously with the portion of

the fluid near the step and below its level moving with a smaller

motion than the portion above it. For $h_1 \simeq 1.0$ inches and $h_2 \simeq .5$

inches the horizontal extent of this region was smaller by about 50% of

the previous case. It is thought that the energy loss is due to the

generation of small secondary motions in the form of an eddy in these

regions and since the extent of this region was greater for $h_1 < h_2$

it is expected that there will be a greater energy loss in this case.

6.3 The Local Surface Disturbances at the Step

An investigation was made into the extent of the local surface
disturbances in the vicinity of the step. Owing to the difficulty in
obtaining accurate wave heights from composite wave height measurements
no results were investigated near the step in region (1). A number of
wave heights were measured in region (2) in the neighbourhood of the
step and far from the step. To ensure that small variations in the
incident wave height did not effect the results, each measurement of
wave height in region (2) was compared to a simultaneous wave record
taken in region _(1) (using only the first portion corresponding to no
reflected component being present.) Figure (33) shows the wave heights
for $h_1 > h_2$ using the 77% glycerol mixture, the solid line shows the
decay coefficient which had previously been found from the wave heights
measured far from the step. The extent of the local disturbance is
seen to be small in that all measurements in the vicinity of the step
lie close to the α_2 line. Using the same fluid, a similar result was
found for $h_1 < h_2$ (Figure (34)). Tap water was used in place of the
viscous glycerol mixture, the results for similar depths as used in the
previous example are shown in Figure (35) for $h_1 > h_2$ and Figure (36)
for $h_1 < h_2$. In both cases the local disturbance of the surface near
the step is much more pronounced than when the more viscous fluid was
used. It therefore appears that the presence of viscosity plays an
important part in damping out the local surface disturbances. Figure
(37) shows wave heights in region (2) for a comparitively large depth

ratio of h_1 = 2.09 inches and h_2 = .35 inches using the 77% glycerol

mixture, again, with this viscous fluid, there is no evidence of any

local surface disturbances (except for the one point at the step

itself).
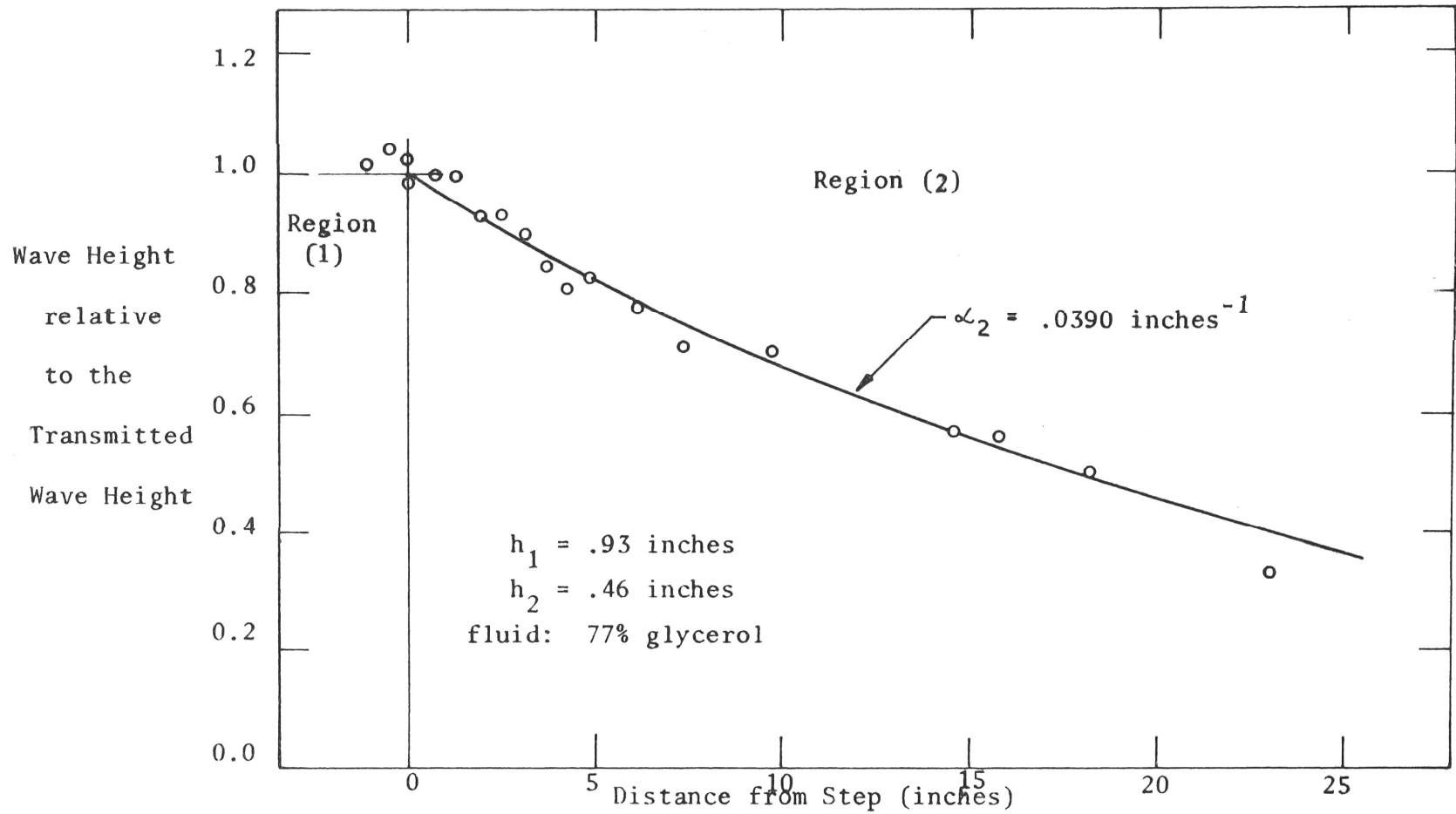
FIGURE 33: MEASURED WAVE HEIGHTS IN REGION (2) VS. DISTANCE FROM STEP IN REGION (2).
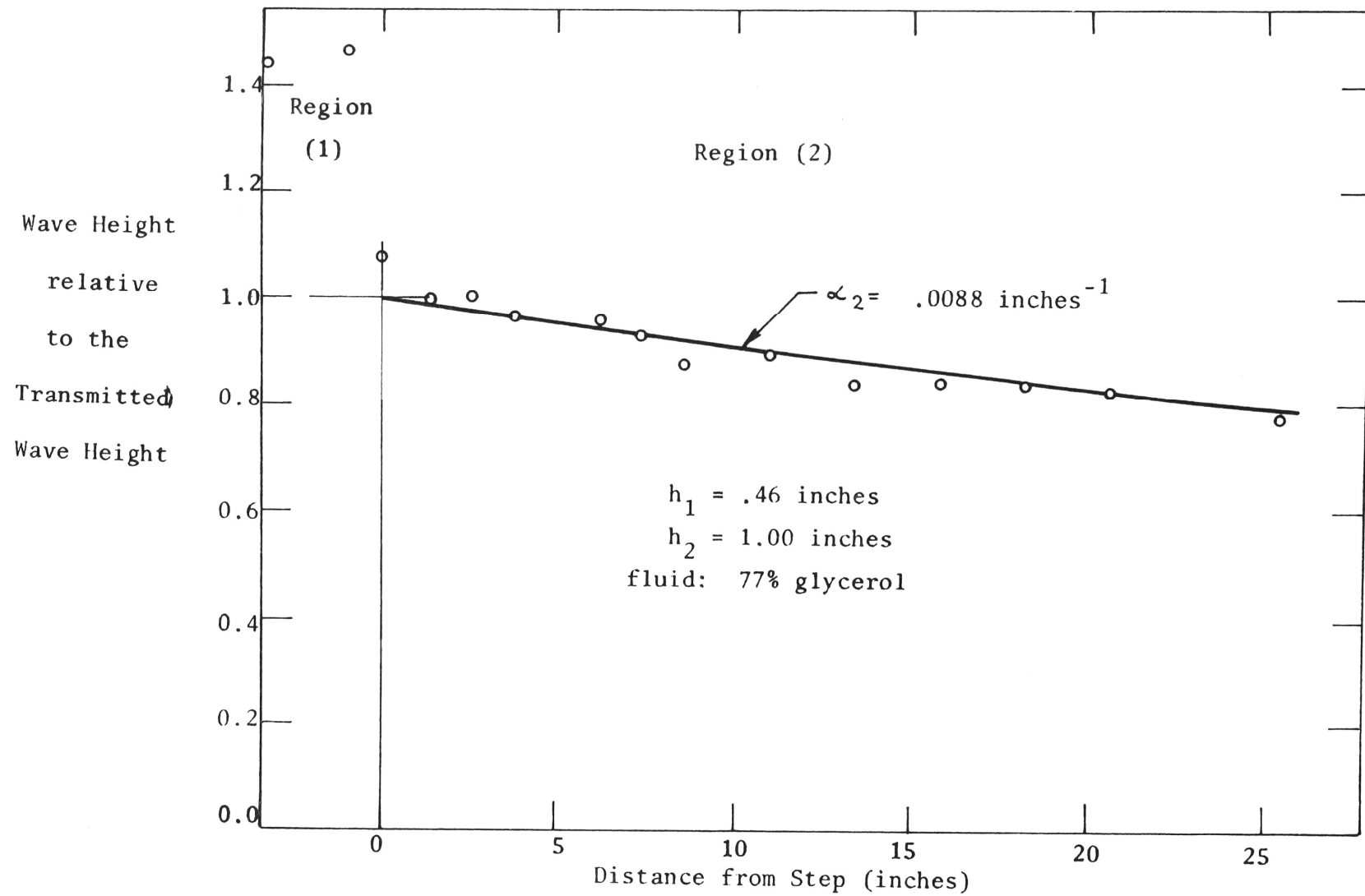
FIGURE 34: MEASURED WAVE HEIGHTS IN REGION (2) VS. DISTANCE FROM STEP
IN REGION (2).
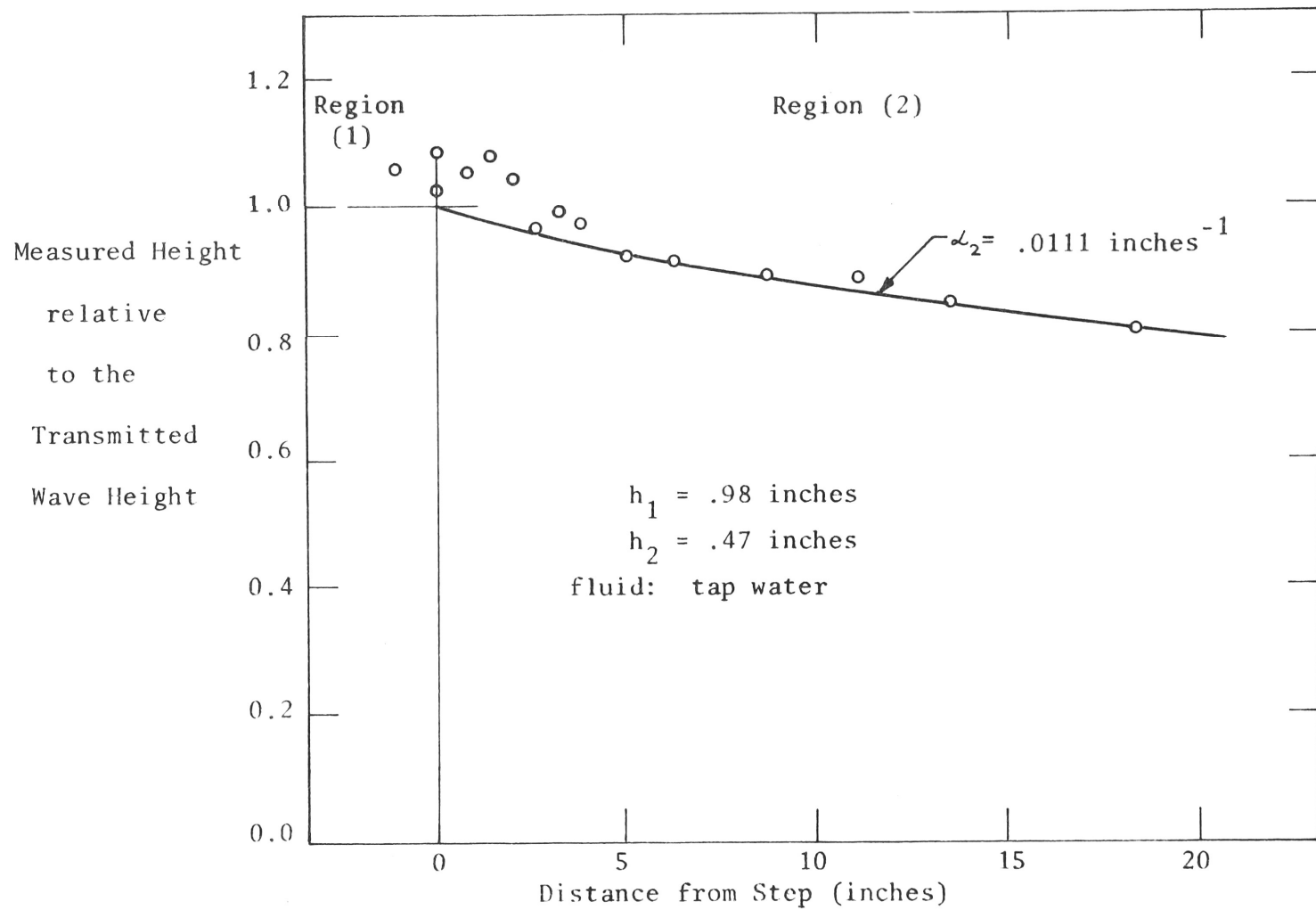
FIGURE 35: MEASURED WAVE HEIGHTS IN REGION (2) VS. DISTANCE FROM STEP IN REGION (2).
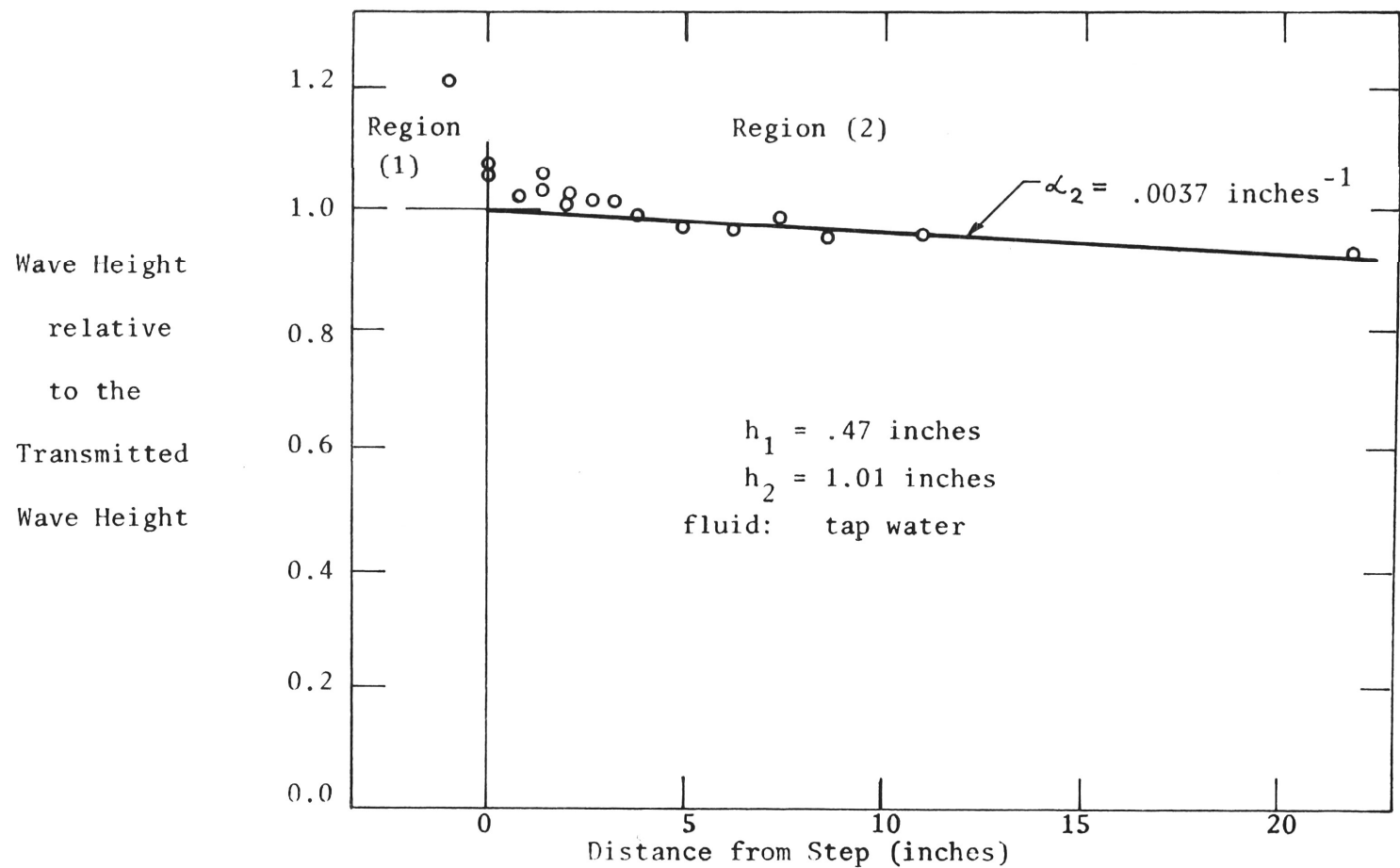
FIGURE 36: MEASURED WAVE HEIGHTS IN REGION (2) VS. DISTANCE FROM STEP IN REGION (2).
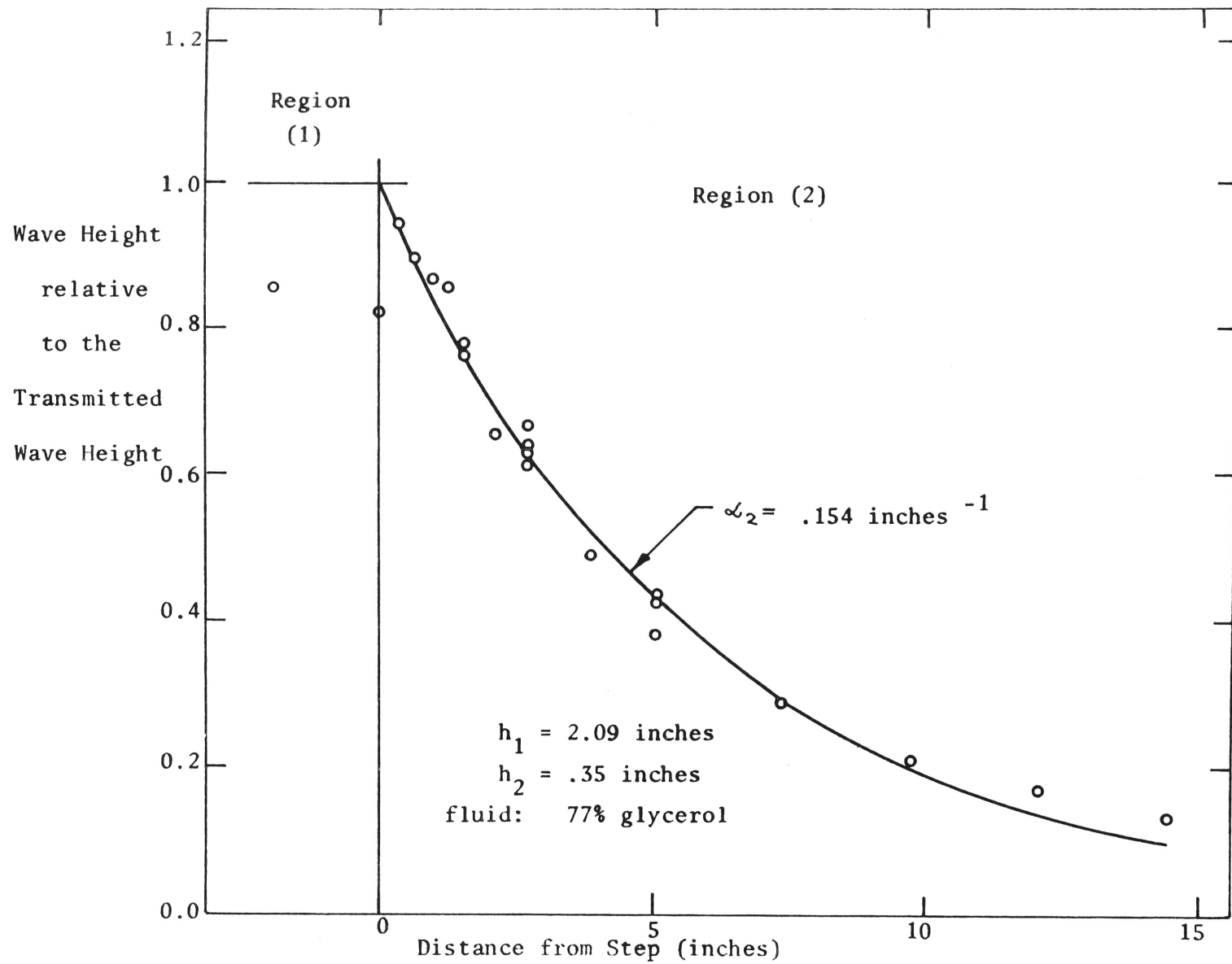
FIGURE 37: MEASURED WAVE HEIGHTS IN REGION (2) VS. DISTANCE FROM STEP IN REGION (2).

CHAPTER 7

THE FORCED EXCITATION OF WAVES OVER A

SUBMERGED CIRCULAR SILL

In this chapter the forced excitation of waves over a circular
sill and the scattering of wave energy away from the sill is invest-
igated in the presence of friction. The circular sill of radius R is
taken to be centred at the origin and to have a fluid depth above it
of h_2. The infinite region outside the sill is considered to have a
constant fluid depth h_1, this region will be designated as the ocean.
Sinusoidal plane waves incident from the ocean travel in a direction
of increasing x such that their crests are perpendicular to the x axis.
These waves constitute the forcing mechanism. Upon reaching the sill
some of the wave energy is transmitted over the sill, once over the
sill the wave energy undergoes multiple reflections at the boundary
of the sill. It has been shown for circular symmetry (Longuet-Higgins
(1967)) that even in the frictionless model, there is always some loss
of energy from the sill to infinity, although this loss may be very
small. The response coefficients using frictionless long-waves have
been derived by Longuet-Higgins (1967) and show the possibility of
(theoretical) large amplifications over the sill for certain forcing
frequencies, the wave energy in these instances is said to be nearly
trapped.

In this investigation the linear friction term is introduced into
the equations of motion and the depths in the ocean and above the sill

are not necessarily in the long-wave region.

7.1 Representation of the Potential Functions

The complex valued potential function for the forcing wave is:
(Equation (2-11)).

$$(\phi_i)_c = \frac{i\sigma A_i \cosh k_1 (z+h_1)}{k_1 \sinh k_1 h_1} e^{i(k_1 x - \sigma t)}$$

$$= f_1(z) e^{i(k_1 x - \sigma t)}$$

Transforming into polar co-ordinates:

$$x = r \cos \theta$$

so:

$$(\phi_i)_c = f_1(z) e^{i(k_1 r \cos \theta - \sigma t)}$$

Which may be rewritten in terms of a series of Bessel functions of the
first kind by use of the identity:

$$e^{i x \cos \theta} = \sum_{n=0}^{\infty} \epsilon_n i^n J_n(x) \cos n \theta$$

where

$$\epsilon_0 = 1 \quad \text{AND} \quad \epsilon_n = 2 \quad \text{FOR} \quad n \gtreqless 1 .$$

Therefore the complex valued potential function is:

$$(\phi_i)_c = f_1(z) e^{-i\sigma t} \sum_{n=0}^{\infty} \epsilon_n i^n J_n(k_1 r) \cos n \theta \qquad (7-1)$$

Since the origin has been excluded from the region designed as
the ocean, the scattered wave may be represented in terms of Hankel
functions of the first kind, $H_n^{(1)}$. Hankel functions of the second

kind must be excluded from the solution since they represent waves travelling inward whereas those of the first kind represent waves travelling outward. This property can be seen most easily from asymptotic expansions of the functions (McLachlan (1955)) where it is shown that for large arguments, $K_1 r$:

(i) $H_n^{(1)} (K_1 r)$ contains a factor $e^{i(K_1 r)}$

and (ii) $H_n^{(2)} (K_1 r)$ contains a factor $e^{-i(K_1 r)}$

The forcing waves, incident from the left, have a factor $e^{i(K_1 r \cos \Theta)}$ associated with them and along the axis $\Theta = \pi$ this factor becomes $e^{-i(K_1 r)}$. This factor is the same as that contained in the asymptotic value of $H_n^{(2)}$ and thus $H_n^{(2)}$ represents a wave travelling inward. It is also clear that $H_n^{(1)} (K_1 r)$ decays and that $H_n^{(2)} (K_1 r)$ grows with increasing r FOR $0 < ARG (K_1) \leqslant \frac{\pi}{2}$.

The scattered wave is thus represented by Equation (2-14) (with $'B_n = 0$) as:

$$(\phi_s)_c = f_1(\xi) e^{-i\sigma t} \sum_{n=0}^{\infty} B_n H_n^{(1)} (K_1 r) \cos n \Theta \qquad (7-2)$$

where B_n is a constant to be evaluated from the matching conditions at the edge of the sill.

The origin has been taken as the centre of the sill; hence, in this region, solutions using Bessel functions of the second kind must be excluded. From Equation (2-13) the complex valued potential function for the waves over the sill is:

$$(\phi_2)_c = f_2(z) e^{-i\sigma t} \sum_{\nu=0}^{\infty} A_\nu J_\nu (K_2 r) \cos \nu \theta \qquad (7\text{-}3)$$

where A_ν is evaluated from matching conditions at the sill.

7.2 The Matching Conditions at $r = R$

The matching condition of a continuous instantaneous energy flux at the edge of the sill is:

$$\lim_{J \to 0} \frac{1}{J} \int_{t}^{t+J} \int_{-h_1}^{0} \left(\frac{\partial(\phi_i + \phi_s)}{\partial t} + \frac{c}{h_1} (\phi_i + \phi_s)_r \right)(u_i + u_s) \, dz \, dt \Big|_{r = R^+}$$

$$= \lim_{J \to 0} \frac{1}{J} \int_{t}^{t+J} \int_{-h_1}^{0} \left(\frac{\partial \phi_2}{\partial t} + \frac{c}{h_2} (\phi_2)_r \right) u_2 \, dz \, dt \Big|_{r = R^-} \qquad (7\text{-}4)$$

where u is the radial particle velocity.

As was shown in Chapter 5, this condition gives 3 equations, only two of which are required (along with 2 from the surface condition) to determine the complex constants A_ν and B_ν . To obtain these three equations, in Chapter 5, the real parts of the dynamic pressure and the horizontal velocity were taken and multiplied to give the integrand. The integration was performed and coefficients of like time dependant trigonometric functions were equated. Instead of this lengthy process, what will be done is to multiply the complex valued

dynamic pressure and radial velocity, integrate and then equate real and imaginary parts of Equation (7-4). That this process gives two of the equations arrived at by the first method is shown by the following argument.

Let $\mathcal{D}_j e^{i d_j} e^{-i\sigma t}$ and $\mathcal{L}_j e^{i g_j} e^{-i\sigma t}$ $(j = 1, 2)$ be four complex numbers that are harmonic with time, then the condition that:

$$\mathcal{R}\{\mathcal{D}_1 e^{i d_1} e^{-i\sigma t}\} \cdot \mathcal{R}\{\mathcal{L}_1 e^{i g_1} e^{-i\sigma t}\} = \mathcal{R}\{\mathcal{D}_2 e^{i d_2} e^{-i\sigma t}\} \cdot \mathcal{R}\{\mathcal{L}_2 e^{i g_2} e^{-i\sigma t}\}$$

is:

$$\mathcal{D}_1 \cos(d_1 - \sigma t) \, \mathcal{L}_1 \cos(g_1 - \sigma t) = \mathcal{D}_2 \cos(d_2 - \sigma t) \, \mathcal{L}_2 \cos(g_2 - \sigma t)$$

or:

$$\mathcal{D}_1 \mathcal{L}_1 [\cos(d_1 + g_1 - 2\sigma t) + \cos(d_1 - g_1)] = \mathcal{D}_2 \mathcal{L}_2 [\cos(d_2 + g_2 - 2\sigma t) + \cos(d_2 - g_2)]$$

Expanding in terms of $\sin 2\sigma t$ and $\cos 2\sigma t$ gives:

$$\mathcal{D}_1 \mathcal{L}_1 [\cos(d_1 + g_1) \cos 2\sigma t + \sin(d_1 + g_1) \sin 2\sigma t + \cos(d_1 - g_1)]$$

$$= \mathcal{D}_2 \mathcal{L}_2 [\cos(d_2 + g_2) \cos 2\sigma t + \sin(d_2 + g_2) \sin 2\sigma t + \cos(d_2 - g_2)]$$

Equating coefficients of like functions of $2\sigma t$ gives the result that:

$$\mathcal{D}_1 \mathcal{L}_1 \cos(d_1 - g_1) = \mathcal{D}_2 \mathcal{L}_2 \cos(d_1 - g_1)$$

$$\mathcal{D}_1 \mathcal{L}_1 \sin(d_1 + g_1) = \mathcal{D}_2 \mathcal{L}_2 \sin(d_2 + g_2)$$

and

$$\mathcal{D}_1 \mathcal{L}_1 \cos(d_1 + g_1) = \mathcal{D}_2 \mathcal{L}_2 \cos(d_2 + g_2)$$

If, instead of taking the real parts and forming the products, the products are taken as:

$$(\mathcal{D}_1 e^{i d_1} e^{-i\sigma t})(\ell_{g_1} e^{i g_1} e^{-i\sigma t}) = (\mathcal{D}_2 e^{i d_2} e^{-i\sigma t})(\ell_{g_2} e^{i g_2} e^{-i\sigma t})$$

then

$$\mathcal{D}_1 \ell_{g_1} e^{i(d_1 + g_2)} = \mathcal{D}_2 \ell_{g_2} e^{i(d_2 + g_2)}$$

and equating real and imaginary parts gives:

$$\mathcal{D}_1 \ell_{g_1} \cos(d_1 + g_1) = \mathcal{D}_2 \ell_{g_2} \cos(d_2 + g_2)$$

and

$$\mathcal{D}_1 \ell_{g_1} \sin(d_1 + g_1) = \mathcal{D}_2 \ell_{g_2} \sin(d_2 + g_2)$$

which are the same as the latter two equations arrived at in the previous development.

The complex valued radial velocity is - for the incident wave:

$$\mathcal{U}_i^c = -\frac{\partial(\phi_i)_c}{\partial r} = -K_1 f_1 e^{-i\sigma t} \sum_{m=0}^{\infty} \epsilon_m i^m J_m'(K_1 r) \cos m\theta \qquad (7\text{-}5)$$

for the scattered wave:

$$\mathcal{U}_s^c = -\frac{\partial(\phi_s)_c}{\partial r} = -K_1 f_1 e^{-i\sigma t} \sum_{m=0}^{\infty} B_m H_m^{(1)}(K_1 r) \cos m\theta \qquad (7\text{-}6)$$

and for the wave over the sill:

$$\mathcal{U}_2^c = -\frac{\partial(\phi_2)_c}{\partial r} = -K_2 f_2 e^{-i\sigma t} \sum_{m=0}^{\infty} A_m J_m'(K_2 r) \cos m\theta \qquad (7\text{-}7)$$

where $\quad J_m'(x) = \dfrac{d}{dx} J_m(x)$

and

$$H_m^{(1)'}(x) = \frac{d}{dx}\, H_m^{(1)}$$

The two equations corresponding to the continuous energy flux condition (Equation 7-4)) will be those obtained by equating real and imaginary parts of:

$$\int_{-h_1}^{0} \left\{ \frac{\partial((\phi_i)_c + (\phi_s)_c)}{\partial t} + \frac{c}{h_1}\,((\phi_i)_c + (\phi_s)_c)_\ell \right\} \left\{ u_i^c + u_s^c \right\} dz \,\Bigg|_{r=R^+}$$

$$= \int_{-h_2}^{0} \left(\frac{\partial(\phi_2)_c}{\partial t} + \frac{c}{h_2}\,((\phi_2)_c)_\ell \right) u_2^c \, dz \,\Bigg|_{r=R^-}$$

or, more explicitely:

$$\sum_{n=0}^{\infty}\sum_{m=0}^{\infty} f_1 (\epsilon_n i^n J_{n_1} + B_n H_{n_1})(\epsilon_m i^m J_{m_1}' + B_m H_{m_1}') \cos n\theta \cos m\theta$$

$$= \sum_{n=0}^{\infty}\sum_{m=0}^{\infty} f_2 A_n A_m J_{n_2} J_{m_2}' \cos n\theta \cos m\theta \qquad\qquad (7\text{-}8)$$

where: $\quad f_j = \int_{-h_j}^{0} \zeta_j K_j \left(\nu\sigma \zeta_j + \frac{c}{h_j} \zeta_{\ell_j} \right) dz$

and:
$$\mathcal{C}_{nj} = \mathcal{C}_n(K_j\,R);\qquad \mathcal{C} \text{ being any of the}$$
cylindrical functions used to define the potential function or radial particle velocity.

The condition of a continuous surface elevation at $r = R$ is:

$$\langle \eta_i + \eta_s \rangle \Big|_{r = R^+} = \eta_2 \Big|_{r = R^-}$$

or that:

$$\sum_{n=0}^{\infty} \left(\epsilon_n i^n J_n(K_1 r) + B_n H_n(K_1 r) \right) \cos n\theta \, e^{-i\sigma t} \Big|_{r = R^+}$$

$$= \sum_{n=0}^{\infty} A_n J_n(K_2 r) \cos n\theta \, e^{-i\sigma t} \Big|_{r = R^-}$$

Equating the nth components at $r = R$ gives:

$$\epsilon_n i^n J_{n_1} + B_n H_n = A_n J_{n_2}$$

$$(7\text{-}9)$$

Using the R.H.S. of equation (7-9) in equation (7-8) and

rearranging gives:

$$\sum_{n=0}^{\infty} \sum_{m=0}^{\infty} A_m J_{m_2} \left\{ \frac{f_1}{f_1} \left(\epsilon_n i^n J'_{n_1} + B_n H'_{n_1} \right) - A_n J'_{n_2} \right\} \cos n\theta \cos m\theta = 0$$

which can be factored into a term depending only on "n" and one

depending only on "m". That is:

$$\sum_{m=0}^{\infty} A_m J_{m_2} \cos m\theta \sum_{n=0}^{\infty} \left\{ \frac{f_1}{f_2} \left(\epsilon_n i^n J'_{n_1} + B_n H'_{n_1} \right) - A_n J'_{n_2} \right\} \cos n\theta = 0$$

Since Am is not in general equal to zero, it follows that:

$$\frac{f_1}{f_2} \left(\epsilon_n i^n J'_{n_1} + B_n H'_{n_1} \right) - A_n J'_{n_2} = 0 \qquad (7\text{-}10)$$

The above equation along with the nth component of the surface boundary condition gives a linear system of equations in 2 unknowns.

Using the relation that for any arguement "X":

$$J_n'(x) H_n^{(1)}(x) - J_n(x) H_n^{(1)'}(x) = -\frac{2i}{\pi x}$$

it follows immediately that:

$$A_n = \frac{f_1}{f_2} \frac{2\epsilon_n i^{n+1}}{\pi K_1 R \left(\frac{f_1}{f_2} J_{n_2} H_{n_1}' - H_{n_1} J_{n_2}'\right)} \tag{7-11}$$

and

$$B_n = \epsilon_n i^n \left\{ \frac{J_{n_1} J_{n_2}' - \frac{f_1}{f_2} J_{n_2} J_{n_1}'}{\frac{f_1}{f_2} J_{n_2} H_{n_1}' - H_{n_1} J_{n_2}'} \right\} \tag{7-12}$$

That these equations reduce to the results for frictionless long-waves found by Longuet-Higgins (1967) is shown in Appendix 11. (A11.3)

The ratio $\frac{f_1}{f_2}$ is evaluated in Appendix 11 (A11.2) and is found to be

$$\frac{K_2^2 \sinh^2 K_2 h_2}{K_1^2 \sinh^2 K_1 h_1} \left\{ \frac{2 K_1 h_1 + \sinh 2 K_1 h_1 + i \frac{4c}{\sigma h_1} \sinh K_1 h_1}{2 K_2 h_2 + \sinh 2 K_2 h_2 + i \frac{4c}{\sigma h_2} \sinh K_2 h_2} \right\} \tag{7-13}$$

which reduces to the ratio of the energy velocities when friction is neglected.

7.3 Asymptotic Behaviour of $|A_n|$ and $|B_n|$ for $K_i R \ll n$

If the wave lengths L_1 and L_2 and the radius of the sill are such that $K_i R \ll n$, n, being the order of the circular functions, then using asymptotic formulae for $n > 0$ (McLachlan (1955)) the function

in the denominator of (7-11) becomes:

$$\frac{\mathcal{f}_1}{\mathcal{f}_2} J_{n_2} H'_{n_2} - H_{n_1} J'_{n_2} \simeq \frac{i}{\pi R} \left(\frac{K_2}{K_1}\right)^n \left\{\frac{\mathcal{f}_1}{\mathcal{f}_2 K_1} + \frac{1}{K_2}\right\}$$

and the response coefficient over the sill is:

$$A_n \simeq \frac{4 i^n \left(\frac{K_1}{K_2}\right)^n}{1 + \frac{\mathcal{f}_2}{\mathcal{f}_1} \frac{K_1}{K_2}} \quad ; \quad n > 0 \qquad (7\text{-}14)$$

Thus, since $K_1 < K_2$, $|A_n|$ becomes smaller and smaller as n increase

and the higher order modes are no longer present over the sill.

For $|A_n|$ to become large and correspond to a (partially) trapped

mode the denominator must become small which in this case is clearly

impossible and thus for $n > 0$ and $K_j R \ll n$ there can be no

trapping of wave energy over the sill. If $n = 0$ and $K_j R \ll 1$,

then the circular functions may be approximated by terms of order $(k_j R)$

or of lower order. In this case the function:

$$\frac{\mathcal{f}_1}{\mathcal{f}_2} J_{0_2} H'_{0_1} - H_{0_1} J'_{0_2} \simeq R \left(K_2 - \frac{\mathcal{f}_1}{\mathcal{f}_2} K_1\right)\left[\frac{1}{2} + \frac{i}{\pi}\left(\gamma + \log_e \frac{K_1 R}{2}\right)\right] + \frac{2 i}{\pi R K_1} \frac{\mathcal{f}_1}{\mathcal{f}_2}$$

and the response coefficient is:

$$A_0 \simeq \frac{2 i \frac{\mathcal{f}_1}{\mathcal{f}_2}}{\pi K_1 R \left[R\left(K_2 - \frac{\mathcal{f}_1}{\mathcal{f}_2} K_1\right)\left(\frac{1}{2} + \frac{i}{\pi}\left(\gamma + \log_e \frac{K_1 R}{2}\right)\right) + \frac{2 i}{\pi R K_1} \frac{\mathcal{f}_1}{\mathcal{f}_2}\right]} \qquad (7\text{-}15)$$

where $\gamma = .5772 \cdots$ is Euler's constant.

For $K_1 R$ sufficiently small, the last term in the square brackets dominates the term containing the log function, and A_o reduces to unity.

It is of interest to note that, for frictionless long-waves, the term $\left(K_2 - \frac{f_1}{f_2} K_1 \right)$ is always zero and so in this asymptotic approximation, (7-15), $A_o = 1$. In this special case the other response coefficients are:

$$A_n \simeq \frac{4 i^n}{1 + \frac{h_2}{h_1}} \left(\frac{h_2}{h_1} \right)^{n/2}$$

Using these same asymptotic approximations to determine the behaviour coefficients for the scattered wave gives:

$$B_n \simeq \frac{2 i^{n-1} \left(\frac{K_1 R}{2} \right)^{2n}}{n! \, (n-1)!} \; \frac{\frac{f_2 K_1}{f_1 K_2} - 1}{\frac{f_2 K_1}{f_1 K_2} + 1} \qquad (7\text{-}16)$$

which is clearly small for $\frac{K_1 R}{2} < 1$ and assuming if $\frac{K_1 R}{2} > 1$, $\left(\text{and } n \gg \left(\frac{K_1 R}{2} \right)^2 \right)$ then $n!$ may be approximated by Sterling's formula:

$$n! \simeq \sqrt{2\pi n} \; n^n e \qquad \qquad \text{so:}$$

$$B_n \simeq \frac{i^{n-1}}{\pi} \left(\frac{K_1 R e}{2 n} \right)^{2n} \left\{ \frac{\frac{f_2 K_2}{f_1 K_1} - 1}{\frac{f_2 K_1}{f_1 K_2} + 1} \right\}$$

which tends to zero for $n \to \infty$.

If $n = 0$:

$$B_0 \simeq \frac{-\frac{R}{2}\left(f_2 K_2 - f_1 K_1\right)}{R\left(f_2 K_2 - f_1 K_1\right)\left(\frac{1}{2} + \frac{i}{\pi}\left(\gamma + \log_e \frac{K_1 R}{2}\right)\right) + \frac{2i}{\pi K_1 R} f_1} \qquad (7\text{-}17)$$

which for $K_1 R$ sufficiently small reduces to:

$$B_0 \simeq \frac{i\pi R^2 K_1}{2 f_1}\left(f_2 K_2 - f_1 K_1\right)$$

For frictionless long-waves B_0 is identically zero and

$$B_n \simeq \frac{\epsilon_n \, i^{n-1} \pi}{n! \, (n-1)!}\left(\frac{\sigma^2 R^2}{g h_1}\right)^n \frac{\frac{h_2}{h_1} - 1}{\frac{h_2}{h_1} + 1}$$

Situations can exist where none of the "nearly trapped" modes can be present over the sea-mount for any forcing frequency. Basically these occur for configurations where the critical angle is not approached by a wave corresponding to the nth harmonic until $K_1 R$ (and thus $K_2 R$) is much smaller than n and here the asymptotic equation for A_n shows that no modes with a high "Q" can exist; in fact, for n large enough $A_n \to 0$. At the other extreme for short wave periods the effect of the bottom topography is insignificant and the waves pass over the sill unobstructed, in this case $A_n = \epsilon_n$ for all n. Table (15) shows numerical results for a situation of the type described above.

TABLE 15

$|A_n|$ FOR A SITUATION WHERE NO HIGH "Q"

RESPONSES EXIST

$T_{sec.}$ \ n	0	1	2	3	4	5	6	7	8	9
1.0	1.000	2.000	2.000	2.000	2.000	2.000	2.000	2.000	2.000	2.000
2.0	0.982	2.002	1.965	1.999	1.970	1.990	1.983	1.974	2.000	1.962
3.0	0.896	2.090	1.804	2.036	1.887	1.866	2.098	1.774	1.941	2.128
4.0	1.136	1.938	2.304	1.922	2.174	2.212	1.744	2.133	2.879	1.176
5.0	1.231	2.311	2.421	2.455	1.991	2.944	1.771	0.549	0.250	0.131
6.0	1.321	2.824	2.604	2.433	4.334	0.819	0.271	0.115	0.054	0.026
7.0	1.683	2.857	2.857	4.877	0.811	0.233	0.087	0.036	0.015	0.007
8.0	1.711	3.123	4.455	1.429	0.307	0.098	0.035	0.013	0.005	0.002
9.0	1.569	4.057	4.442	0.613	0.158	0.050	0.017	0.006	0.002	0.001
10.0	1.592	5.792	2.023	0.355	0.095	0.029	0.009	0.003	0.001	0.000
11.0	1.792	6.689	1.190	0.240	0.064	0.018	0.006	0.002	0.001	0.000
12.0	2.190	5.185	0.833	0.179	0.047	0.013	0.004	0.001	0.000	0.000
13.0	2.878	3.814	0.645	0.142	0.037	0.010	0.003	0.001	0.000	0.000
14.0	4.034	2.994	0.532	0.119	0.030	0.008	0.002	0.001	0.000	0.000
15.0	5.703	2.490	0.459	0.104	0.026	0.007	0.002	0.000	0.000	0.000
16.0	6.508	2.157	0.408	0.092	0.023	0.006	0.001	0.000	0.000	0.000
17.0	5.419	1.925	0.371	0.084	0.020	0.005	0.001	0.000	0.000	0.000
18.0	4.198	1.754	0.343	0.078	0.019	0.005	0.001	0.000	0.000	0.000
19.0	3.381	1.624	0.322	0.073	0.017	0.004	0.001	0.000	0.000	0.000

$$R = 100 \text{ feet}$$
$$h_1 = 200 \text{ feet}$$
$$h_2 = 10 \text{ feet}$$

7.4 Convergence of the Series Representing the Waves over the Sill and the Scattered Wave.

That the series representing the wave over the sill (Equation (7.3)) is absolutely convergent can be seen by considering the ratio of the $(n+1)^{th}$ and the nth term and taking the limit as $n \to \infty$, it is sufficient for absolute convergence that the modulus of this limit is less than 1. Omitting the cosine term in Equation (7-3) since $|\cos n\theta| \le 1$ and using Equation (7-4) gives this limit as:

$$\lim_{n \to \infty} \left| \frac{i^{n+1} \left(\frac{K_1}{K_2}\right)^{n+1} J_{n+1}(K_2 r)}{i^n \left(\frac{K_1}{K_2}\right)^n J_n(K_2 r)} \right|$$

$$= \frac{K_1}{K_2} \lim_{n \to \infty} \left| \frac{\frac{(\frac{1}{2} K_2 r)^{n+1}}{(n+1)!}}{\frac{\frac{1}{2}(K_2 r)^n}{n!}} \right|$$

where $J_n(K_2 r)$ and $J_{n+1}(K_2 r)$ have been approximated for large n.

$$= \frac{K_1 r}{2} \lim_{n \to \infty} \frac{1}{n+1} \to 0 \qquad$$ and Equation (7-3) is absolutely convergent.

The convergence is uniform since it is independant of r and θ and thus there is a continuous distribution of waves over the sill.

Similarly, using Equation (7-2) and the asymptotic representation of B_n (Equation (7-16)), the limit involving the ratio of the $(n+1)^{th}$

and nth terms is:

$$\lim_{n \to \infty} \frac{i^n \left(\frac{K_1 R}{2}\right)^{2(n+1)} H_{n+1}^{(1)}(K_1 r)}{(n+1)! \; n!} \cdot \frac{n! \, (n-1)!}{i^{n-1} \left(\frac{K_1 R}{2}\right)^{2n} H_n^{(1)}(K_1 r)}$$

$$= \left(\frac{1}{2} K_1 R\right)^2 \lim_{n \to \infty} \frac{\left(\frac{2}{K_1 r}\right)^{n+1} n!}{n(n+1)\left(\frac{2}{K_1 r}\right)^n (n-1)!}$$

$$= \frac{K_1 R^2}{2 r} \lim_{n \to \infty} \left|\frac{1}{n+1}\right| \to 0$$

and the series (Equation (7-2)) is again absolutely and uniformly convergent $(r > 0)$ and thus represents a continuous distribution of scattered waves around the sill.

7.5   The Response Coefficients when Friction is neglected.

Figure (38) shows the modulus of the response coefficient, $\left|A_3\right|$, for frictionless surface waves as a function of the wave period. For comparison the response coefficients resulting when the long-wave approximations are used and are also drawn on the figure. It is clear that these latter curves are for comparison only as the long-wave approximations are not strictly valid throughout this whole region. It can be seen that the height of the response peaks is less for the
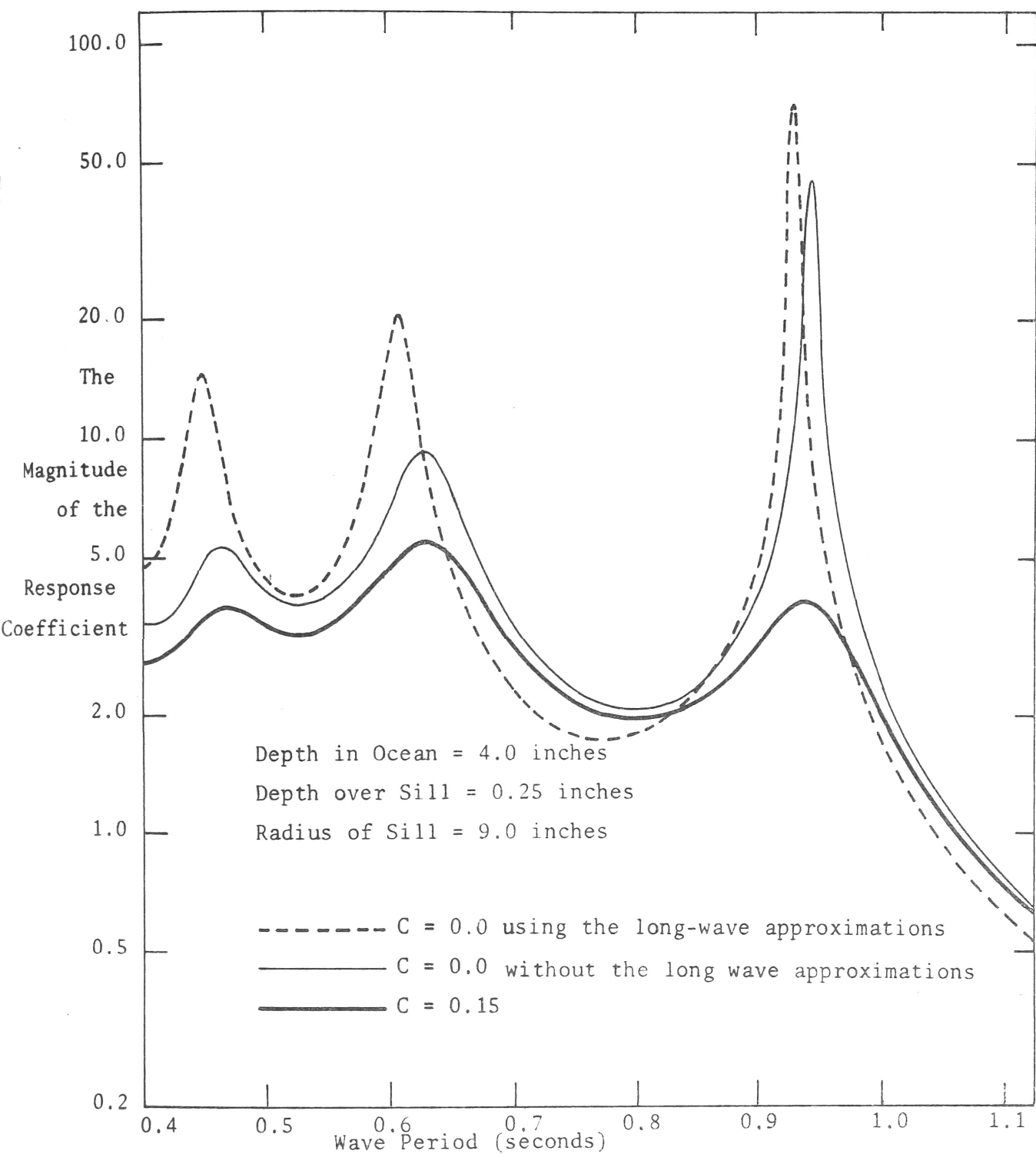
FIGURE 38:   COMPARISON OF THE MAGNITUDE OF THE RESPONSE
              COEFFICIENT $|A_n|$ OVER THE SILL $(n = 3)$

surface waves than for the long-waves but that the position of the

peaks is approximately the same. Two reasons for this reduction in

the responses are:

1) For a given depth, wave period and wave height the

approximations used in arriving at the long-wave solution

always gives a larger value for the energy flux than

would be found using the general equations. (Although,

as $h/L \Rightarrow 0$ the two solutions become the same.)

Therefore, long-wave theory predicts more energy arriving

at the sill and thus a greater $|A_n|$.

2) As pointed out by Longuet-Higgins (1967) and remarked on

by Sommerfield (1969) the response peaks are a consequence

of the waves over the sill being internally reflected at

the edge of the sill and at certain frequencies these waves

reinforce each other. The peaks with a high "Q" (the

highly trapped modes) are formed when the waves meet the

edge at an angle greater than the critical angle (where

the angle at a point on the sill edge is considered in

reference to the tangent drawn at this point to the sill

edge.)

Snell's Law of geometric optics applies to surface waves

travelling from a region where they exhibit one phase

velocity to a region where they exhibit another. (See, Appendix 12). In other words:

$$\frac{v_{P_2}}{v_{P_1}} = \frac{\sin \beta_2}{\sin \beta_1}$$

where β_2 is the angle of incidence (See Figure (A12:1)) and β_1 is the angle of refraction. The critical angle occurs when $\beta_1 = \frac{\pi}{2}$, which from energy considerations is clearly the maximum refracted angle, and thus:

$$\beta_{Crit} = \sin^{-1} \left(\frac{v_{P_2}}{v_{P_1}} \right)$$

For the same depth and wave period the phase velocity found using the long-wave approximation is less than that when the complete equations are used. In the shallower region over the sill the difference between the long-wave solution and the general solution for the phase velocity is less than in the deeper region of the ocean. Therefore

$$\left(\frac{v_{P_2}}{v_{P_1}} \right) \quad \text{for} \quad \text{Long-waves} \quad \leqslant \quad \left(\frac{v_{P_2}}{v_{P_1}} \right) \text{for General Surface}$$

$$\text{Waves}$$

and it follows that for a given incident angle, β_2, of the waves on the sill, that the refraction angle, β_1, is greater when the long-wave phase velocities are used than

when the general equations are used, thus the solutions
show more energy lost from the sill in the latter case
than the former and a reduction in $|A_n|$ is expected.

Sommerfield (1967), remarked that, for frictionless "long-waves",
the response coefficient β_n changed in a monotone manner between
a lower limit of zero and an upper limit of unity with the former
occuring near a minima for $|A_n|$ and the latter near a maxima.
From numerical results calculated for this thesis, somewhat different
conclusions are made in that the maxima for $|A_n|$ corresponded to
one or the other of the extreme values for $|B_n|$, with the phase of
$A_n J_n (K_1 r) \Big|_{r = R^-}$ relative to the phase of the nth component of the
incident wave determining which extreme. Physically, what is taking
place is that there is interference between the waves scattered by
reflection of the incident waves at the sill edge and those scattered
across the sill edge by the waves over the sill. If these scattered
waves are of the same amplitude and out of phase by π then
destructive interference occurs and $|B_n| = 0$. That $|B_n|$ has
a maximum value of ϵ_n can be easily seen from energy considerations;
that is, if $|B_n| > \epsilon_n$ then more energy would be leaving the sill
than arriving at it and the amplitude of oscillation over the sill would
diminish with time contrary to this steady state solution. Evidently,
when $|B_n| = 0$, the nth component of the incident wave scatters none

of its energy and, for the steady state, does not supply energy to the excitation over the sill, thus this incident mode will be transmitted across the sill without 'loss of energy and appear unchanged on arriving outside the sill. This principle of destructive interference between internally and externally reflected waves is employed in optics by "coating" lenses with a thin film which is an integral or half-integral number of wavelengths thick to reduce back scatter. As remarked on by Longuet Higgins (1967) the situation when $|B_n| = 0$ is analagous to the "Ramsauer effect" in which an extremely low scattering cross-section is found for low energy electrons incident to atoms of a noble gas. (See, Eiseberg (1961)).

It should be pointed out that a maximum or minimum for $|B_n|$ does not necessarily take the limiting values of ϵ_n or zero and that each extreme value of $|B_n|$ does not necessarily have a corresponding extreme value for $|A_n|$. The preceding remarks have been found to hold true for solutions not necessarily using the "long-wave" approximations and for solutions where friction is included (in the latter case $|B_n|$ cannot equal ϵ_n or 0). Figure (39) shows the scattered wave amplitude, $|B_3|$, for frictionless surface waves as a function of the wave period. In this instance the maximum value for $|B_3|$ occurs at nearly the same frequency as a maximum for $|A_3|$ but a minimum value for $|B_3|$ and a minimum value for $|A_3|$ correspond only in that there is a minima between adjacent maxima.

Parameters for this Figure correspond to those in Figure (38).

Magnitude

of the

Response

Coefficient

Wave Period (seconds)
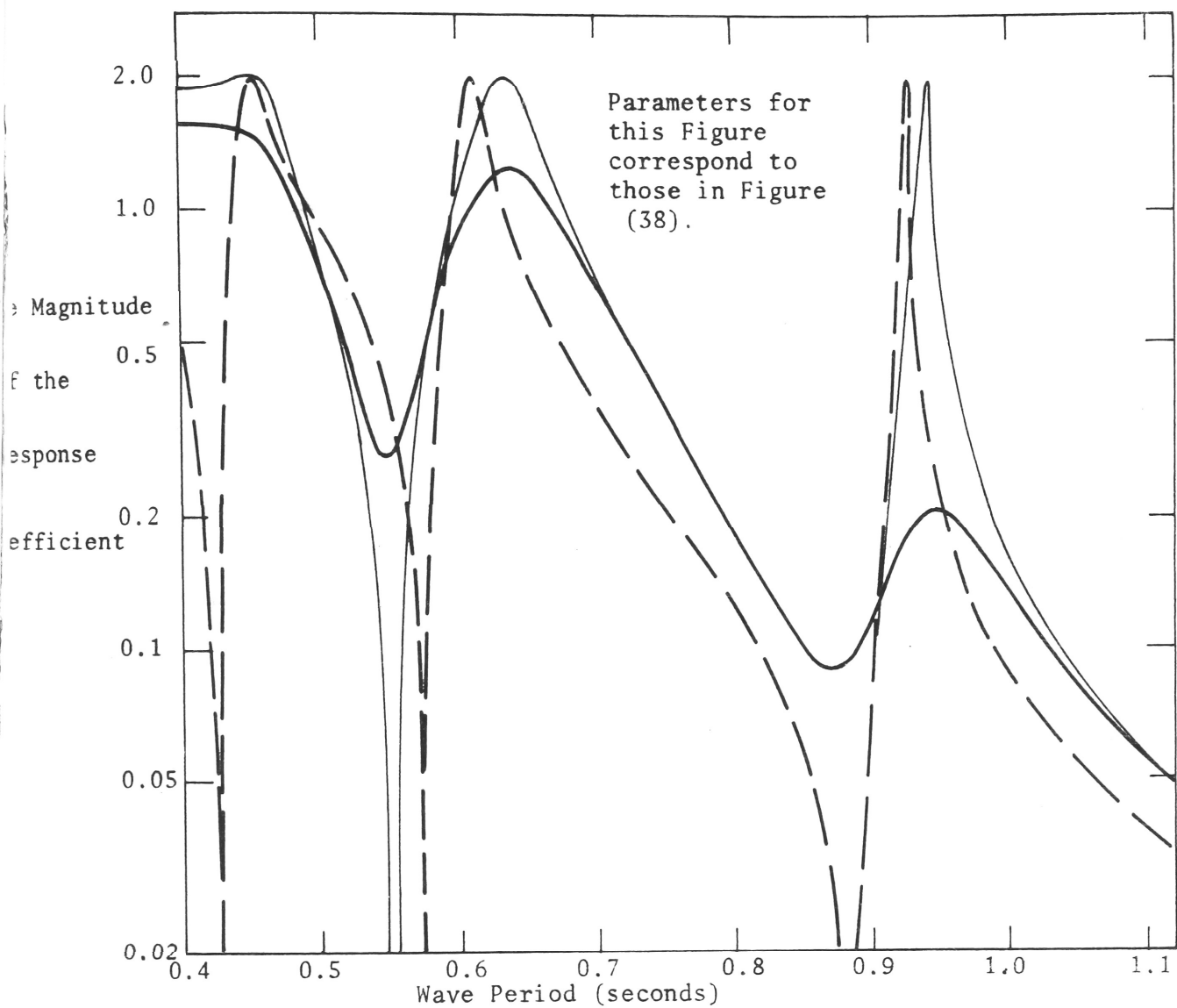
FIGURE 39: COMPARISON OF THE MAGNITUDE OF THE RESPONSE COEFFICIENT $|B_n|$ IN THE OCEAN $(n = 3)$

The wave periods which give the extreme values for the response coefficients are tabulated in Table (16). For comparison the zeroes of $J_3(K_2 R)$ are listed in the same table where it can be seen that when the radius of the sill is such that it corresponds closely to a nodal circle of the waves over the sill then a high response coefficient $|A_n|$ is found. In effect, the amplitude of the wave over the sill adjusts itself until the energy lost to infinity is just balanced by that arriving from the forcing wave. To gain this balance when the sill lies near a nodal circle and the $J_n(K_1 r)_{r=R^-}$ part of the amplitude is small requires a larger response coefficient over the sill than when the sill edge is such that the $J_n(K_1 r)_{r=R^-}$ part of the wave amplitude is comparatively large. A similar result is seen in the large tidal amplifications produced in channels open to the ocean at one end with lengths $\frac{2 m+1}{4 L}$ such that the open end corresponds to a node. Numerical results have shown that as the ratio f_1/f_2 increases the maximum value for $|A_n|$ occurs increasingly near to the value for $K_2 R$ which gives a zero of J_{n_2}. That this must be the case can be seen from Equation (7-11) where, for $|A_n|$ to become large the bracketed term in the denominator must become small which implies, since f_1/f_2 is large, that J_{n_2} or H_{n_1}' must be near zero. The latter choice is excluded since if $K_1 R$ is complex then H_{n_1}' can vanish but this places an added condition on the

single variable $K_1 R$, that is J_{n_1}' must also be small such that

$|B_n| \leq \epsilon_n$ (See, Equation (7-12).

For large values of the argument, the zeros of $J_n(x)$ occur

at intervals of approximately π that is, if x_o is a zero of

$J_n(x)$ then $x_o + \pi, x_o + 2\pi, \cdots$ are near to values which makes $J_n(x)$

vanish. The zeros of $J_n(x)$ are interlaced or, in other words, if

$\gamma_{n,m}$ designates a zero of $J_n(x)$ where m is the rank

of the zero, then:

$$0 < \gamma_{n,m} < \gamma_{n+1,m} < \gamma_{n,m+1} < \gamma_{n+1,m+1} < \cdots \cdots$$

It then follows from the two statements above that if $K_2 R$ is

large, then in an interval between $K_2 R$ and $K_2 R + \pi$;

$J_{0_2}, J_{1_2}, J_{2_2} \cdots J_{(k-1)_2}$ will all have zeros in the interval, but J_{k_2}

and higher order functions will have no zeros in the interval. Therefore,

since the values for $K_2 R$ which produces maxima for $|A_n|$ lie

near zeros of J_{n_2} there will be approximately k maxima for $|A_n|$

in the interval and since the phases of $A_n J_n(K_2 r)$ for various

n are generally different it is expected that the sum of the

responses at a given frequency will mask the individual behaviour of

the separate components. This point is examined in more detail in

Section (7-7). As a numerical example, suppose R = 1 mile and h_2 =

100 feet then values for T of 19.1 seconds and of 21.3 seconds give zeros

of J_{n_2} at $K_2 R = 27.49$ and 30.63. Using the asymptotic expansion

formula for the rank 1 zero of large orders:

$$\gamma_{n,1} \simeq n + 1.856\, n^{1/3} + 1.033\, n^{-1/3} \qquad (7\text{-}18)$$

TABLE 16

THE WAVE PERIODS AT WHICH THE FIRST THREE MAXIMA AND MINIMA OCCUR FOR $n = 3$. THE ZEROS, $j_{3,m}$, ARE GIVEN IN THE FIRST COLUMN

Zeros of J_3			$\lvert A_3 \rvert$ Wave Period for :		$\lvert B_3 \rvert$ Wave Period for:	
m	$j_{3,m}$	$K_1 R$	Maximum (seconds)	Minimum (seconds)	Maximum (seconds)	Minimum (seconds)
				0.407		0.320
3	13.02	12.92	0.465		0.483	
				0.530		0.549
2	9.76	9.26	0.630		0.633	
				0.800		0.878
1	6.38	6.15	0.942		0.942	
				None	None	None
			None			

$$C = 0.0 \text{ inches/second}$$
$$R = 9.0 \text{ inches}$$
$$h_1 = 4.0 \text{ inches}$$
$$h_2 = 0.25 \text{ inches}$$

(H'book Math. Functions (1964)) shows that there is a zero of $J_{24.2}$

in the interval, but no higher order zeros. Thus, using the fact

that the zeros are interlaced and that each zero corresponds (nearly)

to a maximum for $|A_n|$ then in the relatively narrow frequency

band between T = 19.1 seconds and T = 21.3 seconds there will be

26 maxima (2 at the end points of the interval for J_{o_2}).

7.6   The Effects of Frictional Damping on the Response Coefficients

As in any resonating system the effects of a dissipative friction

force will be to reduce the "Q" of the resonance peaks and, for a

given amount of friction, this reduction will be proportionately

greater for the sharp, high "Q" modes than for the ones with a lower

"Q". For the scattered wave in this model it is also expected that

the coefficient $|B_n|$ will not attain its maximum value of ϵ_n

or minimum value of zero since there is an energy loss over the sill.

Or, more explicitly, the former extreme cannot be reached because, if it

were, this would indicate a quantity of energy scattered in the nth

mode which would equal the quantity of energy incident in the same mode,

this is contrary to the model where there are frictional energy losses;

if the latter extreme of zero were reached it would indicate complete

transmission of energy in the incident n^{th} mode, again, because of

energy losses, contrary to the model. Since the phase speed of the waves

is changed only slightly by friction, the value for the critical

angle is altered by only a small amount and the frequency at which

the waves over the sill can reinforce themselves is also changed by

only a small amount, thus it is expected, physically, that the

presence of friction will not significantly alter the resonant

frequency. Figure (38) shows the effects of friction on $\left| A_3 \right|$ and

Figure (39) the effects on $\left| B_3 \right|$. To avoid confusion with a

changing friction coefficient with wave period, a constant value for

this parameter was used. From Figure (18), Chapter 4, it can be seen

that between T = .4 seconds and T = 1.2 seconds the friction coefficient

was found to be greater than .15 inches/sec.; therefore using this

lower limit will give a smaller effect than using the larger one that

was found experimentally. From Figure (38) it can be seen that there is

a large reduction in the height of the maxima for $\left| A_3 \right|$ and this

reduction is proportionally greater for the high "Q" modes, in fact the

most pronounced peak, when C = 0, is reduced by a factor of 12 by

friction whereas the adjacent peak which had a much smaller "Q" when

C = 0 is reduced by a factor of less than 2 and is now of greater

amplitude than the damped maxima corresponding to the originally most

pronounced peak. Figure (39) shows the smoothing effects of frictional

damping on $\left| B_3 \right|$, as in the case of the response coefficient over

the sill these effects are more pronounced for the narrower peaks and

troughs than for the broader ones. From this Figure it is seen that

$\left| B_3 \right|$ no longer takes it maximum value of 2 or minimum value of zero.

The response coefficients, $|A_n|$, $n = 0 \to 5$, for a large scale

oceanographic situation are shown in Figures (40), (41) and (42) for

a sill with a radius of about 12 miles, a depth in the ocean of 3,200

feet and a sill depth of 200 feet. For these parameters, wave periods

of between 8.5 and 13.0 minutes gave maxima that produced as little

overlapping as possible; in fact, they correspond to the zeros

$j_{0,3}$; $j_{1,2}$; $j_{2,2}$; $j_{3,1}$; $j_{4,1}$ and $j_{5,1}$ which are the only zeros in the

interval and hence the only maxima for $|A_n|$. The response curves

have been plotted for frictional coefficients of 0.00, 0.15, 0.50 and

1.00 inches/second, in view of the values used in Section (5.5) for

ocean swell with periods of 10 to 20 seconds and for tidal waves with

periods in the excess of a few hours it is expected that for the periods

used here a realistic value for C would probably be in the neighbour-

hood of 0.50 inches/second. Using Equation (3-4C) to calculate the

decay coefficient, it was found for this value of C that it took

approximately 150 miles for a wave travelling in a constant depth of

200 feet to decay by a factor of e and 9000 miles for waves travelling

in a depth of 3,200 feet. As found previously for the small scale model

the high "Q" modes are reduced in height by a relatively large amount

whereas the broader peaks are reduced comparatively much less. It

therefore appears that in a physical situation where friction is

important that the lower modes will be dominant and the higher modes

will have only a small effect on the surface configuration over the sill.

The response coefficient $|B_n|$ is plotted on Figure (43) for the even modes and again there is a considerable smoothing of the peaks and troughs. It is of interest to note that the "Q" of the response coefficient $|A_n|$ does not determine the sharpness of the maximum or minimum for the corresponding $|B_n|$, for an example illustrating this consider the mode corresponding to n = 0 on Figures (40) and (43) and compare with the mode corresponding to n = 2 on Figures (42) and (43).

7.7   The Maximum Surface Elevation over the Sill and in the Ocean

From a practical standpoint it is not so much of interest what the surface profile is at any given instant but what its extremes are. Since the individual components of the series representing the surface profile are out of phase with each other (the phase being determined by the relative sizes of the real and imaginary parts of the complex amplitudes) it is necessary to determine the times at which the components reinforce each other to give a maximum. The surface profile over the sill is the real part of:

$$\eta_2 = \sum_{n=0}^{\infty} A_n J_n(k_2 r) \cos n\theta \, e^{-i\sigma t} \tag{7-19}$$

where, since friction is introduced $J_n(k_2 r)$ is a complex quantity. Letting

$$J_n(k_2 r) = j_{n_2} e^{i \Omega n_2}$$

$$A_n = a_n e^{i \gamma_{n_2}}$$

and taking the real part of (7-19) gives:

$$\eta_2 = \sum_{n=0}^{\infty} a_n j_{n_2} \cos n\theta \cos(\gamma_{n_2} + \Omega_{n_2} - \sigma t) \tag{7-20}$$

FIGURE 40: COMPARISON OF THE MAGNITUDES OF THE RESPONSE COEFFICIENTS $|A_0|$ AND $|A_5|$ FOR VARIOUS VALUES OF THE FRICTION CONSTANT.
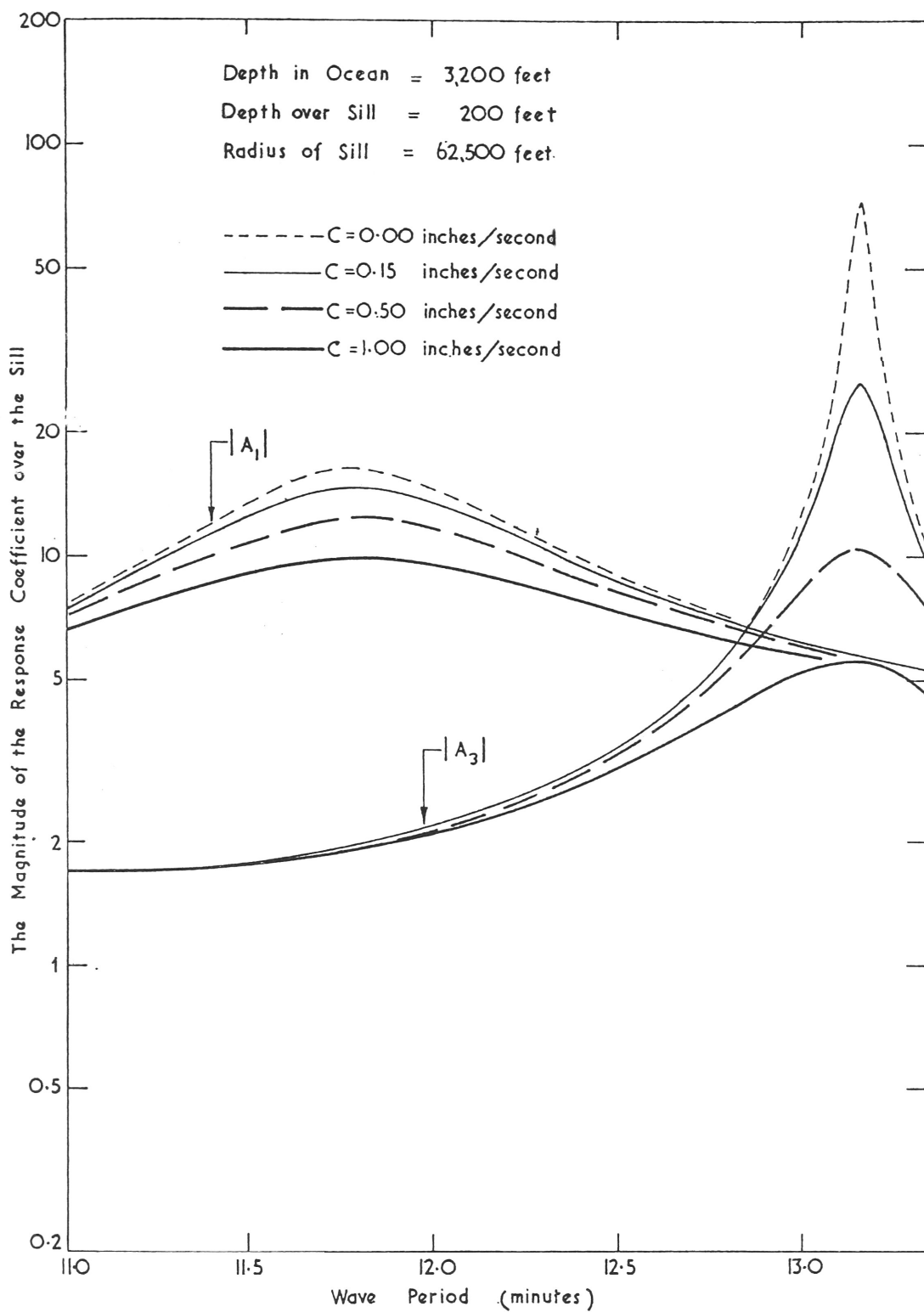
FIGURE 41: COMPARISON OF THE MAGNITUDES OF THE RESPONSE COEFFICIENTS $|A_1|$ AND $|A_3|$ FOR VARIOUS VALUES OF THE FRICTION CONSTANT.
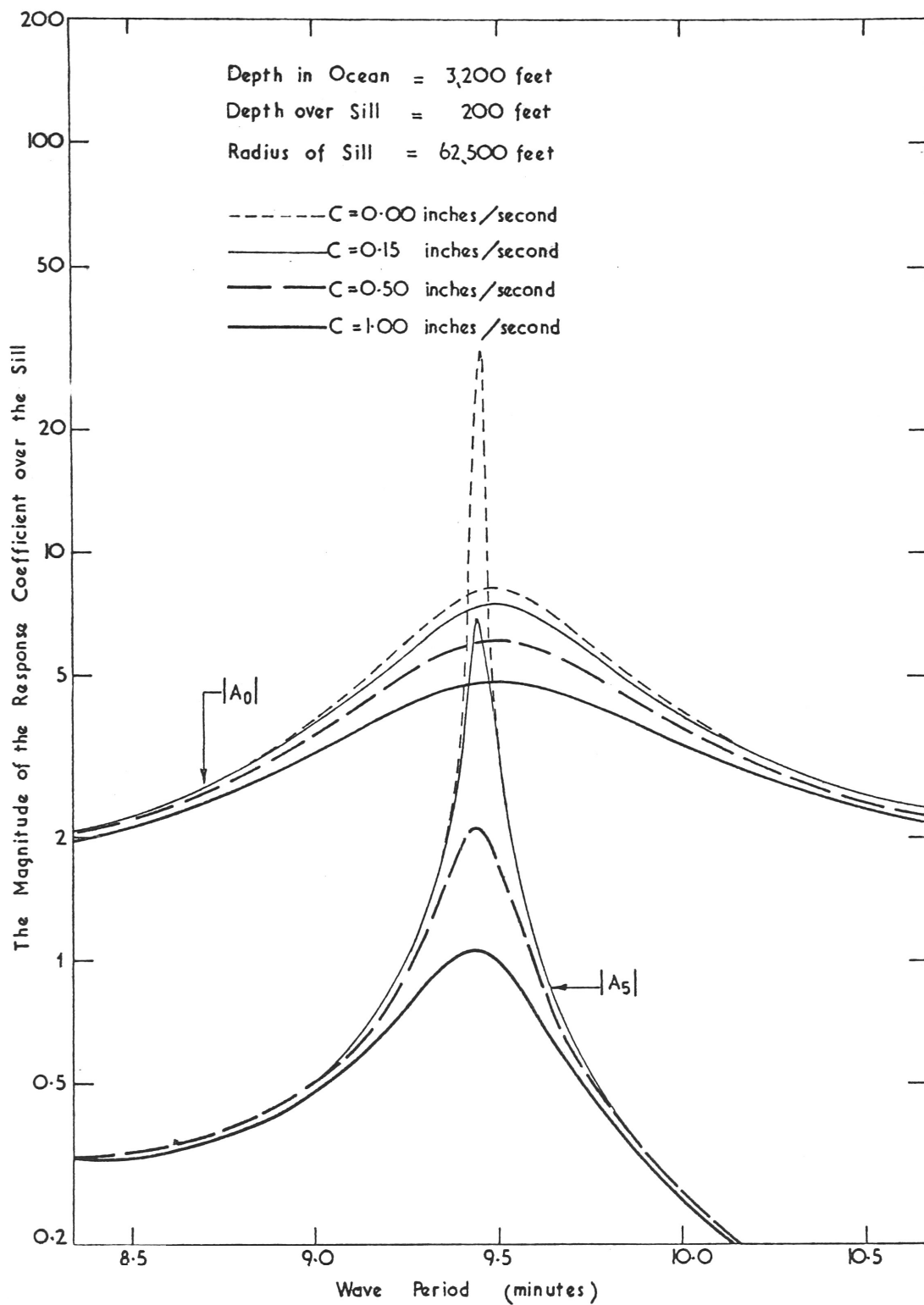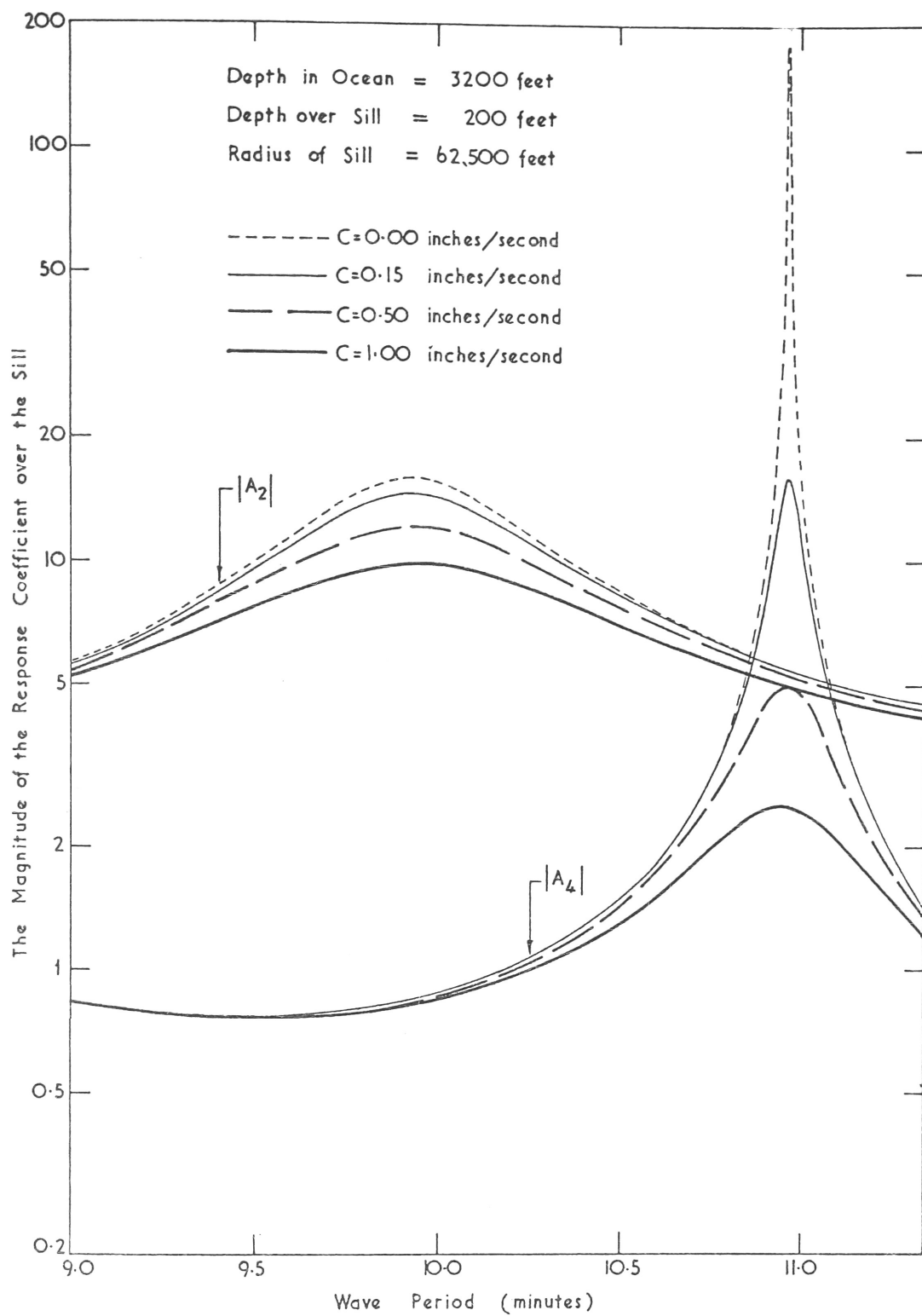
FIGURE 42: COMPARISON OF THE MAGNITUDES OF THE RESPONSE COEFFICIENTS $|A_2|$ AND $|A_4|$ FOR VARIOUS VALUES OF THE FRICTION CONSTANT
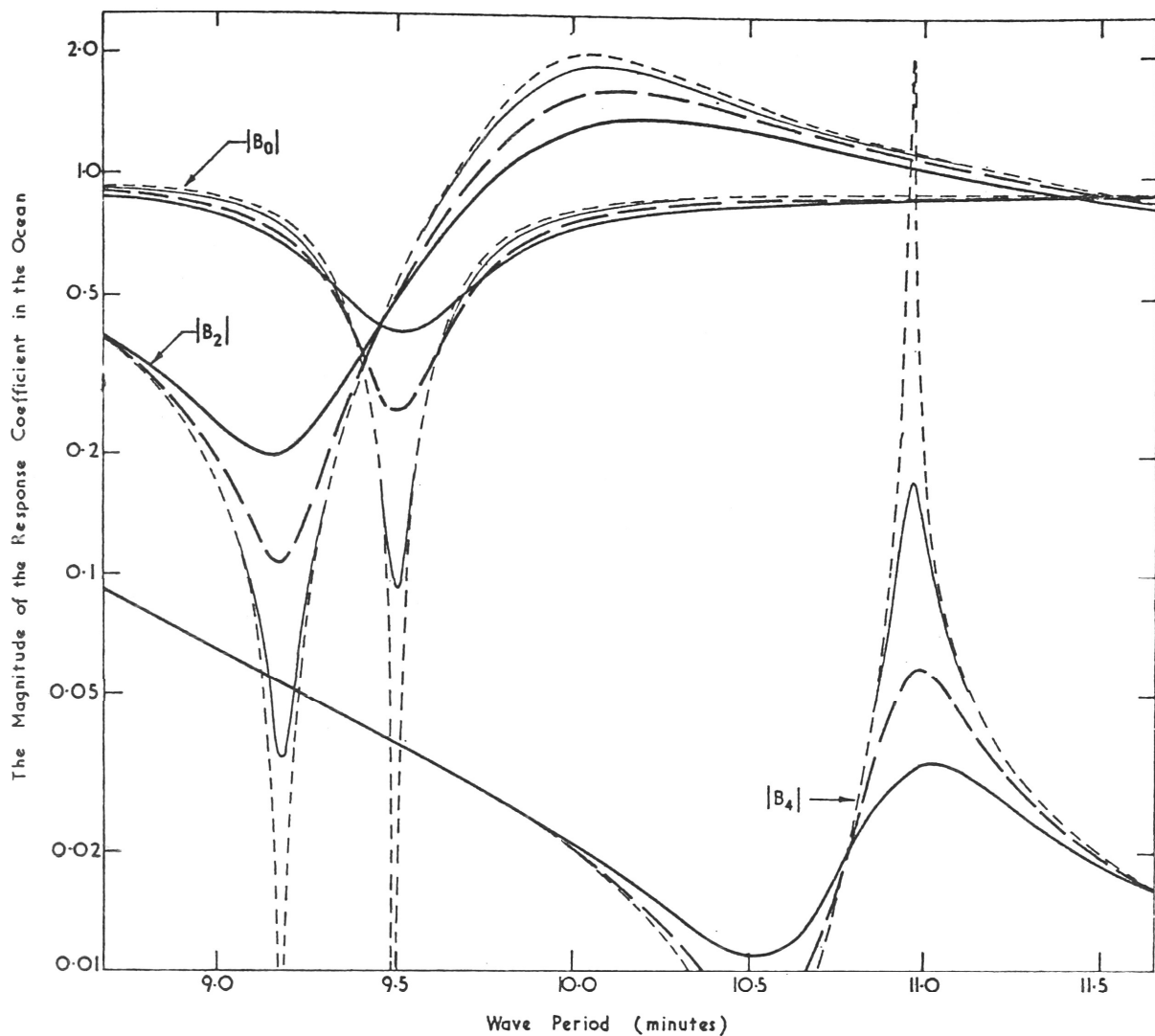
FIGURE 43: COMPARISON OF THE MAGNITUDES OF THE RESPONSE COEFFICIENTS $|B_0|$, $|B_2|$ AND $|B_4|$ FOR VARIOUS VALUES OF THE FRICTION CONSTANT.

To obtain a maximum with respect to the time variable, this expression differentiated term by term with respect to t and set equal to zero, the result is:

$$\frac{\partial \eta_2}{\partial t} = 0 = \sum_{n=0}^{\infty} a_n \, j_{n_2} \cos n\theta \, \sin\left(\gamma_{n_2} + \Omega_{n_2} - \sigma t\right)$$

Solving the the value of t which gives the extremes gives

$$t_{ext_2} = \frac{1}{\sigma} \tan^{-1}\left\{\frac{\sum_{n=0}^{\infty} a_n \, j_{n_2} \cos n\theta \, \sin\left(\gamma_{n_2} + \Omega_{n_2}\right)}{\sum_{n=0}^{\infty} a_n \, j_{n_2} \cos n\theta \, \cos\left(\gamma_{n_2} + \Omega_{n_2}\right)}\right\} \quad (7\text{-}21)$$

The surface profile in the ocean is the real part of:

$$\eta_1 = \sum_{n=0}^{\infty} \left(\epsilon_n i^n J_n(K_1 r) + B_n H_n^{(1)}(K_1 r)\right) \cos n\theta \, e^{-i\sigma t}$$

$$= e^{i(K_1 x - \sigma t)} + \sum_{n=0}^{\infty} B_n H_n^{(1)}(K_1 r) \cos n\theta \, e^{-i\sigma t} \quad (7\text{-}22)$$

Where the incident wave has been transformed from polar co-ordinates back into rectangular co-ordinates. This is convenient since, when evaluating the series only a finite number of terms are used and using the polar representation of the forcing waves requires a prohibitively large number of terms since $J_n(x)$ does not start to decrease monotonically until n and x are of approximately the same value.

Letting $H_n^{(1)} (K_1 \tau) = h_{n_1} e^{i \nu_{n_1}}$

$$B_n = b_n e^{i \gamma_{n_1}}$$

and taking the real part of (7-22) gives

(7-23)

$$\eta_1 = e^{-\alpha_1 x} \cos (k_1 x - \sigma t) + \sum_{n=0}^{\infty} h_{n_1} b_n \cos n \Theta \cos(\nu_{n_1} + \gamma_{n_1} - \sigma t)$$

Differentiating with respect to time, setting the result to zero and solving for the times which gives extremes for the surface profile in the ocean gives:

$$t_{ext_1} = \frac{1}{\sigma} \tan^{-1} \left\{ \frac{e^{-\alpha_1 x} \sin k_1 x + \sum_{n=0}^{\infty} h_{n_1} b_n \cos n \Theta \sin (\nu_{n_1} + \gamma_{n_1})}{e^{-\alpha_1 x} \cos k_1 x + \sum_{n=0}^{\infty} h_{n_1} b_n \cos n \Theta \cos (\nu_{n_1} + \gamma_{n_1})} \right\}$$

(7-24)

Using the values found in Equation (7-21) and (7-24) for the time which gives a maximum (or minimum) response in Equations (7-20) and (7-23) yields the formal solution. That the value for the minimum surface elevation is just the negative of the maximum is clear since all components of the composite wave have the same period.

In any practical calculation it is necessary to terminate the series after a given number of terms to make the calculations tractable. An estimate on the number of terms necessary can be made by determining the order of the function that gives a rank 1 zero $\left(j_{n, 1} \right)$ near to the value of $\mathcal{R} \left\{ K_2 R \right\}$ that is of interest such that $j_{n+1, 1}$ and zeros of higher order do not exist near $\mathcal{R} \left\{ K_2 R \right\}$. This order

can be determined using the approximate relation (7-18). Suppose the physical problem showed that $\mathcal{R}\left\{\kappa_2 R\right\}$ = 31, then from the example given in Section (7-4) if η = 25 there are no higher order zeros until $\gamma_{26,1}$ is reached at 32.63 (See Equation (7-18)). Therefore the series would require at least 26 terms (η = 0, 1, 2 ..... 25) and in a numerical calculation the values for $|B_\eta|$ and $|A_\eta|$ would be found by using a successively higher number of terms in the series until results are found that did not deviate with the addition of more terms past the desired accuracy.

In another example, consider the situation with the parameters as given on Figures (40)-(43) and suppose the value for $\mathcal{R}\left\{\kappa_1 R\right\}$ of interest was 7.5 then since $\gamma_{4,1}$ = 7.588 and $\gamma_{5,1}$ = 8.771 a starting point for the evaluation of the series would be taking η from 0 to 4. The calculated values for $|A_\eta|$ and $|B_\eta|$ for $\mathcal{R}\left\{\kappa_1 R\right\}$ = 7.5 are shown in Table (17-A) and (17-B) and, in this case, taking five terms in the sum neglects the η = 5 term whose magnitude is less than 5% of the smallest entry in the sum. Therefore 5 or possibly 6 terms will give a sufficient number of terms to calculate η_2 and the scattered component of η_1 . The effect of adding the individual components is shown in Figure (44) where the curves have been calculated using Equations (7-10) and (7-21) with one to six terms successively in the series. Figure (45) shows the reduction in height of the composite wave amplitude by friction damping and shows that the reduction is more pronounced for the higher "Q" modes (in this case the η = 4 mode).

CHAPTER 8

EXPERIMENTAL VERIFICATION OF THE AMPLIFICATION AND

SCATTERING OF WAVES BY A SUBMERGED CIRCULAR SILL

In this chapter the experimental verification of some of the results in Chapter 7 is carried out. Basically two experiments were undertaken, the first being the measurement of the wave profile over the sill at a fixed position using a variable wave period; and the second, the measurement of the surface profile at various positions for a fixed wave period.

8.1 The Experimental Equipment

A complete description of the large wave tank and wave generator is given in Appendices 6 and 7. Since a large number of wave periods were used, each of which had to be determined with a high degree of accuracy, it proved too extravagant to use a high chart speed and deduce the wave period from the output. Instead, a rough estimate of the wave period was found by use of a tachometer connected to the output shaft of the reduction gear box. (See, Photograph (A6:1) and (A6:4)). To obtain an accurate value for the period, a gear cog was fitted between the quick start mechanism and the drive plate, a set of automotive breaker points were fixed such that they opened and closed as the teeth on the gear cog rotated past them. (See, Photo (A6:4)). The number of times these points opened and closed during a

TABLE (17-A)

THE RESPONSE COEFFICIENTS $|A_n|$ FOR $R\{k,R\} = 7.5$

n / c in/sec.	0	1	2	3	4	5	6	7	8	9
0.00	2.119	7.092	5.692	1.726	12.528	0.078	0.010	0.002	0.000	0.000
0.15	2.105	6.950	5.626	1.724	9.842	0.078	0.010	0.002	0.000	0.000
0.50	2.069	6.601	5.456	1.715	4.697	0.078	0.009	0.002	0.000	0.000
1.00	2.007	6.008	5.186	1.692	2.512	0.077	0.009	0.002	0.000	0.000

TABLE (17-B)

THE RESPONSE COEFFICIENTS $|B_n|$ FOR $R\{k,R\} = 7.5$

n / c in/sec.	0	1	2	3	4	5	6	7	8	9
0.00	0.915	0.802	1.188	0.174	0.124	0.001	0.000	0.000	0.000	0.000
0.15	0.910	0.786	1.176	0.174	0.094	0.001	0.000	0.000	0.000	0.000
0.50	0.897	0.748	1.143	0.174	0.049	0.001	0.000	0.000	0.000	0.000
1.00	0.881	0.697	1.098	0.174	0.030	0.001	0.000	0.000	0.000	0.000

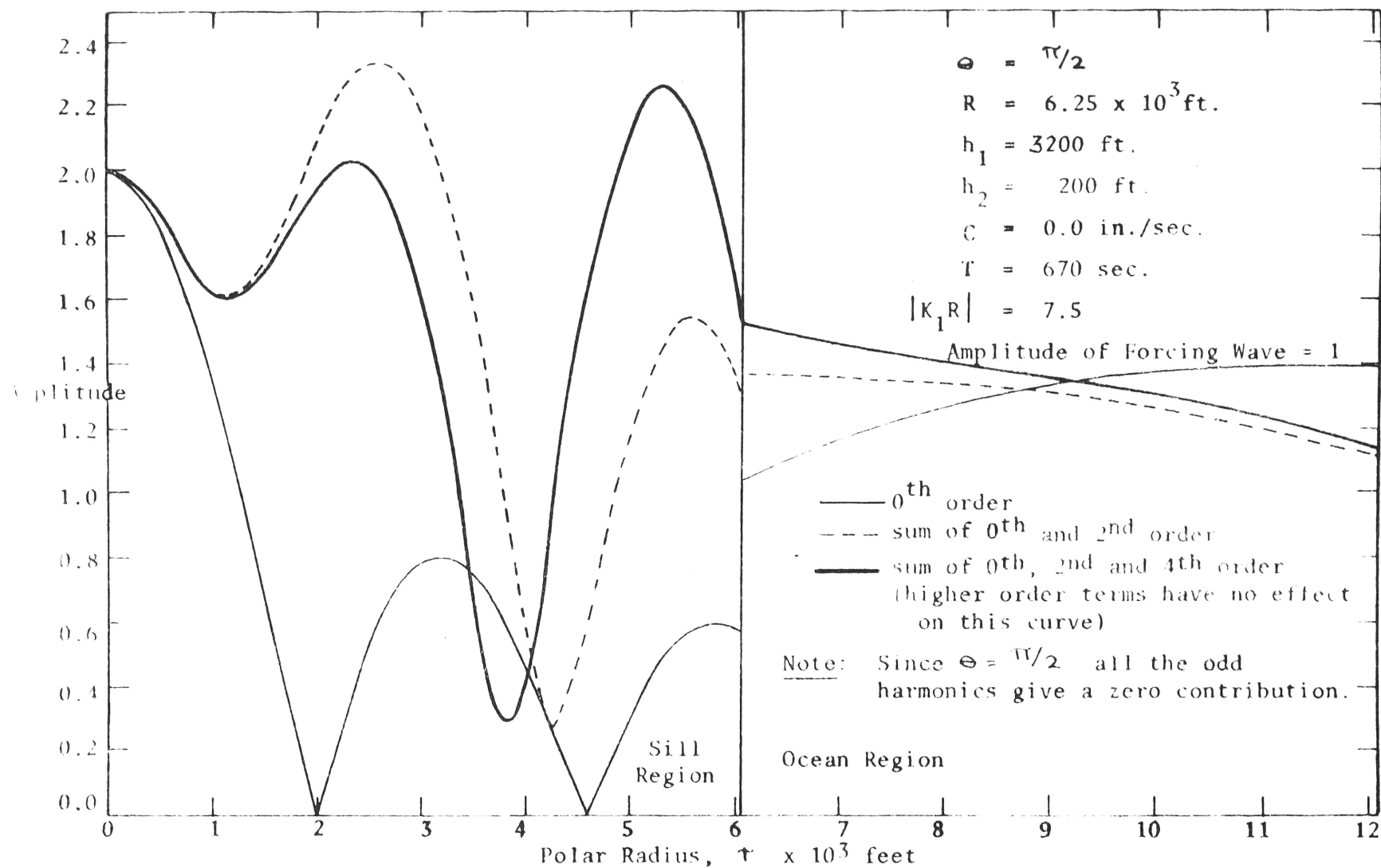$R = 6.25 \times 10^5$ feet; $h_1 = 3600$ feet; $h_2 = 200$ feet

FIGURE 44: THE AMPLITUDE OF THE WAVES OVER THE SILL AND IN THE OCEAN USING VARIOUS NUMBERS OF TERMS IN THE INFINITE SUM
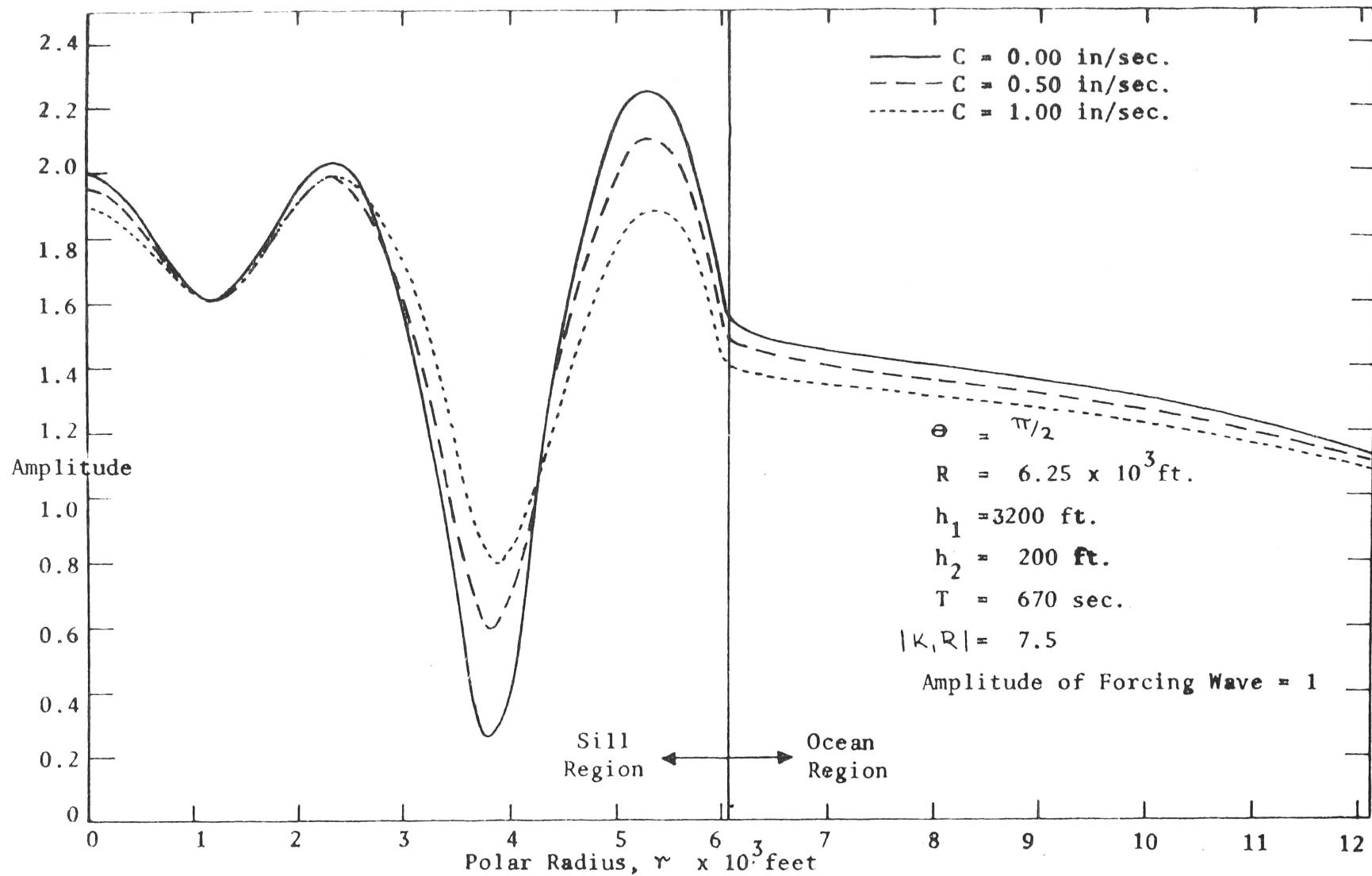
FIGURE 45   THE AMPLITUDE OF THE COMPOSITE WAVES OVER THE SILL AND IN THE OCEAN FOR
VARIOUS FRICTION COEFFICIENTS

fixed time interval was recorded on a digital counter, the time interval was measured using a crystal timer.

The greatest difficulties with this type of experiment, where an infinite ocean is assumed in all directions, is firstly the elimination of reflections from anything but the model itself and, secondly, the production of a plane wave train of constant amplitude along the wave crest. As pointed out in Appendix 7 these difficulties are not exclusive of one another in that it is a relatively simple matter to design absorbers around the tank such that all reflections are less than 8% but this generally renders a poor quality incident wave; on the other hand if the wave absorbers are removed from all but the end of the tank an incident wave of constant height is easily obtained in the model area. Appendix 7 gives details of the wave absorbers and wave guides for various experimental conditions. It is felt that reflections and asymmetries of the incident wave gave the greatest source of error in these experiments. Another source of error was anticipated because of the distance between the sensing wires on the wave probe. This distance was ¼ inch and thus the measured wave heights did not correspond to a point measurement but to the average of the heights existing at the position of each sensing wire.

In all experiments the depth in the ocean was set at 1.33 inches and that over the sill at 0.33 inches. This did not give as high a depth ratio as was desired but it proved too difficult to absorb the

waves successfully if the depth in the ocean was increased greatly.
A reduction of the depth over the sill gave problems with second
order effects caused by the relatively large wave amplitudes generated
over the sill by the forcing waves. The incident wave was typically
.005 inches to .01 inches in height which produced waves of at most
two or three times this size over the sill. A circular sill was
constructed from a flat steel plate 18 inches in diameter and one
inch thick, this plate was surface ground such that its thickness was
constant to within .001 inch.

8.2   Measurement of the Surface Profile over the Sill for Various Wave Periods

The surface probe was set at a fixed position over the sill and
wave heights were measured for a variety of wave periods using a fixed
amplitude of motion of the wave paddle. The circular sill was then
removed from the tank and wave heights were measured at a few positions
in $+ < R$ with the probe situated along the $\theta = \frac{\pi}{2}$ line. These
measurements, when averaged for each period, corresponded to the
incident wave height and from Figure (46) it is seen that the
variation in incident wave height with period generally corresponds to
the variation found in the surface probe tests. (See, Figures (A8-3,4),
the differences between these curves is attributed to the changing
value for the decay constant, C, with wave period. The wave heights
H_2, measured over the sill were compared with the heights of the
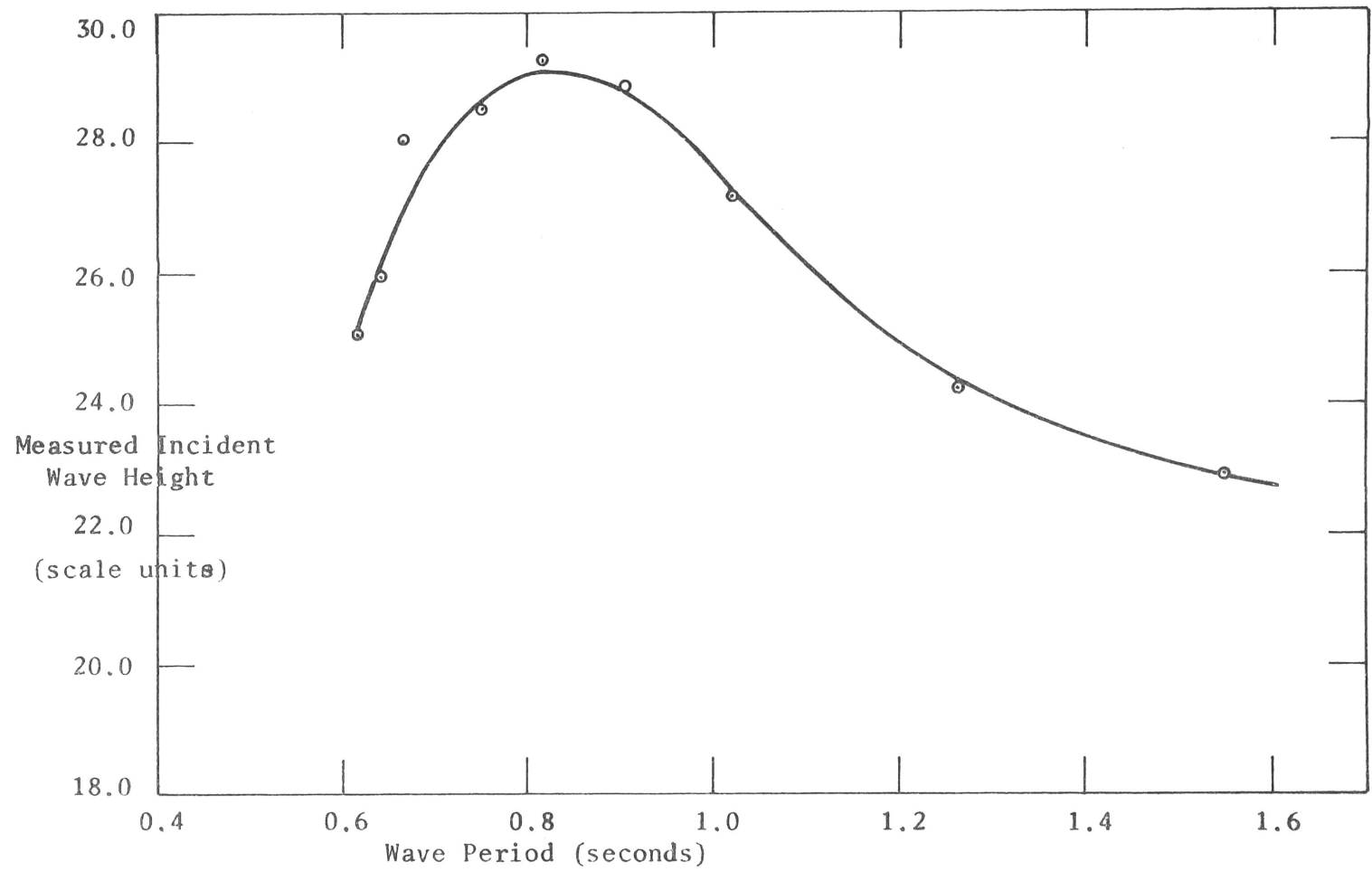
FIGURE: 46   VARIATION OF THE MEASURED INCIDENT WAVE HEIGHT WITH WAVE PERIOD

incident waves, H_i, of the same periods; these latter heights were found from the ordinate on Figure (46). The ratio of these two heights, H_2/H_i, gave the surface response over the sill to a forcing wave of unit amplitude. These results are shown graphically in Figure (47) and compared with the theoretical predictions calculated using Equations 7-20 and 7-21, the friction constant for the various wave periods was calculated from the emperical relation determined experimentally in Chapter 4 (See, Figure (18)). There appears to be reasonably good agreement between the experimental results and those predicted from the theory. For comparison, the theoretical results, when friction is neglected, are plotted on Figure (47). The build up of the wave height over the sill corresponding to the maximum at about 1.2 seconds is shown in Figure (48a) and the reduction in wave height corresponding to the minimum at about 0.92 seconds is shown in Figure (48b), these figures reveal that a steady state wave height was reached after about 8 or 10 cycles.

8.3 Measurement of the Surface Profile at Different Radii using a Constant Wave Period

Using a constant wave period and a fixed value for the angle Θ , wave heights were measured at various radii over the sill and in the ocean. The sill was then removed from the tank and the wave heights were measured along the $\Theta = \dfrac{\pi}{2}$ line, an average of these results

was taken to give the incident wave height. The variation in wave height across the tank was generally ± 5% to 10% from this average and was attributed to interference effects from secondary waves incident from the absorbers.

The wave heights measured with the sill in place were compared with the average incident wave height to give the ratios H_2/H_i over the sill and H_s/H_i in the ocean. These results are shown in Figures (49), (50) and (51) for wave periods of 2.37, 0.977, and 0.604 seconds respectively. The theoretical results are in reasonably good agreement with the experimental ones. The rather large discrepancy near the left hand side of the sill edge on Figure (51) is a consequence of the incident wave in this region having a somewhat lower height than the average: although the results are low in this region, the change in height with radius agrees well with the theoretical ones.

The theoretical curves when friction is neglected are drawn on these figures and indicate a much larger range of wave heights than were found experimentally or theoretically when friction is introduced. Table (18) lists the response coefficients $|A_n|$ and $|B_n|$ corresponding to the wave periods given above and shows that for $T = 2.37$ seconds only the lowest modes are of importance whereas the higher order modes gain importance as T decreases.
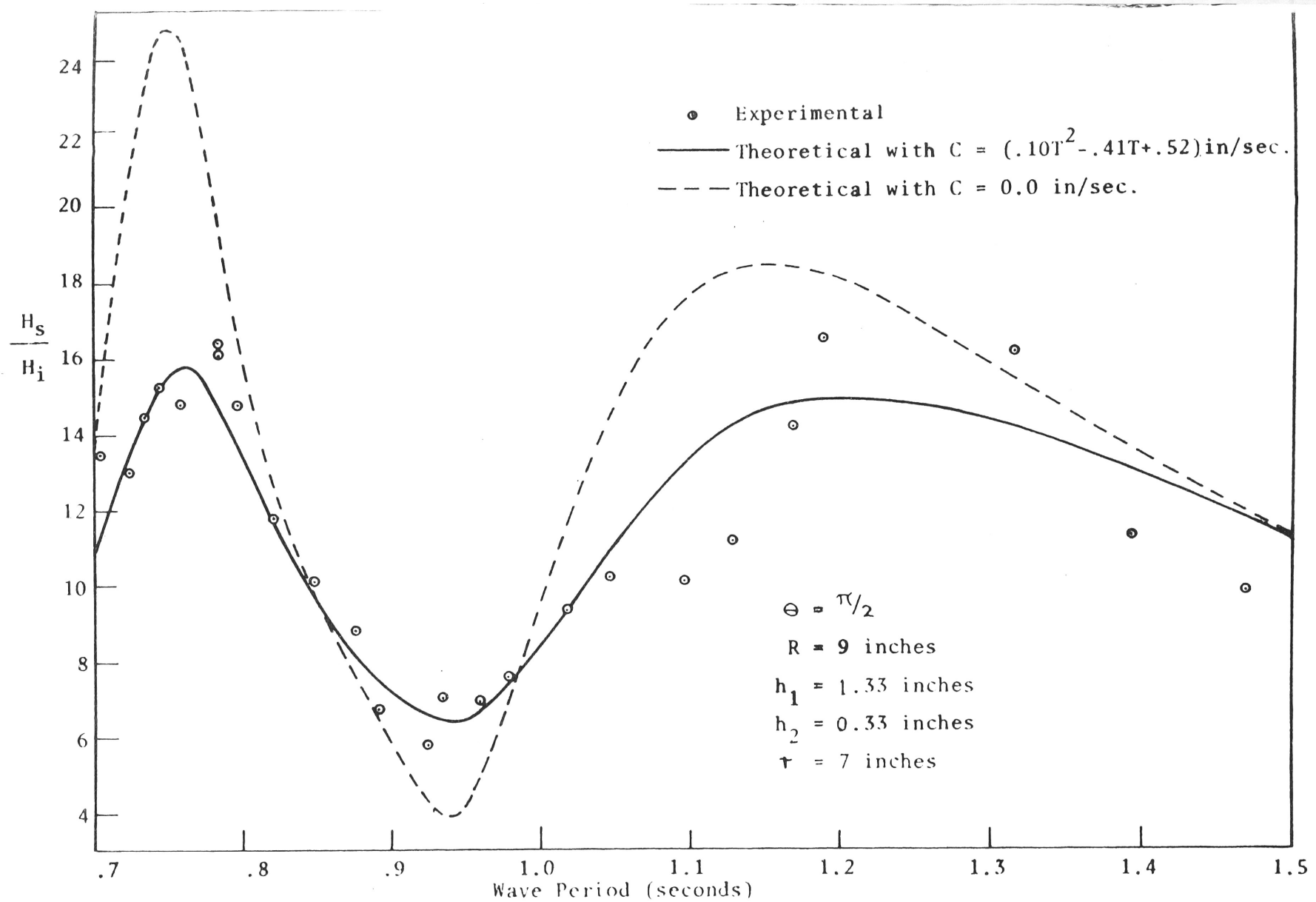
FIGURE 47: THE VARIATION OF THE RELATIVE WAVE HEIGHT OVER THE SILL WITH
WAVE PERIOD (RELATIVE TO A FORCING WAVE OF HEIGHT = H_i)
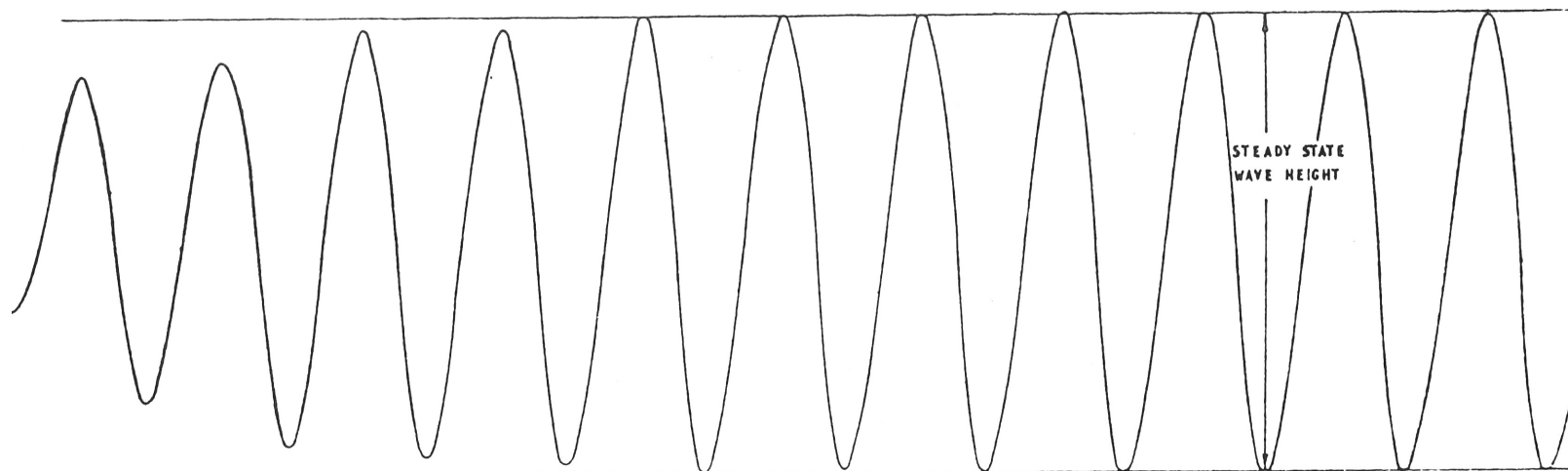
FIGURE 48a. WAVE PROFILE SHOWING BUILD-UP OF WAVE HEIGHT OVER THE SILL (T=1.19 sec.)

STEADY STATE
WAVE HEIGHT
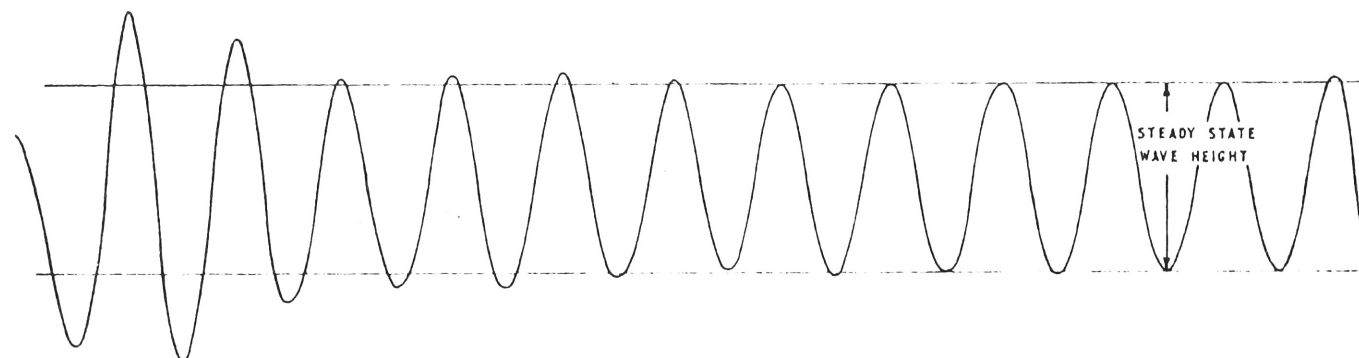
FIGURE 48b. WAVE PROFILE SHOWING REDUCTION OF WAVE HEIGHT OVER THE SILL (T=0.921 sec.)

$\Theta = \frac{\pi}{2}$

$R = 9$ inches

$h_1 = 1.33$ inches

$h_2 = 0.33$ inches

$T = 7$ inches
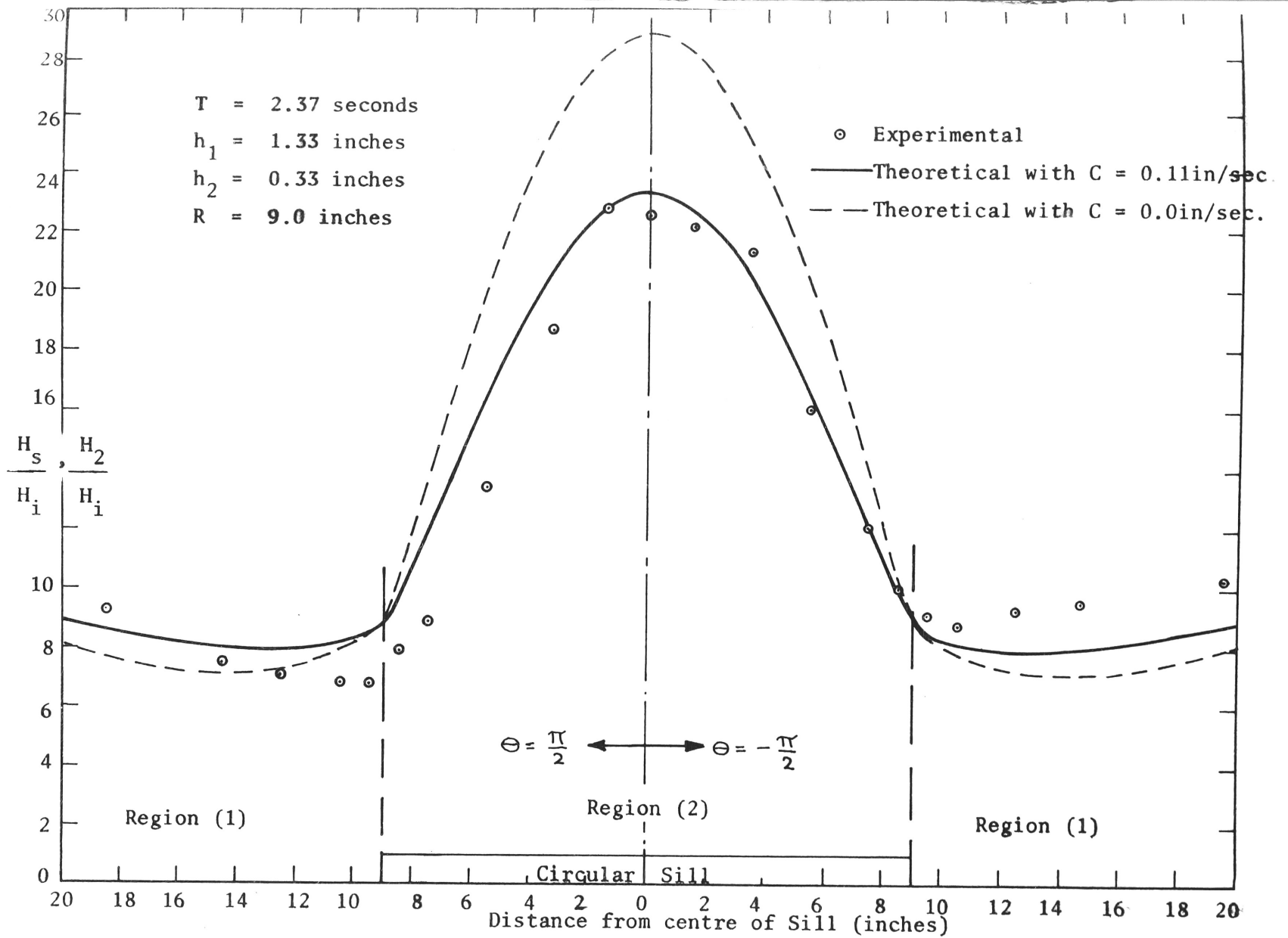
FIGURE 49: THE RELATIVE HEIGHT OF THE WAVES IN THE OCEAN AND OVER THE SILL FOR T = 2.37secs. (RELATIVE TO A FORCING WAVE OF HEIGHT = H_i)
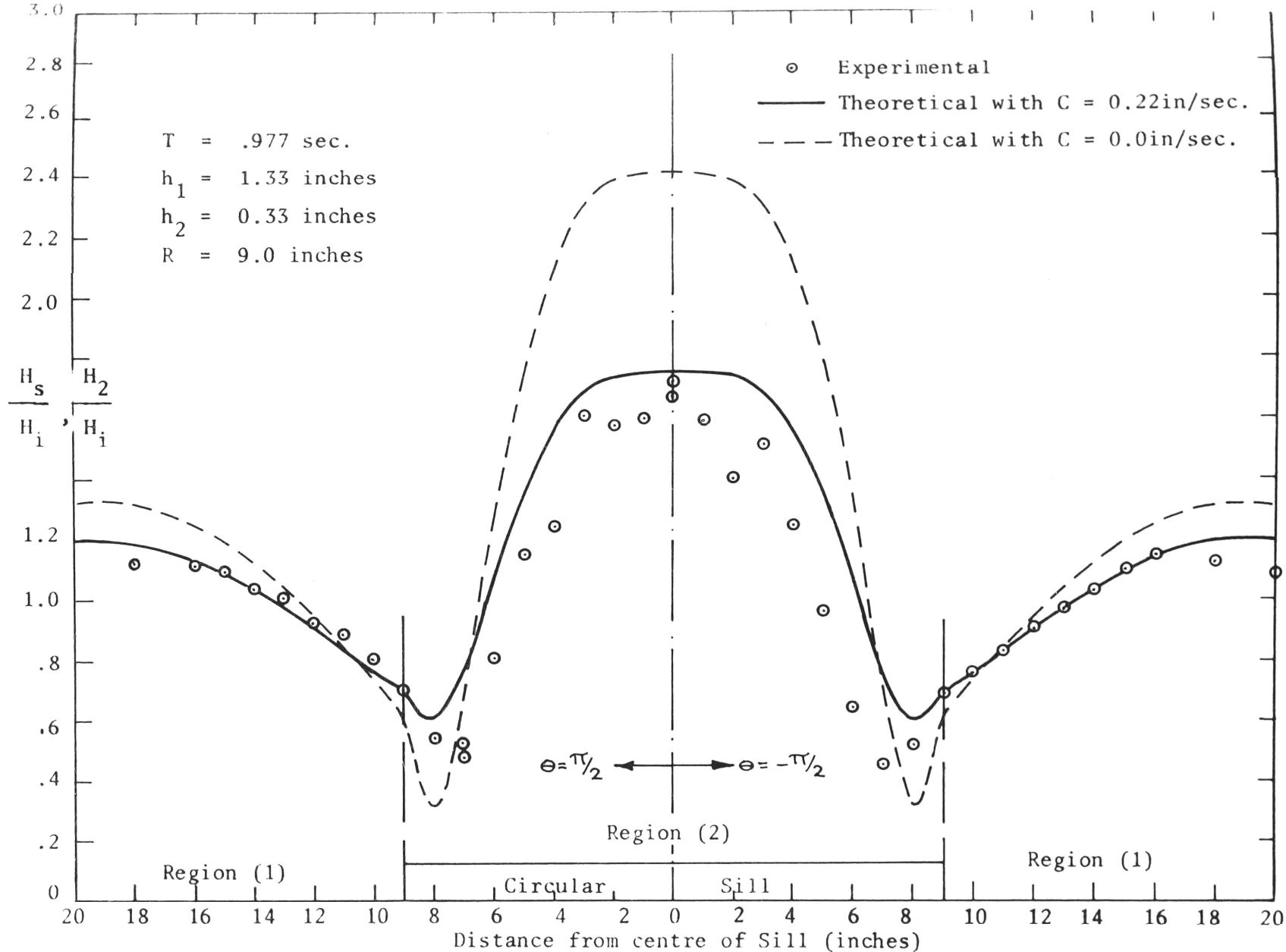
FIGURE 50:   THE RELATIVE HEIGHT OF THE WAVES IN THE OCEAN AND OVER THE SILL FOR T = 0.604
(RELATIVE TO A FORCING WAVE OF HEIGHT = H_i)
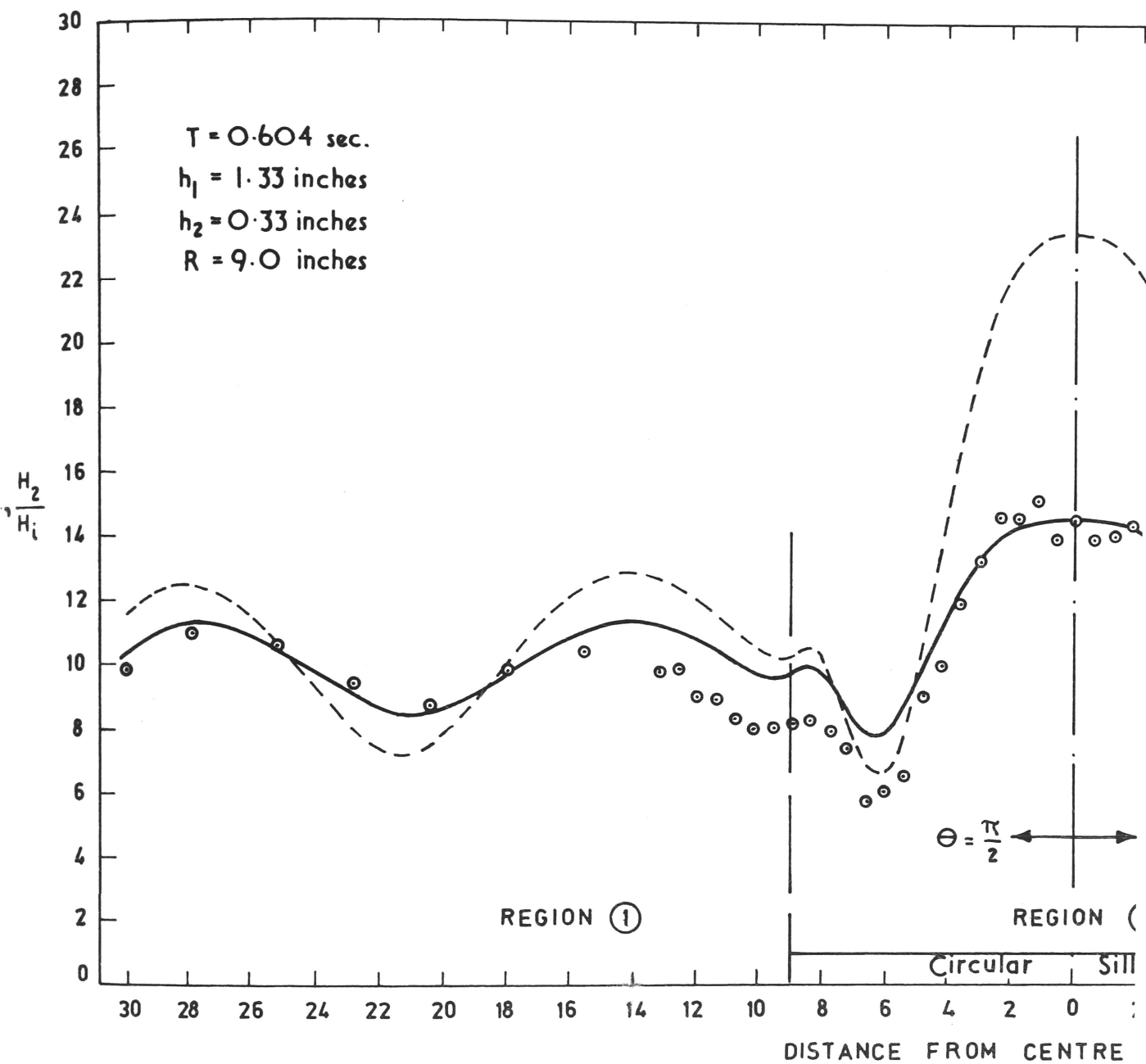
FIGURE 5I: THE RELATIVE HEIGHT OF THE WAVES IN THE OCE.

(Relative to a Forcing Wave of Height =

TABLE 18

THE THEORETICAL RESPONSE COEFFICIENTS

USED TO CALCULATE THE SURFACE PROFILE FOR PARAMETERS

CORRESPONDING TO EXPERIMENTAL CONDITIONS

n	T = 2.37 sec.		T = 0.977 sec.		T = 0.604 sec.	
	$|A_n|$	$|B_n|$	$|A_n|$	$|B_n|$	$|A_n|$	$|B_n|$
0	2.338	0.540	1.749	0.651	1.455	0.479
1	2.450	0.815	2.496	1.171	2.252	1.278
2	1.226	0.141	3.525	1.231	2.896	1.023
3	0.522	0.006	3.107	1.149	2.493	0.404
4	0.242	0.000	0.903	0.153	2.392	0.377
5	0.116	0.000	0.305	0.012	2.799	0.775
6	0.057	0.000	0.125	0.001	1.569	0.329
7	0.028	0.000	0.055	0.000	0.339	0.028
8	0.013	0.000	0.025	0.000	0.113	0.002
9	0.001	0.000	0.012	0.000	0.045	0.000

CONCLUSIONS

The equations of motion were developed for small amplitude
surface waves with a distributed body force associated with them.
Based on these equations it was shown that the effect of friction
was to reduce the average wave energy over the no friction case
as a result of:

(i)   A reduction in wave amplitude due to frictional
      damping.

(ii) A reduction in the water particle velocities
      for a wave of given amplitude.

The velocity of phase, energy and groups was calculated and found,
as in electro-magnetic theory, to be generally different from one
another. There was found to be a continuous reduction in the
energy velocity as friction was increased.

Experiments were carried out using a constant fluid depth to
determine values for the friction constant for different fluids and
different wave periods. It was found the friction coefficient
varied with wave period but was independent of fluid depth. These
findings are in general agreement with the literature but the
functional variation of C with wave period is not. This discrepancy
is attributed to the shallow depths and/or to the moderately
viscous fluids used and thus to a relatively thick boundary layer
which extends throughout a significant portion of the fluid depth.

The results in the literature generally assume parameters such
that the boundary layer thickness is much less than the fluid
depth. This boundary layer necessitated a definition of an
effective depth which was based on the experimental phase velocity;
for the viscous glycerol solutions used in the experiments this
effective depth was measurably different from the measured depth
whereas for water this difference was not evident. The attenuation
of the wave amplitude by surface boundary layer was investigated
and for the parameters used in this experiment, the attenuation
was insignificant compared with that due to the bottom friction. On
the other hand, using the glycerol mixture, the surface appeared to
change from a horizontally fairly mobile one after complete mixing to
an immobile one after the fluid had been let stand for an hour
or so. Phase differences between the horizontal particle motion and
the surface profile showed an increase with time after mixing,
indicating an influence of the surface layer on the particle motion.

The reflection and transmission coefficients for plane waves
incident normally to a depth discontinuity were deduced using an
approximate model. The matching conditions at the depth discontinuity
were that at any instant the flux of energy was continuous and that
the surface was a continuous streamline. The solution of the
problem was carried out under the approximation that the potential
function was discontinuous at the step and the further assumption
was made that the values for the reflection and transmission

coefficients found in this manner would be valid at some distance from the depth discontinuity. The effect of friction was found to increase both α_t and α_r when waves were propagated from deeper to shallower water and to decrease α_t and increase α_r for propagation from shallower to deeper water. This change in the magnitude of the coefficients was a consequence of the greater effect of friction on the wave properties in the shallow than in the deep region, or, more specifically the energy flux was reduced by friction more in the shallow than in the deep region. Limiting values of $\alpha_r \Rightarrow 1$ and $\alpha_t \Rightarrow 2$ were found when $\dfrac{v_{e_1}}{v_{e_2}} \rightarrow \infty$ and of $\alpha_r \Rightarrow 1$ and $\alpha_t \Rightarrow 0$ when $\dfrac{v_{e_1}}{v_{e_2}} \rightarrow 0$ The effect of friction on the reflection and transmission coefficients for large scale oceanographic situations was to produce only a very small difference in their values from the frictionless ones.

Experiments were run using moderately viscous glycerol and water solutions to determine the effects of friction on the reflection and transmission coefficients. These results were compared with the theoretical ones and showed that, as predicted, friction had little effect on either α_r or α_t . Estimations of energy losses in the viscinity of the step were determined using the experimental wave heights measured at some distance from the step. These results showed, within the experimental error, that little

energy was lost when waves were propagated from the deep to the
shallow region. For propagation from the shallow to the deep
region an average loss of about 10 percent was observed. This
loss was attributed to the generation of an eddy in the lee of
the step. The local disturbance downwave of the discontinuity
was examined and showed that for the glycerol mixtures, there was
very little extraneous surface agitation in this region whereas a
marked local disturbance was found when the fluid mixture was
replaced with water. It thus appeared that frictional damping
rapidly reduced the local surface disturbance at such a rate that
they were no longer evident.

The response coefficients over a submerged circular sill
subject to a plane forcing wave from the ocean were found using the
matching conditions at the depth discontinuity as used for the
straight shelf. Physical arguments indicated that the nth response
coefficient over the sill should be a maximum when the sill edge
was near a zero of $J_n(\kappa_1 R)$, numerical calculations showed this to
be the case as well as showing that the response coefficient for the
scattered wave was either near a maximum or minimum when A_n
was a maximum. Therefore as the radius of the sill becomes progress-
ively smaller compared with the wave length fewer and fewer modes are
present over the sill; this finding was also deduced using asymptotic

approximations. The effect of friction was to reduce the response coefficient over the sill and this reduction was found to be proportionately much greater for the high "Q" modes than for the less sharp ones. A reduction in magnitude of the peaks and troughs corresponding to the response coefficient in the ocean was found and, again, this reduction was greatest for the more sharply tuned modes; B_n no longer reached its extreme values of zero or ϵ_n .

Since the zeros of $J_n(\kappa_1 R)$ are interlaced and, for a given with $\kappa_1 R$ sufficiently large, are separated by approximately π then in a relatively narrow frequency band there will be many resonant modes present. With regard to the effect of friction on $|A_n|$ and to the fact that each mode has generally a different phase from any other it is unlikely at the higher frequencies, that any single mode will be dominant over the rest. This is not the case at lower frequencies where only the lower modes are present and their resonant peaks do not overlap greatly.

The theory of forced oscillations (with damping) over a circular sill was verified in two experiments. The first with all parameters held fixed and varying the wave period, and the second varying the position of measurement along a radius with period constant. These results agreed quite well with the theoretical ones and showed a large change from that predicted by frictionless theory.

It was assumed, in the theoretical model, that the friction term could be considered linear with respect to the near bottom particle velocity. This appeared reasonable in that if the particle motion near the bottom was laminar, then, as has been shown by a variety of authors, the friction term, to a first approximation, is linear. In all the experimental work in this thesis, the particle motion was small hence the motion near the bottom was laminar.

In large scale oceanographic situations the motion near the boundary is often turbulent and thus the friction force follows a quadratic law. This quadratic term may be linearized by equating the work done over a complete wave period using the quadractic term to that done using an equivalent linear friction term. Provided this linearization process is valid such that a representative coefficient may be found for the linear friction model, then the theoretical and experimental results presented in this thesis will be expected to apply to the case of turbulent motion near the bottom.

APPENDIX 1

EVALUATION OF THE REAL PART OF THE POTENTIAL FUNCTION

Equation (2-10) expresses the velocity potential in complex form as:

$$\phi_c(x, z, t) = \frac{i \sigma A \cosh K(z+h)}{K \sinh Kh} e^{i(Kx - \sigma t)}$$

ere $K = k + i\alpha$

The hyperbolic functions with complex arguments may be written in terms of functions with real arguments as :

$$\cosh((k+i\alpha)h) = \cosh kh \cos \alpha h + i \sinh kh \sin \alpha h$$

$$\text{and} \quad \sinh((k+i\alpha)h) = \sinh kh \cos \alpha h + i \cosh kh \sin \alpha h$$

Therefore: $\sinh Kh = \Delta e^{i\delta}$

where $\delta = \tan^{-1} \left\{ \dfrac{\cosh kh \sin \alpha h}{\sinh kh \cos \alpha h} \right\}$

and $\Delta = \left\{ (\sinh kh \cos \alpha h)^2 + (\cosh kh \sin \alpha h)^2 \right\}^{1/2}$

$$= \sqrt{\sinh^2 kh + \sin^2 \alpha h}$$

similarly: $K = \mathcal{K} e^{i\Omega}$

where $\Omega = \tan^{-1} \dfrac{\alpha}{k}$

and $\mathcal{K} = \sqrt{k^2 + \alpha^2}$

The complex constant $(K \sinh Kh)$ is then:

$$\frac{1}{\Delta \mathcal{K}} e^{-i(\Omega + \delta)}$$

$$= \frac{1}{\Delta \mathcal{K}} (\cos \epsilon + i \sin \epsilon) \quad ; \quad \epsilon = \Omega + \delta \qquad (A1-1)$$

The variable part of the potential function is:

$$\cosh K (z+h) e^{i(kx-\sigma t)}$$

$$= e^{-\lambda x} \cosh((k+i\lambda)Z) \; e^{i(kx-\sigma t)} \qquad ; \qquad Z = z + h$$

$$= e^{-\lambda x} \{(\cosh kZ \cos \lambda Z + i \sinh kZ \sin \lambda Z)(\cos(kx-\sigma t) + i \sin(kx-\sigma t))\}$$

$$= e^{-\lambda x} \{(\cosh kZ \cos \lambda Z \cos(kx-\sigma t) - \sinh kZ \sin \lambda Z \sin(kx-\sigma t))$$
$$+ i(\cosh kZ \cos \lambda Z \sin(kx-\sigma t) + \sinh kZ \sin \lambda Z \cos(kx-\sigma t)) \}$$

$$(A1-2)$$

The real part of ϕ_c is then:

$$\mathcal{R}\{\phi_c\} = \phi(x, z, t)$$

$$= \frac{\sigma A e^{-\lambda x}}{\Delta K} \{ -\cos \epsilon [\cosh kZ \cos \lambda Z \sin(kx-\sigma t) + \sinh kZ \sin \lambda Z \cos(kx-\sigma t)]$$
$$+ \sin \epsilon [\cosh kZ \cos \lambda Z \cos(kx-\sigma t) - \sinh kZ \sin \lambda Z \sin(kx-\sigma t)] \}$$

$$= \frac{\sigma A e^{-\lambda x}}{\Delta K} \{ -\cosh kZ \cos \lambda Z [-\sin \epsilon \cos(kx-\sigma t) + \cos \epsilon \sin(kx-\sigma t)]$$
$$- \sinh kZ \sin \lambda Z [\cos \epsilon \cos(kx-\sigma t) + \sin \epsilon \sin(kx-\sigma t)] \}$$

$$\phi(x,z,t) = \frac{-\sigma A e^{-\lambda x}}{\Delta K} \{ \cosh kZ \cos \lambda Z \sin(kx-\sigma t-\epsilon)$$
$$+ \sinh kZ \sin \lambda Z \cos(kx-\sigma t-\epsilon) \}$$

$$(A1-3)$$

APPENDIX 2

EVALUATION OF THE WAVE NUMBER "k" AND THE DECAY COEFFICIENT "α"

The free surface Bernoulli equation is:

$$\left\{ \frac{\partial \phi}{\partial t} + \frac{c}{h} \phi_b \right\}_{z \simeq 0} = g \eta$$

where

$$\frac{\partial \phi}{\partial t}\bigg/_{z \simeq 0} = \frac{\sigma^2 A e^{-\alpha x}}{\Delta \kappa} \left\{ \cosh kh \cos \alpha h \cos(kx - \sigma t - \epsilon) - \sinh kh \sin \alpha h \sin(kx - \sigma t - \epsilon) \right\}$$

and

$$\phi_b = \frac{-\sigma A e^{-\alpha x}}{\Delta \kappa} \sin(kx - \sigma t - \epsilon)$$

The surface profile is described as:

$$\eta = R \left\{ A e^{i(kx - \sigma t)} \right.$$
$$= A e^{-\alpha x} \cos(kx - \sigma t)$$

Thus, at the free surface:

$$\frac{\sigma^2}{\Delta \kappa} \left\{ \cosh kh \cos \alpha h \cos(kx - \sigma t - \epsilon) \ \sinh kh \sin \alpha h \sin(kx - \sigma t - \epsilon) \right.$$
$$\left. - \frac{c}{\sigma h} \sin(kx - \sigma t - \epsilon) \right\} = \cos(kx - \sigma t)$$

$$\text{(A2-1)}$$

which is the dispersion relation for k and α.

The evaluation of the constants k and α is most expediently carried out using equation (2-7b), the complex form of the dispersion relation.

$$\phi e^{-i\sigma t} \left\{ \left(\frac{-i\sigma f(z) + \frac{c}{h} f(-h)}{g} \right)_{z \simeq 0} \right\} = A \cdot z e^{-i\sigma t}$$

Two equations in the two unknowns are then obtained by equating the real and imaginary parts of the above equation.

From equation (2-8):

$$f(\mathfrak{z}) = -\frac{\sigma A}{K \sinh Kh} \cosh K (\mathfrak{z} + h)$$

so

$$\frac{\sigma^2}{gK \sinh Kh} \cosh Kh + \frac{i c \sigma}{ghK \sinh Kh} = 1$$

or

$$\frac{\sigma^2}{gK \sinh Kh} \left\{ \cosh Kh + \frac{i c}{\sigma h} \right\} = 1 \qquad\qquad \text{(A2-2)}$$

The complex constant $(K \sinh Kh)$ has been expressed (equation (A1-1)) as

$\dfrac{\cos \epsilon - i \sin \epsilon}{\Delta K}$. Expanding the trigonometric terms in this relation

such that their dependance on k and α is more explicit.

$$\cos \epsilon = \cos (\delta + \Omega) = \cos \delta \cos \Omega - \sin \delta \sin \Omega$$
$$= \frac{1}{\Delta K} \left\{ k \sinh kh \cos \alpha h - \alpha \cosh kh \sin \alpha h \right\}$$

and $\sin \epsilon = \sin (\delta + \Omega) = \sin \delta \cos \Omega + \cos \delta \sin \Omega$
$$= \frac{1}{\Delta K} \left\{ k \cosh kh \sin \alpha h + \alpha \sinh kh \cos \alpha h \right\}$$

Therefore equation (A2-2) becomes:

$$\frac{\sigma^2}{g\Delta^2 K} \left\{ (k \sinh kh \cos \alpha h - \alpha \cosh kh \sin \alpha h) - i (k \cosh kh \sin \alpha h - \alpha \sinh kh \cos \alpha h) \right\}$$
$$\times \left\{ \cosh kh \cos \alpha h + i (\sinh kh \sin \alpha h + \frac{c}{\sigma h}) \right\} = 1$$

Equating real and imaginary parts gives:

$$\frac{\sigma^2}{g\Delta^2 K^2} \left\{ (k \sinh kh \cos \alpha h - \alpha \cosh kh \sin \alpha h)(\cosh kh \cos \alpha h) \right.$$
$$\left. + (k \cosh kh \sin \alpha h + \alpha \sinh kh \cos \alpha h)(\sinh kh \sin \alpha h + \frac{c}{\sigma h}) \right\} = 1$$

$$\text{(A2-3a)}$$

and

$$(k \sinh kh \cos \alpha h - \alpha \cosh kh \sin \alpha h)(\sinh kh \sin \alpha h + \frac{c}{\sigma h}$$

$$-(k \cosh kh \sin \alpha h + \alpha \sinh kh \cos \alpha h) \cosh kh \cos \alpha h \ ) \ = \ 0$$

(A2-4a)

Expanding (A2-3a):

$$\frac{\sigma^2}{g\Delta^2 k^2} \Big\{ k \sinh kh \cosh kh \cos^2 \alpha h - \alpha \cosh^2 kh \sin \alpha h \cos \alpha h$$

$$+ \frac{c}{\sigma h} (k \cosh kh \sin \alpha h + \alpha \sinh kh \cos \alpha h)$$

$$+ k \sinh kh \cosh kh \sin^2 \alpha h + \alpha \sinh^2 kh \sin \alpha h \cos \alpha h \Big\} = 1$$

$$\frac{\sigma^2}{g\Delta^2 k^2} \Big\{ \frac{k}{2} \sinh 2kh (\cos^2 \alpha h + \sin^2 \alpha h) - \frac{\alpha}{2} \sin 2\alpha h (\cosh^2 kh - \sinh^2 kh)$$

$$+ \frac{c}{\sigma h} (k \cosh kh \sin \alpha h + \alpha \sinh kh \cos \alpha h) \Big\} = 1$$

AND

$$\frac{\sigma^2}{2g\Delta^2 k^2} \Big\{ (k \sinh 2kh - \alpha \sin 2\alpha h) + \frac{2c}{\sigma h} (k \cosh kh \sin \alpha h + \alpha \sinh kh \cos \alpha h) \Big\} = 1$$

(A2-3b)

Similarly, expanding (A2-4a) gives:

$$k \sinh^2 kh \cos \alpha h \sin \alpha h - \alpha \cosh kh \sinh kh \sin^2 \alpha h$$

$$- k \cosh^2 kh \cos \alpha h \sin \alpha h - \alpha \cosh kh \sinh kh \cos^2 \alpha h$$

$$+ \frac{c}{\sigma h} (k \sinh kh \cos \alpha h - \alpha \cosh kh \sin \alpha h) = 0$$

thus:

$$k \sin 2\alpha h + \alpha \sinh 2kh - \frac{2c}{\sigma h}(k \sinh kh \cos \alpha h - \alpha \cosh kh \sin \alpha h) = 0$$

<div align="right">(A2-4b)</div>

Rewriting equation (A2-3b) as:

$$k\left(\sinh 2kh + \frac{2c}{\sigma h}\cosh kh \sin \alpha h\right) - \alpha\left(\sin 2\alpha h - \frac{2c}{\sigma h}\sinh kh \cos \alpha h\right)$$

$$= \frac{2g\Delta^2 K^2}{\sigma^2}$$

and (A2-4b) as:

$$\sinh 2kh + \frac{2c}{\sigma h}\cosh kh \sin \alpha h = \frac{k}{\alpha}\left(-\sin 2\alpha h + \frac{2c}{\sigma h}\sinh kh \cos \alpha h\right)$$

Using the R.H.S. of the above in (A2-3b) yields:

$$\frac{k^2}{\alpha}\left(-\sin 2\alpha h + \frac{2c}{\sigma h}\sinh kh \cos \alpha h\right) + \alpha\left(-\sin 2\alpha h + \frac{2c}{\sigma h}\sinh kh \cos \alpha h\right)$$

$$= \frac{2g\Delta^2 K^2}{\sigma^2}$$

or:

$$\frac{k^2 + \alpha^2}{\alpha}\left(-\sin 2\alpha h + \frac{2c}{\sigma h}\sinh kh \cos \alpha h\right) = \frac{2g\Delta^2 K^2}{\sigma^2}$$

Thus:

<div align="right">(A2-5)</div>

$$\alpha = \frac{\sigma^2}{2g}\left\{\frac{-\sin 2\alpha h + \frac{2c}{\sigma h}\sinh kh \cos \alpha h}{\sinh^2 kh + \sin^2 \alpha h}\right\}$$

Again, rewriting (A2-3b) as:

$$\left(-\sin 2\alpha h + \frac{2c}{\sigma h}\sinh kh \cos \alpha h\right) = \frac{\alpha}{k}\left(\sinh 2kh + \frac{2c}{\sigma h}\cosh kh \sin \alpha h\right)$$

and using this in (A2-3b) results in:

$$k\left(\sinh 2kh + \frac{2c}{\sigma h}\cosh kh \sin \alpha h\right) + \frac{\alpha^2}{k}\left(\sinh 2kh + \frac{2c}{\sigma h}\cosh kh \sin \alpha h\right)$$

$$= \frac{2g\Delta^2 K^2}{\sigma^2}$$

or:

$$\frac{k^2+\alpha^2}{k} \left(\sinh 2kh + \frac{2c}{\sigma h} \cosh kh \sin \alpha h \right) = \frac{2g\Delta^2 k^2}{\sigma^2}$$

thus:

$$k = \frac{\sigma^2}{2g} \left\{ \frac{\sinh 2kh + \frac{2c}{\sigma h} \cosh kh \sin \alpha h}{\sinh^2 kh + \sin^2 \alpha h} \right\}$$ (A2-6)

From equation (A2-5) and (A2-6) it will be shown that if k is small, then it follows that α is also small. Writing equation (A2-6) as:

$$\frac{2k}{M} = \sinh 2kh + \frac{2c}{\sigma h} \cosh kh \sin \alpha h$$

or:

$$\frac{k}{M} = \cosh kh \left(\sinh kh + \frac{c}{\sigma h} \sin \alpha h \right)$$ (A2-6a)

and equation (A2-5) as:

$$\frac{\alpha}{M} = \cos \alpha h \left(-\sin \alpha h + \frac{c}{\sigma h} \sinh kh \right)$$ (A2-5a)

Now, since α and M are positive it follows that:

$$\frac{c}{\sigma h} = \sinh kh \geqslant \sin \alpha h \quad \text{in} \quad 0 \leqslant \alpha h \leqslant \frac{\pi}{2}$$

This restriction on the angle αh is justified in Section 3.3A. The above inequality reduces to $\frac{c}{\sigma h} kh \geqslant \sin \alpha h$ for $kh \ll 1$ (long-waves), and in this case the inequality can be formed:

$$\frac{k}{M} \geqslant \left(\frac{\sigma h}{c} + \frac{c}{\sigma h} \right) \sin \alpha h$$

or:

$$\frac{k}{M \sin \alpha h} - \frac{\sigma h}{c} \geqslant \frac{c}{\sigma h}$$

from equation (A2-6a).

Since $0 \le \cos \alpha h \le 1$ in $0 \le \alpha h \le \dfrac{\pi}{2}$ gives, from equation (A2-5a), the relation:

$$\frac{\alpha}{M} \le \left(-\sin \alpha h + \frac{c}{\sigma h} (kh) \right) \le \frac{c}{\sigma h} (kh)$$

and:

$$\frac{\alpha}{M(kh)} < \frac{c}{\sigma h}$$

Thus the inequality that:

$$\frac{\alpha}{M(kh)} < \left(\frac{k}{M \sin \alpha h} - \frac{\sigma h}{c} \right)$$

or:

$$\frac{\alpha}{M(kh)} < \frac{k}{M \sin \alpha h}$$

and arrive at:

$$\alpha \sin \alpha h < k (kh)$$

which, by virtue of $kh \ll 1$ can be expressed as:

$$\alpha h \sin \alpha h \ll kh \ll 1$$

Therefore $\alpha h \ll 1$, and if k is small it follows that α is also small: Hence for long-waves ($kh \ll 1$) the approximations used in the functions involving arguments of kh can also be used for those involving αh

Evaluation of k and α for Long-waves
_____

Retaining only the first term in the Taylor's series expansions for the functions having kh or αh as arguments, reduces equation (A2-6) to:

$$k \simeq g \, \frac{\sigma^2}{((kh)^2 + (\alpha h)^2)} \left\{ \frac{2kh}{2} + \frac{c}{\sigma h}(1)(\alpha h) \right\}$$

$$\simeq \frac{\sigma^2}{gh^2(k^2 + \alpha^2)} \left\{ kh + \frac{c}{\sigma h} \alpha h \right\}$$

Therefore:

$$k \simeq \frac{\sigma^2}{gh(k^2 + \alpha^2)} \left(k + \frac{c}{\sigma h} \alpha \right) \tag{A2-7}$$

Similarly, equation (A2-5) reduces to:

$$\alpha \simeq \frac{\sigma^2}{gh^2(k^2 + \alpha^2)} \left(-\alpha h + \frac{c}{\sigma h} kh \right)$$

Therefore:

$$\alpha \simeq \frac{\sigma^2}{gh(k^2 + \alpha^2)} \left(-\alpha + \frac{c}{\sigma h} k \right) \tag{A2-8}$$

Equations (A2-7) and (A2-8) may be rearranged to obtain explicit solutions for k and α .

Equation (A2-7) can be written as:

$$k \left\{ (k^2 + \alpha^2) - \frac{\sigma^2}{gh} \right\} \frac{c\alpha}{\sigma h} \tag{A2-7a}$$

and equation (A2-8) as:

$$\alpha \left\{ (k^2 + \alpha^2) + \frac{\sigma^2}{gh} \right\} = \frac{\sigma^2}{gh} \frac{ck}{\sigma h} \qquad \text{(A2-8a)}$$

After multiplying (A2-7a) by $1/\alpha$ and (A2-8a) by $1/k$ and combining the two equations -

$$\frac{k}{\alpha} \left(k^2 + \alpha^2 - \frac{\sigma^2}{gh} \right) = \frac{\alpha}{k} \left(k^2 + \alpha^2 + \frac{\sigma^2}{gh} \right)$$

rearranging·

$$k^2 \left(\frac{k}{\alpha} - \frac{\alpha}{k} \right) + \alpha^2 \left(\frac{k}{\alpha} - \frac{\alpha}{k} \right) = \frac{\sigma^2}{gh} \left(\frac{k}{\alpha} + \frac{\alpha}{k} \right)$$

or:

$$k^2 (k^2 - \alpha^2) + \alpha^2 (k^2 - \alpha^2) = \frac{\sigma^2}{gh} (k^2 + \alpha^2)$$

$$(k^2 + \alpha^2) \qquad (k^2 - \alpha^2) = \frac{\sigma^2}{gh} (k^2 + \alpha^2)$$

therefore:

$$k^2 - \alpha^2 = \frac{\sigma^2}{gh} \qquad \text{(A2-9)}$$

Using this result in (A2-7a):

$$k \left[(k^2 + \alpha^2) - (k^2 - \alpha^2) \right] = \frac{\sigma^2}{gh} \left(\frac{c\alpha}{\sigma h} \right)$$

$$k (2\alpha^2) = \frac{\sigma^2}{gh} \left(\frac{c\alpha}{\sigma h} \right)$$

thus:

$$2\alpha k = \frac{\sigma^2}{gh} \left(\frac{c}{\sigma h} \right) \qquad \text{(A2-10)}$$

Eliminating α between (A2-9) and (A2-10) -

From (A2-10): $\qquad \alpha = \frac{\sigma^2}{2ghk} \left(\frac{c}{\sigma h} \right)$

Using this in (A2-9):

$$k^2 - \frac{1}{k^2}\left(\frac{c\sigma}{2gh^2}\right)^2 - \frac{\sigma^2}{gh} = 0$$

$$k^4 - k^2 \frac{\sigma^2}{gh} - \left(\frac{c\sigma}{2gh^2}\right)^2 = 0$$

Solving for k^2 :

$$k^2 = \frac{\sigma^2}{2gh} \pm \frac{1}{2}\sqrt{\left(\frac{\sigma^2}{gh}\right)^2 + \left(\frac{c\sigma}{gh^2}\right)^2}$$

$$= \frac{\sigma^2}{2gh}\left\{1 \pm \sqrt{1 + \left(\frac{c}{\sigma h}\right)^2}\right\}$$

Taking the positive square-root since, for the frictionless model $(c=0), k \neq 0$,

Therefore:

$$k^2 = \frac{\sigma^2}{2gh}\left\{1 + \sqrt{1 + \left(\frac{c}{\sigma h}\right)^2}\right\} \qquad\qquad\text{(A2-11)}$$

Similarly, from (A2-10):

$$k = \frac{\sigma^2}{2gh\alpha}\left(\frac{c}{\sigma h}\right)$$

using this value for k **in (A2-9) results in:**

$$\left(\frac{c\sigma}{2gh^2}\right)^2 \frac{1}{\alpha^2} - \alpha^2 - \frac{\sigma^2}{gh} = 0$$

Rearranging:

$$\alpha^4 + \frac{\sigma^2}{gh}\alpha^2 - \left(\frac{c\sigma}{2gh^2}\right)^2 = 0$$

Solving for α^2 :

$$\alpha^2 = -\frac{\sigma^2}{2gh} \pm \frac{1}{2} \sqrt{\left(\frac{\sigma^2}{gh}\right)^2 + \left(\frac{c\sigma}{gh^2}\right)^2}$$

$$= \frac{\sigma^2}{2gh} \left\{ -1 \pm \sqrt{1 + \left(\frac{c}{\sigma h}\right)^2} \right\}$$

Again taking the positive sign for the square-root, since α must vanish for $c = 0$

Therefore:

$$\alpha^2 = \frac{\sigma^2}{2gh} \left\{ -1 + \sqrt{1 + \left(\frac{c}{\sigma h}\right)^2} \right\} \tag{A2-12}$$

Finally arriving at:

$$k = \frac{\sigma}{\sqrt{2gh}} \left\{ 1 + \sqrt{1 + \left(\frac{c}{\sigma h}\right)^2} \right\}^{1/2} \tag{A2-13}$$

and:

$$\alpha = \frac{\sigma}{\sqrt{2gh}} \left\{ -1 + \sqrt{1 + \left(\frac{c}{\sigma h}\right)^2} \right\}^{1/2} \tag{A2-14}$$

Where the positive square-roots have been taken since it was stipulated that both k and α are positive numbers.

These equations, (A2-13) and (A2-14), may be further simplified if $\frac{c}{\sigma h} \ll 1$

Letting $\frac{c}{\sigma h} = \sinh \Theta$

then $\sqrt{1. + \left(\frac{c}{\sigma h}\right)^2} = \cosh \Theta$

and $\quad k = \frac{\sigma}{\sqrt{2gh}} \quad \sqrt{1 + \cosh \Theta}$

$\quad\quad = \frac{\sigma}{\sqrt{gh}} \quad \cosh \frac{\Theta}{2}$

similarly: $\quad \measuredangle = \frac{\sigma}{\sqrt{gh}} \quad \sinh \frac{\Theta}{2}$

But, for Θ small; $\sinh \Theta \simeq \Theta \simeq \frac{c}{\sigma h}$

so:

$\quad k \simeq \frac{\sigma}{\sqrt{gh}} \left(1 + O \left(\frac{c}{2\sigma h}\right)^2\right)$

and:

$\quad \measuredangle \simeq \frac{\sigma}{\sqrt{gh}} \left(\frac{c}{2\sigma h} + O \left(\frac{c}{2\sigma h}\right)^3\right)$

APPENDIX 3

THE ENERGIES OF THE WAVE

(A3.1) The Average Potential Energy:

In a section from x to $x+dx$ the time average potential energy

is:

$$d(PE)_{AVG.} = \left\{ \frac{\rho g}{2} \frac{1}{T} \int_{t}^{t+T} \eta^2 \, dt \right\} dx$$

where the assumption has been made that the wave has a constant amplitude

across the infinitesimal section.

$$d(PE)_{AVG.} = \left\{ \frac{\rho g}{2} A^2 e^{-2\alpha x} \frac{1}{T} \int_{t}^{t+T} \cos^2(kx - \sigma t) \, dt \right\} dx$$

$$= \frac{\rho g}{4} A^2 e^{-2\alpha x} \frac{1}{T} \left[t - \frac{\sin 2(kx - \sigma t)}{2\sigma} \right]_{t}^{t+T} dx$$

$$= \left\{ \frac{\rho g}{4} A^2 e^{-2\alpha x} \right\} dx$$

(A3-1)

(A3.2) The Average Kinetic Energy:

With the same stipulation as was used in calculating the average

potential energy, the average kinetic energy is:

$$d(KE)_{AVG.} = \left\{ \frac{\rho}{2} \int_{\eta \simeq 0}^{h} \frac{1}{T} \int_{t}^{t+T} (u^2 + w^2) \, dt \, dz \right\} dx$$

where u and w are the particle velocities as defined in equations

(3-6A) and (3-7) respectively.

The integrand is:

$$\mu^2 + w^2 = \frac{\sigma^2 A^2 e^{-2\alpha x}}{\Delta^2} \left\{ \sinh^2 k\bar{z} \sin^2 \alpha\bar{z} \sin^2 X_\delta + \sinh^2 k\bar{z} \cos^2 \alpha\bar{z} \sin^2 X_\delta \right.$$

$$\left. + \cosh^2 k\bar{z} \cos^2 \alpha\bar{z} \cos^2 X_\delta + \cosh^2 k\bar{z} \sin^2 \alpha\bar{z} \cos^2 X_\delta \right\}$$

where

$$X_\delta = kx - \sigma t - \delta$$

$$\mu^2 + w^2 = \frac{\sigma^2 A^2 e^{-2\alpha x}}{\Delta^2} \left\{ \sinh^2 k\bar{z} \sin^2 X_\delta + \cosh^2 k\bar{z} \cos^2 X_\delta \right\}$$

Hence:

$$d(KE)_{AVG} = \left\{ \frac{\rho}{2} \int_o^h d\bar{z} \, \frac{1}{T} \int_t^{t+T} \frac{\sigma^2 A^2 e^{-2\alpha x}}{\Delta^2} \left[\sinh^2 k\bar{z} \sin^2 X_\delta + \cosh^2 k\bar{z} \cos^2 X_\delta \right] dt \right\} dx$$

Expanding the hyperbolic functions and integrating gives:

$$d(KE)_{AVG} = \left\{ \frac{\rho\sigma^2 A^2 e^{-2\alpha x}}{4\Delta^2} \frac{1}{T} \int_t^{t+T} \left[\left(-h + \frac{\sinh 2kh}{2k} \right) \sin^2 X_\delta + \left(h + \frac{\sinh 2kh}{2k} \right) \cos^2 X_\delta \right] dt \right\} dx$$

Collecting terms:

$$= \left\{ \frac{\rho\sigma^2 A^2 e^{-2\alpha x}}{4\Delta^2} \frac{1}{T} \int_t^{t+T} \left[h \cos 2 X_\delta + \frac{\sinh 2kh}{2k} \right] dt \right\} dx$$

$$= \left\{ \frac{\rho\sigma^2 A^2 e^{-2\alpha x}}{8k\Delta^2} \sinh 2kh \right\} dx$$

$$(A3\text{-}2a)$$

With the use of equation (3-3A), equation (A3-2) can be rewritten as:

$$d(KE)_{AVG} = \left\{ \frac{\rho\sigma^2 A^2 e^{-2\alpha x}}{8\Delta^2} \frac{\sinh 2kh}{\frac{\sigma^2}{g\Delta^2} \left(\frac{1}{2} \sinh 2kh + \frac{c}{\sigma h} \cosh kh \sin \alpha h \right)} \right\} dx$$

$$= \left\{ \frac{\rho g A^2 e^{-2\alpha x}}{4 \left[1 + \frac{c}{\sigma h} \frac{\sin \alpha h}{\sinh kh} \right]} \right\} dx$$

$$(A3\text{-}2b)$$

Thus the average kinetic energy is less than the average potential energy by an amount:

$$d(\Delta E)_{AVG.} = \frac{\rho g A^2 e^{-2\alpha x}}{4} \left\{ 1 - \frac{1}{1 + \frac{c}{\sigma h} \frac{\sin \alpha h}{\sinh kh}} \right\} dx$$

$$= \frac{\rho g A^2 e^{-2\alpha x}}{4} \left\{ \frac{\frac{c}{\sigma h} \frac{\sin \alpha h}{\sinh kh}}{1 + \frac{c}{\sigma h} \frac{\sin \alpha h}{\sinh kh}} \right\} dx$$

or, using (A3-2a)

$$d(\Delta E)_{AVG.} = \left(\frac{\rho g}{4} - \frac{\rho \sigma^2}{8 k \Delta^2} \sinh 2kh \right) A^2 e^{-2\alpha x} dx$$

eliminating g by use of equation (3-3a):

$$= \left[\frac{\rho}{4} \frac{\sigma^2}{2k\Delta^2} \left\{ \sinh 2kh + \frac{2c}{\sigma h} \cosh kh \sin \alpha h \right\} - \frac{\rho \sigma^2}{8 k \Delta^2} \sinh 2kh \right] A^2 e^{-2\alpha x} dx$$

$$= \left\{ \frac{c \rho \sigma}{4 kh \Delta} \cdot \frac{\cosh kh \sin \alpha h}{\Delta} A^2 e^{-2\alpha x} \right\} dx$$

$$= \frac{c \rho \sigma}{4 kh \Delta} \sin \delta \left(A^2 e^{-2\alpha x} \right) dx$$

(A3.3)   <u>The Total Average Energy:</u>

$$d(E)_{AVG.} = d(PE)_{AVG.} + d(KE)_{AVG.}$$

$$= \frac{\rho g A^2 e^{-2\alpha x}}{4} \left\{ 1 + \frac{1}{1 + \frac{c}{\sigma h} \frac{\sin \alpha h}{\sinh kh}} \right\} dx \qquad \text{(A3-4a)}$$

or, again using (3-3a):

$$d(E)_{AVG.} = \left\{\frac{c\rho\sigma}{4\Delta kh} \sin S + \frac{\rho}{4}\frac{\sigma^2}{k\Delta^2} \sinh 2kh \right\} A^2 e^{-2\alpha x} \, dx$$

$$= \frac{\rho\sigma^2}{4\Delta k} \left\{\frac{c}{\sigma h} \sin S + \frac{\sinh 2kh}{\Delta} \right\} A^2 e^{-2\alpha x} \, dx \qquad (A3\text{-}4b)$$

which, for a given amplitude ($Ae^{-\alpha x}$) is always less than the friction-less average energy. The wave energy per wave length between x' and $x'+L$ can be found by directly integrating equation (A3-4a).

That is:

$$E_{AVG.} = \frac{\rho g A^2}{4} \left\{1 + \frac{1}{1+\frac{c}{\sigma h}\frac{\sin \alpha h}{\sinh kh}} \right\} \int_{x'}^{x'+L} z^{-2\alpha x} \, dx$$

$$= \frac{\rho g A^2 e^{-2\alpha x'}}{4} \left\{1 + \frac{1}{1+\frac{c}{\sigma h}\frac{\sin \alpha h}{\sinh kh}} \right\} \left(\frac{1-e^{-2\alpha L}}{2\alpha} \right). \qquad (A3\text{-}5)$$

APPENDIX 4

EVALUATION OF THE AVERAGE ENERGY FLUX

The average energy flux or power across a plane extending from the bottom to the surface and one unit in the y direction is:

$$P_{AVG.} = \frac{\rho}{T} \int_{t}^{t+T} \int_{0}^{h} \left(\frac{\partial \phi}{\partial t} + \frac{c}{h} \phi_{b} \right) u \, dZ \, dt$$

(A4-1)

The average being taken over one wave period, $T = \frac{2\pi}{\sigma}$. The integration over the depth is carried out first. Splitting the integrand into two parts gives:

$$\int_{0}^{h} \frac{\partial \phi}{\partial t} u \, dZ$$

(A4-2)

and

$$\frac{c}{h} \phi_{b} \int_{0}^{h} u \, dZ$$

(A4-3)

Expanding the integrand of (A4-2) explicitly:

$$\frac{\partial \phi}{\partial t} u = \frac{\sigma^{3} A^{2} e^{-2\alpha x}}{\Delta^{2} k} \left\{ (\cosh kZ \cos \alpha Z \cos X_{\epsilon} - \sinh kZ \sin \alpha Z \sin X_{\epsilon}) \right.$$
$$\left. \times (\cosh kZ \cos \alpha Z \sin X_{\delta} - \sinh kZ \sin \alpha Z \sin X_{\delta}) \right\}$$

where $X_{\epsilon} = kx - \sigma t - \epsilon$

and $X_{\delta} = kx - \sigma t - \delta$

Multiplying and using double angle relations gives:

$$\frac{\partial \phi}{\partial t} \mu = \frac{\sigma^3 A^2 e^{-2\alpha x}}{\Delta^2 K} \Big\{ (1 + \cosh 2kZ)(1 + \cos 2\alpha Z) \cos X_E \cos X_\delta$$

$$+ (-1 + \cosh 2kZ)(1 - \cos 2\alpha Z) \sin X_E \sin X_\delta$$

$$- \sinh 2kZ \sin 2\alpha Z \sin(X_E + X_\delta) \Big\}$$

Collecting terms in the z dependance;

$$\frac{\partial \phi}{\partial z} \mu = \frac{\sigma^3 A^2 e^{-2\alpha x}}{4\Delta^2 K} \Big\{ (\cos X_E \cos X_\delta - \sin X_E \sin X_\delta)$$

$$+ \cosh 2kZ(\cos X_E \cos X_\delta + \sin X_E \sin X_\delta)$$

$$+ \cos 2\alpha Z(\cos X_E \cos X_\delta + \sin X_E \sin X_\delta)$$

$$+ \cosh 2kZ \cos 2\alpha Z(\cos X_E \cos X_\delta - \sin X_E \sin X_\delta)$$

$$- \sinh 2kZ \sin 2\alpha Z \sin(X_E + X_\delta) \Big\}$$

$$= \frac{\sigma^3 A^2 e^{-2\alpha x}}{4\Delta^2 K} \Big\{ \cos(X_E + X_\delta) + (\cosh 2kZ + \cos 2\alpha Z)\cos(X_E - X_\delta)$$

$$+ \cosh 2kZ \cos 2\alpha Z \cos(X_E + X_\delta)$$

$$- \sinh 2kZ \sin 2\alpha Z \sin(X_E + X_\delta) \Big\}$$

Using the method of integration by parts gives:

$$\int_0^h \cosh 2k\bar{z} \cos 2\alpha\bar{z} \, d\bar{z} = \frac{1}{2K^2} \left\{ k \sinh 2k\bar{z} \cos 2\alpha\bar{z} + \alpha \cosh 2k\bar{z} \sin 2\alpha\bar{z} \right\} \Big|_0^h$$

$$= \frac{1}{2K^2} \left\{ k \sinh 2kh \cos 2\alpha h + \alpha \cosh 2kh \sin 2\alpha h \right\}$$

$$(A4\text{-}4)$$

and similarly:

$$\int_0^h \sinh 2k\bar{z} \sin 2\alpha\bar{z} \, d\bar{z} = \frac{1}{2K^2} \left\{ k \cosh 2kh \sin 2\alpha h \right.$$

$$\left. - \alpha \sinh 2kh \cos 2\alpha h \right\}$$

$$(A4\text{-}5)$$

Therefore:

$$\int_0^h \frac{\partial \phi}{\partial t} \, u \, d\bar{z} = \frac{\sigma^3 A^2 e^{-2\alpha x}}{4 \Delta^2 K} \left\{ h \cos(X_\epsilon - X_\delta) + \left(\frac{\sinh 2kh}{2k} + \frac{\sin 2\alpha h}{2\alpha} \right) \cos(X_\epsilon - X_\delta) \right.$$

$$+ \frac{1}{2K^2} \left[\sinh 2kh \cos 2\alpha h (k \cos(X_\epsilon + X_\delta) + \alpha \sin(X_\epsilon + X_\delta)) \right.$$

$$\left. \left. + \cosh 2kh \sin 2\alpha h (\alpha \cos(X_\epsilon + X_\delta) - k \sin(X_\epsilon + X_\delta)) \right] \right\}$$

Using the definition of K and Ω yields the relations:

$$k \cos(X_\epsilon + X_\delta) + \alpha \sin(X_\epsilon + X_\delta) = K \cos(X_\epsilon + X_\delta - \Omega) = K \cos 2X_\epsilon$$

and

$$\alpha \cos(X_\epsilon + X_\delta) - k \sin(X_\epsilon + X_\delta) = K \sin(-X_\epsilon - X_\delta + \Omega) = -K \sin 2X_\epsilon$$

So:

$$\int_0^h \frac{\partial \phi}{\partial t} \, u \, dz = \frac{\sigma^3 A^2 e^{-2\alpha x}}{4 \Delta^2 k} \left\{ h \cos(X_\epsilon - X_\delta) + \left(\frac{\sinh 2kh}{2k} + \frac{\sin 2\alpha h}{2\alpha} \right) \cos(X_\epsilon - Y_\delta) \right.$$

$$+ \frac{1}{2k} \left[\sinh 2kh \cos 2\alpha h \, \cos 2 X_\epsilon \right.$$

$$\left. \left. - \cosh 2kh \sin 2\alpha h \sin 2 X_\epsilon \right] \right\} \qquad (A4\text{-}6)$$

The second integral (A4-3) is:

$$\frac{c}{h} \phi_b \int_0^h u \, dz$$

$$= \frac{c}{h} \left(- \frac{A \sigma e^{-\alpha x}}{\Delta k} \sin X_\epsilon \right) \Big|_0^h \left[-\psi \right]$$

since $\quad u = - \dfrac{\partial \psi}{\partial z}$

Using the value for ψ determined previously (equation (3-3)) and inserting limits of integration results in:

$$\frac{c}{h} \phi_b \int_0^h u \, dz = \left(\frac{4c}{\sigma h} \right) \frac{\sigma^3 A^2 e^{-2\alpha x}}{4 \Delta^2 k^2} \sin X_\epsilon \left\{ -\sinh kh \cos \alpha h \, \cos X_\epsilon \right.$$

$$\left. + \cosh kh \sin \alpha h \sin X_\epsilon \right\}$$

$$= \frac{4c}{\sigma h} \frac{\sigma^3 A^2 e^{-2\alpha x}}{4 \Delta^2 k^2} \sin X_\epsilon \left\{ \Delta \left(- \cos \delta \cos X_\epsilon + \sin \delta \sin X_\epsilon \right) \right\}$$

$$= \frac{4c}{\sigma h} \frac{\sigma^3 A^2 e^{-2\alpha x}}{4 \Delta^2 k^2} \sin X_\epsilon \left\{ \Delta \cos (X_\epsilon + \delta) \right\}$$

$$= - \frac{4c}{\sigma h} \frac{\sigma^3 A^2 e^{-2\alpha x}}{4 \Delta^2 k^2} \sin X_\epsilon \left\{ \Delta \cos X \, \Omega \right\}$$

where $X_\Omega = (kx - \sigma t - \Omega)$

Combining the trigonometric terms:

$$\frac{c}{h} \phi_b \int_0^h \mu \, dz = -\frac{2c}{\sigma h} \frac{\sigma^3 \Delta^2 e^{-2\alpha x}}{4 \Delta^2 K^2} \left\{ \Delta \left[\sin(X_\epsilon + X_\Omega) + \sin(X_\epsilon - X_\Omega) \right] \right\}$$ (A4-7)

Using (A3-6) and (A3-7) the average power expression is:

$$P_{AVG.} \frac{\rho \sigma^3 \Delta^2 e^{-2\alpha x}}{4\Delta^2 K^2} \cdot \frac{1}{T} \int_t^{t+T} \left\{ h \cos(X_\epsilon + X_\delta) + \left(\frac{\sinh 2kh}{2k} - \frac{\sin 2\alpha h}{2\alpha} \right) \cos(X_\epsilon - X_\delta) \right.$$

$$+ \frac{1}{2k} \left[\sinh 2kh \cos 2\alpha h \, \cos 2X_\epsilon \right.$$

$$\left. - \cosh 2kh \sin 2\alpha h \sin 2X_\epsilon \right]$$

$$\left. - \frac{2c}{\sigma h k} \left[\Delta \left[\sin(X_\epsilon + X_\Omega) + \sin(X_\epsilon - X_\delta) \right] \right] \right]$$

Examining the arguments for the trigonometric functions:

$X_\epsilon + X_\delta = 2(kx - \sigma t - \delta) - \Omega$

$X_\epsilon - X_\delta = -\Omega$

$X_\epsilon + X_\Omega = 2(kx - \sigma t - \Omega) - \delta$

$X_\epsilon - X_\Omega = -\delta$

$2X_\epsilon = 2(kx - \sigma t - \epsilon)$

and using the identity that states that integrals of the form

$$\int_t^{t+2\pi} \cos(p + nt)\, dt$$

and

$$\int_t^{t+2\pi} \sin(p + nt)\, dt$$

where p is independant of t and n is an interger, are zero;

allows simplification of the average power expression to:

$$P_{AVG} = \frac{\rho \sigma^3 A^2 e^{-2\alpha x}}{4\Delta^2 K} \frac{1}{T} \int_t^{t+T} \left\{ \left[\frac{\sinh 2kh}{2k} + \frac{\sin 2\alpha h}{2\alpha} \right] \cos \Omega \right. \tag{A4-8}$$

and, upon integrating:

$$P_{AVG} = \frac{\rho \sigma^3 A^2 e^{-2\alpha x}}{4\Delta^2 K} \left\{ \left[\frac{\sinh 2kh}{2k} + \frac{\sin 2\alpha h}{2\alpha} \right] \cos \Omega + \frac{2c\Delta}{\sigma h K} \sin \delta \right\}$$

$$= \frac{\rho \sigma^3 A^2 e^{-2\alpha x}}{8\Delta^2 K} \left\{ \left(\frac{\sinh 2kh}{k} + \frac{\sin 2\alpha h}{\alpha} \right) \frac{k}{K} + \frac{4c}{\sigma h} \frac{\Delta}{K} \frac{\cosh kh \sin \alpha h}{\Delta} \right.$$

$$P_{AVG} = \frac{\rho \sigma^3 A^2 e^{-2\alpha x}}{8\Delta^2 K^2} \left\{ \left(\sinh 2kh + \frac{k}{\alpha} \sin 2\alpha h \right) + \frac{4c}{\sigma h} \cosh kh \sin \alpha h \right\} \tag{A4-9}$$

Appendix 5   -   The Wave Tanks .

A5.1 The Large Wave Tank

A 10 foot by 20 foot wave tank was constructed to investigate surface waves travelling in two dimensions. The tank was basically a shallow tray which allowed for a maximum water depth of 6 inches, the tray was supported by a rigid base made from 3 x 9 inches channel iron (Figure (A5:1)). Two 99½ inches by 75½ inches glass plates supported on all edges were used for the bottom of the model region, the remainder of the tray bottom and the sides were constructed from ¼ inch iron sheeting (Photo (A5:1)). The bottom sheeting was set about ¼ inch below the level of the glass and covered with a sand-cement mixture to make the two levels equal. This area was used for wave generation and absorption.

The glass was used on the bottom to allow for visual observations through the tray bottom of the wave action and also because of the flatness of the glass plates over a large area. The sheet of glass used near the wave paddle was a piece of 5/8 inch surface toughened plate which was found to be rather flexible, hence making it necessary to provide an additional support across its centre. The other glass sheet was 1 1/8 inch thick polished plate which was used in the model area and was rigid enough so that no additional supports were necessary. This allowed for an unobstructed 6 foot by 8 foot area in which to view the wave action. The edge supports for the thinner sheet of glass were built up to make both levels of the glass plates equal.

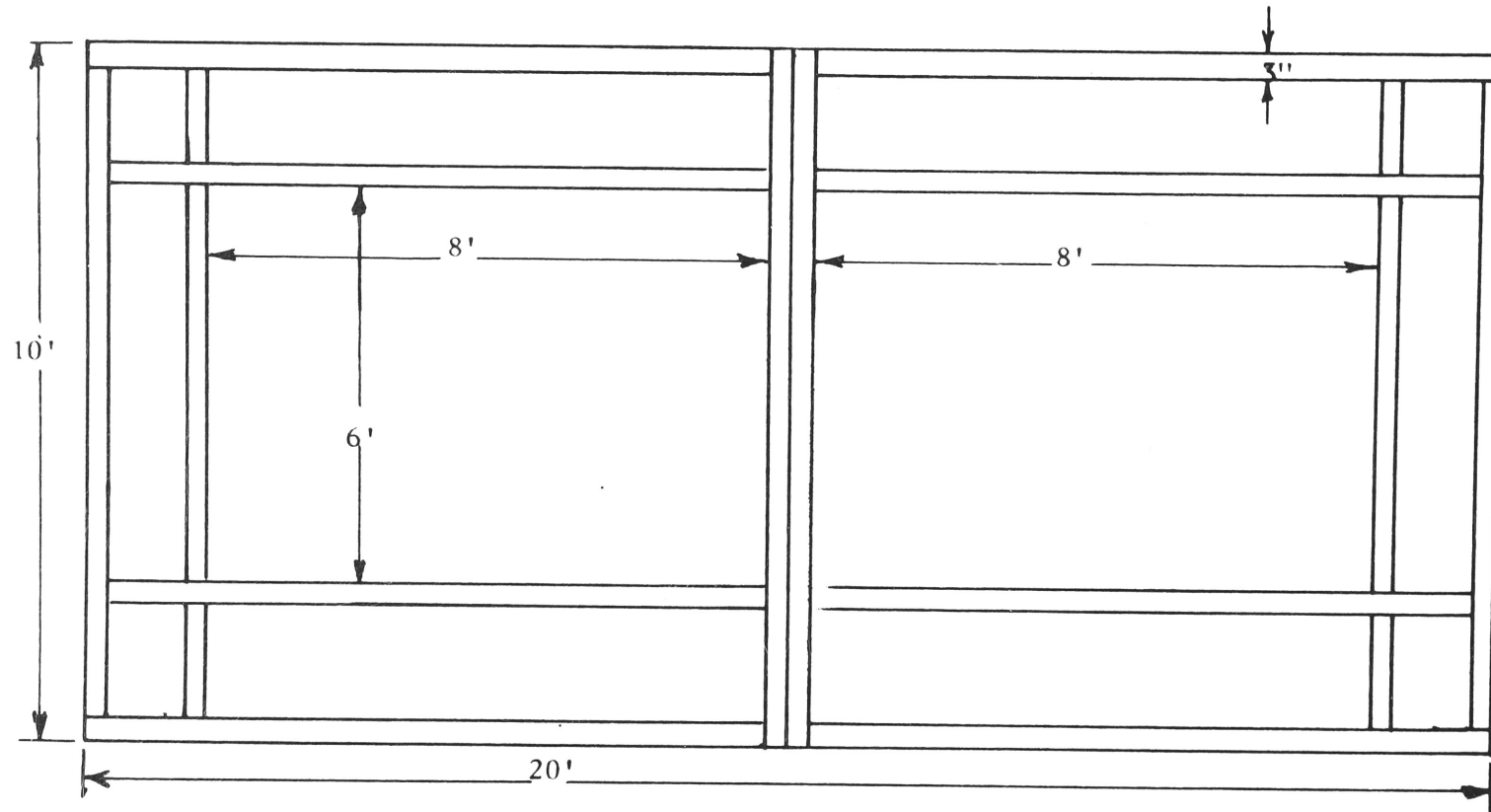All structural members 3 X 9 channel iron
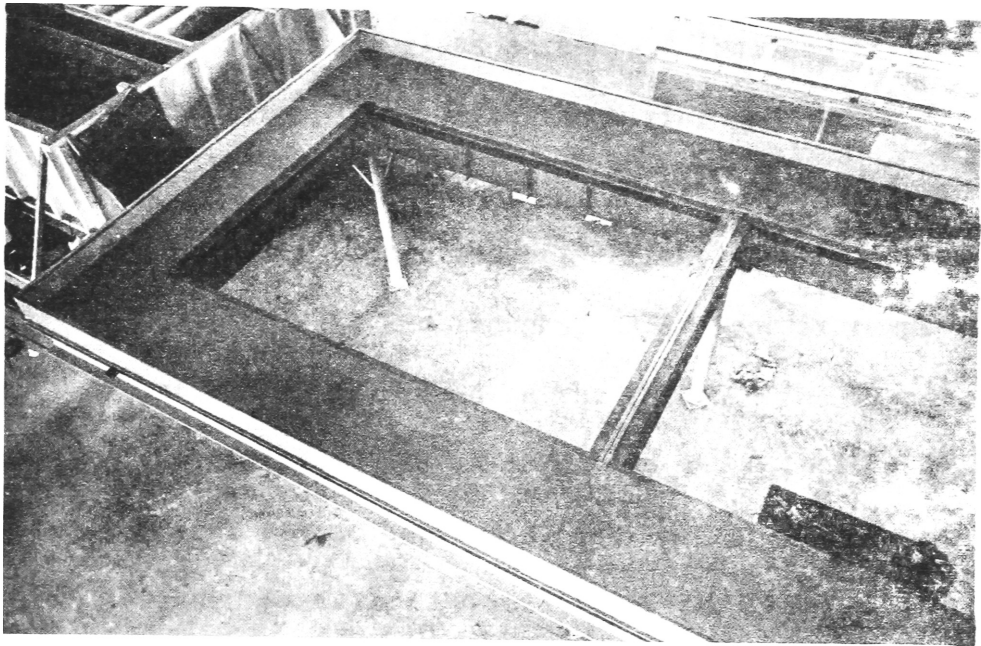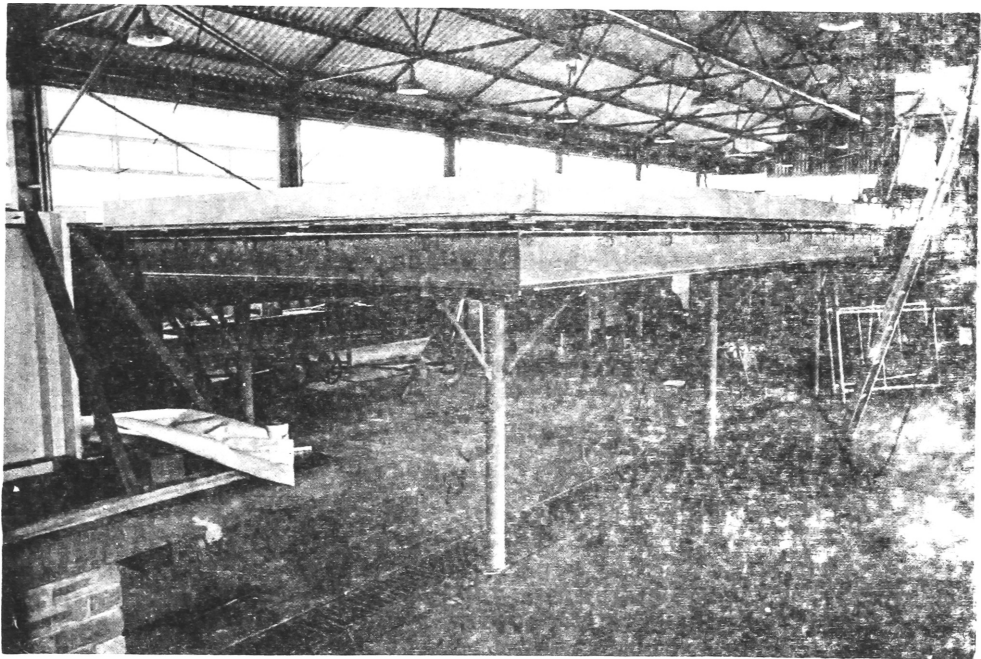

FIGURE A5:1   BASE FOR WAVE TRAY

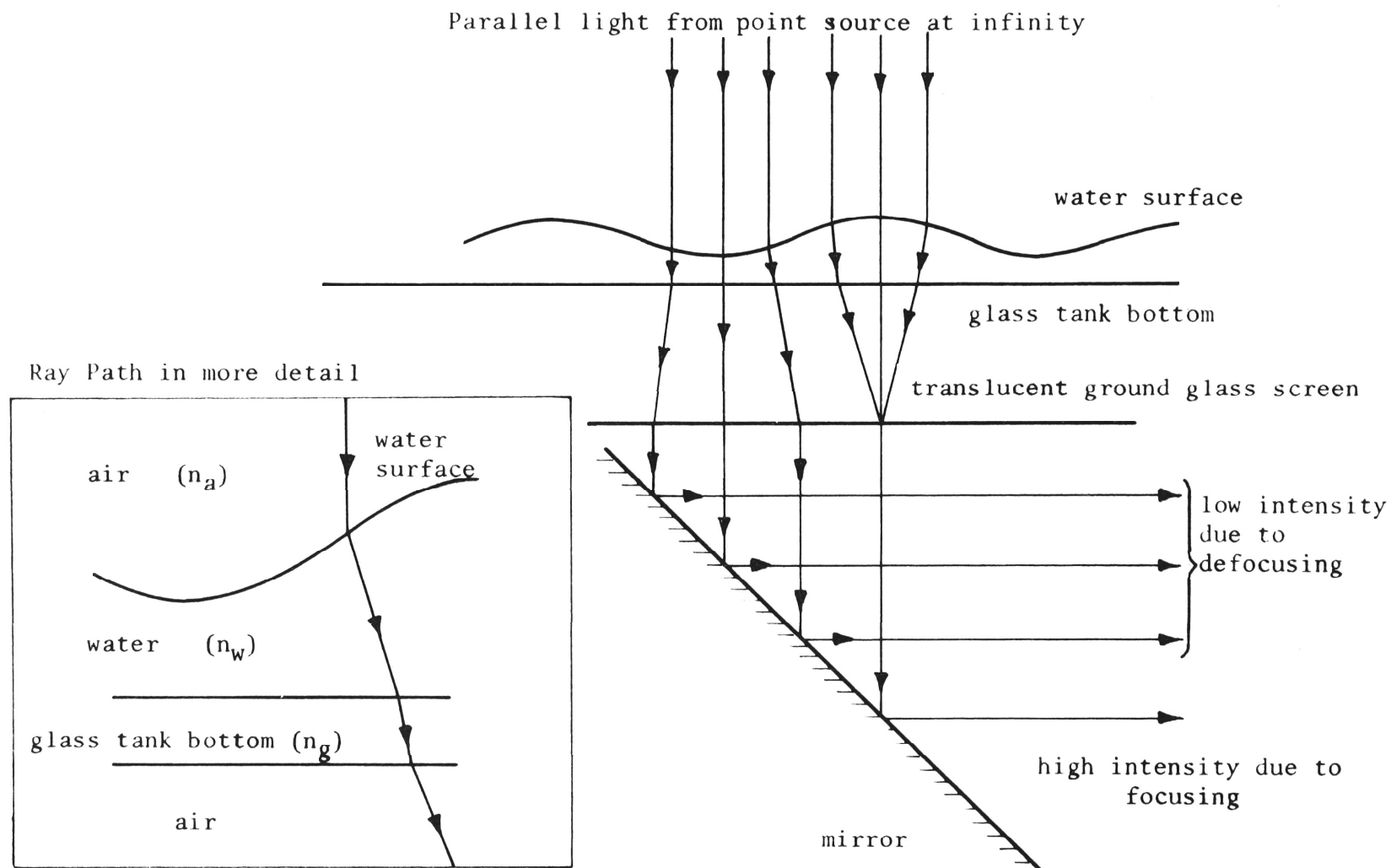PHOTOGRAPH A5:1   Top view of the Wave Tray.

PHOTOGRAPH A5:2   The Channel Iron Tank Base
                   supported by the Columns.

The channel iron base was set on six steel columns 54 inches high (Photo (A5:2)) so that a ground glass screen and inclined mirror could be situated under the tray. Thus, with the mirror and screen the wave tank could be used as a ripple tank whose principle of operation is that light, from a point source above the tank, is focused and defocused by the wave's crests and troughs, this light is transmitted through the tank bottom and displayed on the screen. The mirror, set at 45 degrees to the vertical, serves to change the direction of the light from the vertical to the horizontal thus making visual observations easier. (Figure (A5:2)). Visibility of the image on the mirror was increased by sheeting in 3 sides of the area under the tray, this reduced extraneous light from reaching the mirror. The level of the tray was adjusted by using levelling screws situated around the periphery of the tray and under the supports for the glass. (Figure (A5:3)). With water in the tray and using a surveyor's level the glass plates were set level to within 1/100th inch. A movable gantry was built that spanned the tank and allowed for model adjustments to be carried out in the tank. The gantry was mounted on wheels which ran along a track set on the concrete floor; no part of the tank came in contact with the gantry thus unwanted disturbances in the tank caused by the uneven loading of the gantry were eliminated.

The instrument carriage was a 10 foot square frame made from 2 inch square steel tubing. A round brass tube was bolted along one of the longer steel tubes and a brass angle section along the other.

These brass rails were situated a distance apart so that the small
instrument carriage (See (A5.2) used in the other tank could be
mounted on them. The instruments were connected to the small carriage
(Photo (A5:3)). Two rectangular steel tracks were bolted to lengths
of angle iron which, in turn, were bolted to the sides of the tray.
The bolts securing the track and the rails were used for adjustment of
the level of the carriage. Four steel wheels were machined to fit the
track and were connected to the instrument carriage. A small amount
of end float was allowed on the wheel axles to prevent binding on the
track.

A rough level of the tracks and rails was obtained by using a
spirit level. The accurate level of one of the tracks was set by
placing a wave probe (along with the small carriage) on the carriage
and situating the probe as near as possible to one of the tracks. The
probe wires were immersed in the water in the tank and different
deflections of the bridge galvanometer were found for different positions
of the carriage along the tracks. Adjustments were made on the track
so that a constant deflection of the bridge balance was obtained from
point to point as the carriage was moved along the track. The wave
probe was moved to the other side of the tank and the other track levell-
ed in the same manner. With both tracks now level, the wave probe was
moved on the carriage from point to point across the tank and the brass
rails were set level. Levelling the instrument carriage in this way
proved very quick and accurate as well as compensating for deflections of
the carriage caused by the weight of the small carriage and wave probe.

Parallel light from point source at infinity

water surface

glass tank bottom

translucent ground glass screen

Ray Path in more detail

air (n_a)

water
surface

water (n_w)

glass tank bottom (n_g)

air

low intensity
due to
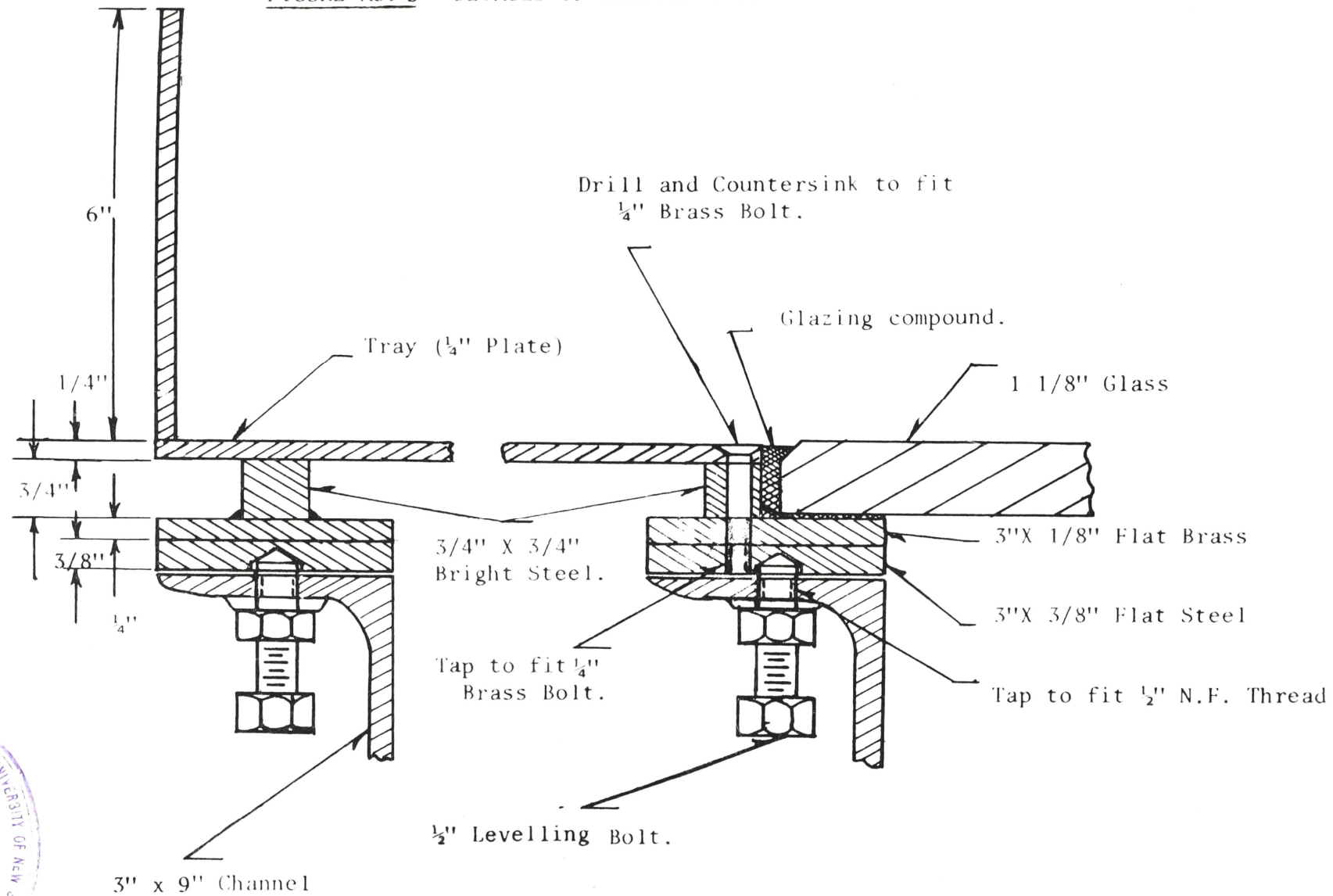defocusing

high intensity due to
focusing

mirror

n = refractive index

$n_a < n_w < n_g$

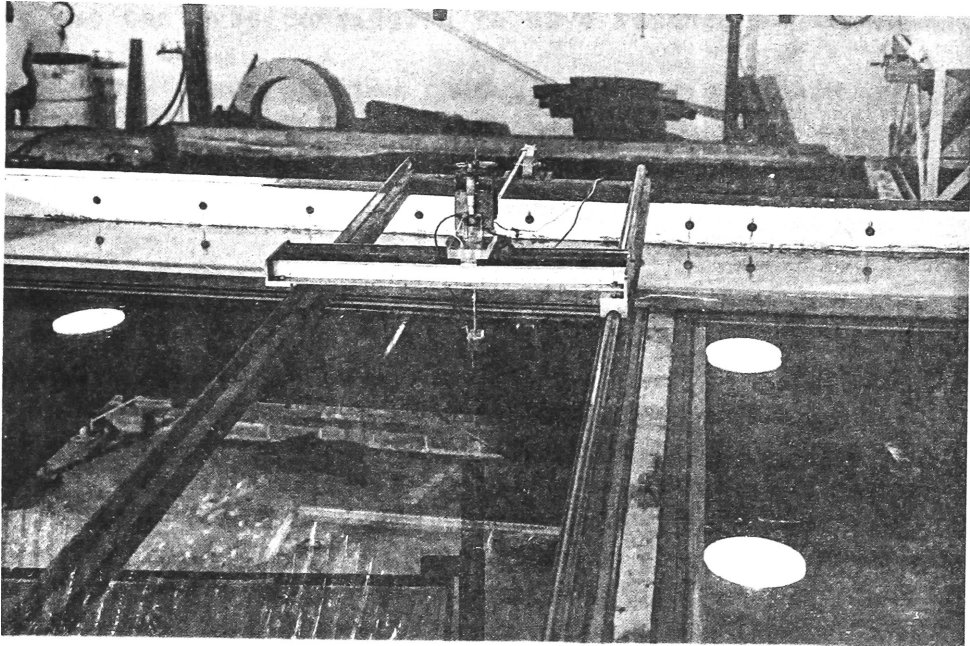FIGURE A5:2   SCHEMATIC DIAGRAM OF THE OPERATION OF A RIPPLE TANK

FIGURE A5: 3   DETAILS OF LEVELLING BLOCKS AND BOLTS.

6"

1/4"

3/4"

3/8"

¼"

Tray (¼" Plate)

3/4" X 3/4"
Bright Steel.

Tap to fit ¼"
Brass Bolt.

3" x 9" Channel

½" Levelling Bolt.

Drill and Countersink to fit
¼" Brass Bolt.

Glazing compound.

1 1/8" Glass

3"X 1/8" Flat Brass

3"X 3/8" Flat Steel

Tap to fit ½" N.F. Thread
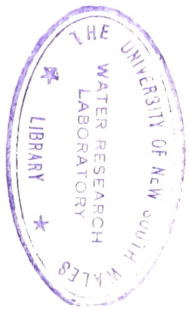
PHOTOGRAPH A5:3   The Instrument Carriages mounted
on the Large Wave Tank.
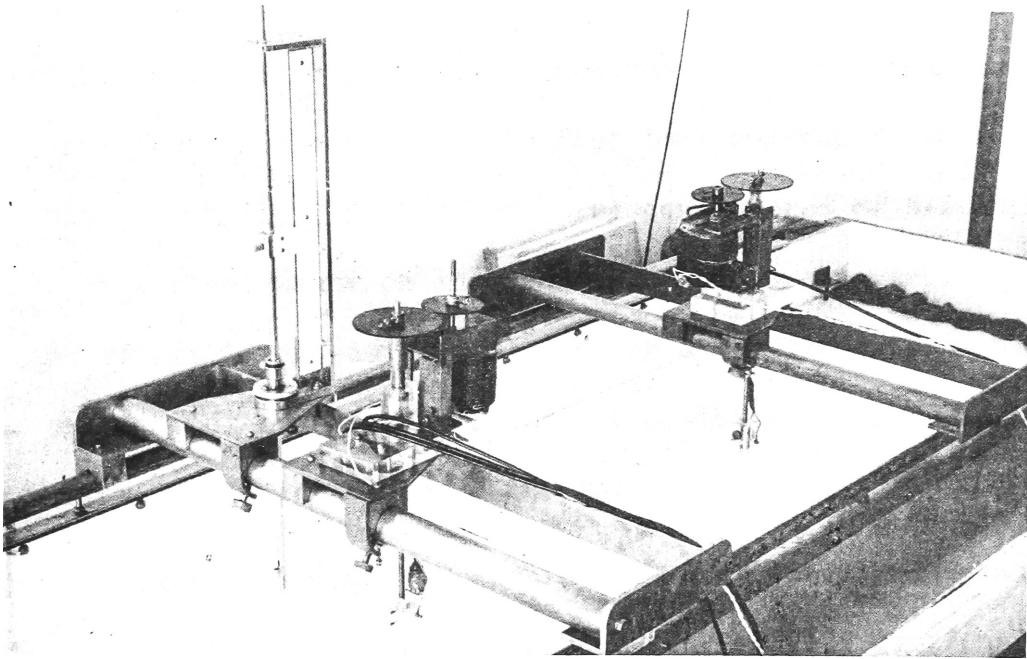
PHOTOGRAPH A5:4   The Instrument Carriages mounted
on the Small Wave Flume.

The water in the tank was considered to have reached a uniform
temperature and any discrepancies caused by changing conductivity of
the water from point to point were considered negligible.

A5.2   The Small Wave Flume

A small wave flume was constructed to examine one dimensional
wave properties in a viscous fluid. This wave flume was 2 feet wide
by 10 feet long and built of wood. The bottom was made in three
sections:

1)   the wave generation and runup region

2)   the fixed flat bottom

3)   the movable flat bottom   (See Figure (A5:4))

The generation region was 10 inches long and 3 inches below
the level of the fixed bottom; a 20 inch run up region connected these
two levels. The fixed bottom was 3½ feet long and the movable
portion was 4 feet long, the latter being constructed of 5/8 inch
plywood with a steel frame on its underside to prevent warping.
Adjustment of its level was accomplished by a levelling screw situated
in each of its four corners, the vertical position could be adjusted
2 inches above and 2 inches below the level of the fixed bottom.

This movable bottom gave a simple method of quickly and easily
changing the ratios of the depths between the two flat portions of
the flume. The flume was set on two sturdy channel iron trestles
and the level of the fixed bottom adjusted by levelling screws
between the foot of the trestles and pads set on the concrete floor.

A brass tube was bolted along one side of the flume and a brass angle section along the other. The small instrument carriage was designed to run along these brass rails; twisting of the carriage was prevented by mounting brass blocks, which had been machined to fit the tubular rail, on its underside. The other side of the carriage was allowed to run free along the top of the brass section. Levelling of the rails was accomplished as described in (A5.1). The instrument carriage supported the platform to which point gauges, wave gauges etc. could be mounted. It ran along the carriage on a similar but narrower set of rails as were mounted on the flume. A scale was put on the side of the tank and on the instrument carriage so that positions along the tank and across the flume could be found. A cursor was connected to the instrument carriage and to the instrument platform. Photo (A5:4) shows the instrument carriage arrangement.
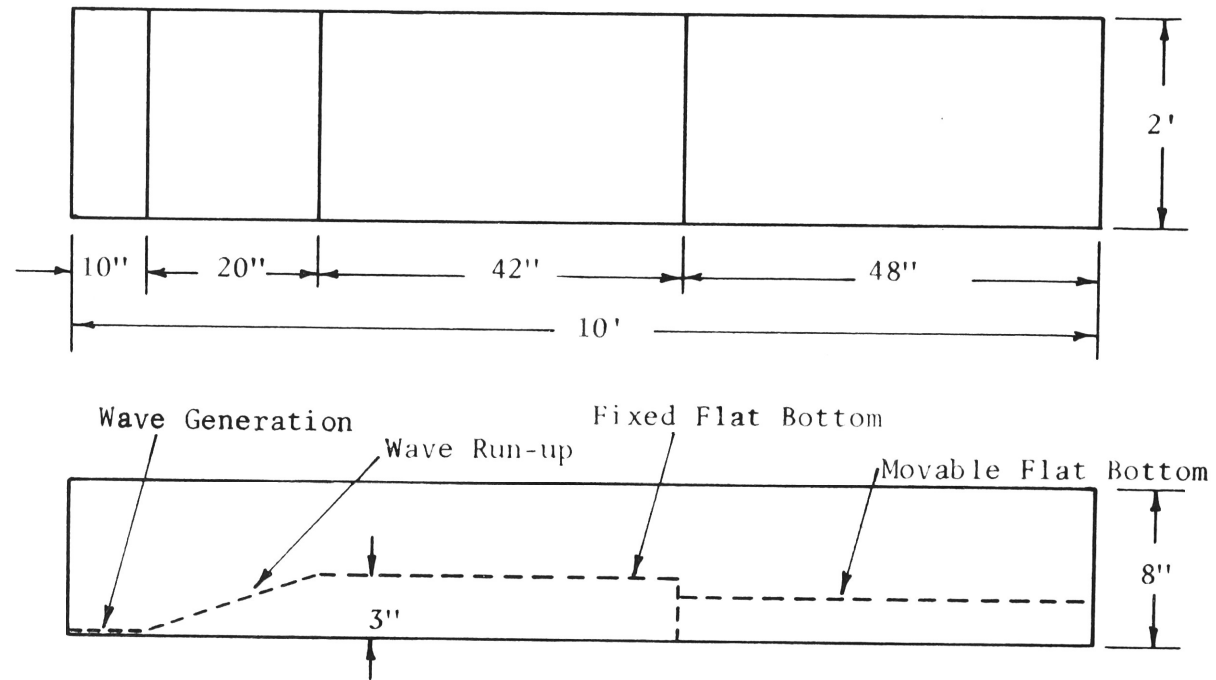
FIGURE A5:4 SCHEMATIC DIAGRAM OF BOTTOM LEVELS IN THE SMALL WAVE FLUME
(not to scale)

Appendix 6 - The Wave Generators

A6.1 The Wave Generator in the Large Tank

The wave generating mechanism was of the piston type and consisted of a driving unit, a quick start mechanism, a crank plate, a connecting yoke and a wave paddle.

The power supply for the driving unit was a C & H two horsepower variable speed drive with a range of 400 to 100 R.P.M. This speed was reduced by use of a reduction gearbox with a further range of speeds being supplied by a set of pulleys and V-belts. (See photo (A6:1)). This arrangement gave a variation in speeds from 23 to 270 R.P.M. and a corresponding period of 2.6 seconds and .22 seconds respectively.

A quick start mechanism was incorporated between the output shaft from the gearbox and the crank plate to provide a means of allowing the drive unit to build up to speed and then to instantaneously start the crank plate in motion. A small flywheel with a hole drilled in its outer edge was fixed to the gearbox shaft and a plate with a spring loaded pin connected to the drive shaft of the crank plate. The pin, when dropped into the hole on the flywheel, provided the coupling between the drive unit and the wave paddle. Photo (A6.2) shows this mechanism.

The pin mechanism and the crank plate were connected by a shaft running in two bronze bushes which were mounted on a rigid steel frame. A piece of steel machined with a slot so that a drive pin could

move up and down it was bolted to the crank plate. The amplitude
of motion of the wave paddle was adjusted by adjusting the eccentricity
of the drive pin with respect to the centre of the crank plate. A
lock nut was used to securely fix the position of the drive pin after
the desired amplitude had been obtained. (Photo (A6:3)). The
complete power supply mechanism for the wave paddle is shown in Photo
(A6:4).

The connecting rod between the wave paddle and the drive
pin was made in the form of a stiff yoke to help reduce racking of
the paddle. A self aligning ball race was used between the connecting
yoke and the drive pin to eliminate binding and racking of the wave
paddle, caused by small amounts of misalignment between the drive pin
the paddle. Two bronze bushes, positioned a distance 68 inches apart,
provided the connection between the two ends of the yoke and the wave
paddle.

The wave paddle consisted of a heavy 9 2/3 foot by 2 foot
channel iron frame to which was mounted a piece of ¼ inch x 8 inch
steel plate 10 feet long. The edge of this plate was set near to the
bottom to prevent, as much as possible, any flow under the paddle when
in motion. The frame ran on four roller bearings, two on one side were
allowed to run free on a flat steel block while the two on the other
side ran in machined slot (Photo (A6:5)) to help prevent racking and
sideward motions of the paddle.
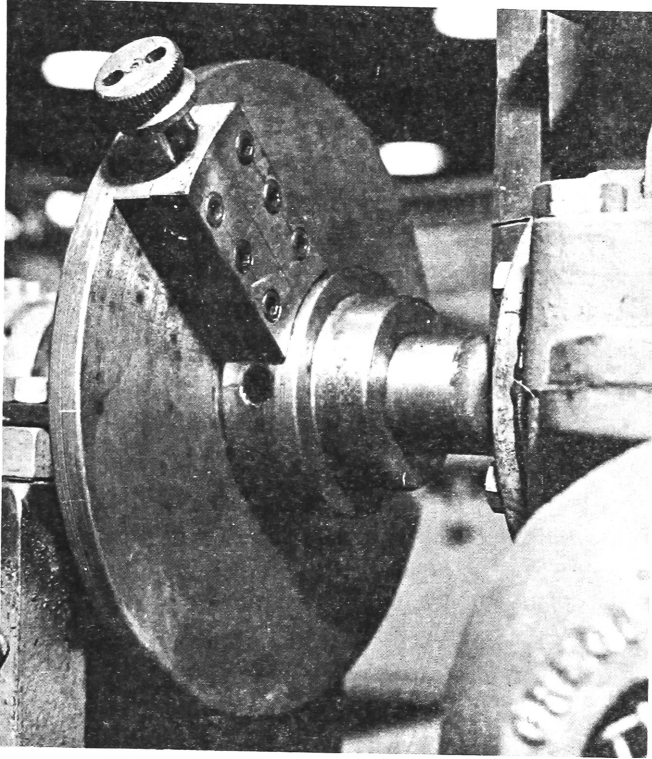
PHOTOGRAPH A6:2   The Quick Start Mechanism.
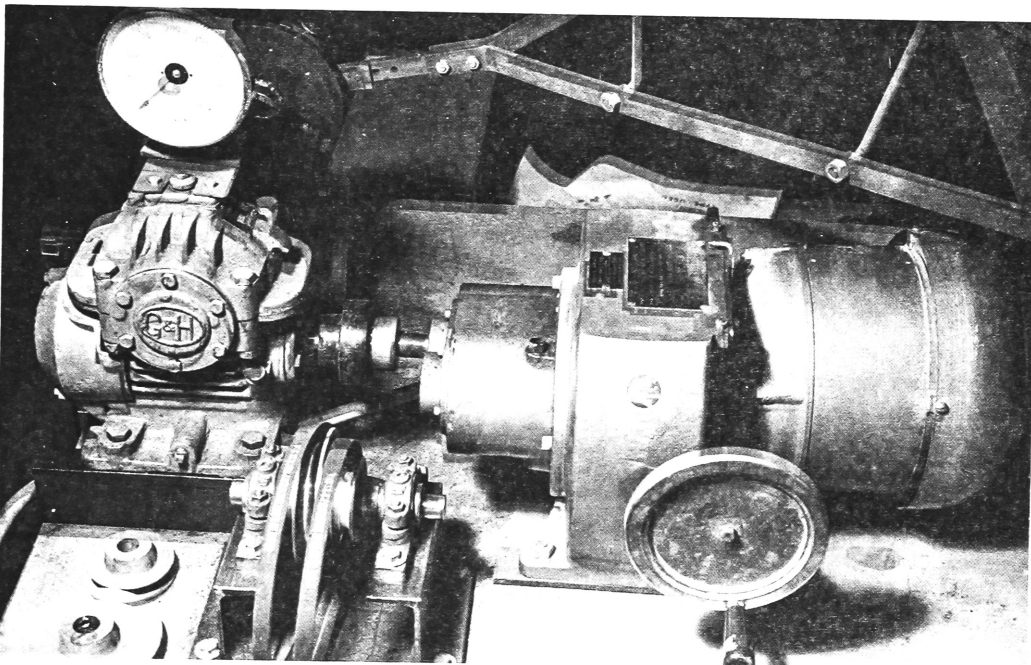
PHOTOGRAPH A6:1   The Variable Speed Drive Unit,
Reduction Pulleys (disconnected)
and the Reduction Box.
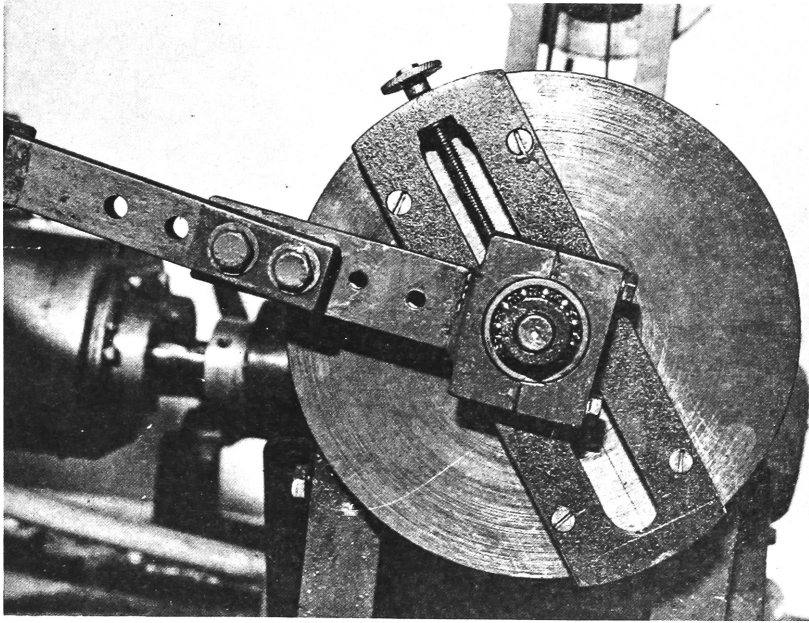
PHOTOGRAPH A6:3   The Crank Plate Assembly.

PHOTOGRAPH A6:4   The complete power supply
mechanism.

PHOTOGRAPH A6:5   The Machined Slot and Roller
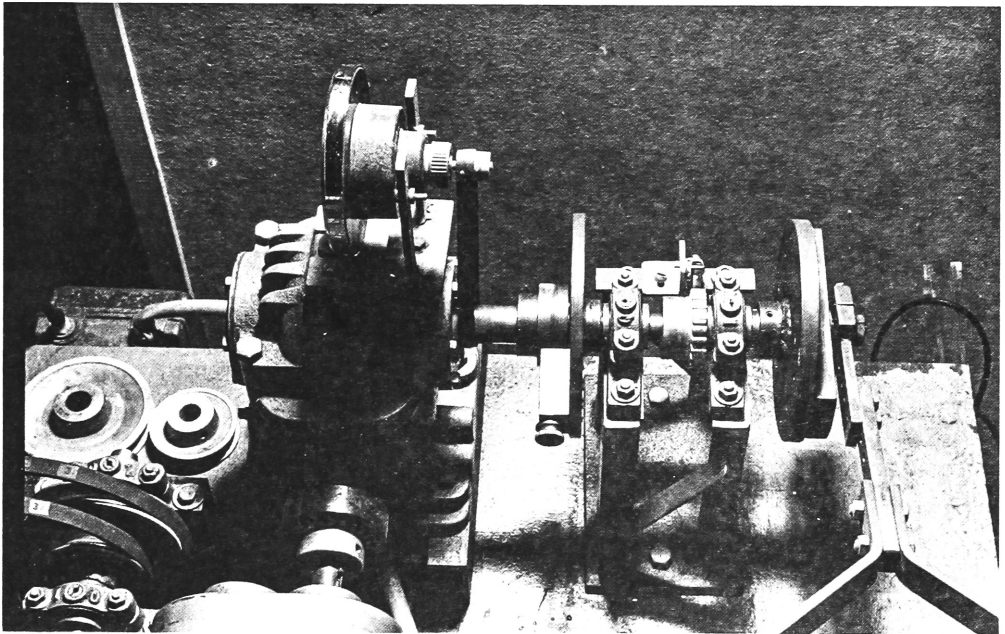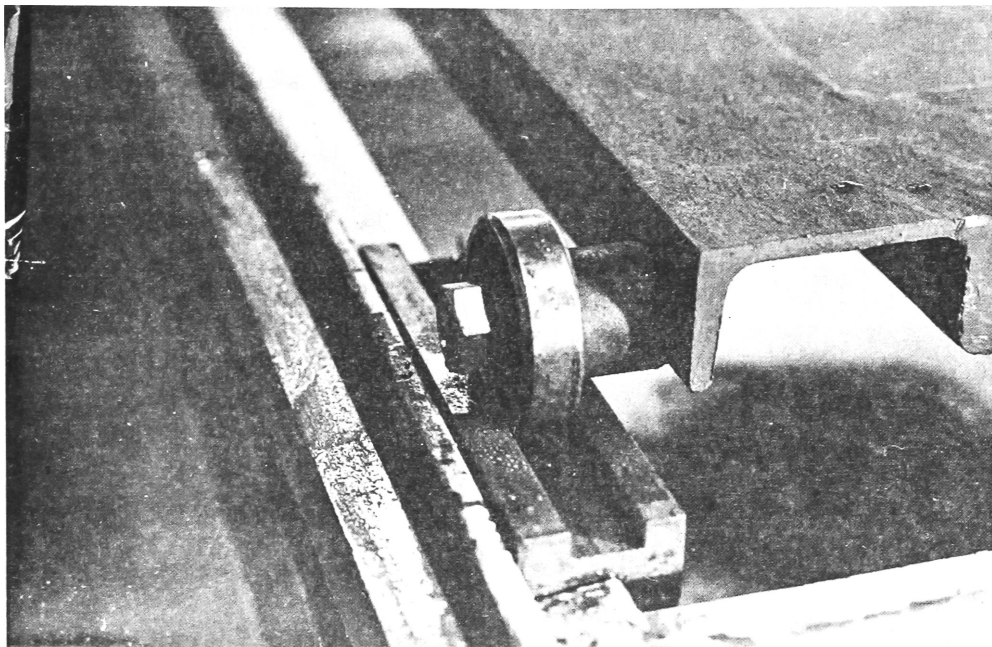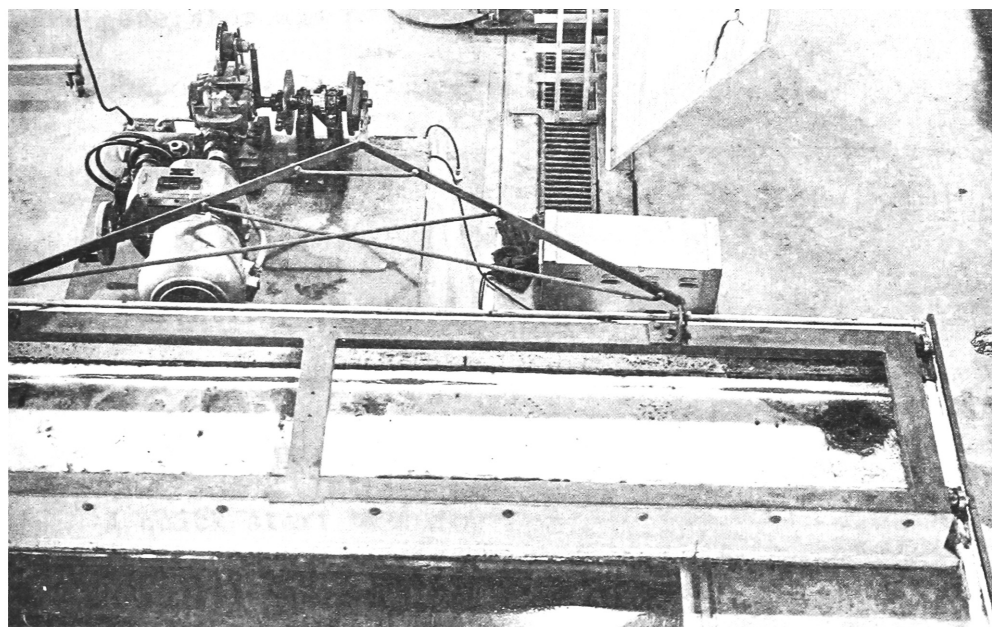Bearing carrying the Wave Paddle.

PHOTOGRAPH A6:6   The overall Wave Generator for
the Large Wave Tank.

The amplitudes were small compared with the length of the connecting rod so that very nearly true simple harmonic motion of the paddle was achieved. The drive unit, the quick start mechanism and the crank plate were all mounted on a rigid steel platform which was separate from the wave tank, this partially eliminating problems of vibration between the two components. Photo (A6:6) shows the overall wave generator and Figure (A6:1A) shows a typical profile of the waves generated by the mechanism. A check was run to determine the uniformity of the wave heights across the tank, these results are shown in Figure (A6:2).

A6.2 .The Wave Generator for the Small Flume

This wave generator was of the same type and consisted of a similar set of components as described in A6.1.

A 1/3 horsepower A.C. motor supplied the power to the system, a reduction box reduced the speed of rotation to the desired range of frequencies and variations in speed were set by using a continually a adjustable pulley V-belt unit. This gave a speed range of from about 63 to 170 R.P.M. and a corresponding period of .95 seconds to .35 seconds respectively. A quick start mechanism was incorporated between the output from the reduction box and the crank plate which worked on the spring loaded pin method as described previously. The crank plate and drive pin were similar to the ones used in the generator for the large tank. It was found more convenient to connect the drive pin and the wave paddle through a system of levers (Photo (A6:7)), than by a

direct connection. A connecting rod was used to connect the drive pin to one end of a steel lever, the lever being allowed to swivel about its centre on a bronze bushing fixed to a steel frame. The other end of the lever held a rod which was connected to the wave paddle. The rods had yokes welded to one of their ends so that the lever would just fit between the arms of the yoke. The connections between the lever and yokes were made through a rubber bushing set in a hole in the lever and a ¼ inch pin passing through the bushing and threaded to the yoke. The fit was tight enough between the bushing and pin so that the small amount of rotation was taken up by the elasticity of the rubber. A ball race connected the drive pin to one of the connecting rods while the other was fixed to the middle of the wave paddle with a bronze bushing. Since the flume was quite narrow, it proved unnecessary to use a yoke type connecting rod to prevent racking of the paddle.

A relatively heavy 16 inch by 20 inch steel frame was used to carry the actual paddle and was mounted on roller bearings in the manner described previously. The paddle was a piece of ½ inch plywood trimmed so that there was a close fit between it and the flume sides and bottom. It was stiffened with brass angle pieces on the back and any bending due to forces on the fluid were eliminated by the use of struts from the bottom of the paddle to the frame.

Vibrations between the mechanical drive and the wave paddle were essentially eliminated by separate mountings for the two components and

Wave Period = .64sec.
Fluid Depth = .33 inches
Wave Height = .0050 inches
Fluid   = Tap water
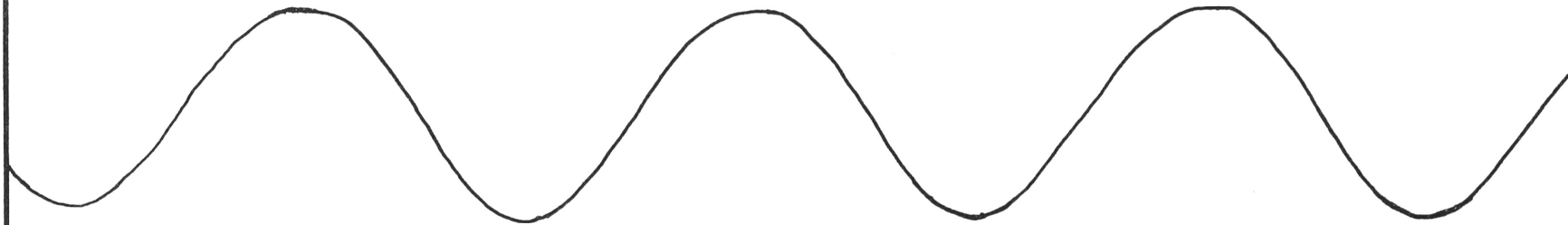
FIGURE A6:1A   WAVE FORM GENERATED IN LARGE WAVE TANK

Wave Period = .63sec.
Fluid Depth = .51 inches
Wave Height = .0153 inches
Fluid   = 77% glycerol
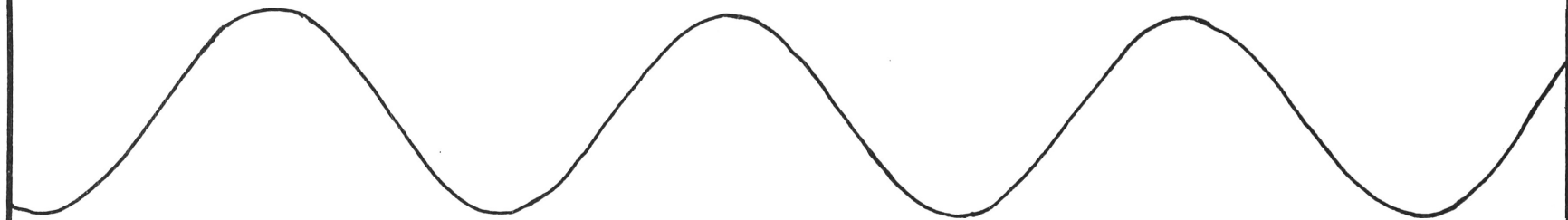
FIGURE A6:1B   WAVE FORM GENERATED IN SMALL FLUME

FIGURE A6:2   THE VARIATION IN WAVE HEIGHT ACROSS THE TANK
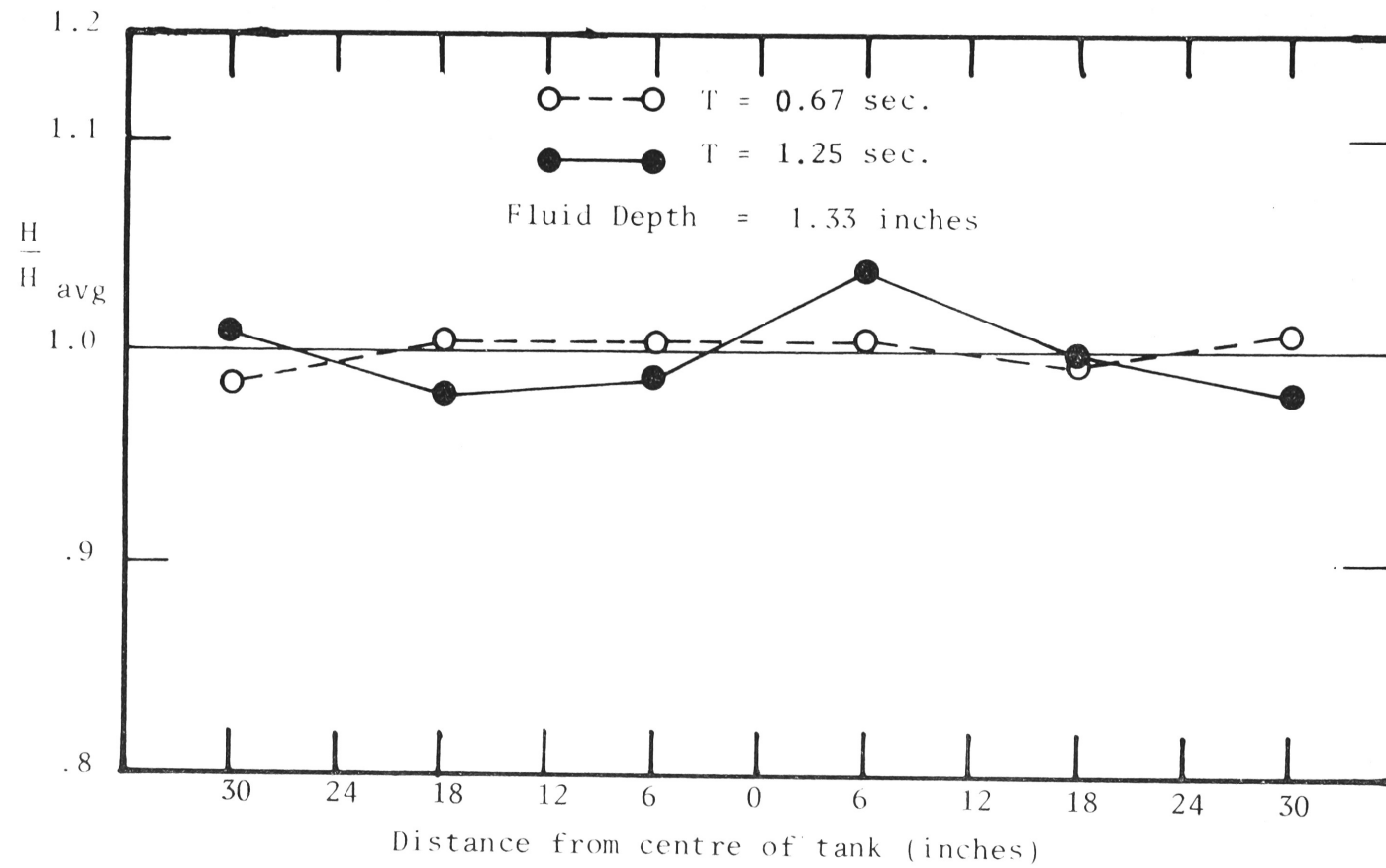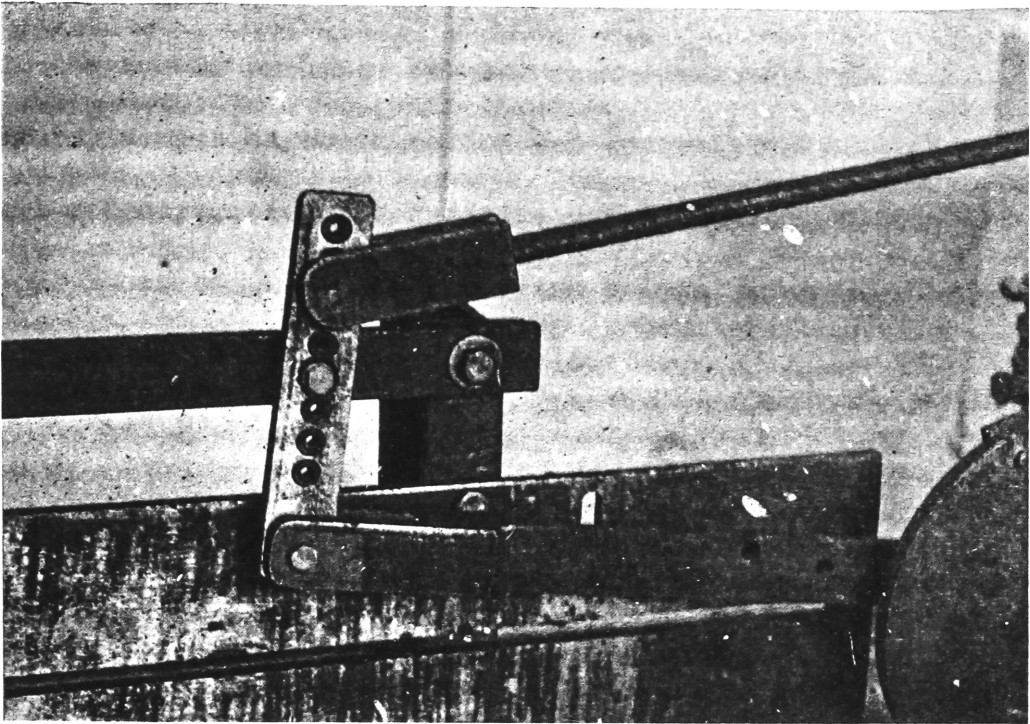
PHOTOGRAPH A6:7   The Lever Set Up for the Wave
Generator used for the Small Flume.
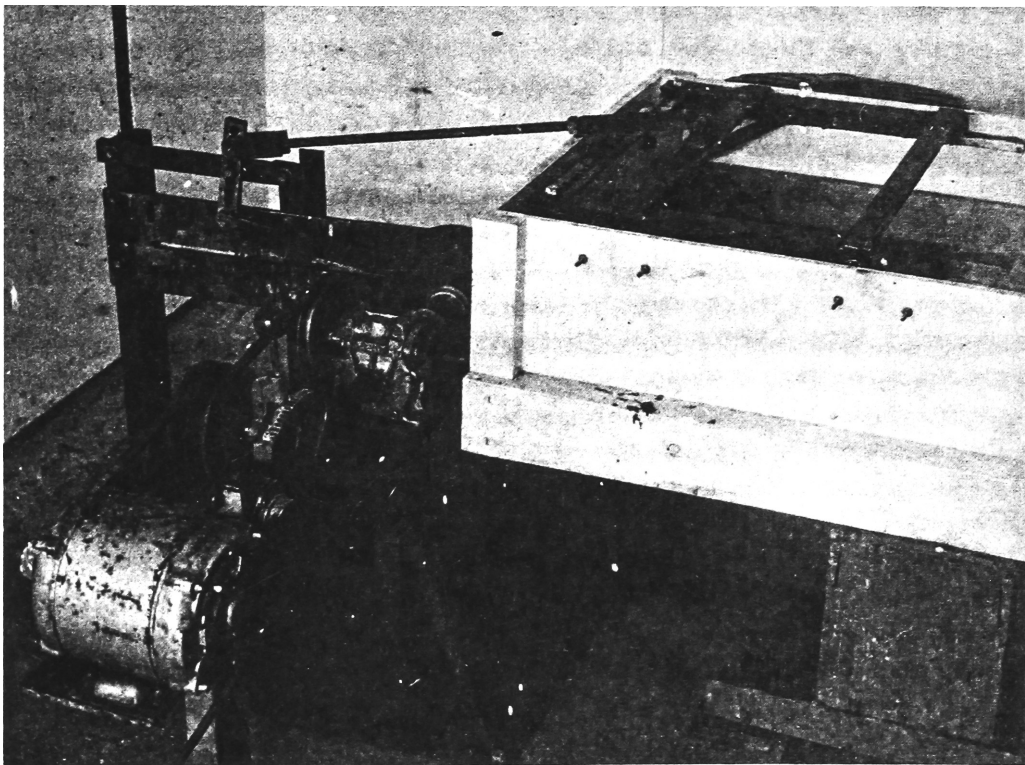
PHOTOGRAPH A6:8   The Overall Wave Generator for
the Small Wave Flume.

the use of the rubber bushings between the connecting rods and the lever. Again, simple harmonic motion was approximately obtained using small eccentricities and relatively long connecting rods. Photo (A6:8) shows the wave generator and a typical wave profile from this generator is shown in Figure (A6:1B).

Appendix 7 - Wave Absorbers in Large Tank

The laboratory study of waves travelling in two dimensions
presents considerable problems in the elimination of unwanted
reflections from the tank boundaries. Firstly, there is the incident
wave that must be absorbed to prevent reflections from the end of the
tank and secondly, there is the scattered wave that must be absorbed
on all boundaries. The wave absorbers upstream (toward the wave
paddle) from the model must be of a design so that they interfere as
little as possible with the incident wave train while providing
efficient damping of the scattered wave. The problem can be broken
up into three regions namely:

1) the end absorber

2) the absorber in front of the wave paddle

3) the side absorbers

Since fairly long period waves and shallow water were used in
all the experiments the use of parallel plate absorbers (Biesel (1948))
which depend on viscous damping between the plates and the fluid
proved unsuccessful. This was because of the large number of plates,
and hence a relatively large frontal area, required to produce
damping. Again, because of the nature of the waves, absorption of
energy by wave breaking on beaches or through perforated plates
(Hamill (1963)) could not be achieved. Rubbarized horse hair was
found to be a satisfactory material for the wave absorbers. As well
as being a good wave absorber it also had the advantage of being

easily cut to any desired shape and was commercially available in

3 foot by 6 foot sheets 2 inches thick.

A7.1   The End Absorbers

The reflection coefficients from the end of the wave tank were

determined by producing a short train of waves and measuring their

height as they passed through the model area.   The corresponding

wave train was measured as it again passed through the model area

after reflection from the end of the tank.   All the determinations of

the reflection were carried out in water about 1.3 inches deep as this

corresponded to the depth used in the experiments.

Figure (A7:1) shows the multiple reflections resulting when no

absorbers are in the tank.   The reduction in size of the waves

indicates that viscous bottom damping is of considerable importance

in reducing unwanted reflections arriving at the model region.   It

was found that the horse hair appeared somewhat opaque to the waves

because of its large frontal area and hence produced considerable

reflection.   (Figure (A7:2)).   The frontal area was reduced by using

wedge shaped sections instead of a flat surface, this gave a large

reduction in the reflection coefficient (Figures (A7:3A), (A7:3B)).

Comparison of these two figures show that the reflection increases at

the period increases.   For wave periods greater than about one second

the simple wedge design was replaced by one that further reduced the

frontal area.   (Figure (A7:4)).   It was found that for periods of

above two seconds the reflected wave had a height of at most 8% of that of the incident wave. For periods of about one second the reflection was approximately 5% and using the design as in Figure (A7:3) for periods less than one second, the reflection was further reduced.

A7.2   The Absorber in Front of the Wave Paddle

This absorber must fulfil two requirements, firstly, it must allow waves generated from the wave paddle to pass through it with as little distortion of the waves as possible and, secondly, must be able to absorb wave energy incident from downstream of the wave paddle.

The second requirement is easily fulfilled by using a sawtoothed arrangement as in Figure (A7:3). Unfortunately, this distorts the wave travelling through it from the wave paddle; this is due to the unequal length of absorber that the waves must transverse and hence the result of an uneven wave height and differences in phase across any line parallel to the wave paddle. It is thus clear that the wave absorber must have symmetry along its length if distortion is to be kept to a minimum. An eighteen inch wide strip of rubberized horse hair placed about 1 inch in front of the paddle was found to give sufficiently good absorption and, for periods greater than about .8 seconds, a fairly undistorted incident wave. For shorter periods the differences in density of the horse hair along the length of the absorber produced irregularities in the incident wave which were too

1. Incident wave.
2. Reflected wave from tank end.
3. Re-reflected wave from wave paddle.
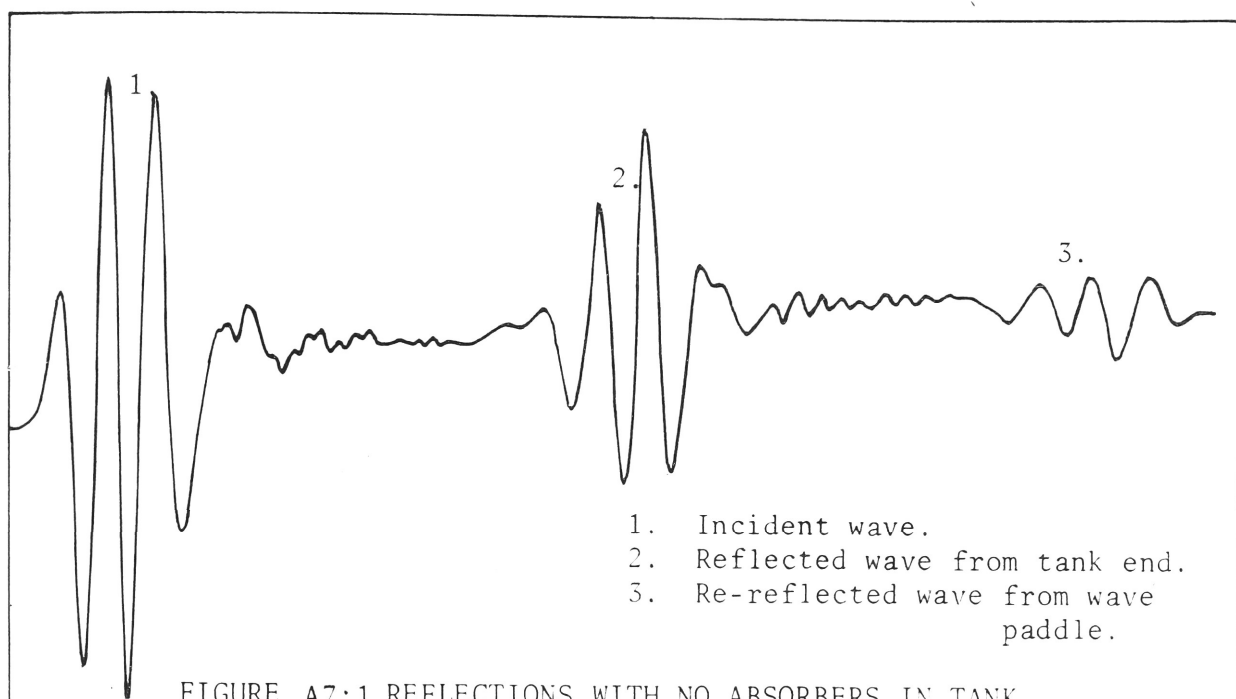
FIGURE A7:1 REFLECTIONS WITH NO ABSORBERS IN TANK

rubberized horsehair

24"

incident wave
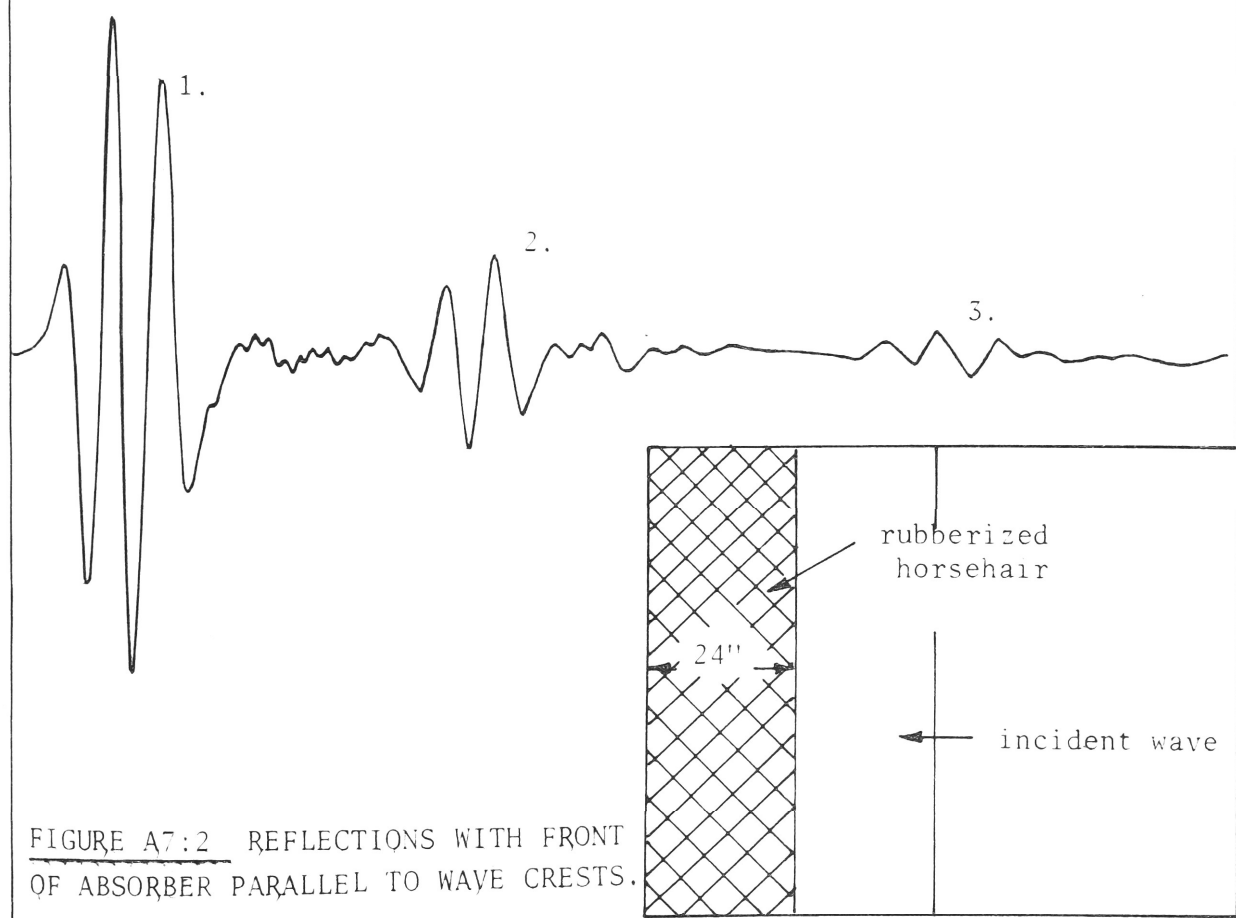
FIGURE A7:2 REFLECTIONS WITH FRONT OF ABSORBER PARALLEL TO WAVE CRESTS.
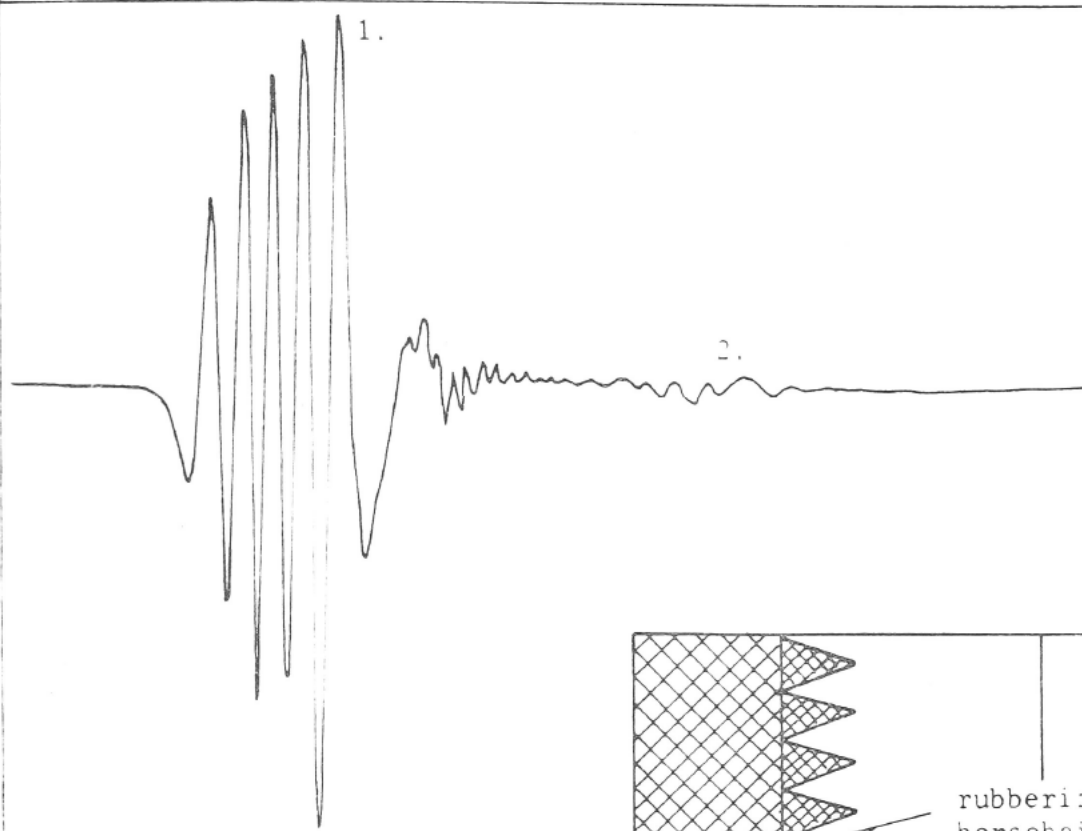
FIGURE A7:3A   REFLECTIONS
WITH SAW-TOOTH SHAPED FRONT ON
ABSORBER.   T ≃ .6sec.

rubberized
horsehair

incident
wave

5"

24"   12'
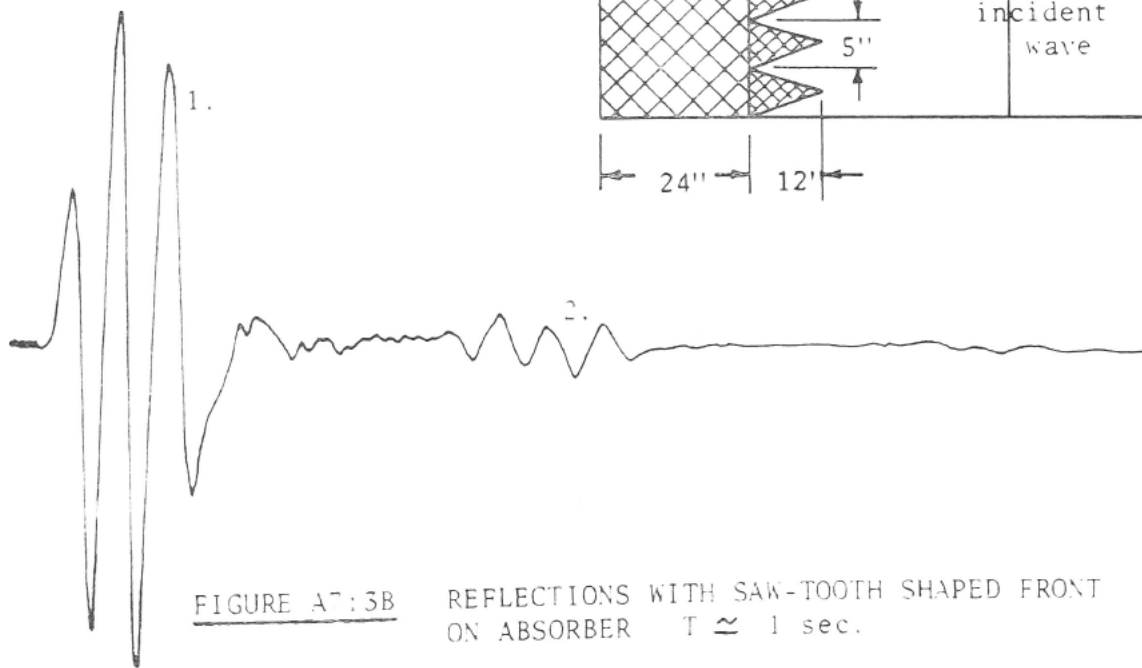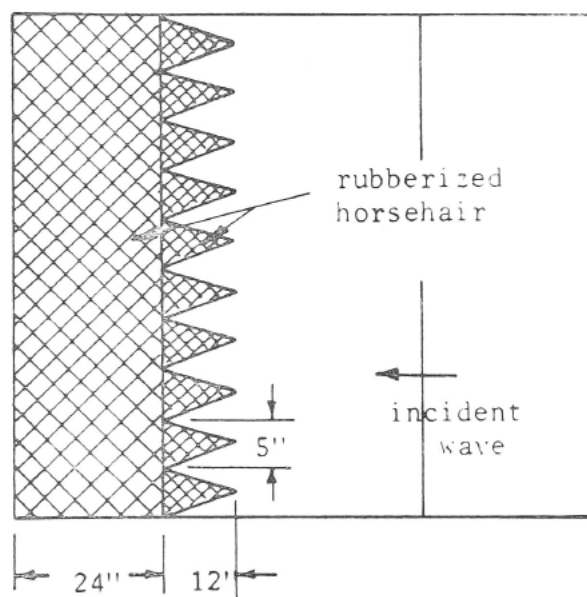
FIGURE A7:3B   REFLECTIONS WITH SAW-TOOTH SHAPED FRONT
ON ABSORBER   T ≃ 1 sec.

1.

2.

rubberized
horsehair

incident
wave

5"

1½"

24"

12"

28"
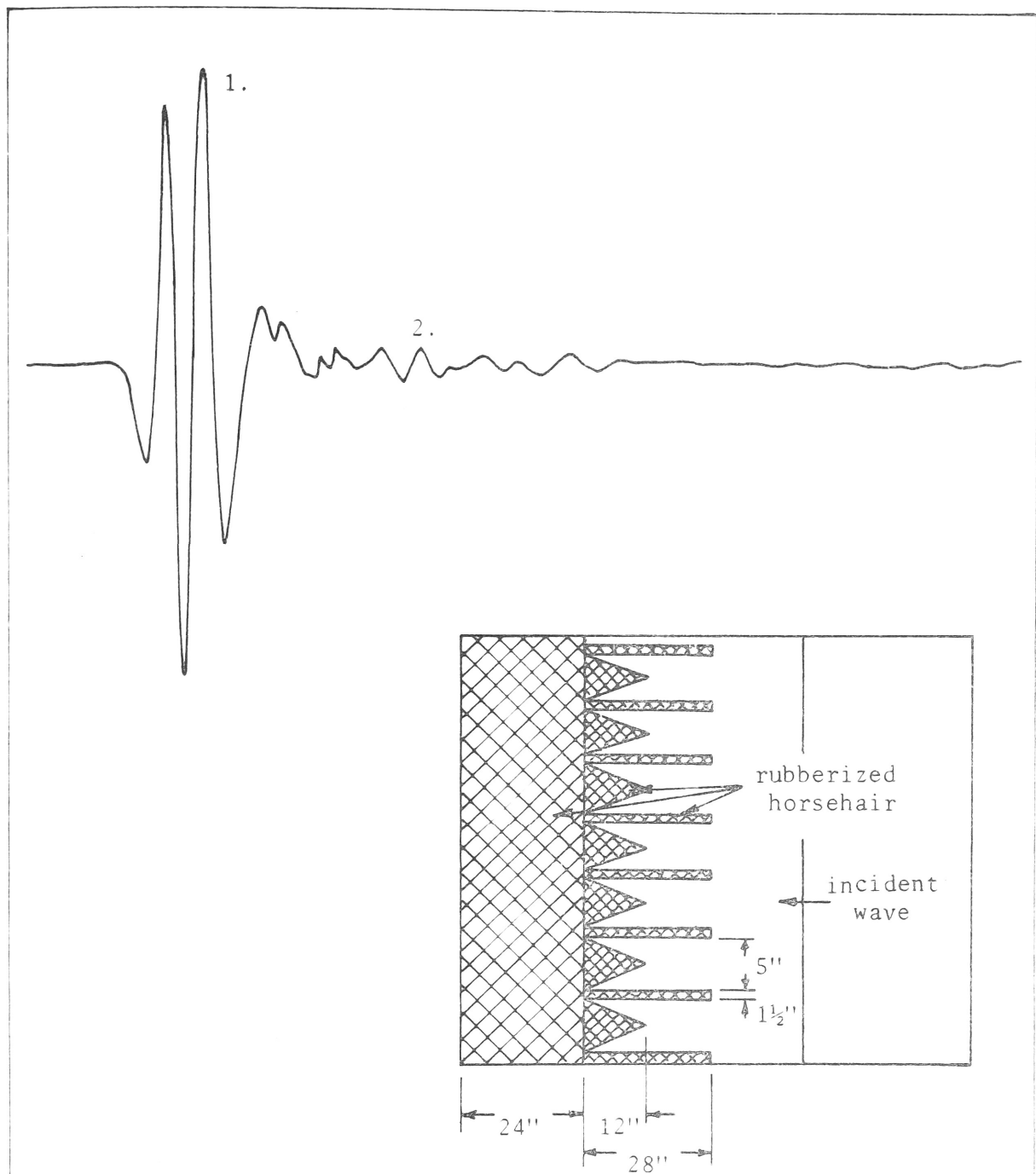
FIGURE **A7:4**   REFLECTIONS WITH FRONTAL AREA OF ABSORBER REDUCED.

large. It was found that suitable absorption could be obtained for these shorter periods by using ½ inch diameter glass marbles. These were tightly packed in a single four foot wide layer across the tank, with the inner edge situated just far enough from the wave paddle to avoid being in contact. To check the consistency of the wave heights across the tank, a series of wave measurements were taken a few inches in front of the absorber. These results are plotted in Figure (A7:5B) for the horse hair absorber and in Figure (A7:5A) for the marble absorber.

The efficiency of the marble absorber was tested by placing a wave reflector across the tank in the model area. A short train of waves was generated by the wave paddle and measurements were taken of the incident and reflected waves. The first reflection (from the wave reflector) was taken to be the wave generated in the model area and the second was the reflection from the wave paddle absorber. These two heights were compared and the percent reduction due to absorption by the wave absorber and to viscous damping was calculated. From Figure (A7:6) it is found that there is a reduction in height of about 87% for the marble absorber using a wave period of about .67 seconds; for the longer period waves it was found that the reflection after crossing and recrossing the absorber was greater than that for the horse hair (30%), (See Figure (A7:2)). Therefore the marble absorber was used for wave periods less than .8 seconds and horse hair was used for chose greater. These absorbers were felt to be sufficient since, in the circular model under study, it was expected that the scattered waves would be much

smaller than the incident waves and that they would be diverging from the model area, this divergence would also reduce the height when the waves reached the wave paddle.

A7.3   The Side Absorbers

These absorbers must fulfil the requirements that waves generated in the model area are absorbed as much as possible while being of a design that has a minimum amount of influence on the incident wav·s. The use of horse hair with a reduced frontal area as in Figure (A7:3A), (A7:3B) or Figure (A7:4) provided good absorption, but produced unwanted disturbances on the incident wave in the form of secondary waves travelling across the tank. Therefore, in the region between the wave paddle and the model area it was necessary to have parallel sides of some sort. These parallel sides ran along the edge of the glass and were wider than the reduced frontal area absorbers in the model region. Thus a wave generated by the wave paddle travelled between the two parallel sides until it came to the model area, here the width of the water surface was greater and it was found that only small disturbances were created by the absorbers in this area. This was due to the relatively small amount of wave energy reaching the side absorbers by diffraction and thus the even smaller secondary disturbances that could be generated by them. This method was generally employed for all the periods used in the model tests. Three examples of the configuration used are:

(a)   For wave periods greater than about .8 seconds

FIGURE A7:5A   MARBLE ABSORBER

FIGURE A7:5B   HORSEHAIR ABSORBER
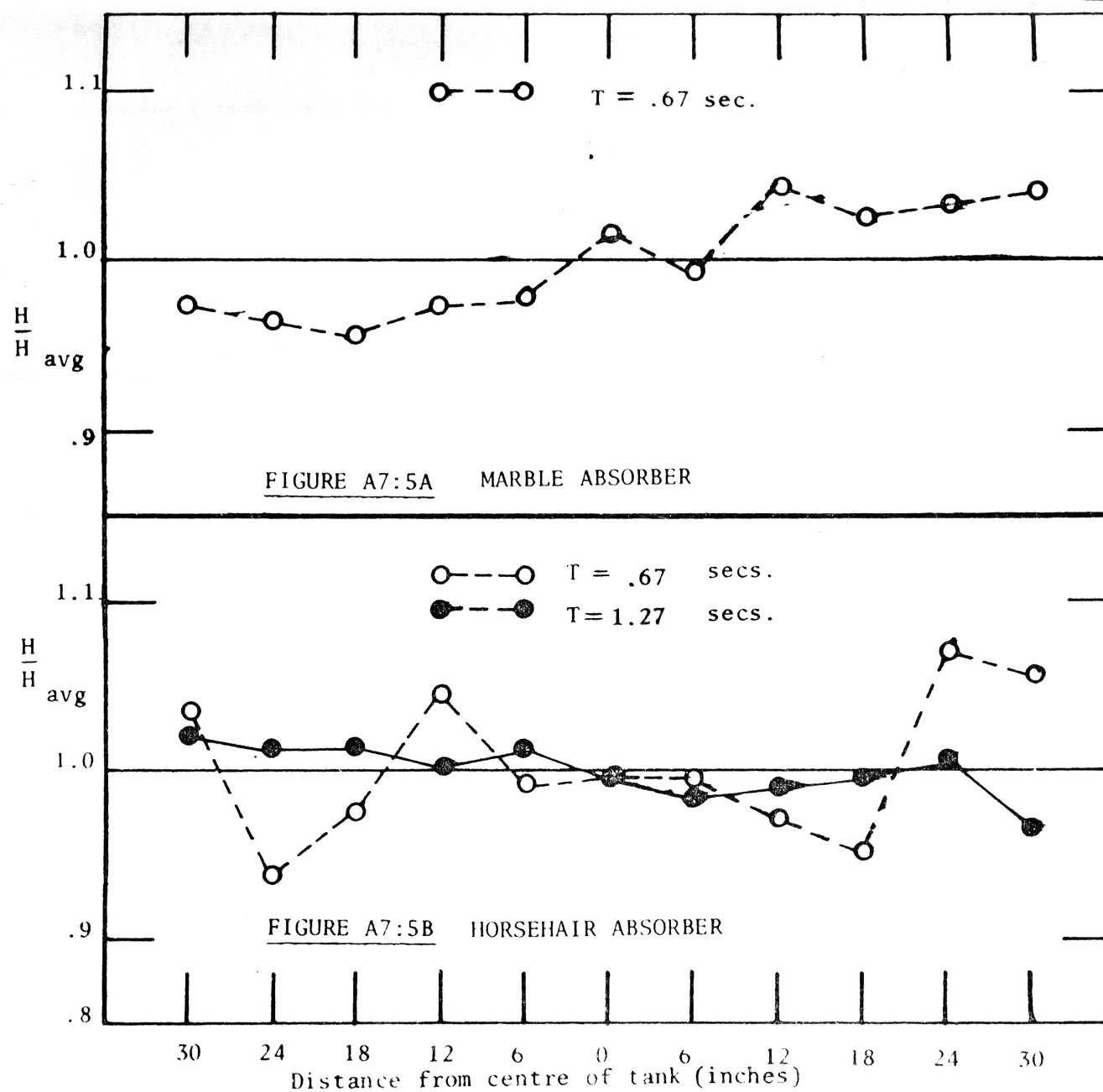
VARIATION OF WAVE HEIGHT ACROSS TANK

① Incident Waves from Wave Paddle

② Reflected Waves from Reflector Downstream of Wave Probe

③ Re-reflected Waves from Wave Paddle ($\simeq$ 13% of ②)
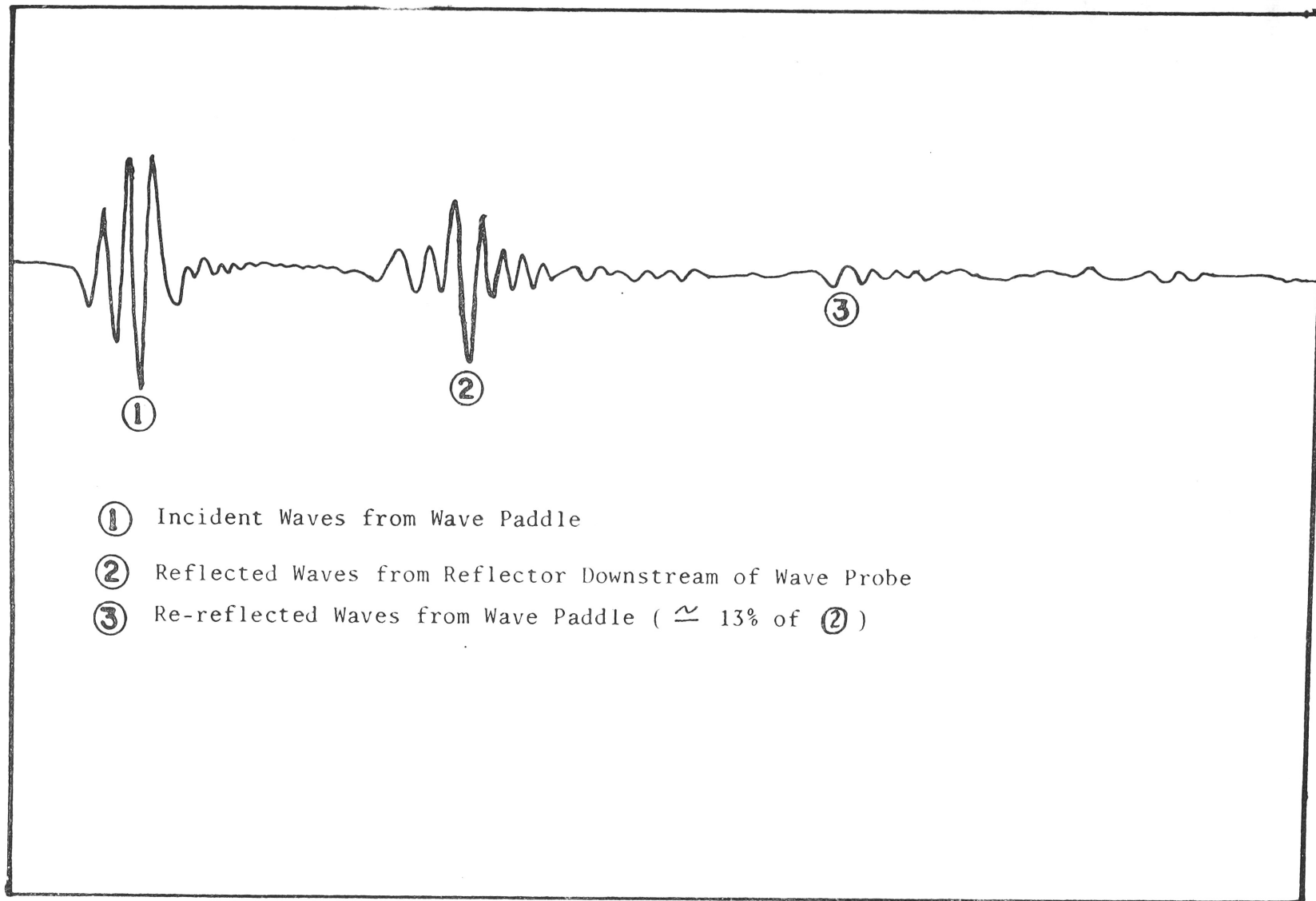
FIGURE A7:6.   DETERMINATION OF EFFICIENCY OF THE MARBLER
ABSORBER IN FRONT OF THE WAVE PADDLE.

the arrangement was as in Figure (A7:7). It was found that few secondary effects were produced by the parallel horse hair sides and it has already been shown that the reduced-frontal area absorbers of this type were very effective.

(b)   For wave periods less than .5 seconds it was found that the parallel sides as described in (a) produced secondary disturbances which were too large. To eliminate this, two rigid brass angle sections were placed along the edge of the glass to form solid parallel wave guides. This created the problem that disturbances were produced at the ends of these sides where the effective width of the tank became greater. It was found that a circular secondary wave was generated in this region, this was eliminated by using curved sections at the ends of the parallel guides to reduce the end effects. These peices were made from tin-plate and had a radius of about one foot. Reflections from these solid boundaries were considered negligible; firstly, because any waves from the model area striking the parallel guides would do so obliquely and thus be reflected away from the model area to be absorbed through viscous damping or at the wave paddle absorber. And secondly, any wave incident on the curved sections could only be reflected back to the model in the form of a diverging wave. Slots were cut in the paddle so it could slide over the parallel guides thus preventing any pumping between the wave paddle and the end of the guides. The system of absorbers and wave guides is shown in Figure (A7:8).

(c) For wave periods between .5 and .8 seconds, essentially

the same arrangement as in (b) was used with the exception of the curved

sections. These were replaced by a tin plate baffle whose plates

were 6 inches apart and 10 inches long. This had the effect of re-

flecting into the horse hair absorbers any waves generated at the

ends of the parallel guides. This arrangement is shown in Figure

(A7:9).
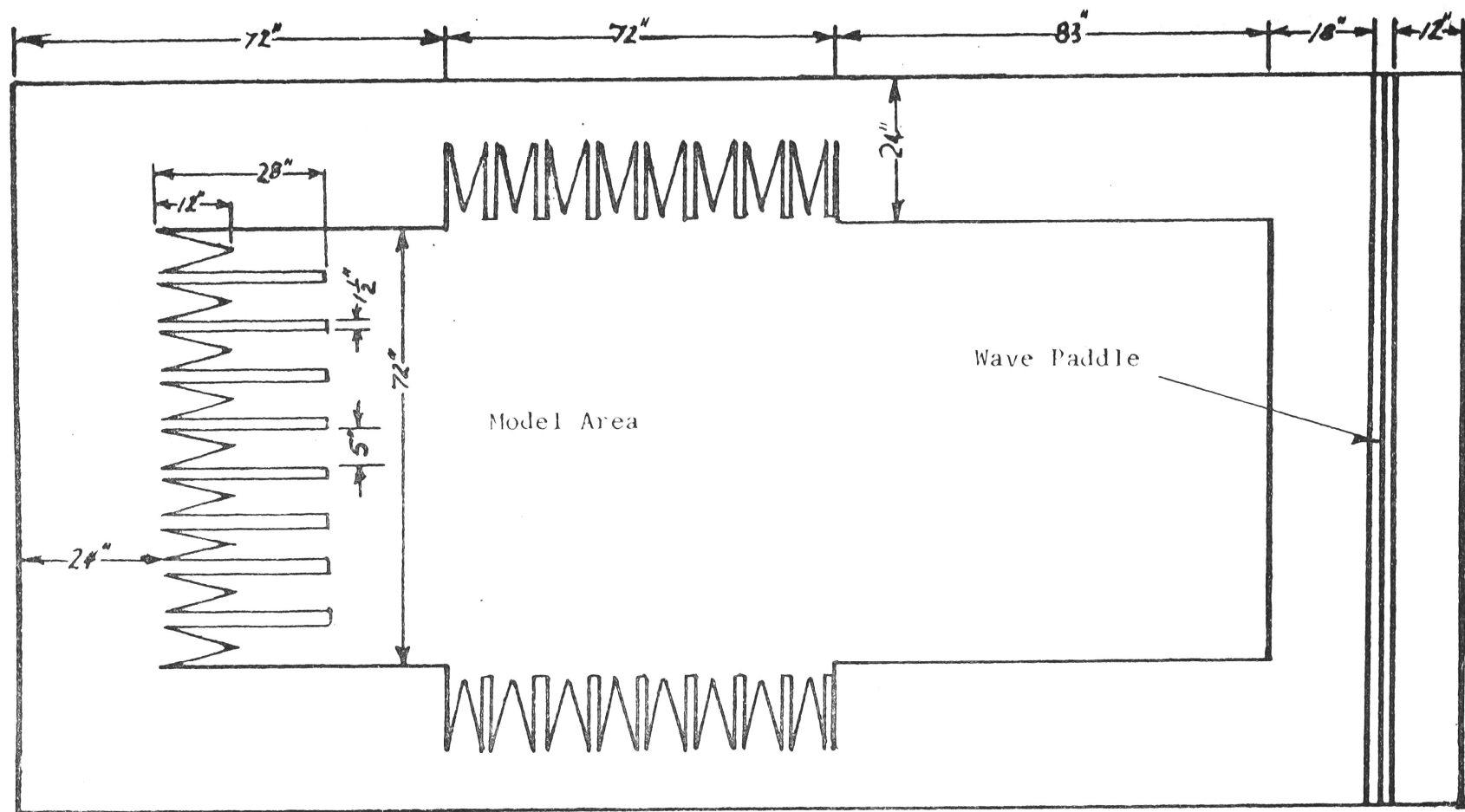
FIGURE A7:7.   ABSORBER ARRANGEMENT FOR T > .8 SECS.
(NOT TO SCALE)

Wave Guides

½" Diameter Marbles

Wave Paddle
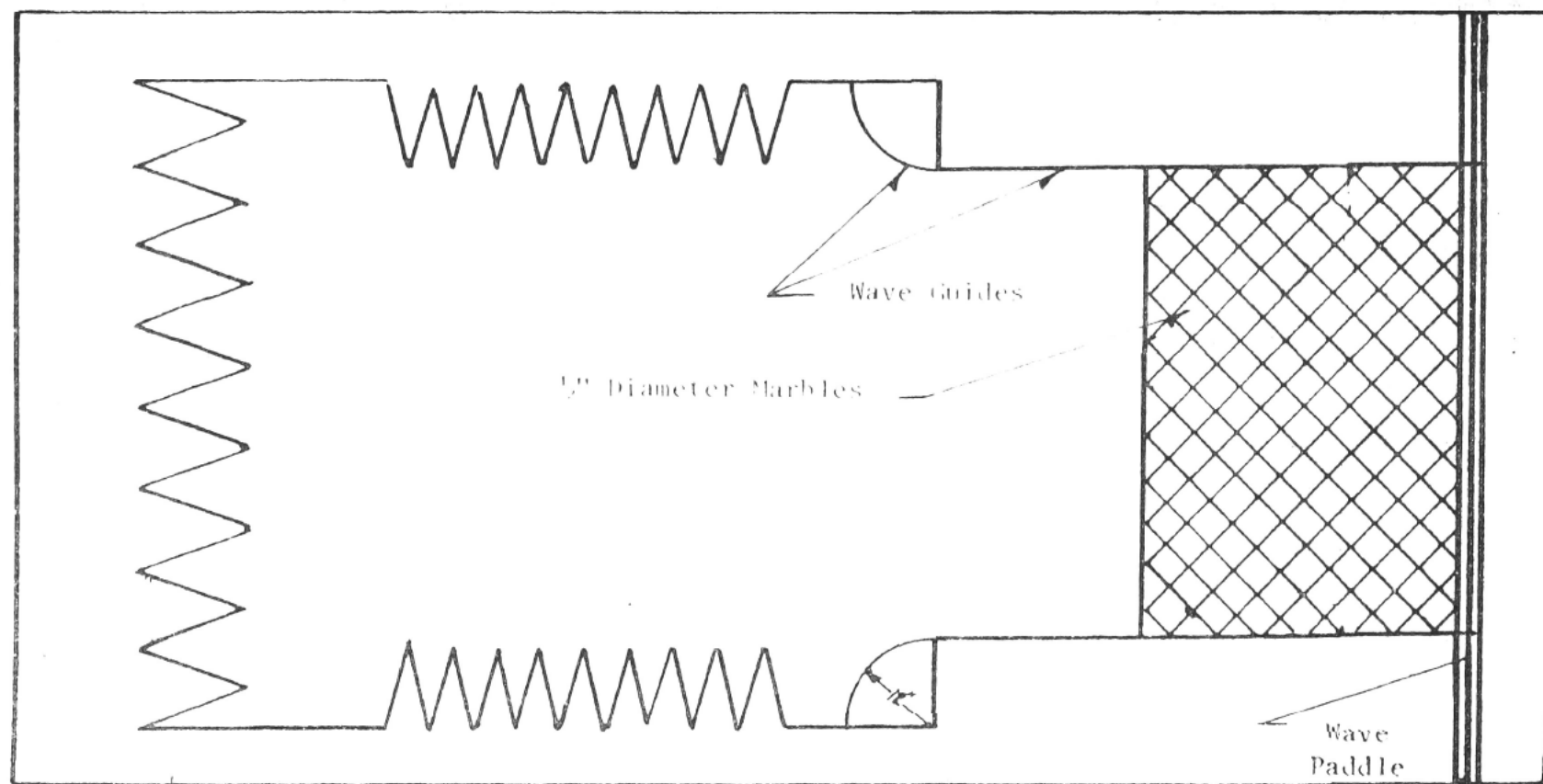
FIGURE A7:8.   THE ABSORBER ARRANGEMENT FOR T < .5 SEC.

(NOT TO SCALE)
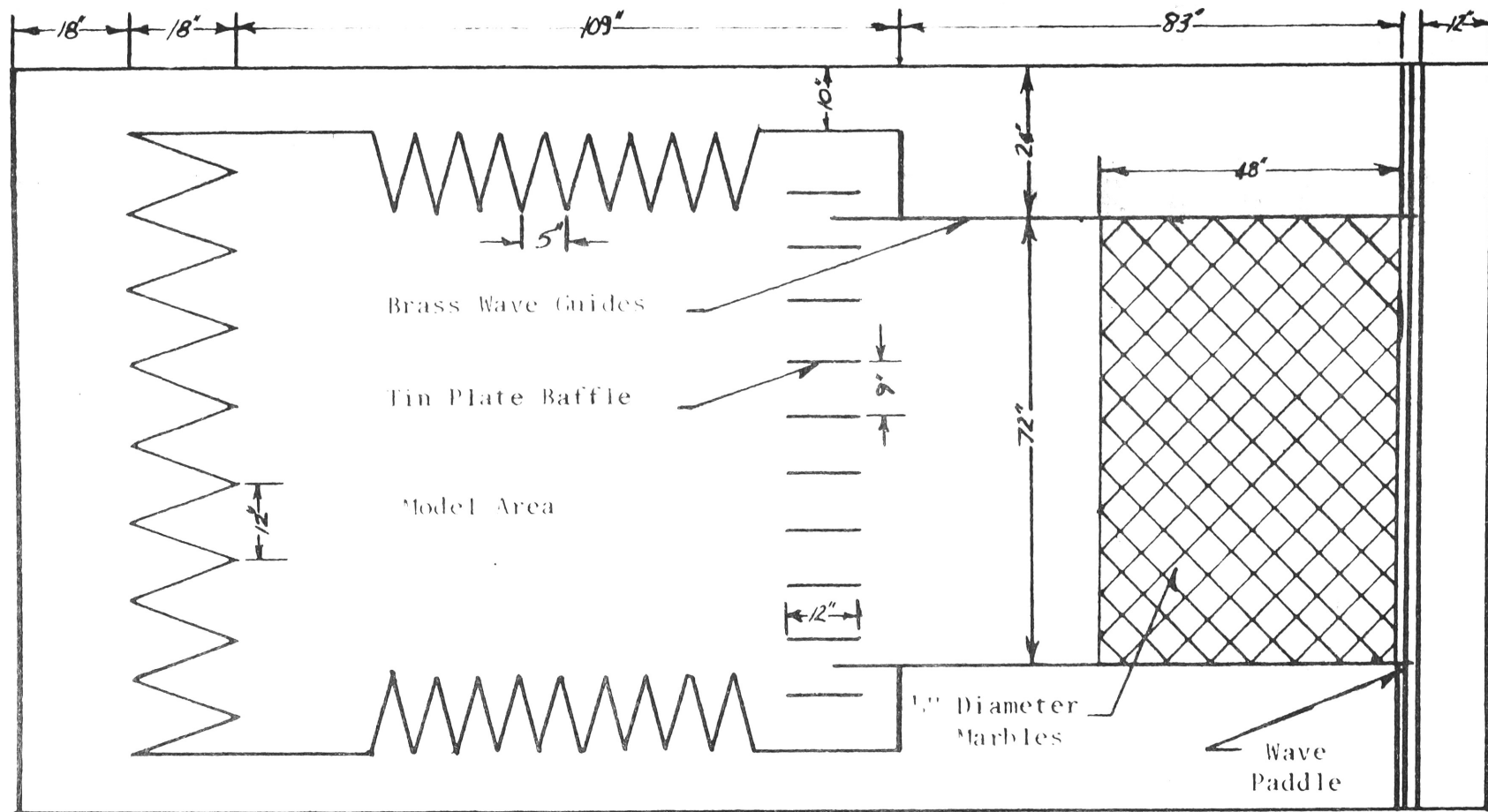
FIGURE A-9. THE ABSORBER ARRANGEMENT FOR .5 SEC. < T < .8 SEC.
(NOT TO SCALE)

Appendix 8 - The Wave Probe

Introduction

In laboratory experiments involving surface waves it is often desirable to eliminate as much as possible, the effect of finite amplitude on the wave properties. The experiments studying inter- actions between surface waves and solid structures usually exhibit a large range of wave amplitudes, all of which, to remain within a linear theory, must be small in the sense of Stokes (1880).

The use of a parallel wire resistance probe provides a relatively rugged, simple and inexpensive means of measuring surface wave profiles. The principle of operation is basically that, as the depth of immersion of two vertical wires in a conducting fluid changes the electrical resistance between them changes. This change in resist- ance is observed by use of a suitable bridge circuit in conjunction with a recording system. Unfortunately, this method proves somewhat unreliable for measurement of small as well as large amplitude waves. This un- reliability stems from a number of causes which can, in most cases, be traced to extraneous changes in the resistance between the two wires or to the effects of the miniscus.

These effects can be corrected, for if, at each point (or time) where an experimental measurement of the wave profile is taken, the probe can be calibrated against a known wave profile.

A known profile is produced by moving the probe wires up and down a fixed distance in oscillatory motion to simulate the effect of a falling and rising water surface.

The method of wave measurement is then to:

1) Move the probe and calibrator to a desired position in the wave tank and measure a few waves to determine a profile, or more specifically a wave height (H_{exp}).

2) Switch off the wave maker, and when the free surface has come to rest, oscillate the probe vertically through a known distance "d". This will determine a recorded calibration wave height of H_c.

3) From the recorder output measure graphically both (H_{exp}) and (H_c) and correct both for variations caused by the response of the electrical system to obtain (H'_{exp}) and (H'_c).

4) The actual wave height H can now be deduced from calibration curves of recorded height against actual height. It was found for the system used that the calibration curves were linear, hence:

$$H = \frac{H'_{exp}}{H'_c} d \qquad\qquad (A8-1)$$

Although the standard and experimental wave profiles did not have exactly the same form, the assumption was made that the calibration curves were valid when applied to the experimental results.

One obvious shortcoming of this system is the necessity of a still water surface for calibration. This entails stopping the wave maker and waiting for all the waves to be absorbed or damped out.

Tests were carried out on the probe to determine:

1. The change in recorded wave height as a function of -

(i)   the actual wave heignt.

(ii)   the period of oscillation.

(iii) the temperature of the fluid.

(iv)   the depth of probe wire immersion.

(v)   the proximity of the probe wires to a
       conducting submerged structure.

2. The change in phase and wave form between the recorded
    oscillatory motion and the actual motion for various
    wave heights and periods.

Experimental Equipment

The probe was cf the micrometer type and was basically the same design as that described by Wong, Ippen and Harleman (1963). A separate description is given here:

A micrometer head was fixed to a perspex stand such that vertical movements of the micrometer spindle could be transferred to a sliding

brass rod extending through the stand. This rod was spring loaded to permit continuous contact with a small ball bearing fitted to the end of the micrometer spindle. On the lower end of the rod was fastened a perspex block which held and insulated two .020 inch diameter stainless steel wires a distance of ¼ inch apart. These wires protruded about 1½ inches outside the block and provided the contact with the fluid. An electrical connection was made through the perspex block to each of the wires. The thimble of the micrometer was driven in oscillatory circular motion by an electric windscreen wiper motor, the motion was converted into vertical oscillatory motion by the micrometer. The motor shaft and the micrometer were connected by a set of "MECANNO" gear cogs. Various amplitudes of motion of the micrometer spindle were obtained by using a variety of gear ratios. The speed of the motor and hence its period was varied by use of a variable-output transformer connected through a half-wave rectifier to the power mains.

A PHILLIPS PM9300 strain gauge bridge was used for all of the tests on the characteristics of the probe with the exception of one calibration curve using an Automation Sperry bridge.

Both bridges incorporated the desirable features of:

1) A high frequency signal used in the bridge
    circuit which prevents electrolysis on the
    probe wires.

2) A filtering circuit to remove the high

frequency carrier from the low frequency

modulated wave produced by the charging

resistance across the probe wires.

3) An output amplifier.

4) A galvanometer which permits continuous

visual observations of resistance charges.

5) An attenuation switch which allows a large

range of wave amplitudes to be measured.

The recorder used was a HONEYWELL 1943 four channel ultraviolet recorder which gave a rapid response and a good range of chart speeds. Due to the high resistance of the fluid it was found that the system was extremely sensitive to small changes in capacitance and to static charges accumulating on the components, both of which caused a fairly rapid drift of the bridge balance. To eliminate this, all the components including the fluid were fixed to a common earth wire and 780 OHM shunt resistors were placed across both arms of the bridge. It was found that the balance controls incorporated in the bridge then had sufficient range to permit the bridge to be balanced when the probe wires were immersed in the fluid.

For a number of the tests, it was necessary to know the exact motion of the probe as it was driven up and down by the motor. This was accomplished by use of a PHILLIPS PM1843 linear transducer mounted on the probe. The body of the transducer was fixed in a

stationary position on the probe and the movable pin driven off the oscillating brass rod. An adjustment screw was incorporated to allow zeroing of the transducer.

The fluid temperature was measured by use of a chromel-alumel thermocouple in line with a vacuum-tube voltmeter. These measurements of temperature were taken as near as possible to the probe wires and at approximately the same depth as their ends.

Most of the tests on the probe were made in conjunction with experiments involving the decay of waves in a viscous fluid. The fluid used was 77% glycerol and 23% distilled water with the addition of 6gm of N_aCl per gallon to increase the electrical conductivity. Tap water was used in the tests involving the submerged conducting structure.

Photo (A8:1) shows the wave probe and calibrator unit with the linear transducer in position and the thermocouple taped to the movable perspex block. All the tests on the probe except the one concerned with conducting structures were carried out on a vibration free bench. The probe was supported above the bench by concrete blocks and the fluid was held in a suitable small container under the probe. (Photo (A8:2)). This arrangement was felt to give a higher degree of experimental control than that which could be obtained by using the large volume of fluid in the wave tank. For the tests not involving changes in temperature the fluid was held in a glass thermos flask.
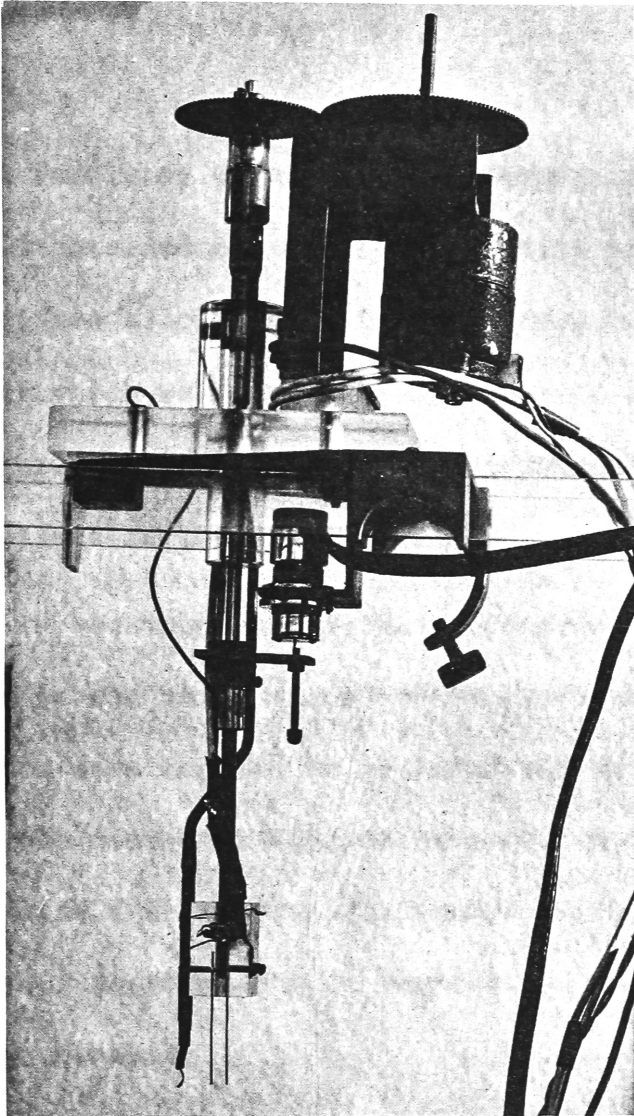
PHOTOGRAPH A8:1

The Wave Probe with the Linear Displacement Transducer and Thermocouple Sensor attached.

PHOTOGRAPH A8:2 (Below) The Experimental Set Up for the tests on the Wave Probe.
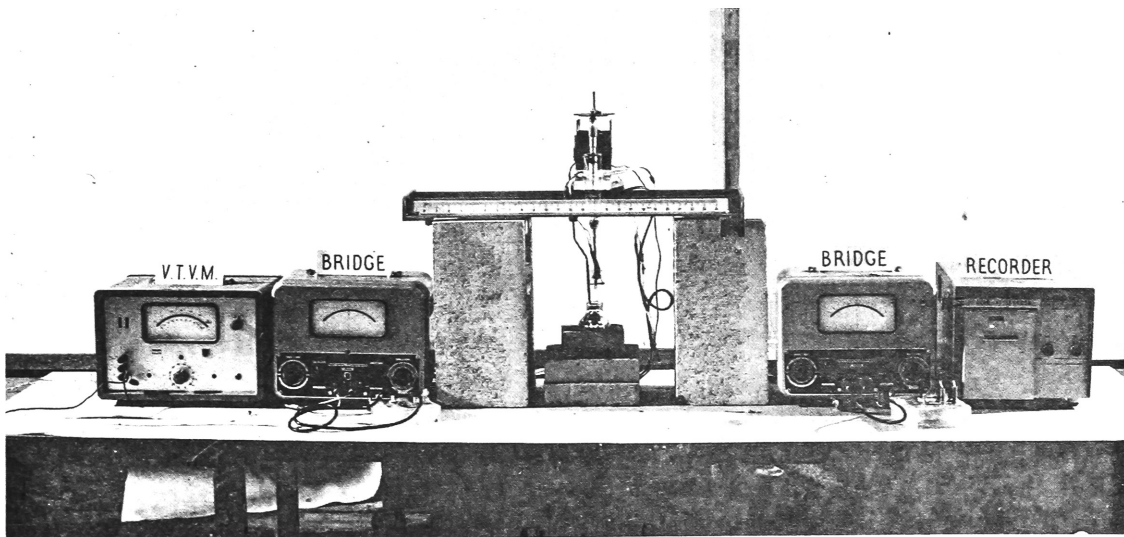
For the test involving changing fluid temperatures, the variation in temperature was obtained by heating a quantity of the fluid in a 250ml. beaker and then allowing the fluid to cool by placing the beaker in a 500ml. beaker which was partially filled with ice water. Coincidental measurements of temperature and recorded amplitude were taken at various times as the fluid cooled.

The changes in recorded wave heights caused by a conducting structure were investigated in the large glass bottom wave tank. The dimensions of the glass bottom were assumed to be large enough to prevent any effects on the probe caused by conducting parts of the tank. A 1 inch thick steel disc with a diameter of 18 inches was placed in the centre of the tank. Measurements of recorded wave heights were taken at intervals across a diameter.

To examine the effect of the miniscus on the form and phase of the wave a second identical bridge was used in conjunction with the linear transducer. Two simultaneous tracers were obtained on the recorder and compared.

Discussion of Results

(1)   Change in Recorded Wave Height as a Function of the Actual Wave Height:

For the range of wave heights tested these results (Figure (A8:1)), Figure (A8:2)) show that a 1 near relation exists between the output

from the recorder and the actual motion of the probe wires. Thus the experimental wave heights can be easily deduced by knowing the recorded and the actual wave heights of the standard, provided the periods of the experimental waves and standard are the same. (Equation (A8-1)).

(2)   Change in Recorded Wave Height as a Function of
       the Period of Oscillation:

These results are plotted in Figure (A8:3) and Figure (A8:4) for heights of .0022 inches and .0058 inches respectively with periods ranging from about .4 seconds to 1.8 seconds. Similar results to those in Figure (A8:3) were obtained for a height of .0014 inches and to those in Figure (A8:4) for a height of .0116 inches. It was found that there was a resonance type of curve produced from both the transducer and probe outputs. This resonance was felt to be caused by the output circuit of the bridge. The maximum recorded wave height on the curves was at about .62 seconds for the transducer output in comparison with a maximum from the probe output of about .70 seconds for the two smaller and about .62 seconds for the two larger wave heights tested. The difference between the recorded wave heights from the transducer and probe at any one period was at most 3%. Most of these errors were attributed to errors in graphical measurements from the wave record, although there generally appears to be a slightly larger attenuation of the probe output for the higher frequencies. This is probably due to the greater effect of the meniscus for rapid motions of the probe
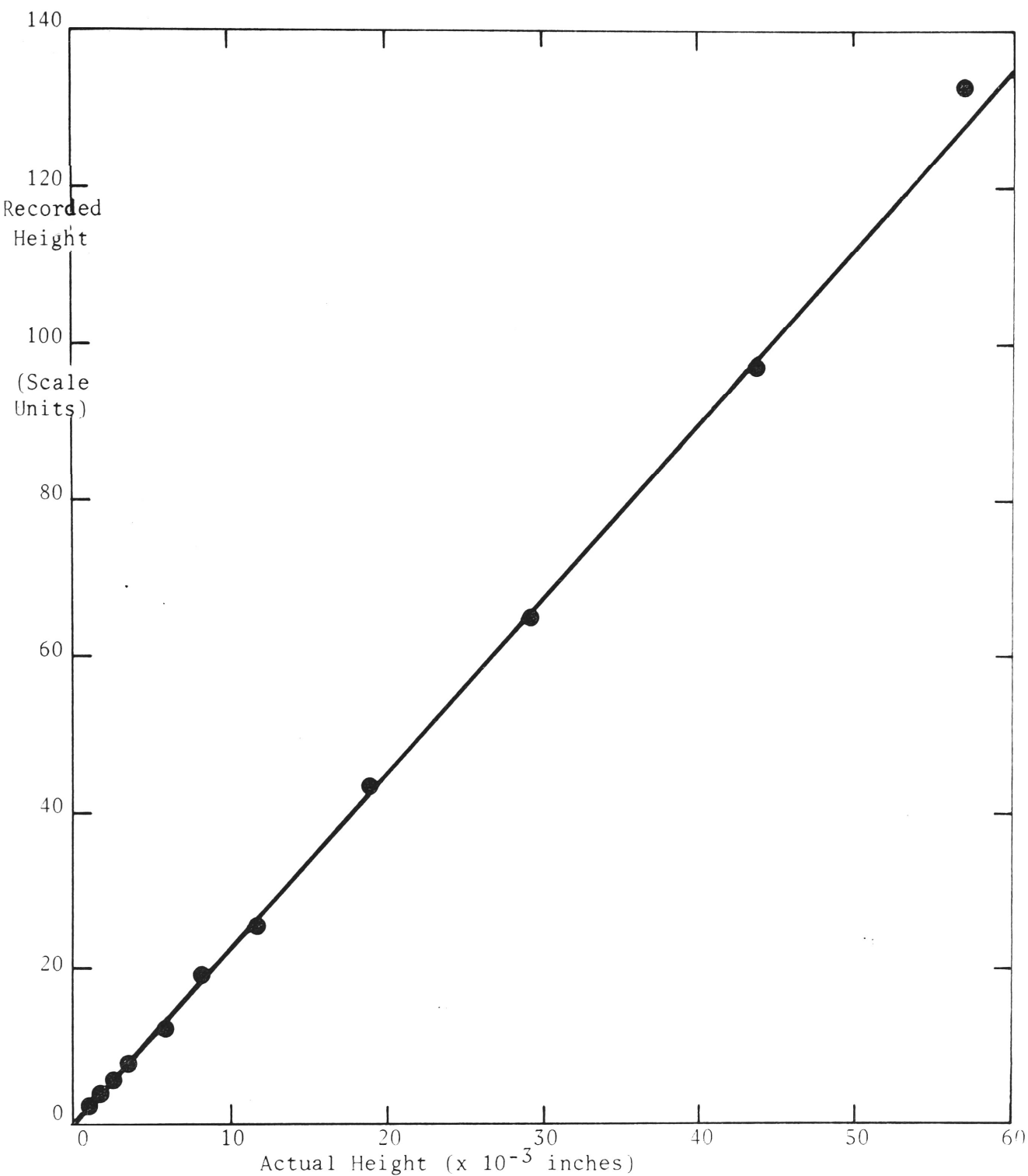
FIGURE A8:1 RECORDED HEIGHT AS A FUNCTION OF THE ACTUAL HEIGHT FOR THE "PHILLIPS" BRIDGE.
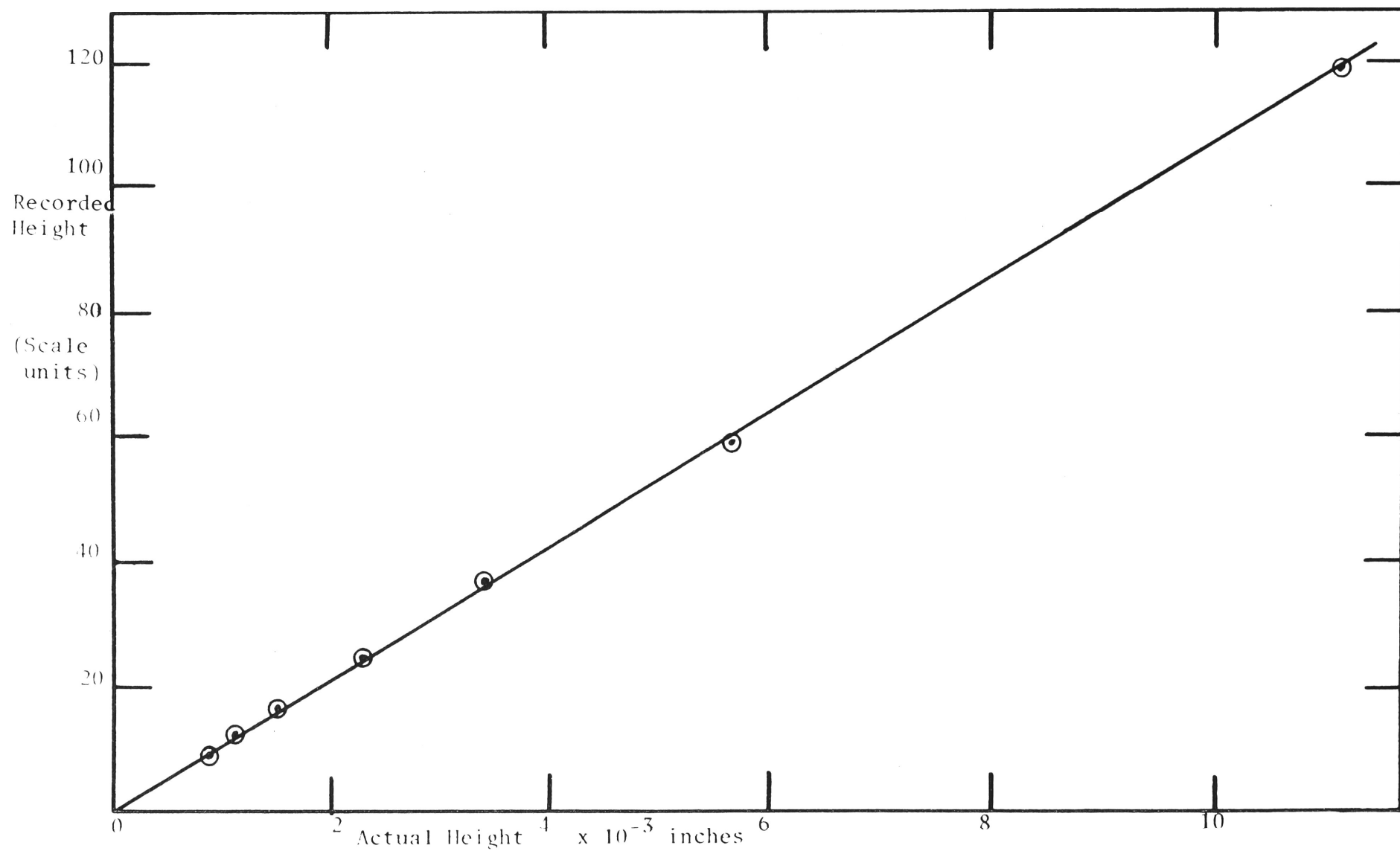
FIGURE A8:2 RECORDED HEIGHT AS A FUNCTION OF THE ACTUAL HEIGHT USING THE "AUTOMATION SPERRY" BRIDGE.
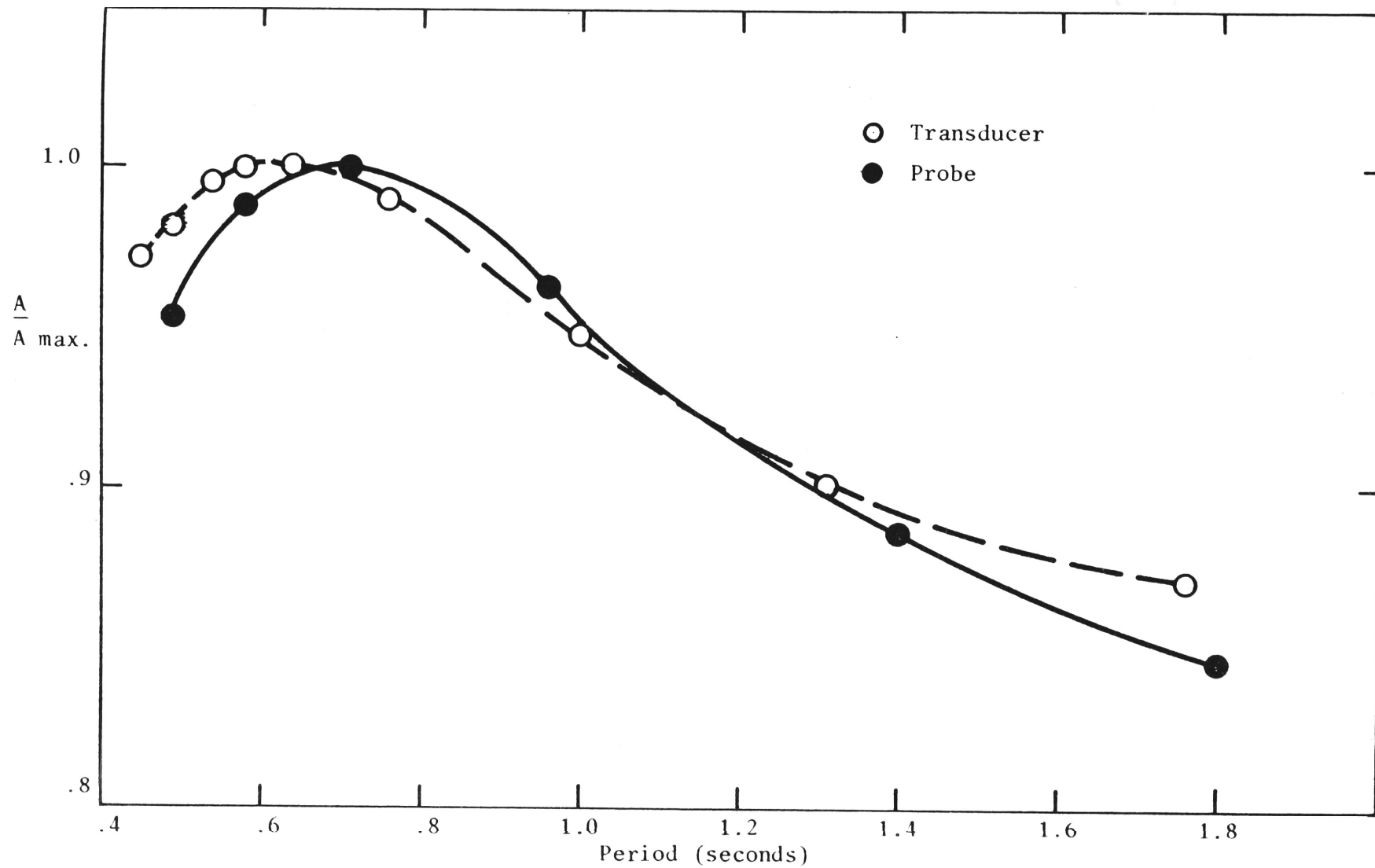
FIGURE A8:3 RELATIVE RECORDED HEIGHT AS A FUNCTION OF THE WAVE PERIOD
(H = .0022 INCHES)
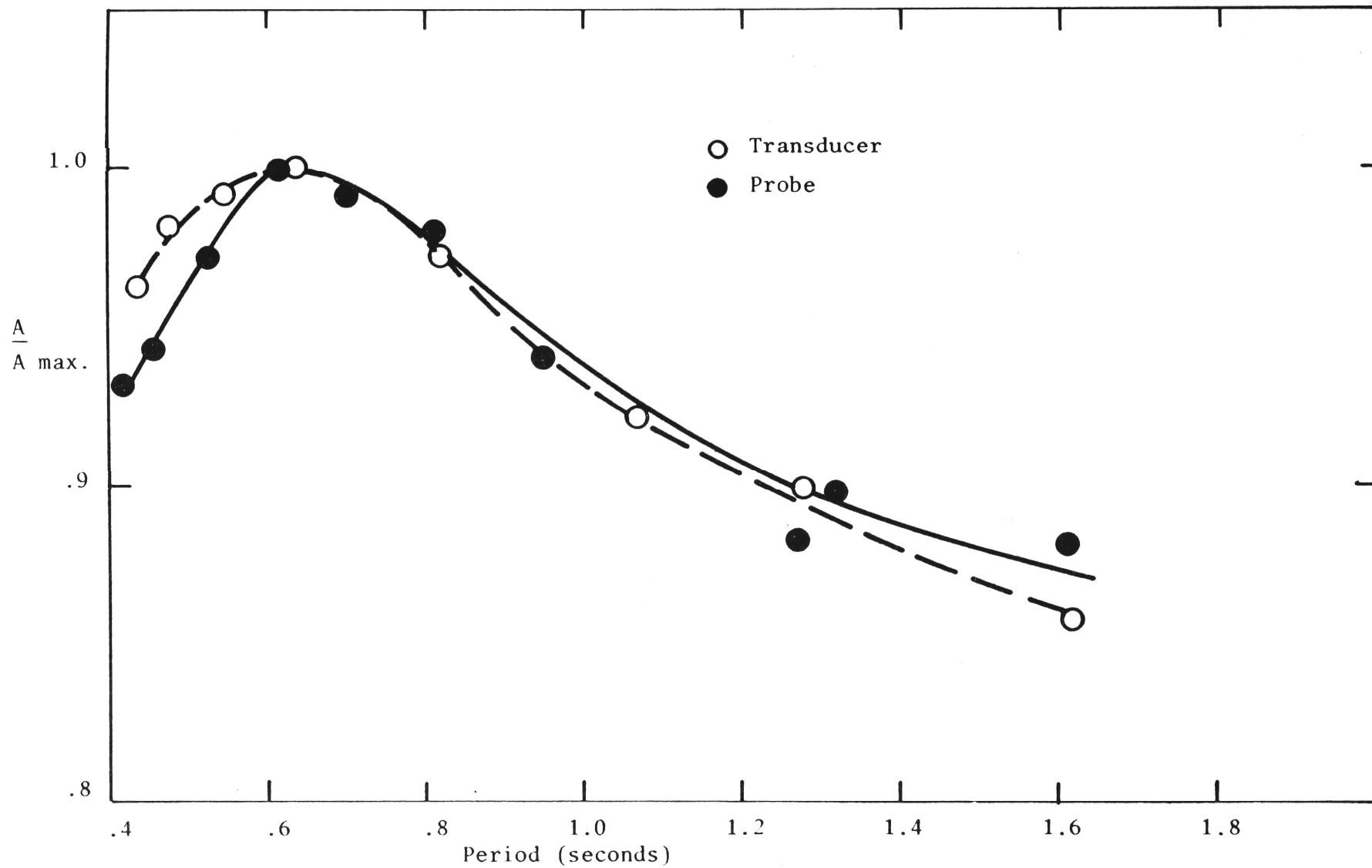
FIGURE A8:4   RELATIVE RECORDED HEIGHT AS A FUNCTION OF THE WAVE PERIOD
(H = .0058 INCHES)

wires.

Because of this change in recorded wave height with period it is necessary to either ensure that the standard and experimental waves have the same period or to correct one of the recorded wave heights by use of calibration curves such as Figure (A8:3) or Figure (A8:4) so that they are compatible with the other record.

(3) The Change in Recorded Wave Height as a Function
of the Fluid Temperature:

In the range of temperatures tested there was a linear relation between the recorded wave height and the fluid temperature (Figure (A8:5)). It is worth noting that a small change in temperature, say 2 degrees C. or 3 degrees C, which could easily arise in a laboratory experiment, gives (at 15 degrees C.) a change in recorded wave height of around 12% to 17%. Thus it is clear that it is necessary to compensate for changing fluid temperature if an acceptable degree of accuracy in wave height measurements is to be obtained. A method for temperature compensation other than the one described in this paper is presented by "Hydro Delft" (1968).

(4) Change in Recorded Wave Height as a Function
of the Depth of Probe Immersion:

Figure (A8:6) shows that when the mean position of the end of the probe wires is below the free surface a linear relation is obtained between the measured wave height and the depth of immersion. The portion of the abscissa in Figure (A8:6) that is negative corresponds

to the probe wires being above the free surface, but maintaining contact with the fluid through the meniscus. The linear relation was found to be no longer valid in this region. In a large wave tank it would be difficult to adjust and maintain the track for the probe carriage to much better than ± .01 inches from a mean position. This irregularity would result in a difference in the measured wave height of about 7% for waves of .0063 inches in height. It would be possible, of course, to maintain a constant depth of immersion for all points in the tank by adjustment of the micrometer. This process is somewhat tedious if a large number of experimental points are to be used and, in fact, is unnecessary since changes in recorded wave height caused by changes in probe wire immersion are automatically compensated for by the calibration of the probe at each experimental position.

(5)   Change in Recorded Wave Height as a Function of the Proximity of the Probe Wires to a Conducting Submerged Structure:

The presence of a submerged conductor had the effect of increasing the measured wave height by about 11% and 6.5% for water depths of .33 inches and 1.00 inches respectively. (Figure (A8:7)). These increases were essentially the same for the two wave heights of .0063 inches and .0122 inches that were used. This would imply that the changing proximity of the probe wires to the conductor caused by the vertical motion of the probe wires did not produce the increase in measured wave height. An explanation for this increase is that, since one of the probe wires is on a common earth with the fluid, it is probable that
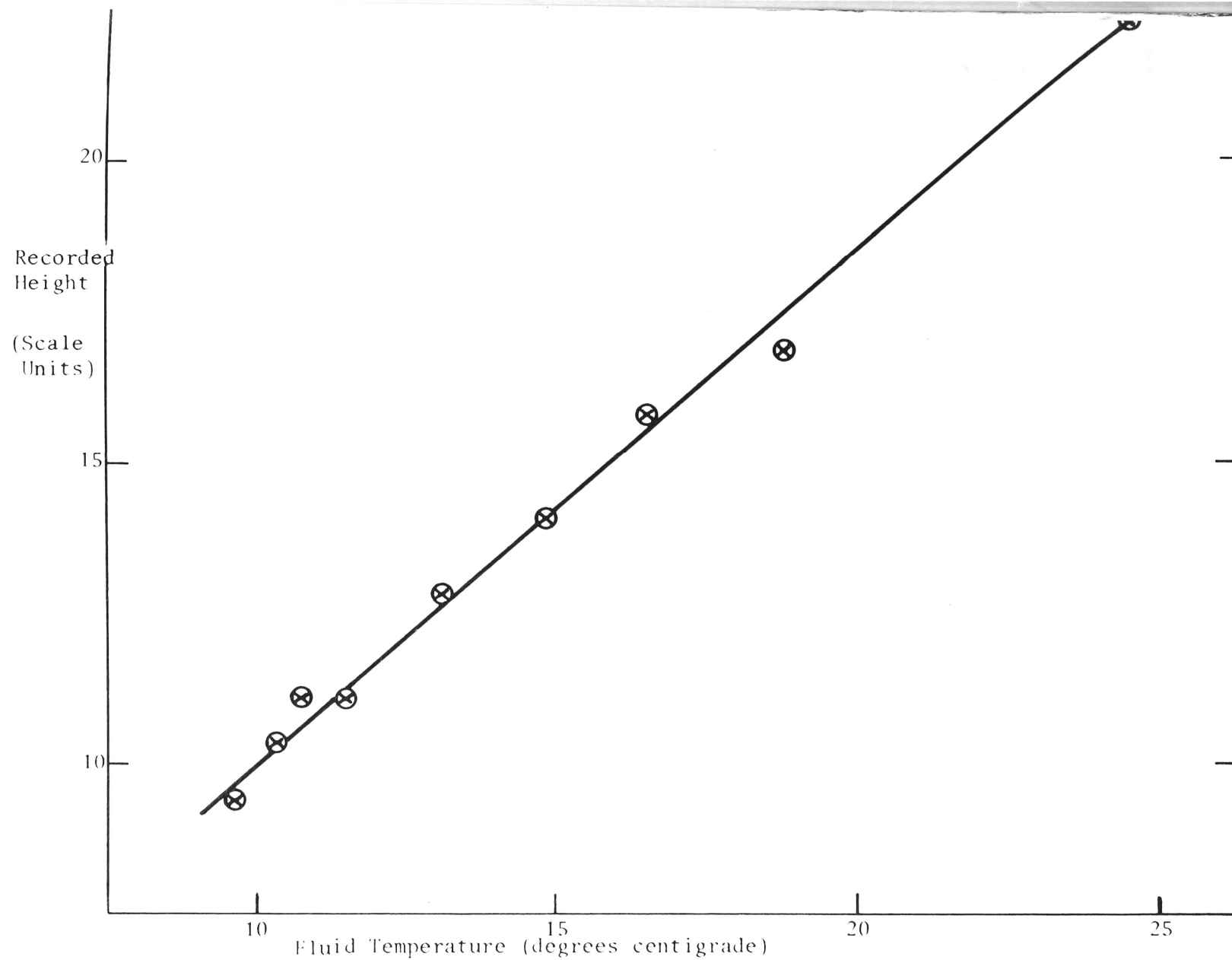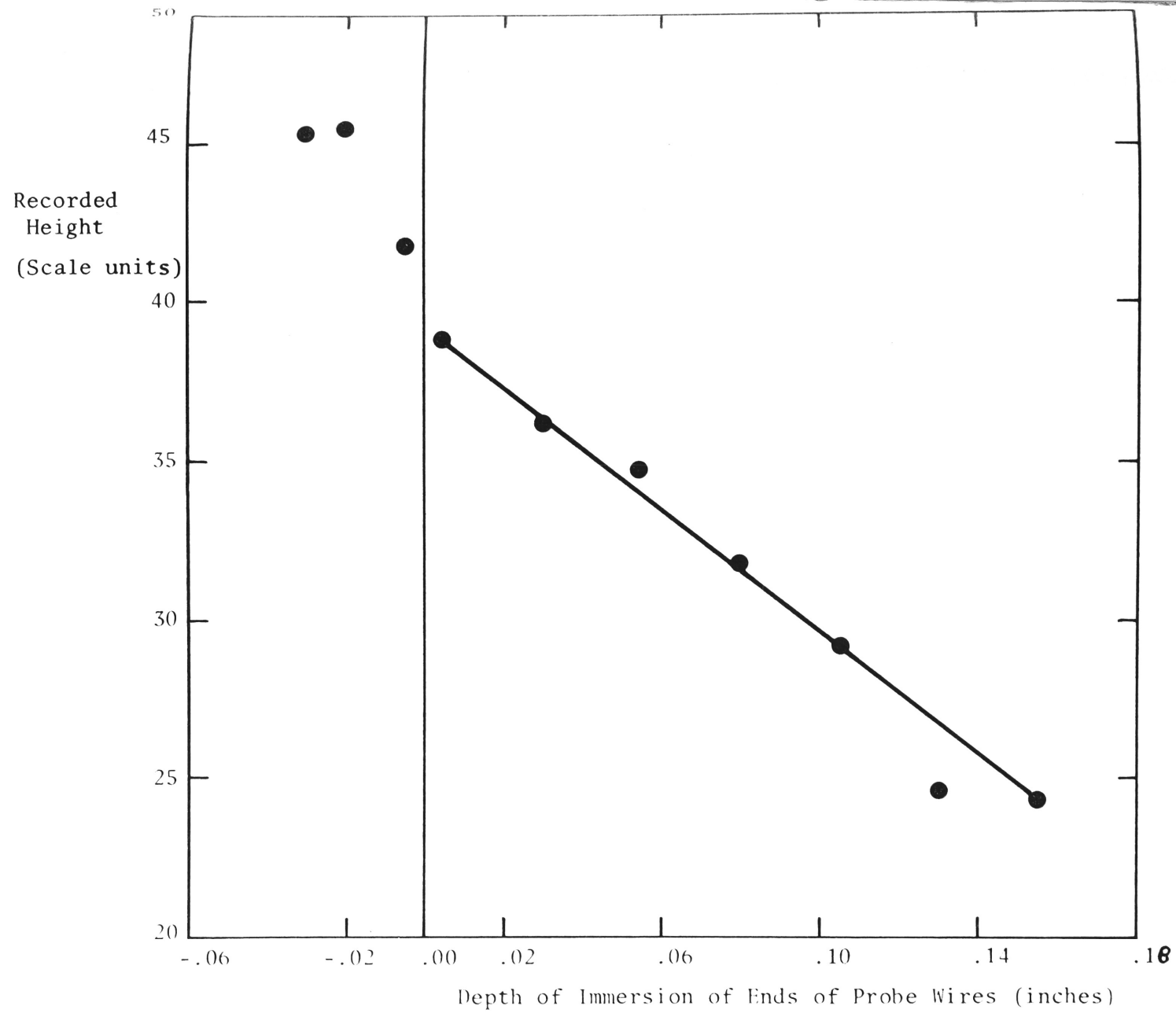
FIGURE A8:6   RECORDED HEIGHT AS A FUNCTION OF THE PROBE WIRE IMMERSION.
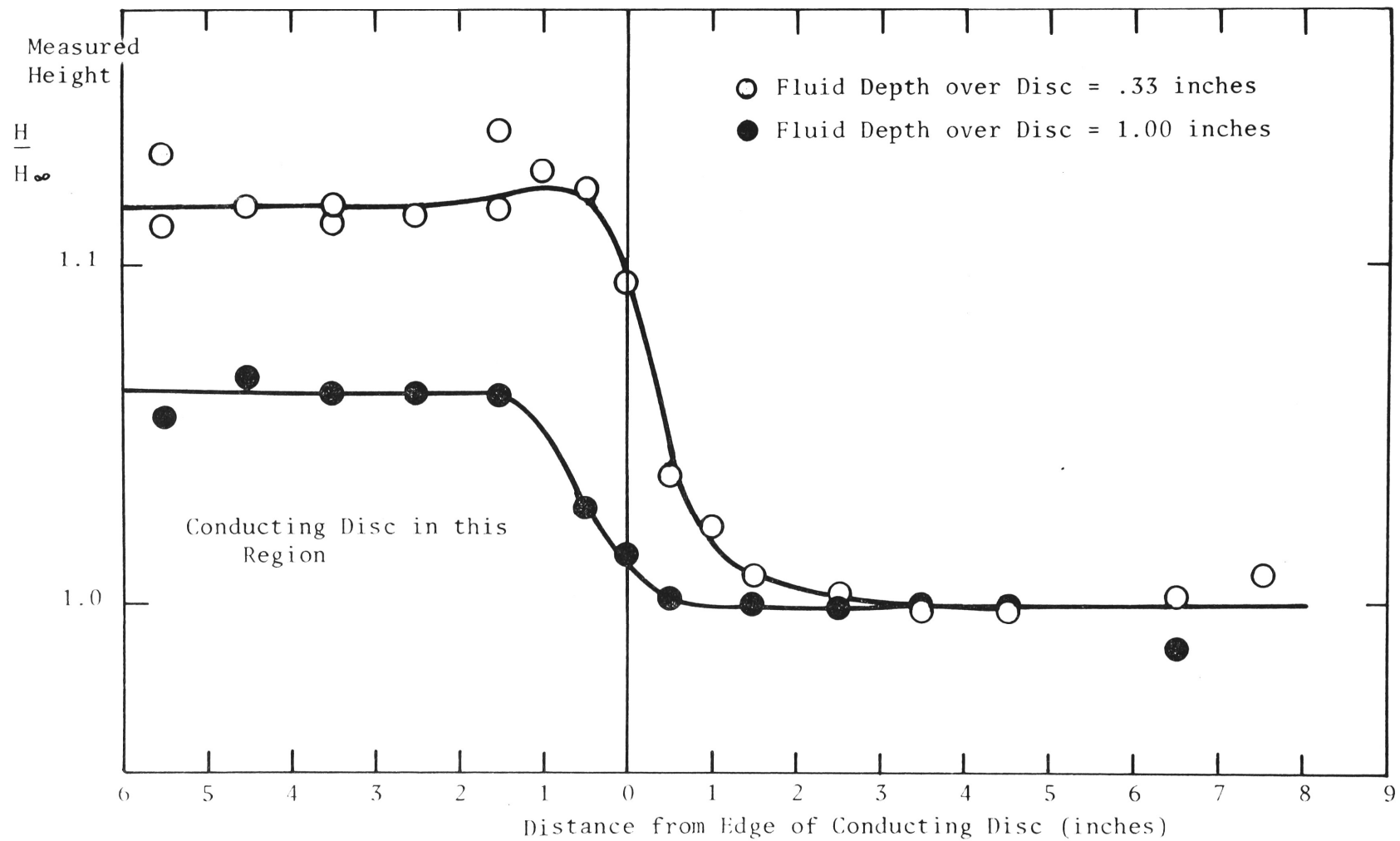
FIGURE A8:7   RELATIVE RECORDED HEIGHT AS A FUNCTION OF THE DISTANCE
FROM THE EDGE OF A SUBMERGED CONDUCTING DISC.

the conducting bottom in conjunction with the active probe wire acts as a single wire wave probe of the type discussed by Wiegel (1955). Thus, in effect, this system may be considered as being two probes coupled together that simultaneously measure the change in the probe wire immersion.

(6)   Difference in Phase and Wave Form between the
      Actual and Recorded Motion of the Probe:

The phase of the recorded motion was found to lag that of the actual motion. This lag was greatest for the higher frequencies tested (Figure (A8:8)) and was found to be about 7 milliseconds behind the actual motion for a period of .4 seconds and a wave height of .0063 inches. The lag was also found to increase as the amplitude of motion was increased (Figure (A8:9)).

A typical example of the output from the probe is shown in Figure (A8:10) by the solid curve. The dotted curve is the trace from the linear transducer which has been redrawn for comparison such that its height coincides with that from the probe. The phase difference was taken as the mean of that found for a rising and for a falling water surface, the measurements being taken midway between crest and trough.

These tests show that is is necessary to calibrate the probe at all experimental positions (or times) to compensate for extraneous changes in the still water resistance as seen by the probe. The effect of the miniscus appears small although there is evidence of a small

attenuation (approximately 3%) at the higher frequencies tested. The

wave form was found to be reproduced almost exactly by the probe except

for a small time lag between the actual and measured motion. Since

the bridge used in these tests had a resonant condition in its output

circuit it was necessary either to ensure that the period of the

waves and of the calibrator were the same or to correct for different

periods using calibration curves as in Figures (A8:3) and (A8:4). The

linearity of the plot connecting the recorded wave heights and the

actual wave heights (for a fixed period) enable a very simple means

of calibrating the probe at each experimental point. Experience has

shown that wave heights of .002 inches or less may be measured with a

repeatability of within 5%. Larger wave heights had in general a

greater degree of repeatability.
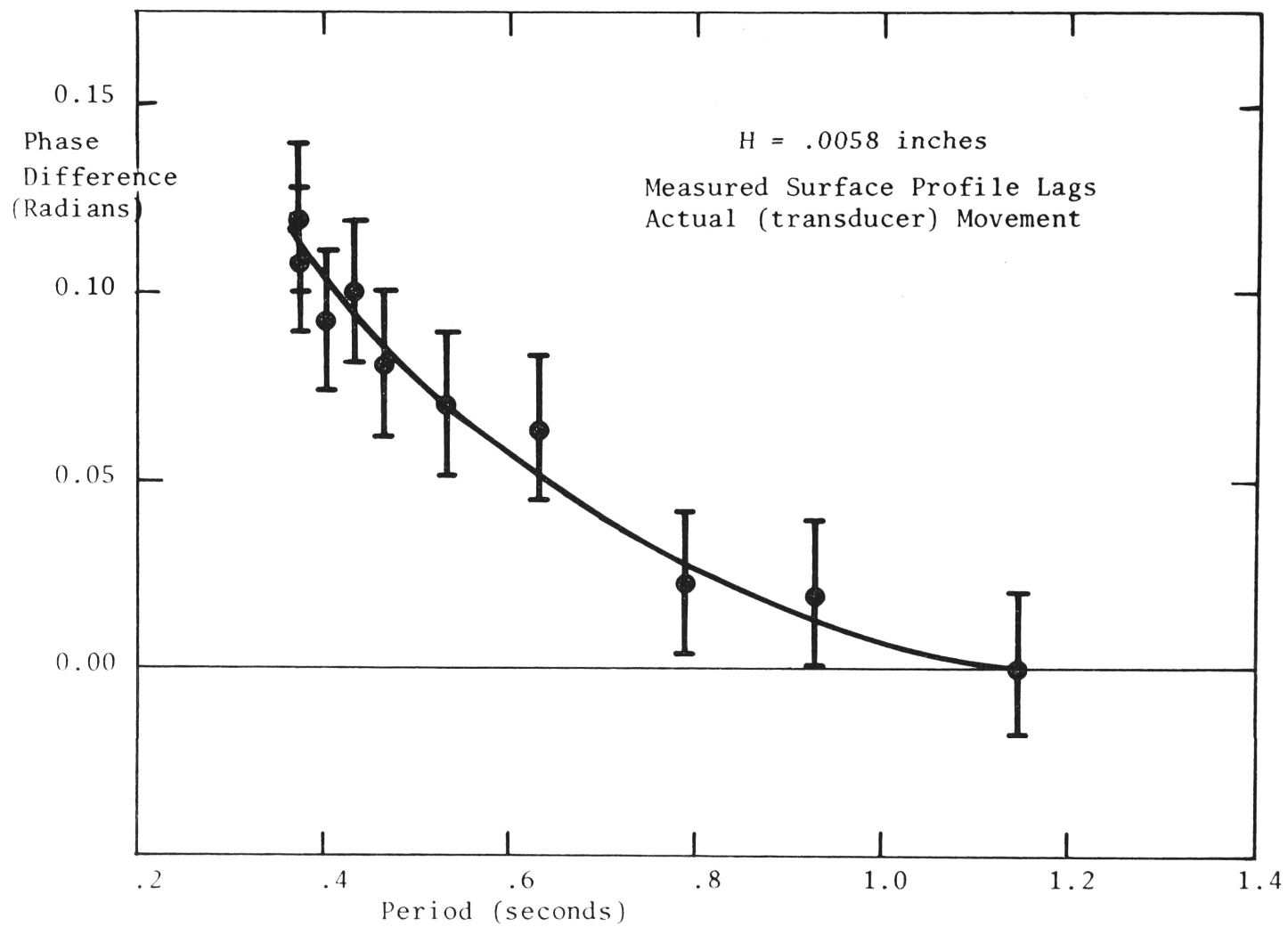
FIGURE A8:8   PHASE LAG AS A FUNCTION OF THE WAVE PERIOD.

0.15

Phase
Difference

(Radians)

0.10

0.05

0.00

T = .9 seconds

Measured Surface Profile
Lags Actual (transducer) Movement

0   1   2   3   4   5   6

Height (x10^{-2} inches)
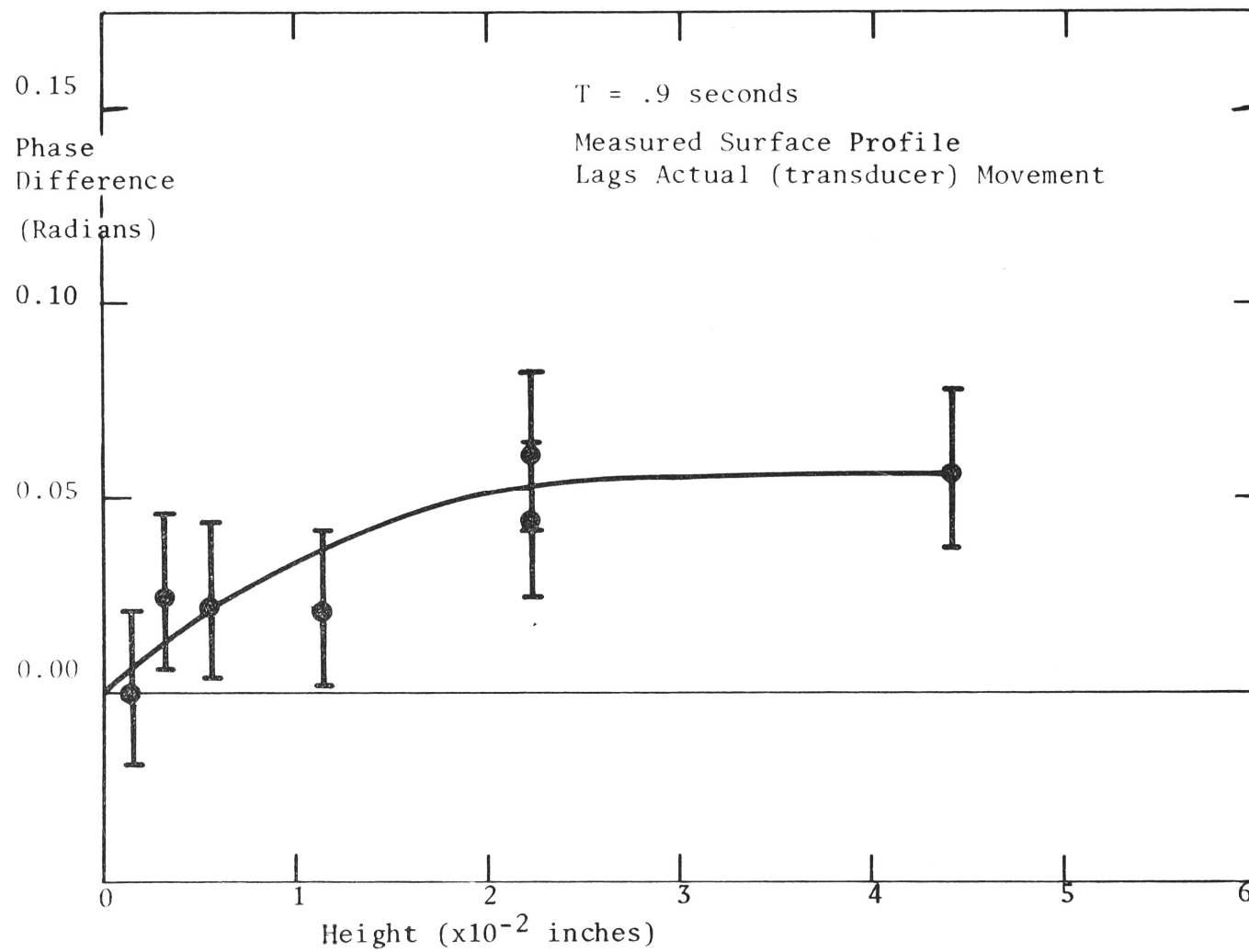
FIGURE A8:9.   PHASE LAG AS A FUNCTION OF THE WAVE HEIGHT.

T = .65 seconds

H = .0058 inches

– – –Transducer

———Probe
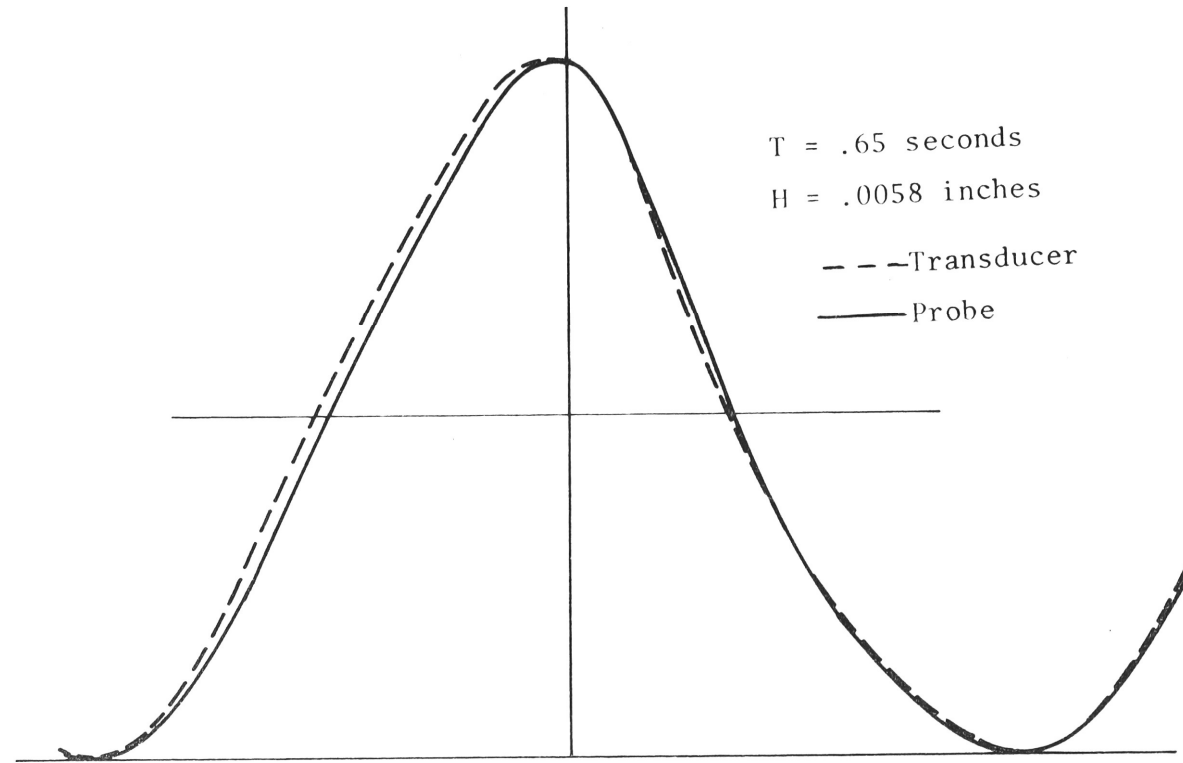
FIGURE A8:10. COMPARISON OF THE WAVE FORM FROM THE TRANSDUCER AND THE SURFACE MEASUREMENTS.

Appendix 9 - The Fluid Particle Follower

Introduction

A fluid particle follower was designed to determine the time at which a horizontally oscillating fluid particle passed through its equilibrium position. For the experiments undertaken the requirements for the device were to have:

1) as little interference with the fluid flow as possible.

2) an accurate means of determining the time when the particle passed through its equilibrium position.

3) a relatively simple construction and method of use.

These requirements were fulfilled by using a small rectangular paddle which moved with the fluid particles in conjunction with a fixed conductor. The paddle was suspended from a relatively long thin wire such that the system could be considered a physical pendulum executing small motions. The finite area of the paddle thus made it necessary to consider the average particle motion over this area and not that at a point. This introduced little complication in the experiments since long period waves were used in relatively shallow water. As the paddle moved away or towards the conductor, the electrical resistance between them increased or decreased. The change

in resistance was detected with a bridge and recorded in a similar

manner as described in Appendix 8 for the wave probe. Due to the weight

of the pendulum it was not expected that its motion would correspond

exactly to the fluid motion.

A theoretical relationship between the pendulum motion and the

fluid motion was derived and the constants in the equation of motion

were found experimentally. An experiment was also run to find the

recorded displacement as a function of the actual displacement.

Derivation of the Equation of Motion:

The problem under consideration will be the motion of a physical

pendulum in a viscous fluid that is oscillating harmonically with time.

The equation of the pendulum motion in the absence of all but buoyant

effects of the fluid was derived under the assumption that the paddle

at the end of the pendulum could be considered as a point mass so

that its moment of inertia about the point of suspension was:

$$I_p = m_p L^2$$

where m_p is the mass of the paddle

and L is the length of the suspension taken to be the distance

from the centre of mass of the paddle to the suspension point. It was

also assumed that the paddle and suspension rotated about the point of

suspension such that at any time the angle between the vertical and

all points on the pendulum were constant. In all strictness the

suspension should be considered as a cantilever which would give

different angular deflections along its length. But, since the

motions were small ($\simeq .1$ inch) compared with the length of the suspension

($\simeq$ 4.5 inches) and the weight of the paddl was about ten times

that of the suspension, it was considered that this assumption was

justified. The moment of inertia of the suspension wire was then

taken to be:

$$I_s = \frac{m_s}{3} L^2$$

where m_s is the mass of the suspension.

The centre of gravity is:

$$\ell_g = \frac{L}{2(W_s + W_p^*)} (W_s + 2 W_p^*)$$

where W_p^* is the weight of the pendulum in the fluid and the

suspension is taken to be completely outisde the fluid. The acceler-

ation of the pendulum in the absence of all but bouyancy effects of the

fluid is:

$$\ddot{x} = - \frac{(W_s + W_p^*)}{(I_s + I_p)} \ell_g x$$

for small displacements.

Where x and $\ddot{x}$ refer to the horizontal distance and acceleration of

the centre of oscillation, $\ell_c = \dfrac{I_s + I_p}{(m_s + m_g)} \ell_g$, from the

vertical. That is, the total mass $m = m_g + m_p$ is considered to be

concentrated at a point a distance ℓ_c from the point of suspension.

If the rather large value for $m_s = \cdot 2\, m_p$ is taken and

$W_p^* = \cdot 9\, m_p g = \cdot 9 W_p$ the value for ℓ_c becomes: $\ell_c = \cdot 98 L$

Thus, with only a small error, ℓ_c can be considered the length "L" of the pendulum.

The acceleration due to gravity is then approximately:

$$\ddot{x} \simeq -\frac{3}{2}\, \frac{g(W_s + 2 W_p^*)}{L\,(W_s + 3 W_p)}\, x$$

and the gravity force is:

$$F_g = m\ddot{x} = \frac{3}{2}\, \frac{(W_s + W_p)(W_s + 2 W_p^*)}{L\,(W_s + 3 W_p)}\, x \quad (A9\text{-}1A)$$

or

$$F_g = -K_g\, x \qquad\qquad (A9\text{-}1B)$$

Taking into account the viscous force on the paddle is probably most easily visualized by considering the system of coupled oscillators as shown in Figure (A9:1).

In this analogy, a flat plate moves horizontally in oscillatory motion (corresponding to the fluid). Resting on the plate is a mass m which corresponds to the pendulum, the plate and the mass are coupled through the friction between them. The influence of the mass on the oscillations of the plate are considered to be negligible, corresponding to the condition that the fluid flow is unaltered by the

Displacement $\rightarrow$ x $\leftarrow$

Mass "m"

Spring

Rigid connectors

$\frac{A\sigma}{kh} \cos \sigma t$

Oscillating plate

Fixed Wall

$x = 0$ (Equilibrium position)
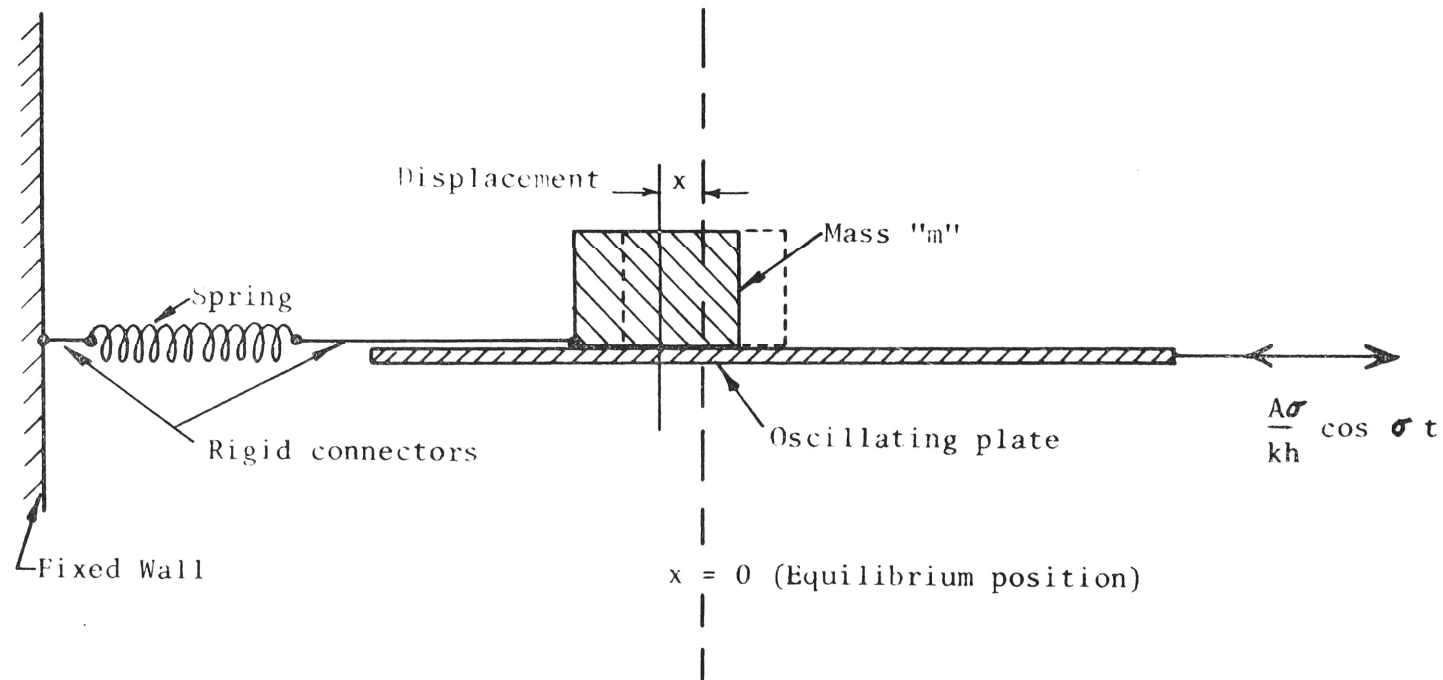
FIGURE A9:1   SCHEMATIC DIAGRAM OF FRICTIONALLY COUPLED OSCILLATORS

presence of the pendulum. This friction force is taken to be pro-
portional to some power of the relative velocity between the plate
and the mass, it corresponds to the viscous force of the fluid on
the pendulum; that is:

$$F_v = K_v V^{X_v} \qquad\qquad \text{(A9-2)}$$

where K_v is the constant of proportionality.

One end of a massless compression and tension spring is connected
to a fixed wall and the other to the mass, the spring constant is defin-
ed to be K_g to correspond to the restoring force due to gravity.
The forces on the mass are:

F = spring force + friction force

or

$$F = K_g \, x + K_v \left| f(t,x) - \frac{dx}{dt} \right|^{X_v} sgn \left(f - \frac{dx}{dt} \right)$$

where K_v and X_v are to be determined experimentally.

$$sgn(G) = \begin{cases} -1 \; ; & G < 0 \\ 0 \; ; & G = 0 \\ 1 \; ; & G > 0 \end{cases}$$

and

$$f(t, x) = \frac{A}{kh} \cos(kx - \sigma t)$$

is the fluid velocity.

The inviscid form of the fluid velocity has been used since the
wave number k is altered only slightly by friction in the model and

the frictional phase shift (Equation (3-6A)) has been eliminated by a translation of the axes. Taking the equilibrium position as $x_{eq} = 0$ and assuming that the particle velocity is very nearly constant at any time in $x_1 \leq 0$ and in $x_2 \geq c$ where $x_1 \leq x \leq x_2$; $f(t,x)$ can be expressed as:

$$f(t) = \frac{A}{kh} \cos \sigma t$$

The equation of motion is then:

$$\frac{d^2x}{dt^2} = \frac{3}{2} \frac{g}{L} \frac{(W_s + 2W_p^*)}{W_x + 3W_p} x + \frac{gK_v}{W_s + W_p} \left\{ \frac{A}{kh} \cos \sigma t - \frac{dx}{dt} \right\}^{X_v} \text{SGN} \left\{ \frac{A}{kh} \cos \sigma t \frac{dx}{dt} \right\}$$

$$(A9-3)$$

or

$$\frac{d^2x}{dt^2} = ax + b \left(c \cos \sigma t - \frac{dx}{dt} \right)^{X_v} \text{sgn} \left(c \cos \sigma t \frac{dx}{dt} \right)$$

Case 1.

If $X_v = 1$, then (A9-3A) becomes the linear nonhomogeneous differential equation:

$$\frac{d^2x}{dt^2} + b \frac{dx}{dt} + ax = bc \cos t \qquad (A9-4)$$

which is easily solved using the method of undetermined coefficients.

A solution is:

$$x = A_1 e^{r_1 t} + A_2 e^{r_2 t} + \sqrt{\frac{bc}{(a-\sigma^2+(b\sigma)^2}} \; \text{SIN} \, (\sigma t + \phi) \qquad \text{(A9-5A)}$$

where

$$r_1 = \frac{1}{2} \left(-b + \sqrt{b^2 - 4a}\right)$$

$$r_2 = \frac{1}{2} \left(-b - \sqrt{b^2 - 4a}\right)$$

$$\phi = \text{TAN}^{-1} \left(\frac{a - \sigma^2}{b}\right)$$

and A_1, and A_2 are constants of integration.

The terms involving the exponential functions always have the real part of their exponents being negative and hence tend to zero for t sufficiently large. In the case $t \to \infty$:

$$x = \frac{bc}{\sqrt{(a-\sigma^2) + (b\sigma)^2}} \; \text{SIN} \, (\sigma t + \phi) \qquad \text{(A9-5B)}$$

or

$$x = \frac{c}{\sigma} \frac{1}{\sqrt{\left(\frac{a}{\sigma^2} - 1\right)^2 + b^2}} \; \text{SIN} \, (\sigma t + \phi) .$$

if the motion of the mass followed that of the plate exactly then its position would be:

$$x_o = \frac{c}{\sigma} \; \text{SIN} \, \sigma t$$

Thus the presence of the frictional coupling is to introduce a reduction in amplitude of the motion of the mass compared with the motion of the

plate and to introduce a phase difference between them. If

$$\frac{3}{2} \frac{g}{L} \frac{(W_s + 2W_p^*)}{(W_s + 3W_p)} > \sigma^2$$, then the position of the mass precedes

that of the plate.

Case 2.

If $X_v \neq 1$, then a non-linear, non-homogeneous equation results

that must be solved using numerical techniques:

Equation (9-3A) can be written as:

$$\frac{d^2x}{dt^2} = a\,x + b\left(c\,\cos\sigma t - \frac{dx}{dt}\right)\left|c\,\cos\sigma t - \frac{dx}{dt}\right|^{X_v - 1} \qquad (A9\text{-}6)$$

Experimental Equipment:

The pendulum was made from a piece of .0015 inch steel shim cut

in the form of a 1.25 inch long by .10 inch wide rectangle. Electrical

connection was made to the pendulum by means of a .0035 inch diameter

enamelled copper wire formed into a yoke and lightly soldered to each

end of the pendulum. This wire also served as the pendulum suspension

and had a length of 4½ inches which was considered to be sufficiently

great so that, for the small motions involved, the vertical component

of the pendulum's motion was negligible. The weight of the pendulum

and suspension was about 1.46 x 10^{-4} pounds. The stationary conductor

was a 4½ inch length of 1/32 inch diameter stainless steel wire which

was insulated along its length except for a 1/20 inch portion at its lower end. The insulation was necessary to prevent extraneous resistance changes between the wire and the pendulum caused by the rising and falling water surface of a passing wave. The fixed end of both wires was held in a horizontally movable perspex block through which connections were made to a strain gauge bridge. Vertical positioning was obtained by connecting the unit to the shaft of a micrometer gauge of the same construction as that which held the sensor for the wave probe. The particle follower is shown in Figure (A9:2).

Due to the lightness of the suspension, it was difficult to obtain, from run to run, a constant still-fluid separation of the pendulum and fixed conductor. This prevented the measurement of absolute amplitudes of the particle motion.

Experimental Procedure

For the tests on the particle follower a motionless fluid was used and the pendulum motion was achieved by pulling the pendulum a known distance from its equilibrium position and allowing it to return under the influence of gravity. A thin piece of wire bent into a right angle and connected to a movable vernier scale was hooked around the lower part of the pendulum suspension. The wire was drawn slowly back by use of the vernier adjustment and released from the suspension by gently sliding the wire off the suspension. The changing resistance between the moving pendulum and the fixed conductor was recorded as a function of time as the pendulum returned to its equilibrium position.

A calibration curve for the actual displacement of the pendulum from its equilibrium position as a function of the recorded displacement was obtained by pulling the pendulum away from its equilibrium position a known amount, allowing any small oscillations to damp out, and then recording the change in the bridge balance. These results are shown in Figure (A9:3) and for the displacements used there is a linear relation between the actual and recorded displacement. The equilibrium position was about .2 inches from the fixed probe wire; trials using different equilibrium positions yielded similar results to the above.

Using graphical differentiation (Hall, (1958)) the velocity and acceleration were deduced as a function of the distance of the pendulum from its equilibrium position. The displacement, the velocity and the acceleration of the pendulum are shown in Figures (A9:4), (A9:5) and (A9:6) respectively. From Figure (A9:4) it can be seen that the pendulum is over-damped by the viscous glycerol mixture and there is no "over-shoot" past its equilibrium position. A trial using tap water showed a highly damped motion of the pendulum about its equilibrium position with the observable motion ceasing after having crossed the equilibrium position one or two times.

To calculate the viscous force on the pendulum the restoring forces due to the bending of the suspension and to gravity were calculated, then, knowing the acceleration of the pendulum, the viscous force was deduced.

To micrometer
spindle

Set screws and electrical
connections

Hypodermic tube
holding suspension
wire

Sliding perspex block

Horizontal
adjustment screw

Suspension wire

Insulated
fixed wire

Paddle

Uninsulated tip
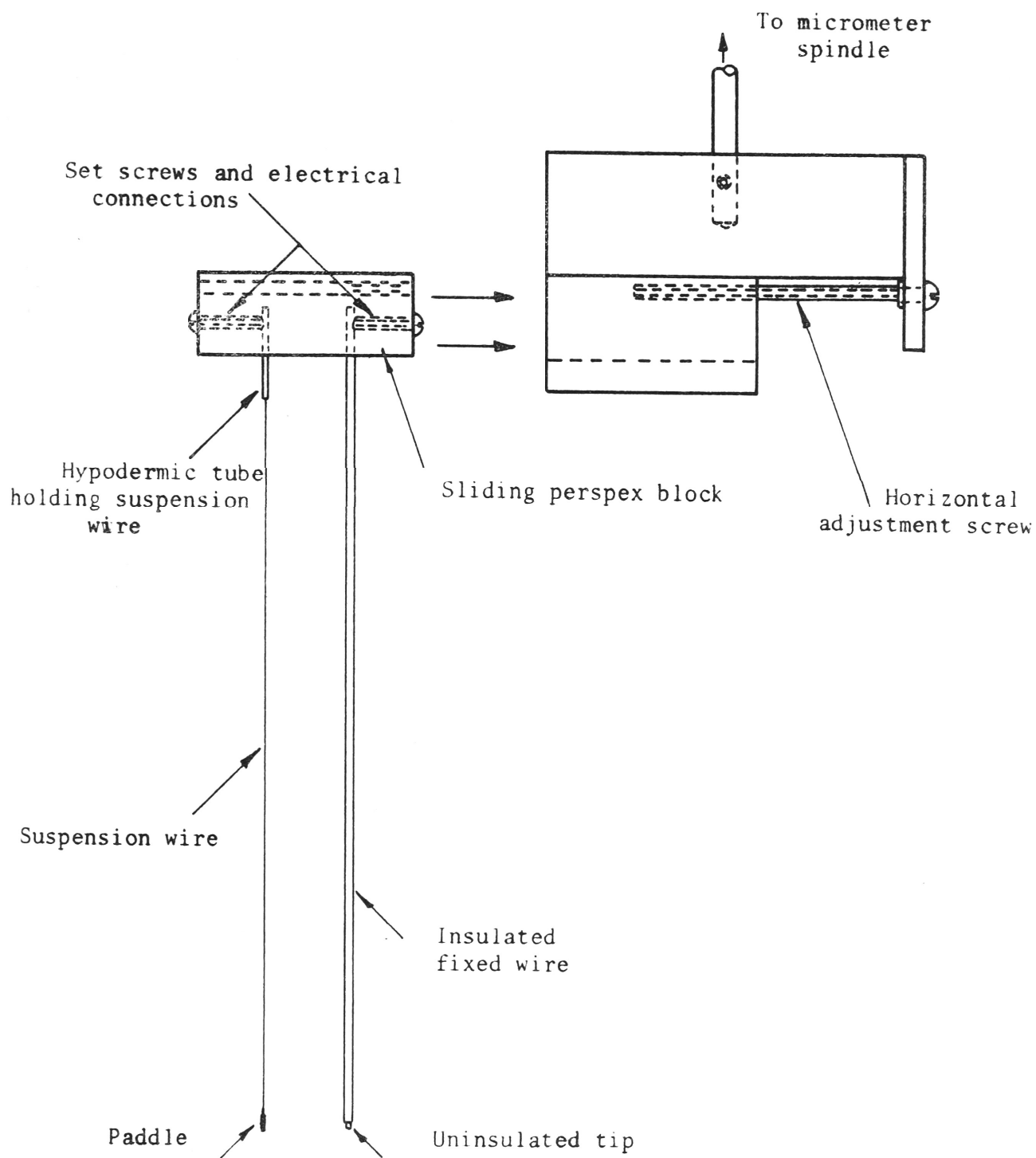
FIGURE A9:2.   THE FLUID PARTICLE FOLLOWER
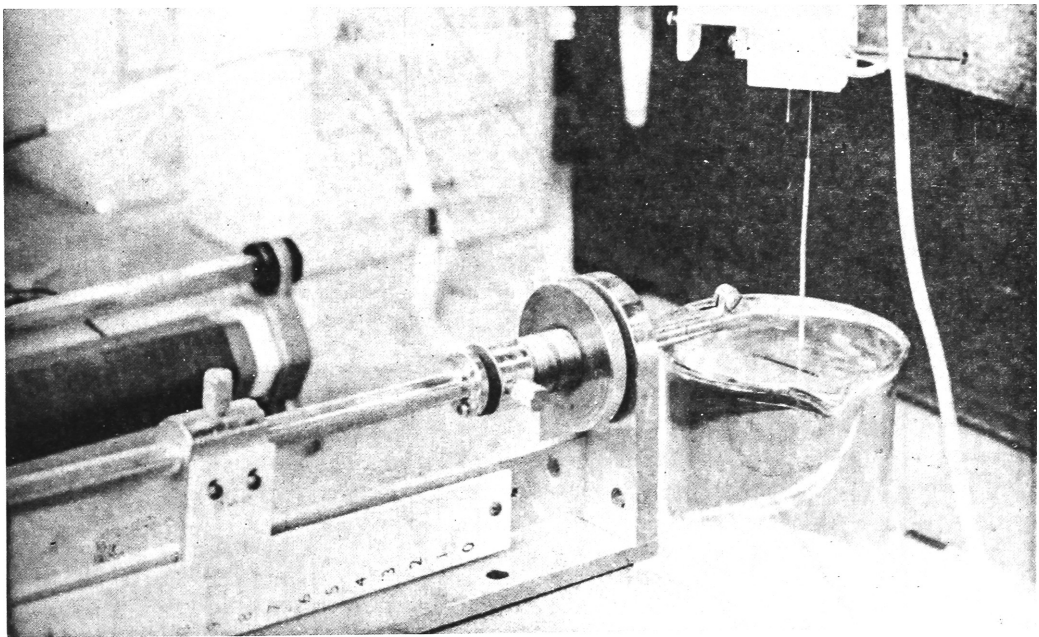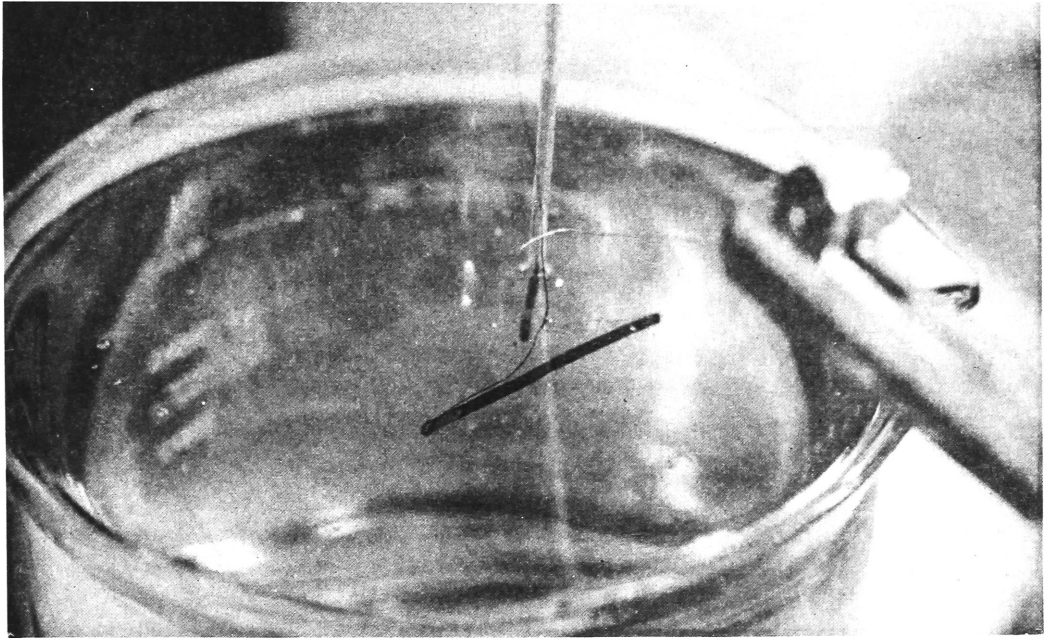
PHOTOGRAPHS A9:1   The Pendulum and the "Draw-Back"
Hook connected to a Vernier Scale.
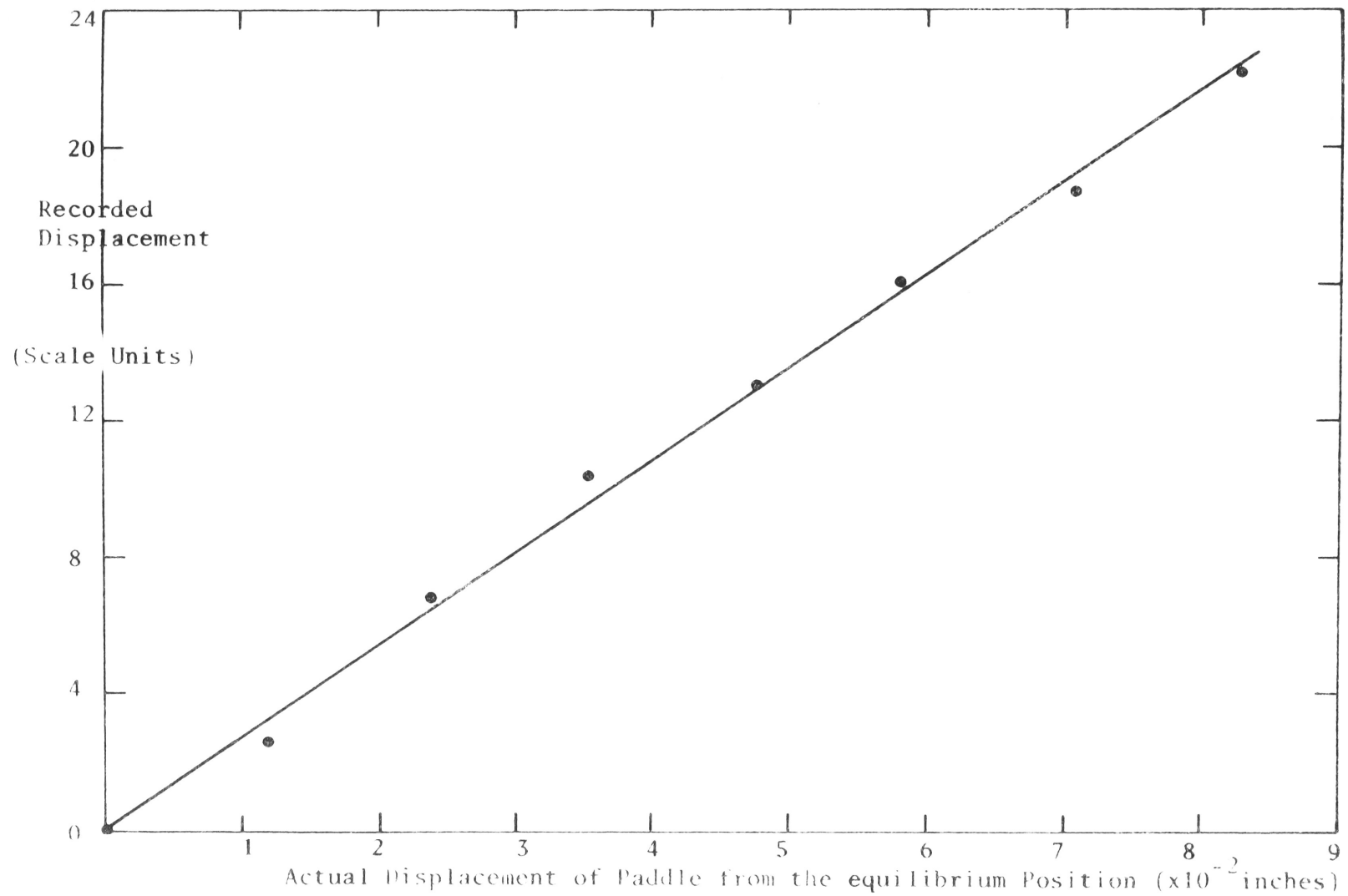
FIGURE A9:3. THE RECORDED DISPLACEMENT AS A FUNCTION OF THE ACTUAL DISPLACEMENT OF THE PADDLE FROM THE EQUILIBRIUM POSITION.
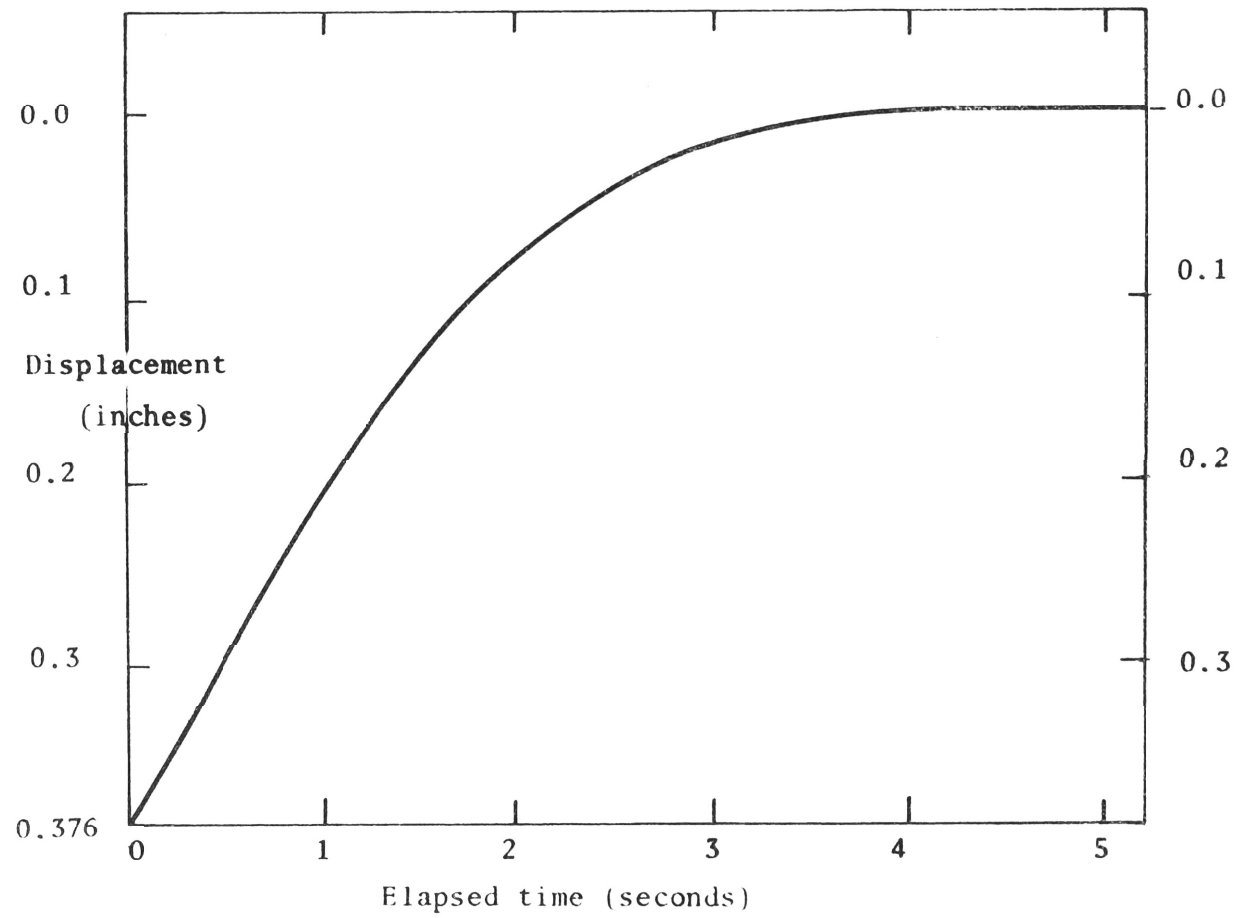
FIGURE A9:4. THE PADDLE DISPLACEMENT AS A FUNCTION OF TIME
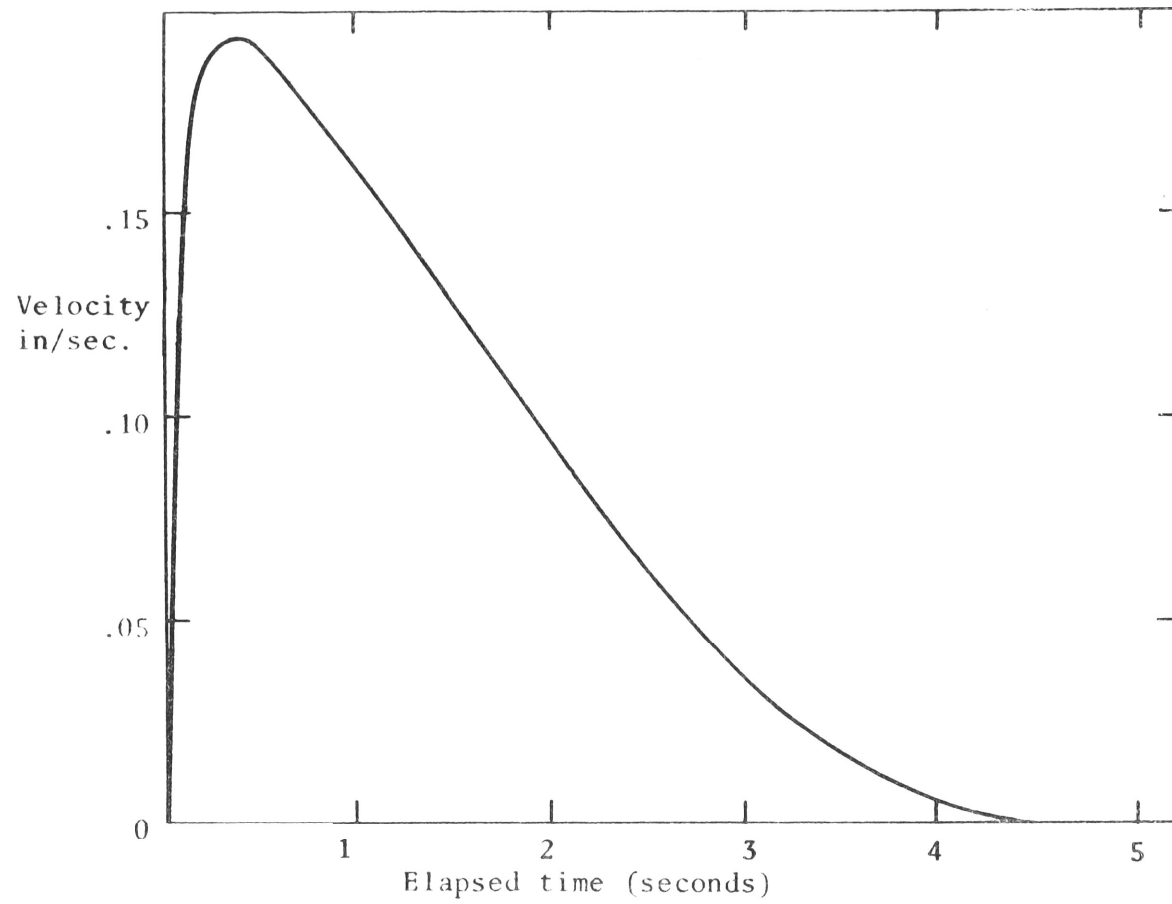
FIGURE A9:5. THE PADDLE VELOCITY AS A FUNCTION OF TIME
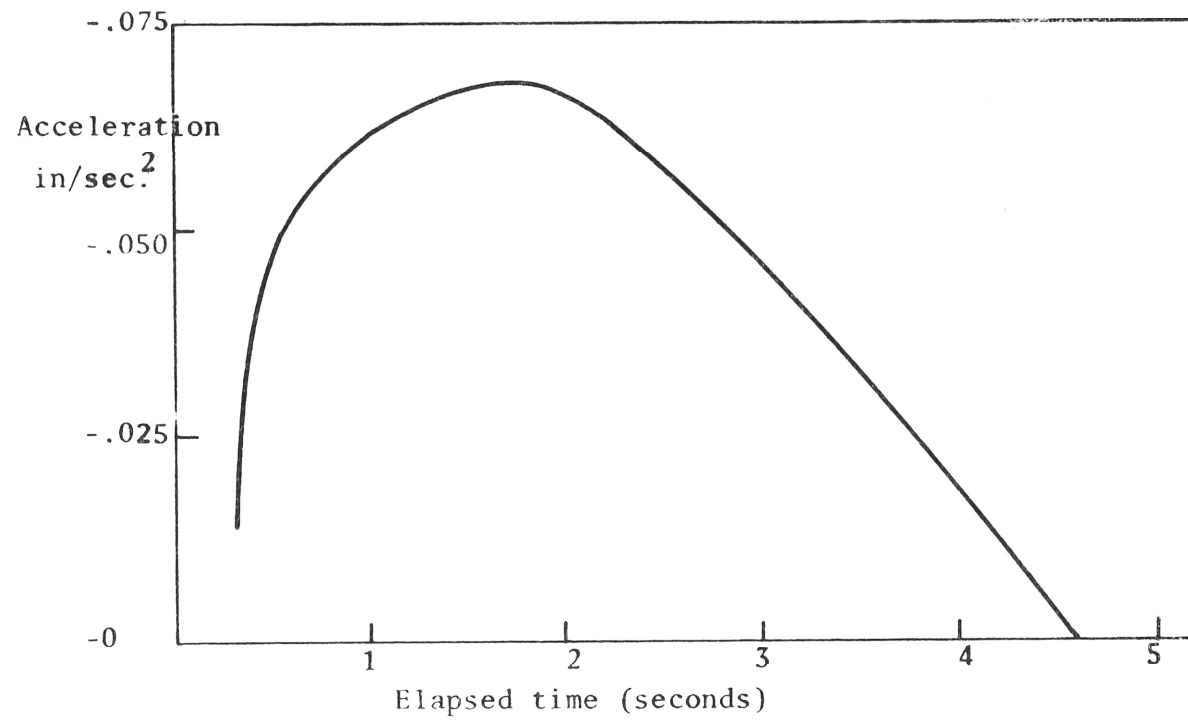
FIGURE A9:6.   THE PADDLE ACCELERATION AS A FUNCTION OF TIME

The weight of the pendulum in air was found by cutting the suspension wires near the pendulum and weighing on a mono-pan balance. This was done after the completion of the experiments and gave the combined weight of the soldered joints and the steel shim. This was found to be 1.30×10^{-4} pounds in comparison with $.16 \times 10^{-4}$ pounds for the suspension wire. Thus the weight of the suspension could not be neglected when the gravity forces were calculated.

1) Bending of Suspension:

The restoring force is given as (Steel Designers Manual (1969))

$$F_s = \frac{3x\,EI}{L^3} \quad ; \quad I = \frac{\pi D^4}{64} \qquad\qquad (A9:7)$$

where

$$D = \text{diameter of suspension}$$
$$E = \text{Young's modulus}$$
$$L = \text{length of suspension}$$
$$\text{and} \quad x = \text{displacement in inches}$$

Thus:
$$F_s = (5.1 \times 10^{-8})\,x \text{ pounds} \qquad\qquad (A9:8)$$

2) Gravity Force:

The gravity force is given approximately by Equation (A9:1) as:

$$F_g \simeq \frac{3}{2}\frac{(W_s + W_p)(W_s + 2W_p^*)}{L(W_s + 3W_p)}\,x$$

where
$$W_p \quad = \quad 1.30 \times 10^{-4} \text{ pounds}$$
$$W_p^* \quad = \quad .88 \times W_p$$
$$W_s \quad = \quad .16 \times 10^{-4} \text{ pounds}$$

which gives:

$$F_g \simeq \left(2 \cdot 72 \times 10^{-5}\right) x \text{ LBS.} \tag{A9:9}$$

Thus F_s is negligible in comparison with F_g .

If the gravity force had been calculated by assuming a massless suspension a value of 2.54×10^{-5} pounds would have been obtained or a difference of about 7%. In view of this relatively small difference it is believed that the simplifications concerning the suspension made in deriving Equation (A9:1) will introduce only a very small departure form the actual motion.

Using Figure (A9:4) the distance of the pendulum from its equilibrium position was found for various times, the origin of the time co-ordinate being the instant that the pendulum was released from th vernier scale. The gravity force was then calculated for these times using Equation (A9-9). The total unbalanced force on the pendulum was found at various times using the values for the acceleration taken from Figure (A9:6). It was then a simple matter to deduce the viscous force F_v from:

$$F = ma \simeq F_v - F_g$$

These results are tabulated in Table (A9:1) where it can be seen that the gravity force and the viscous force are nearly in balance, or that the decelerating force is small. The viscous force was plotted against the pendulum velocity (taken from Figure (A9:5) on a log-log scale. (Figure (A9:7). A straight line was drawn through the points and it was found that the Equation:

$$F_v = 10.4 \times 10^{-5} \, v^{1.61} \qquad \text{(pounds)} \qquad \text{(A9:10)}$$

described the relation between the two variables; thus determining the constants in Equation (A9-2). The exponent in this equation is in fair agreement with Hoerner's (1965) result of 3/2 found for laminar (skin-friction) drag.

A scale using the laminar Reynolds number, $R = \dfrac{v \, \ell}{\nu}$ is included in Figure (A9:6). The characteristic dimension ℓ was taken as .10 inches, the paddle width, and the viscosity as ·127 in.^{2}/second. (77% glycerol at 12.8 degrees C.)

The constants in Equation (A9-10) will be valid for pendulums of different weights other than the one used in this test provided they are of approximately the same thickness and have the same width and length. The constants will only be valid if the viscosity of the fluid used in any later wave test is the same as that used to determine Equation (A9-10). A small amount of fluid was taken from the wave flume and used in the above determination thus ensuring that the concentration of glycerol was the same as for the wave tests. The

temperature of the sample was set equal to that of the fluid in the
flume when the wave measurements had been carried out. This latter
point is the greatest draw-back to the use of the instrument since it
requires a separate determination of the constants in Equation (A9-10)
for every temperature used.

If extensive use were to be made of this particle follower it
would be desirable to compile a set of constants for various viscosities
using a standard pendulum size. This was not done as only one set of
wave measurements were taken and thus only the one determination of the
constants was required.

For the wave measurements a brass shim pendulum with the same
frontal area as the one described and a weight of 7.05×10^{-5} pounds
was used. Using the physical parameters of this pendulum allowed Equation
(A9-6) to be written as:

$$\frac{d^2x}{dt^2} = -79\,x + 460\left(c\cos\sigma t - \frac{dx}{dt}\right)\left|c\cos\sigma t - \frac{dx}{dt}\right|^{.61} \qquad (A9-11)$$

The constants c and σ relate to the wave motion of the fluid and
are evaluated in Section (4-3) for certain instances.

TABLE A9:1

THE POSITION, VELOCITY, ACCELERATION, FORCES
AND REYNOLDS NUMBER ASSOCIATED WITH THE PENDULUM

t seconds	x inches	dx/dt in/sec.	d^2x/dt^2 in/sec.^{2}	F_g $\times 10^{-6}$ lbs.	F $\times 10^{-8}$ lbs.	F_v $\times 10^{-6}$ lbs.	$\mathbb{R}$
0	.376	.000	-	10.2	-	-	.000
.5	.289	.190	.045	7.86	1.7	7.84	.149
1.0	.206	.161	.062	5.60	2.3	5.58	.127
1.5	.135	.128	.066	3.67	2.5	3.65	.100
2.0	.082	.095	.066	2.23	2.5	2.21	.075
2.5	.043	.062	.057	1.17	2.2	1.15	.049
3.0	.020	.037	.045	0.54	1.7	0.52	.029
3.5	.007	.017	.032	0.19	1.2	0.18	.013
4.0	.001	.006	.019	0.03	0.7	0.02	.005
4.5	.000	.000	.003	0.00	0.1	0.00	.000
5.0	.000	.000	.000	0.00	0.0	0.00	.000
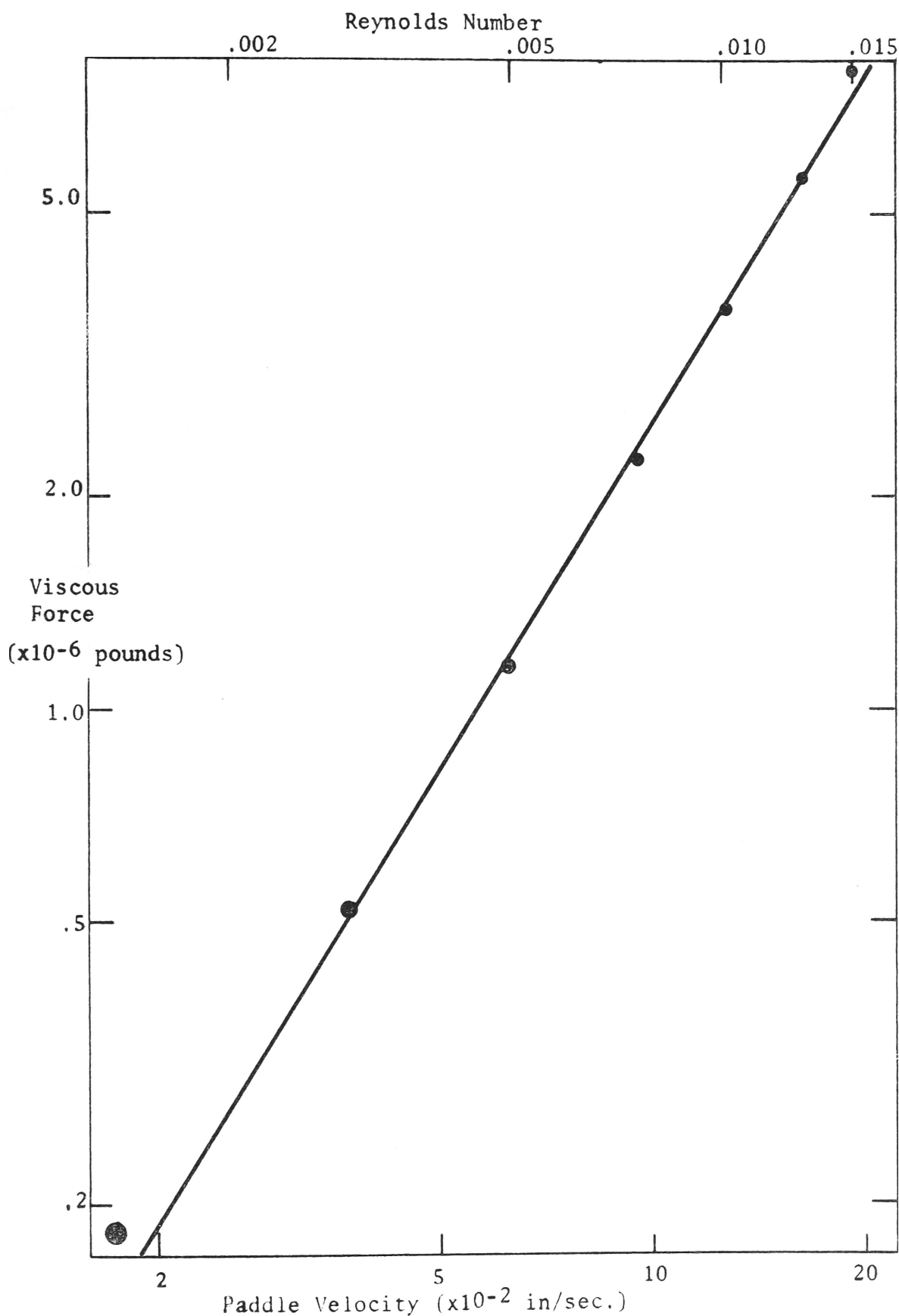
FIGURE A9:7. THE VISCOUS FORCE ON THE PADDLE AS A FUNCTION OF ITS VELOCITY.

APPENDIX 10

EVALUATION OF THE ENERGY FLUXES AT THE DISCONTINUITY

The instantaneous energy flux at x = o has been given by (Equation (5-1)):

$$\underset{\tau \to 0}{Lim} \frac{1}{\tau} \int_{t}^{t+\tau} \int_{-h_1}^{o} (P_{\sigma})_1 \, \mu_1 \, dz \, dt \Bigg|_{x=o^-} = \underset{\tau \to 0}{Lim} \frac{1}{\tau} \int_{t}^{t+\tau} \int_{-h_2}^{o} (P_{\sigma})_2 \, \mu_2 \, dz \, dt \Bigg|_{x=o^+}$$

(A10-1)

A10.1 Integration of the L.H.S. of the energy flux equation over the Depth

The integral is:

$$\int_{-h_1}^{o} (P_{\sigma_1} \mu_1) dz = \rho \int_{-h_1}^{o} \left\{ \frac{\partial(\phi_i + \phi_r)}{\partial t} - \frac{c}{h_1} \left((\phi_b)_i + (\phi_b)_r \right) \right\} (\mu_i + \mu_r) \, dz$$

Let

$$I_A = \int_{-h_1}^{o} \left(\frac{\partial(\phi_i + \phi_r)}{\partial t} \right) (\mu_i + \mu_r) \, dz$$

and

$$I_B = -\frac{c}{h_1} \left((\phi_b)_i + (\phi_b)_r \right) \int_{-h_1}^{o} (\mu_i + \mu_r) \, dz$$

since $(\phi_b)_{i,r}$ is independant of z.

Evaluation of I_A :

ϕ_i is given by Equation (3-1) as:

$$\phi_i = \frac{-\sigma A_i e^{-\alpha_1 x}}{\Delta_1 K_1} \left\{ \cosh k_1 Z \cos \alpha_1 Z \; \sin(k_1 x - \sigma t - \epsilon_1) \right. $$
$$\left. + \sinh k_1 Z \sin \alpha_1 Z \cos(k_1 x - \sigma t - \epsilon_1) \right\}$$

(A10-2)

then

$$\phi_r = \frac{-\sigma A_r e^{\alpha_1 x}}{\Delta_1 K_1} \left\{ \cosh k_1 Z \cos \alpha_1 Z \; \sin(-k_1 x - \sigma t - \epsilon_1 + \gamma_r) \right.$$
$$\left. + \sinh k_1 Z \sin \alpha_1 Z \cos(-k_1 x - \sigma t - \epsilon_1 + \gamma_r) \right\}$$

(A10-3)

where γ_r is the difference in phase between the incident and reflected waves.

Letting $X_i = -\sigma t - \epsilon_1$

and $X_r = -\sigma t - \epsilon_1 + \gamma_r$

then, at x = o

$$\frac{\partial(\phi_i + \phi_r)}{\partial t} \bigg|_{x=o} = \frac{\sigma^2}{\Delta_1 K_1} \left\{ \cosh k_1 Z \cos \alpha_1 Z \; (A_i \cos X_i + A_r \cos X_r) \right.$$
$$\left. - \sinh k_1 Z \sin \alpha_1 Z \; (A_i \sin X_i + A_r \sin X_r) \right\}$$

The horizontal velocity μ is given by Equation (3-6) as:

$$\mu_i = \frac{\sigma A_i e^{-\alpha_1 x}}{\Delta_1}\left\{\cosh k_1 z \cos \alpha_1 z \cos(k_1 x - \sigma t - \delta_1)\right.$$
$$\left. - \sinh k_1 z \sin \alpha_1 z \sin(k_1 x - \sigma t - \delta_1)\right\}$$

so:

$$\mu_r = \frac{-\sigma A_r e^{-\alpha_1 x}}{\Delta_1}\left\{\cosh k_1 z \cos \alpha_1 z \cos(-k_1 x - \sigma t - \delta_1 + \gamma_r)\right.$$
$$\left. - \sinh k_1 z \sin \alpha_1 z \sin(-k_1 x - \sigma t - \delta_1 + \gamma_r)\right\}$$

then, at $x = 0$ and using $\quad \epsilon = \delta + \Omega$

$$(\mu_i + \mu_r)\Big|_{x=0} = \frac{\sigma}{\Delta_1}\left\{\cosh k_1 z \cos \alpha_1 z \left(A_i \cos(X_i + \Omega_1) - A_r \cos(X_r + \Omega_1)\right)\right.$$
$$\left. - \sinh k_1 z \sin \alpha_1 z \left(A_i \sin(X_i + \Omega_1) - A_r \sin(X_r + \Omega_1)\right)\right.$$

$$(A10\text{-}4)$$

The intergrand is:

$$\frac{\partial(\phi_i + \phi_r)}{\partial t}(\mu_i + \mu_r)\Big|_{x=0}$$

$$= \frac{\sigma^3}{\Delta_1^2 K_1}\left\{\cosh^2 k_1 z \cos^2 \alpha_1 z \left(A_i \cos X_i + A_r \cos X_r\right)A_i \cos(X_i + \Omega_1) - A_r \cos(X_r + \Omega_1)\right.$$

$$+ \sinh^2 k_1 z \sin^2 \alpha_1 z \left(A_i \sin X_i + A_r \sin X_r\right)\left(A_i \sin(X_i + \Omega_1) - A_r \sin(X_r + \Omega_1)\right)$$

$$- \frac{1}{4}\sinh 2k_1 z \sin 2\alpha_1 z \left[A_i^2 \sin X_i \cos(X_i + \Omega_1) - A_r^2 \sin X_r \cos(X_r + \Omega_1)\right.$$

$$+ A_i^2 \cos X_i \sin(X_i + \Omega_1) - A_r^2 \cos X_r \sin(X_r + \Omega_1)$$

$$+ A_i A_r\left(-\sin X_i \cos(X_r + \Omega_1) + \sin X_r \cos(X_i + \Omega_1)\right.$$

$$\left.\left.\left. - \cos X_i \sin(X_r + \Omega_1) + \cos X_r \sin(X_i + \Omega_1)\right)\right]\right\}$$

$$= \frac{\sigma^3}{4\Delta_1^2 k_1} \left\{ (1+\cosh 2k_1 z)(1+\cos 2\alpha_1 z)(A_i \cos X_i + A_r \cos X_r)(A_i \cos(X_i + \theta_i) - A_r \cos(X_r + \Omega_1)) \right.$$

$$+ (-1+\cosh 2k_1 z)(1-\cos 2\alpha_1 z)(A_i \sin X_i + A_r \sin X_r)(A_i \sin(X_i + \Omega_1) - A_r \sin(X_r + \Omega_1))$$

$$- \sinh 2k_1 z \sin 2\alpha_1 z \left[A_i^2 \sin(2X_i + \Omega_1) - A_r^2 \sin(2X_r + \Omega_1) \right.$$

$$\left. \left. + A_i A_r (\sin(X_i + X_r + \Omega_1) - \sin(X_i + X_r + \Omega_1)) \right] \right\}$$

$$= \frac{\sigma^3}{4\Delta_1^2 k_1} \left\{ (1+\cosh 2k_1 z \cos 2\alpha_1 z) \left[A_i^2 \cos(2X_i + \Omega_1) - A_r^2 \cos(2X_r + \Omega_1) + A_i A_r (-\cos(X_r + X_i + \Omega_1) \right.\right.$$

$$\left. + \cos(X_r + X_i + \Omega_1)) \right]$$

$$+ (\cosh 2k_1 z + \cos 2\alpha_1 z) \left[A_i^2 \cos \Omega_1 - A_r^2 \cos \Omega_1 + A_i A_r (-\cos(X_r + \Omega_1 - X_i) + \cos(X_r - \Omega_1 - X_i)) \right]$$

$$\left. - \sinh 2k_1 z \sin 2\alpha_1 z \left[A_i^2 \sin(2X_i + \Omega_1) - A_r^2 \sin(2X_r + \Omega_1) \right] \right\}$$

The term $-\cos(X_r + \Omega_1 - X_i) + \cos(X_r - \Omega_1 - X_i) = -\cos(\gamma_r + \Omega_1) + \cos(\gamma_r - \Omega_1)$

$$= 2 \sin \gamma_r \sin \Omega_1$$

so the integrand is:

$$\frac{\partial(\phi_i + \phi_r)}{\partial t}(u_1 + u_r) \bigg|_{x=0.} = \frac{\sigma^3}{4\Delta_1^2 k_1} \left\{ (1+\cosh 2k_1 z \cos 2\alpha_1 z) \left[A_i^2 \cos(2X_i + \Omega_1) - A_r^2 \cos(2X_r + \Omega_1) \right] \right.$$

$$+ (\cosh 2k_1 z + \cos 2\alpha_1 z) \left[(A_i^2 - A_r^2) \cos \Omega_1 + 2 A_i A_r \sin \gamma_r \sin \Omega_1 \right]$$

$$\left. - \sinh 2k_1 z \sin 2\alpha_1 z \left[A_i^2 \sin(2X_i + \Omega_1) - A_r^2 \sin(2X_r + \Omega_1) \right] \right]$$

Integrating over the depth yields:

$$I_A = \frac{\sigma^3}{8\Delta_1^2 \kappa_1} \left\{ \begin{array}{l} a_1 \left[A_i^2 \cos(2X_i + \Omega_1) - A_r^2 \cos(2X_r + \Omega_1) \right] \\[2mm] -b_1 \left[A_i^2 \sin(2X_i + \Omega_1) - A_r^2 \sin(2X_r + \Omega_1) \right] \\[2mm] +d_1 \left[(A_i^2 - A_r^2)\cos\Omega_1 + 2 A_i A_r \sin\gamma_r \sin\Omega_1 \right] \end{array} \right.$$

where:

$$a_1 = 2 \int_0^{h_1} (1 + \cosh 2k_1 Z \cos 2\alpha_1 Z) dZ = 2h_1 + \frac{1}{\kappa_1^2}\left[k_1 \sinh 2k_1 h_1 \cos 2\alpha_1 h_1 \right.$$
$$\left. + \alpha_1 \cosh 2k_1 h_1 \sin 2\alpha_1 h_1 \right]$$

$$b_1 = 2 \int_0^{h_1} \sinh 2k_1 Z \sin 2\alpha_1 Z \, dZ = \frac{1}{\kappa_1^2} \left[k_1 \cosh 2k_1 h_1 \sin 2\alpha_1 h_1 \right.$$
$$\left. - \alpha_1 \sinh 2k_1 h_1 \cos 2\alpha_1 h_1 \right]$$

and

$$d_1 = 2 \int_0^{h_1} (\cosh 2k_1 Z + \sin 2\alpha_1 Z) dZ = \frac{\sinh 2k_1 h}{k_1} + \frac{\sin 2\alpha_1 h_1}{\alpha_1}$$

Rewriting I_A such that the time dependance is shown explicitly:

$$I_A = \frac{\sigma^3}{8\Delta_1^2 \kappa_1} \left\{ a_1 \left[A_i^2 \cos(2\sigma t + 2\epsilon_1 - \Omega_1) - A_r^2 \cos(2\sigma t + 2\epsilon_1 - \Omega_1 - 2\gamma_r) \right] \right.$$

$$-b_1 \left[-A_i^2 \sin(2\sigma t + 2\epsilon_1 - \Omega_1) + A_r^2 \sin(2\sigma t + 2\epsilon_1 - \Omega_1 - 2\gamma_r) \right]$$

$$\left. + d_1 \left[(A_i^2 - A_r^2)\cos\Omega_1 + 2 A_i A_r \sin\gamma_r \sin\Omega \right] \right\}$$

$$= \frac{\sigma^3}{8 \Delta_i^2 \kappa_1} \Big\{ a_1 \big[A_i^2 (\cos 2\sigma t \cos \theta_1 - \sin 2\sigma t \sin \theta_1) - A_r^2 (\cos 2\sigma t \cos(\theta_1 - 2\gamma_r) $$
$$- \sin 2\sigma t \sin(\theta_1 - 2\gamma_r)) \big]$$

$$+ b_1 \big[A_i^2 (\sin 2\sigma t \cos \theta_1 + \cos 2\sigma t \sin \theta_1) - A_r^2 (\sin 2\sigma t \cos(\theta_1 - 2\gamma_r) $$
$$+ \cos 2\sigma t \sin(\theta_1 - 2\gamma_r)) \big]$$

$$+ d_1 \big[(A_i^2 - A_r^2) \cos \Omega_1 + 2 A_i A_r \sin \gamma_r \sin \Omega_1 \big] \Big\}$$

Collecting terms in $\sin 2\sigma t$ and $\cos 2\sigma t$

$$I_A = \frac{\sigma^3}{8 \Delta_i^2 \kappa_1} \Big\{ \cos 2\sigma t \big[A_i^2 (a_1 \cos \theta_1 + b_1 \sin \theta_1) - A_r^2 (a_1 \cos(\theta_1 - 2\gamma_r) + b_1 \sin(\theta_1 - 2\gamma_r)) \big]$$

$$+ \sin 2\sigma t \big[A_i^2 (-a_1 \sin \theta_1 + b_1 \cos \theta_1) - A_r^2 (-a_1 \sin(\theta_1 - 2\gamma_r) + b_1 \cos(\theta_1 - 2\gamma_r)) \big]$$

$$+ d_1 \big[(A_i^2 - A_r^2) \cos \Omega_1 + 2 A_i A_r \sin \gamma_r \sin \Omega_1 \big] \Big\}$$

$$= \frac{\sigma^3}{8 \Delta_i^2 \kappa_1} \Big\{ \cos 2\sigma t \big[A_i^2 (a_1 \cos \theta_1 + b_1 \sin \theta_1) - A_r^2 (a_1 (\cos \theta_1 \cos 2\gamma_r + \sin \theta_1 \sin 2\gamma_r) $$
$$+ b_1 (\sin \theta_1 \cos 2\gamma_r - \cos \theta_1 \sin 2\gamma_r)) \big]$$

$$+ \sin 2\sigma t \big[-A_i^2 (a_1 \sin \theta_1 - b_1 \cos \theta_1) - A_r^2 (a_1 (-\sin \theta_1 \cos 2\gamma_r + \cos \theta_1 \sin 2\gamma_r) $$
$$+ b_1 (\cos \theta_1 \cos 2\gamma_r + \sin \theta_1 \sin 2\gamma_r)) \big]$$

$$+ d_1 \big[(A_i^2 - A_r^2) \cos \Omega_1 + 2 A_i A_r \sin \gamma_r \sin \Omega_1 \big] \Big\}$$

$$I_A = \frac{\sigma^3}{8\Delta_1^2 K_1} \left\{ \cos 2\sigma t \left[(A_i^2 - A_r^2 \cos 2\gamma_r)(a_1 \cos \Theta_1 + b_1 \sin \Theta_1) - A_r^2 \sin 2\gamma_r (a_1 \sin \Theta_1 - b_1 \cos \Theta_1) \right] \right.$$

$$- \sin 2\sigma t \left[(A_i^2 - A_r^2 \cos 2\gamma_r)(a_1 \sin \Theta_1 - b_1 \cos \Theta_1) + A_r^2 \sin 2\gamma_r (a_1 \cos \Theta_1 + b_1 \sin \Theta_1) \right]$$

$$\left. + d_1 \left[(A_i^2 - A_r^2) \cos \Omega_1 + 2 A_i A_r \sin \gamma_r \sin \Omega_1 \right] \right\}$$

where

$$\Theta_1 = 2\epsilon_1 - \Omega_1 = 2\delta_1 + \Omega_1$$

Evaluation of I_B

Evaluating the potential functions given in Equations (A10-2) and (A10-3) at the bottom ($Z = 0$) gives:

$$(\phi_b)_i + (\phi_b)_r = \frac{-\sigma}{\Delta_1 K_1} \left\{ A_i \sin X_i + A_r \sin X_r \right\}$$

and from Equation (A10-4)

$$\int_{-h}^{0} (\mu_i + \mu_r) \Big|_{x=0} dz = \frac{\sigma}{\Delta_1} \left[A_i \cos(X_i + \Omega_1) - A_r \cos(X_r + \Omega_1) \right] \int_{0}^{h_1} \cosh k_1 Z \cos \alpha_1 Z \, dZ$$

$$- \frac{\sigma}{\Delta_1} \left[A_i \sin(X_i + \Omega_1) - A_r \sin(X_r + \Omega_1) \right] \int_{0}^{h_1} \sinh k_1 Z \sin \alpha_1 Z \, dZ$$

Evaluating the integrals:

$$\int_{0}^{h_1} \cosh k_1 Z \cos \alpha_1 Z \, dZ = \frac{1}{k_1^2 + \alpha_1^2} \left\{ k_1 \sinh k_1 h_1 \cos \alpha_1 h_1 + \alpha_1 \cosh k_1 h_1 \sin \alpha_1 h_1 \right\}$$

$$= \frac{\Delta_1 K_1}{K_1^2} \left\{ \cos \Omega_1 \cos \delta_1 + \sin \Omega_1 \sin \delta_1 \right\}$$

$$= \frac{\Delta_1}{K_1^2} \left\{ \cos(\delta_1 - \Omega_1) \right\}$$

and:

$$\int_0^{h_1} \sinh k_1 Z \sin \alpha_1 Z \, dZ = \frac{1}{K_1^2} \left\{ k_1 \cosh k_1 h_1 \sin \alpha_1 h_1 - \alpha_1 \sinh k_1 h_1 \cos \alpha_1 h_1 \right\}$$

$$= \frac{\Delta_1}{K_1} \left\{ \cos \Omega_1 \sin \delta_1 - \sin \Omega_1 \cos \delta_1 \right\}$$

$$= \frac{\Delta_1}{K_1} \left\{ \sin \left(\delta_1 - \Omega_1 \right) \right\}$$

Therefore I_B becomes:

$$I_B = \frac{c \sigma^2}{h_1 \Delta_1 K_1^2} \left(A_i \sin X_i + A_r \sin X_r \right) \left\{ \left(A_i \cos(X_i + \Omega_1) - A_r \cos(X_r + \Omega_1) \right) \cos(\delta_1 - \Omega_1) \right.$$

$$\left. - \left(A_i \sin(X_i + \Omega_1) - A_r \sin(X_r + \Omega_1) \right) \sin(\delta_1 - \Omega_1) \right\}$$

$$= \frac{c \sigma^2}{h_1 \Delta_1 K_1^2} \left(A_i \sin X_i + A_r \sin X_r \right) \left\{ A_i \cos(X_i + \Omega_1 + \delta_1 - \Omega_1) - A_r \cos(X_r + \Omega_1 + \delta_1 - \Omega_1) \right\}$$

$$= \frac{c \sigma^2}{h_1 \Delta_1 K_1^2} \left\{ A_i^2 \sin X_i \cos(X_i + \delta_1) - A_r^2 \sin X_r \cos(X_r + \delta_1) \right.$$

$$\left. + A_i A_r \left(\sin X_r \cos(X_i + \delta_1) - \sin X_i \cos(X_r + \delta_1) \right) \right\}$$

Eliminating the products of the trigonometric functions:

$$I_B = \frac{c \sigma^2}{2 h_1 \Delta_1 K_1^2} \left\{ A_i^2 \left(\sin(2X_i + \delta_1) - \sin \delta_1 \right) - A_r^2 \left(\sin(2X_r + \delta_1) - \sin \delta_1 \right) \right.$$

$$\left. + A_i A_r \left[\sin(X_r + X_i + \delta_1) + \sin(X_r - X_i - \delta_1) - \sin(X_i + X_r + \delta_1) - \sin(X_i - X_r - \delta_1) \right] \right\}$$

$$I_B = \frac{c\sigma^2}{2h_1\Delta_1 K_1^2} \left\{ A_i^2 \left(\sin(-2\sigma t - 2\epsilon_1 + \delta_1) - \sin\delta_1\right) - A_r^2 \left(\sin(-2\sigma t - 2\epsilon_1 + \delta_1 + 2\gamma_r) - \sin\delta_1\right) \right.$$

$$\left. + A_i A_r \left(\sin(-\delta_1 + \gamma_r) - \sin(-\gamma_r - \delta_1)\right) \right\}$$

$$I_B = \frac{c\sigma^2}{2h_1\Delta_1 K_1} \left\{ A_i^2 \left(\cos 2\sigma t \sin(\delta_1 - 2\epsilon_1) - \sin 2\sigma t \cos(\delta_1 - 2\epsilon_1) - \sin\delta_1\right) \right.$$

$$- A_r^2 \left(\cos 2\sigma t \sin(\delta_1 - 2\epsilon_1 + 2\gamma_r) - \sin 2\sigma t \cos(\delta_1 - 2\epsilon_1 + 2\gamma_r) - \sin\delta_1\right)$$

$$\left. + A_i A_r \left(\sin(\gamma_r - \delta_1) + \sin(\gamma_r + \delta_1)\right) \right\}$$

Collecting terms in $\sin 2\sigma t$ and $\cos 2\sigma t$

$$I_B = \frac{c\sigma^2}{2h_1\Delta_1 K_1^2} \left\{ \cos 2\sigma t \left[A_i^2 \sin(\delta_1 - 2\epsilon_1) - A_r^2 \sin(\delta_1 - 2\epsilon_1 + 2\gamma_r) \right] \right.$$

$$- \sin 2\sigma t \left[A_i^2 \cos(\delta_1 - 2\epsilon_1) - A_r^2 \cos(\delta_1 - 2\epsilon_1 + 2\gamma_r) \right]$$

$$\left. + (-A_i^2 + A_r^2) \sin\delta_1 + A_i A_r \left(\sin(\gamma_r - \delta_1) + \sin(\gamma_r + \delta_1)\right) \right\}$$

$$= \frac{c\sigma^2}{2h_1\Delta_1 K_1^2} \left\{ \cos 2\sigma t \left[-A_i^2 \sin\beta_1 - A_r^2 \left(\sin 2\gamma_r \cos\beta_1 - \cos 2\gamma_r \sin\beta_1\right) \right] \right.$$

$$- \sin 2\sigma t \left[A_i^2 \cos\beta_1 - A_r^2 \left(\sin 2\gamma_r \sin\beta_1 + \cos 2\gamma_r \cos\beta_1\right) \right]$$

$$\left. + (-A_i^2 + A_r^2) \sin\delta_1 + A_i A_r \sin\gamma_r \cos\delta_1 \right\}$$

$$I_B = \frac{c\sigma^2}{2h_1\Delta_1 K_1^2}\left\{\cos 2\sigma t\left[(-A_i^2 + A_r^2\cos 2\gamma_r)\sin\beta_1 - A_r^2\sin 2\gamma_r\cos\beta_1\right]\right.$$

$$+ \sin 2\sigma t\left[(-A_i^2 + A_r^2\cos 2\gamma_r)\cos\beta_1 + A_r^2\sin 2\gamma_r\sin\beta_1\right.$$

$$+ (-A_i^2 + A_r^2)\sin\delta_1 + 2A_i A_r\sin\gamma_r\cos\delta_1$$

where $\qquad \beta_1 = 2\epsilon_1 - \delta_1 = 2\Omega_1 + \delta_1$

Thus:

$$\int_{-h_1}^{0}(p_\sigma)_1\,\mu_1\,dz\,\Bigg|_{x=0} = \rho(I_A + I_B)$$

L.H.S. $= \dfrac{\rho\sigma^3}{8\Delta_1^2 K_1}\left\{(A_i^2 - A_r^2)(d_1\cos\Omega_1 + \dfrac{\Delta_1}{K_1}\dfrac{4c}{\sigma h_1}\sin\delta_1) - 2A_i A_r\sin\gamma_r(d_1\sin\Omega_1 - \dfrac{\Delta_1}{K_1}\dfrac{4c}{\sigma h_1}\cos\delta_1)\right.$

$$+ \cos 2\sigma t\left[(A_i^2 - A_r^2\cos 2\gamma_r)(a_1\cos\Theta_1 + b_1\sin\Theta_1 + \dfrac{\Delta_1}{K_1}\dfrac{4c}{\sigma h_1}\sin\beta_1)\right.$$

$$\left. - A_r^2\sin 2\gamma_r(a_1\sin\Theta_1 - b_1\cos\Theta_1 - \dfrac{\Delta_1}{K_1}\dfrac{4c}{\sigma h_1}\cos\beta_1)\right]$$

$$- \sin 2\sigma t\left[(A_i^2 - A_r^2\cos 2\gamma_r)(a_1\sin\Theta_1 - b_1\cos\Theta_1 - \dfrac{\Delta_1}{K_1}\dfrac{4c}{\sigma h_1}\cos\beta_1)\right.$$

$$\left.\left. + A_r^2\sin 2\gamma_r(a_1\cos\Theta_1 + b_1\sin\Theta_1 + \dfrac{\Delta_1}{K_1}\dfrac{4c}{\sigma h_1}\sin\beta_1)\right]\right\}.$$

$$(A10-5)$$

The evaluation of $\lim\limits_{\tau\to 0}\int_{t}^{t+\tau}\rho(I_A + I_B)\,dt$ obviously yields Equation (A10-5) thus this is the instantaneous energy flux on the L.H.S. of the step.

A10.2   Evaluation of the R.H.S. of the Energy Flux Equation

Instead of integrating the R.H.S. of Equation (A10-1) use will be made of Equation (A10-5) to evaluate the energy flux.

If in Equation (A10-5):

1) A_r is set to zero

2)   subscript 1 is changed to 2 and subscript

   i is changed to t

and   3) $\cos 2\sigma t$ is replaced by $\cos(2\sigma t - 2\gamma_t)$

   and $\sin \sigma t$ is replaced by $\sin(2\sigma t - 2\gamma_t)$

Then the result will be:

$$\lim_{\tau \to 0} \frac{1}{\tau} \int_t^{t+\tau} \int_{h_2}^{0} (p_v)_2 \, \mu_2 \, dz \, dt$$

$$= \frac{\sigma^3}{8 \Delta_2^2 \, \kappa_2} \left\{ A_t^2 \left(\alpha_2 \cos \Omega_2 + \frac{\Delta_2}{\kappa_2} \frac{4c}{\sigma h_2} \sin \delta_2 \right) \right.$$

$$+ \cos 2(\sigma t - \gamma_t) \left[A_t^2 \left(\alpha_2 \cos \Theta_2 + b_2 \sin \Theta_2 + \frac{\Delta_2}{\kappa_2} \frac{4c}{\sigma h_2} \sin \beta_2 \right) \right]$$

$$\left. - \sin 2(\sigma t - \gamma_t) \left[A_t^2 \left(\alpha_2 \sin \Theta_2 - b_2 \cos \Theta_2 - \frac{\Delta_2}{\kappa_2} \frac{4c}{\sigma h_2} \cos \beta_2 \right) \right] \right\}$$

$$R.H.S. = \frac{\sigma^3 A_t^2}{8\Delta_2^2 \kappa_2} \left\{ \left(\alpha_2 \cos \Omega_2 + \frac{\Delta_2}{\kappa_2} \frac{4c}{\sigma h_2} \sin \delta_2 \right) \right.$$

$$+ \cos 2\sigma t \left[\cos 2\gamma_t \left(\alpha_2 \cos \Theta_2 + b_2 \sin \Theta_2 + \frac{\Delta_2}{\kappa_2} \frac{4c}{\sigma h_2} \sin \beta_2 \right) \right.$$

$$\left. + \sin 2\gamma_t \left(\alpha_2 \sin \Theta_2 - b_2 \cos \Theta_2 - \frac{\Delta_2}{\kappa_2} \frac{4c}{\sigma h_2} \cos \beta_2 \right) \right]$$

$$- \sin 2\sigma t \left[\cos 2\gamma_t \left(\alpha_2 \sin \Theta_2 - b_2 \cos \Theta_2 - \frac{\Delta_2}{\kappa_2} \frac{4c}{\sigma h_2} \cos \beta_2 \right) \right.$$

$$\left. \left. - \sin 2\gamma_t \left(\alpha_2 \cos \Theta_2 + b_2 \sin \Theta_2 + \frac{\Delta_2}{\kappa_2} \frac{4c}{\sigma h_2} \sin \beta_2 \right) \right] \right\}$$

$$(A10\text{-}6)$$

APPENDIX II

THE RESPONSE COEFFICIENTS A AND B

A11.1   Evaluation of $\dfrac{f_1}{f_2}$

Neglecting the subscript for the moment:

$$f = \int_{-h}^{0} \phi \kappa \left(-i\sigma \phi + \frac{c}{h} \phi_b \right) \, dz$$

where from Equation (2-8):

$$\phi = \frac{i\sigma \cosh \kappa (z+h)}{\kappa \sinh \kappa h} \qquad\qquad \text{for a unit amplitude}$$

and

$$\phi_b = \frac{i\sigma}{\kappa \sinh \kappa h}$$

so:

$$f = \int_{-h}^{0} \left\{ \frac{i\sigma^3 \cosh^2 \kappa (z+h)}{\kappa \sinh^2 \kappa h} - \frac{c\sigma^2 \cosh \kappa (z+h)}{\kappa^2 h \sinh^2 \kappa h} \right\} \, dz$$

$$= \frac{\sigma^2}{\kappa \sinh^2 \kappa h} \int_{0}^{h} \left(i\sigma \cosh^2 \kappa z - \frac{c}{\kappa h} \cosh \kappa z \right) \, dz$$

$$= \frac{i\sigma^2}{k^2 \sinh^2 kh} \left\{ \frac{\sigma}{4} (2kh + \sinh 2kh) + \frac{ic}{h} \sinh kh \right\}$$

(A11-11)

Therefore the ratio $\dfrac{f_1}{f_2}$ is:

$$\frac{f_1}{f_2} = \frac{k_2^2 \sinh^2 k_2 h_2}{k_1^2 \sinh^2 k_1 h_1} \left\{ \frac{2k_1 h_1 + \sinh 2k_1 h_1 + i\frac{4c}{\sigma h_1} \sinh k_1 h_1}{2k_2 h_2 + \sinh 2k_2 h_2 + i\frac{4c}{\sigma h_2} \sin k_2 h_2} \right\}$$

(A11-12)

A11.3 Evaluation of A_n and B_n for Frictionless Long-Waves.

If there is no friction then: $K_j \equiv (k_j + i\alpha_j) = k_j ; \quad j = 1,2$

and the ratio $\dfrac{f_1}{f_2}$ becomes:

$$\frac{f_1}{f_2} = \frac{k_2^2 \sinh^2 k_2 h_2}{k_1^2 \sinh^2 k_1 h_1} \cdot \frac{2k_1 h_1 + \sinh 2k_1 h_1}{2k_2 h_2 + \sinh 2k_2 h_2}$$

which is the ratio of the energy (or group in this case) velocities which

for long-waves is:

$$\frac{f_1}{f_2} = \frac{v_{e_1}}{v_{e_2}} \simeq \frac{\sqrt{h_1}}{\sqrt{h_2}}$$

Therefore the coefficient A_n is:

$$A_n = \frac{2\epsilon_n i^{n+1}}{\pi k_1 R} \left\{ \frac{\sqrt{\frac{h_1}{h_2}}}{\sqrt{\frac{h_1}{h_2}} J_n(k_1 R) H_n'(k_1 R) - J_n'(k_1 R) H_n(k_1 R)} \right\}$$

and:

$$B_n = \epsilon_n \iota^n \left\{ \frac{J_n(k_1 R) J_n'(k_2 R) - \sqrt{\frac{h_1}{h_2}} J_n(k_2 R) J_n'(k_1 R)}{-H_n(k_1 R) J_n'(k_2 R) + \sqrt{\frac{h_1}{h_2}} J_n(k_2 R) H_n'(k_1 R)} \right\}$$

(A11-13)

where $\quad k_i = \dfrac{\sigma}{\sqrt{gh_i}} \cdot \qquad$ for long-waves.

That these results are the same as those found by Longuet-Higgins (1967) can be seen from his representation (for example) of the wave over the sea mount:

$$\eta_2^* = e^{-\iota \sigma t} \sum_{n=-\infty}^{\infty} A_n' J_n(k_1 r) e^{\iota n \theta}$$

where

$$A_n' = \frac{2 \iota^{n+1}}{\pi k_1 R} \frac{\sqrt{\frac{h_2}{h_1}}}{\sqrt{\frac{h_1}{h_2}} J_n(k_1 R) H_n'(k_1 R) - J_n'(k_1 R) H_n(k_1 R)}$$

Selecting the $n^{th.}$ and $-n^{th.}$ component and using the relation that $\mathcal{C}_n = (-1)^n \mathcal{C}_{-n}$ where $\mathcal{C}$ is a cylindrical function, then the sum of the $n^{th.}$ and $-n^{th.}$ components is: $(n \neq 0)$

$$\left(\eta_2\right)_n + \left(\eta_2\right)_{-n} = \frac{e^{-\iota \sigma t} 2 \iota \sqrt{\frac{h_2}{h_1}} J_n(k_1 r)}{\pi k_1 R \left(\sqrt{\frac{h_1}{h_2}} J_n(k_1 R) H_n'(k_1 R) - J_n'(k_1 R) H_n(k_1 R) \right)} \left[\iota^n e^{\iota n \theta} + (-1)^n \iota^{-n} e^{-\iota n \theta} \right]$$

Examining the term in square brackets:

$$i^n e^{in\theta} + (-1)^n i^{-n} e^{-in\theta} = i^n (e^{in\theta} + e^{-in\theta})$$

$$= 2 i^n \cos n\theta$$

by virtue of the easily verified relation that:

$$i^n = (-1)^n i^{-n}$$

Therefore:

$$(\eta_2^*)_n + (\eta_2^*)_{-n} = \frac{e^{-i\sigma t} 4 i^{n+1} J_n(k_1 r) \cos n\theta}{\pi k_1 R (\sqrt{\frac{h_1}{h_2}} J_n(k_1 R) H_n'(k_1 R) - J_n'(k_1 R) H_n(k_1 R))}$$

and since the R.H.S. is the same as obtained by the representation in this thesis

i.e. $$(\eta_2)_{n \neq 0} = 2 e^{-i\sigma t} A_n i^n J_n(k_1 r) \cos n\theta$$

and for $n = 0$ both representations $(\eta_2^*)_0$ and $(\eta_2)_0$ are the same, it is concluded that the results found here are in agreement with those found by Longuet-Higgins (1967). The same arguments would hold for η_i and η_s

A11.4 Asymptotic Approximations for A_n and B_n for Small Arguments

If $n \gg \left(\frac{k_{\gamma} R}{2}\right)^2$ and $n > 0$ then:

$$J_n(k_\gamma R) \simeq \frac{\left(\frac{1}{2} k_\gamma R\right)^n}{n!}$$

and

$$H_n^{(1)}(k_\gamma R) \simeq -\frac{i\left(\frac{2}{k_\gamma R}\right)^n (n-1)!}{\pi}$$

(See, for example, McLachlan (1961) p.86)

The asymptotic behavior of the derivatives is found from the recurrence formula:

$$C_n'(z) = \frac{n}{z} C_n(z) - C_{n+1}(z)$$

Therefore:

$$J_n'(k_\gamma R) \simeq \frac{n}{k_\gamma R} \frac{\left(\frac{1}{2} k_\gamma R\right)^n}{n!} - \frac{\left(\frac{1}{2} k_\gamma R\right)^{n+1}}{(n+1)!}$$

$$\simeq \frac{\left(\frac{1}{2} k_\gamma R\right)^n}{k_\gamma R (n-1)!} \left(1 - \frac{\left(\frac{1}{2} k_\gamma R\right)^2}{n(n+1)}\right)$$

and, since $\left(\frac{1}{2} k_\gamma R\right)^2 \ll n$ the second term may be neglected and:

$$J_n'(k_\gamma R) \simeq \frac{\left(\frac{1}{2} k_\gamma R\right)^n}{k_\gamma R (n-1)!}$$

Similarly:

$$H_n^{(1)'}(k_\gamma R) \simeq \frac{-in\left(\frac{2}{k_\gamma R}\right)^n (n-1)!}{\pi k_\gamma R} + \frac{i\left(\frac{2}{k_\gamma R}\right)^{n+1} n!}{\pi}$$

$$\simeq \frac{-in!}{\pi} \left(\frac{2}{k_\gamma R}\right)^n \left(\frac{1}{k_\gamma R} - \frac{2}{k_\gamma R}\right)$$

$$\simeq \frac{i\,n!}{\pi\,k_i\,R} \left(\frac{2}{k_i\,R}\right)^{n}$$

The bracketed function in the denominator of the equation defining A_n and B_n is (for $n \gg \left(\frac{k_i R}{2}\right)^{2}$):

$$\left(\frac{f_1}{f_2}\,H'_{n_1}\,J_{n_2} - H_{n_1}\,J'_{n_2}\right) \simeq \frac{f_1}{f_2}\,\frac{i\,n!\left(\frac{2}{k_1 R}\right)^{n}\left(\frac{k_2 R}{2}\right)^{n}}{\pi\,k_1\,R\,n!} + \frac{i(n-1)!\left(\frac{2}{k_1 R}\right)^{n}\left(\frac{k_2 R}{2}\right)^{n}}{\pi\,k_2\,R\,(n-1)!}$$

$$\simeq \frac{i}{\pi R}\left(\frac{k_2}{k_1}\right)^{n}\left\{\frac{f_1}{f_2 k_1} + \frac{1}{k_2}\right\} \qquad\qquad\text{(A11-14)}$$

From Equation (A11-10) defining A_n :

$$A_n \simeq \frac{\frac{f_1}{f_2}\,2\,\epsilon_n\,i^{n+1}}{\pi\,k_1\,R\,\frac{i}{\pi R}\left(\frac{k_2}{k_1}\right)^{n}\left\{\frac{f_1}{f_2 k_1} + \frac{1}{k_2}\right\}}$$

so $\quad A_n \simeq \dfrac{4\,i^{n}\left(\frac{k_1}{k_2}\right)^{n}}{1 + \frac{f_2\,k_1}{f_1\,k_2}}$ \qquad\qquad\text{(A11-15)}

Using the frictionless long-wave approximations gives:

$$\left(\frac{k_1}{k_2}\right) = \frac{v_{p_2}}{v_{p_1}} = \sqrt{\frac{h_2}{h_1}}$$

and

$$\frac{f_1}{f_2} = \frac{v_{e_1}}{v_{e_2}} = \sqrt{\frac{h_1}{h_2}}$$

Therefore in this special case Equation (A11-15) becomes:

$$A_n \simeq \frac{4\,i^{n}\left(\frac{h_2}{h_1}\right)^{n/2}}{1 + \frac{h_2}{h_1}}$$

From Equation (A11-11) defining B_n gives (for $n \gg \left(\frac{k_1 R}{2} \right)^2$):

$$B_n \simeq \epsilon_n i^n \frac{\left(\frac{k_1 R}{2} \right)^n \frac{\left(\frac{k_2 R}{2} \right)}{k_2 R (n-1)!} - \frac{f_1}{f_2} \frac{\left(\frac{k_1 R}{2} \right)^n}{k_1 R (n-1)!} \frac{\left(\frac{k_2 R}{2} \right)}{n!}}{\frac{i}{\pi R} \left(\frac{k_2}{k_1} \right)^n \left\{ \frac{f_1}{f_2 k_1} + \frac{1}{k_2} \right\}}$$

$$B_n \simeq 2 i^n \frac{\frac{\left(\frac{R}{2} \right)^{2n} (k_1 k_2)^n}{n! (n-1)!} \left(\frac{1}{k_2 R} - \frac{f_1}{f_2 k_1 R} \right)}{\frac{i}{\pi R} \left(\frac{k_2}{k_1} \right)^n \left\{ \frac{f_1}{f_2 k_1} + \frac{1}{k_2} \right\}}$$

$$\simeq \frac{2 i^{n-1} \cdot \left(\frac{k_1 R}{2} \right)^{2n}}{n! (n-1)!} \left\{ \frac{\frac{f_2 k_1}{f_1 k_2} - 1}{\frac{f_2 k_1}{f_1 k_2} + 1} \right\} \tag{A11-16}$$

which is small for $\frac{k_1 R}{2} < 1$.

If $\left(\frac{k_1 R}{2} \right)^2 \ll n$ and $\frac{k_1 R}{2} \gtrsim 1$ then n will be large

enough such that Sterling's formula will be valid. i.e.

$$n! \simeq \sqrt{2 \pi n} \; n^n e^{-n}$$

Therefore the function

$$\frac{\left(\frac{k_1 R}{2} \right)^{2n}}{n! (n-1)!} = \frac{n \left(\frac{k_1 R}{2} \right)^{2n}}{(n!)^2}$$

$$\simeq \frac{n \left(\frac{k_1 R}{2} \right)^{2n}}{2 \pi n \, n^{2n} e^{-2n}}$$

$$\simeq \frac{1}{2\pi} \left(\frac{K_1 R}{2n} \right)^{2n} e^{2n}$$

For the limit as $n \to \infty$ this becomes:

$$F = \lim_{n \to \infty} \frac{1}{2\pi} \left(\frac{K_1 Re}{2n} \right)^{2n}$$ which is of the indeterminant form

0^∞ . Taking logs gives:

$$\log_e F = \lim_{n \to \infty} \left\{ \log_e \frac{1}{2\pi} + 2n \log_e \frac{K_1 Re}{2n} \right\}$$

which in the limit tends to negative infinity of which the antilog

is zero and thus $F \to 0$:

$$\lim_{n \to \infty} \frac{1}{2\pi} \left(\frac{K_1 Re}{2n} \right)^{2n} \Rightarrow 0.$$

For the special case of frictionless long-waves Equation (A11-16)

becomes:

$$B_n \simeq \frac{\epsilon_n \, \mu^{n-1} \, \pi \left(\frac{\sigma 2}{\sqrt{gh_1}} R^2 \right)^n}{n! \, (n-1)!} \cdot \left(\frac{h_2 - h_1}{h_2 + h_1} \right)$$

If $n = 0$ and $K_j R \ll 1$ then:

$$J_0 (K_j R) \simeq 1 + 0 (K_j R)^2$$

$$\text{AND} \quad J_0' (K_j R) \simeq - \frac{K_j R}{2} + 0 (K_j R)^3$$

Similarly using no higher order terms than first order in $(K_j R)$ gives:

$$H_0 \simeq 1 + \frac{2\iota}{\pi}\left(\gamma + Log_e \frac{K_j R}{2}\right)$$

and $$H_0' \simeq -\frac{K_j R}{2} + \frac{2\iota}{\pi}\left(\frac{2}{K_j R} - \frac{K_j R}{2}\left(\gamma + Log_e \frac{K_j R}{2}\right)\right)$$

(See, for example, MacLachlan (1955) p.197)

where $\gamma = .5772$ is Euler's constant.

Using these asymptotic values gives, after rearranging:

$$\left(\frac{f_1}{f_2} J_{0_2} H_{0_1}' - H_{0_1} J_{0_2}'\right) \simeq R\left(K_2 - \frac{f_1 K_1}{f_2}\right)\left\{\frac{1}{2} + \frac{\iota}{\pi}\left(\gamma + Log_e \frac{K_1 R}{2}\right)\right\} + \frac{2\iota}{\pi R K_1}\frac{f_1}{f_2}$$

so:

$$A_0 \simeq \frac{2\iota \frac{f_1}{f_2}}{\pi K_1 R\left[(R K_2 - \frac{f_1}{f_2}K_1)(\frac{1}{2} + \frac{\iota}{\pi}(\gamma + Log_e \frac{K_1 R}{2})) + \frac{2\iota f_1}{\pi R K_1 f_2}\right]} \qquad \text{(A11-17)}$$

and $$B_0 \simeq \frac{-\frac{K_2 R}{2} + \frac{f_1}{f_2}\frac{K_1 R}{2}}{R(K_2 - \frac{f_1}{f_2}K_1)(\frac{1}{2} + \frac{\iota}{\pi}(\gamma + Log_e \frac{K_1 R}{2})) + \frac{2\iota}{\pi R K_1}\frac{f_1}{f_2}}$$

$$\simeq \frac{-\frac{R}{2}(f_2 K_2 - f_1 K_1)}{R(f_2 K_2 - f_1 K_1)(\frac{1}{2} + \frac{\iota}{\pi}(\gamma + Log_e \frac{K_1 R}{2})) + \frac{2\iota}{\pi R K_1}f_1} \qquad \text{(A11-18)}$$

For the special case of frictionless long-waves the function

$$f_2 K_2 - f_1 K_1 = 0 \qquad \text{so:} \qquad A_0 \simeq 1$$

and $$B_0 \simeq 0$$

APPENDIX 12

THE REFRACTION AND REFLECTION OF FRICTIONLESS

WAVES INCIDENT OBLIQUELY TO A DEPTH DISCONTINUITY

Figure (A12.1) depicts a situation where plane (frictionless) sinusoidal waves are incident at an angle β_2 along the line x = 0. A refracted and reflected wave train are expected to be generated along this line with a refraction angle of β_1 and a reflection angle of β_2 . The incident wave may be described as: (the real part of)

$$\eta_i = A_i e^{i(\vec{K_i} \cdot \vec{x} - \sigma t)}$$

the refracted wave as: (the real part of)

$$\eta_r = A_r e^{i(\vec{K_r} \cdot \vec{x} - \sigma t)}$$

and the refracted wave as: (the real part of)

$$\eta_t = A_t e^{i(\vec{K_t} \cdot \vec{x} - \sigma t)}$$

where

$$\vec{K_i} = \hat{i} \, \ell_2 + \hat{j} \, m$$
$$\vec{K_r} = \hat{i} \, \ell_2 + \hat{j} \, m$$
$$\vec{K_t} = \hat{i} \, \ell_1 + \hat{j} \, m$$
$$\vec{x} = \hat{i} \, x + \hat{j} \, y$$

and $\ell_{1,2}$ and m are the wave numbers in the x and y directions respectively. It is clear from Figure (39) that $m = \dfrac{2\pi}{L_y}$ must be the same for the three waves. To arrive at Snell's law consider:

$$K_t^2 = \ell_1^2 + m^2$$
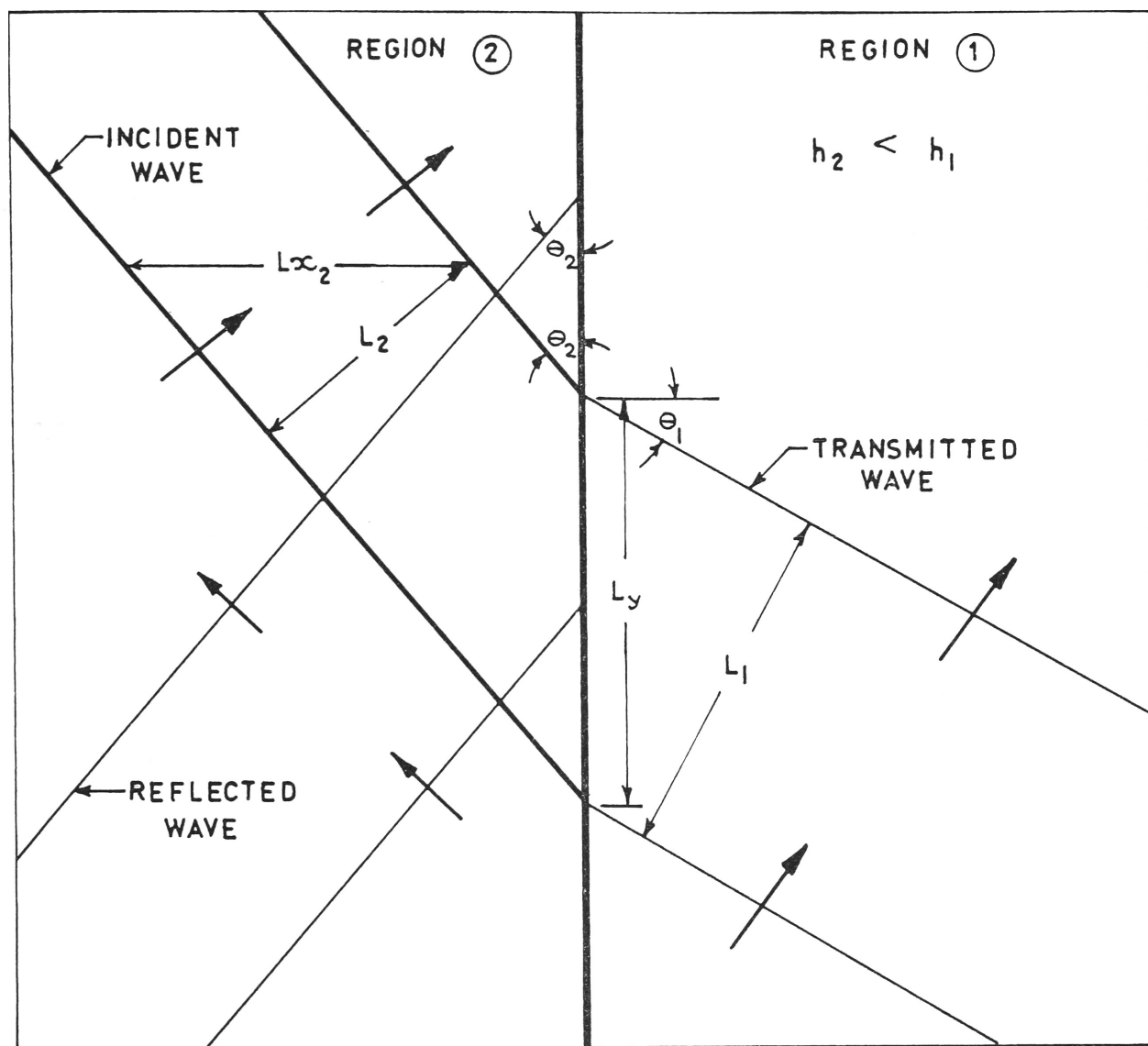
FIGURE A12:1 SCHEMATIC DIAGRAM OF REFRACTION AND REFLECTION FOR WAVES INCIDENT AT AN ANGLE TO A DEPTH DISCONTINUITY.

and $\quad K_i^2 = \ell_2^2 + m^2$

so $\quad K_t^2 = \ell_1^2 + K_i^2 - \ell_2^2$

but $\quad \ell_2 = K_i \cos \beta_2$

and $\quad \ell_1 = K_t \cos \beta_1$

Therefore arriving at:

$$K_t^2 - K_t^2 \cos^2 \Theta_1 = K_i^2 - K_i^2 \cos^2 \Theta_2$$

and, since $\quad \dfrac{\sigma}{K_t} = \upsilon_{P_1}$ AND $\dfrac{\sigma}{K_i} = \upsilon_{P_2}$ $\qquad$ gives

Snell's Law:

$$\frac{\upsilon_{P_2}}{\upsilon_{P_1}} = \frac{\sin \beta_2}{\sin \beta_1} .$$

REFERENCES

1. Anonymous   Conductivity Compensated Wave-Height Meter, Hydro Delft No. 10, January 1968. pp. 1-2.

2. Bartholomeusz, E.F.   The Reflection of Long-waves at a Step, Cambridge Phil. Soc. Proc., Vol. 54, 1958, pp. 106-118.

3. Biesel, F.   The Wave Filter NEYRPIC Method, La Houille Blanche, 1948, Vol. 4, pp. 285-190.

4. Biesel, F.   Calculation of Wave Damping in a Viscous Liquid of known Depth, La Houille Blanche, 1949, Vol. 4, pp. 630-634.

5. Bretschneider, C.L.   Field Investigation of Energy Loss in shallow water Ocean Waves, Beach Erosion Board, Tech. Memo No. 46, 1965, pp. 1-12.

6. Brillouin, L.   Wave Propagation and Group Velocity, Academic Press, New York, 1961, pp. 1, pp. 123.

7. Defant, A.   "Physical Oceanography", Vol. 2, Pergamon Press, The MacMillan Co., New York, 1961, pp. 155-156.

8. Dore, B.D.   Viscous Damping Effects in Long-waves on the Rotating Earth, Quarterly Journal of Mechanical and Applied Mathematics, Vol. 21, Part 1, 1969, pp. 105-114.

9. Einstein, H.A. and Fuchs, R.A.

The Prediction of Tidal Flows in Canals and Estuaries, Report to Committee on Tidal Hydraulics, Corps. of Engineers, U.S. Army, 1954.

10. Eiseberg, R.M.

Fundamentals of Modern Physics, John Wiley and Sons Inc., New York, 1961, pp. 235.

11. Fjeldstat, J.

Contributions to the Dynamics of Free Progressive Tidal Waves, Norwegian North Polar Expedition with the "Maud" (1918-1925), Scientific Results, Vol. 4, No. 3.

12. Gagnon, M.L. and Bocco, M.V.

The Effect of a Gradual Change of Depth on a Train of Surface Waves, S.M. Thesis, Dept. of Civil Eng., M.I.T., Cambridge Mass., May (1962) (Unpublished).

13. Hall, A.S.

The Construction of Graphs and Charts, Sir Isaac Pitman and Sons Ltd., Melbourne, 1958, pp. 70-82.

14. Hamill, P.A.

Experimental Development of a Perforated Wave Absorber of simple construction and minimum length, N.R.C. Report No. 7472, Ottawa, Canada (1963).

15. Handbook of Chem-   The Chemical Rubber Publishing Co., Cleveland,
    istry and Physics   Ohio, 1962, pp. 2273.

16. Handbook of   (Ed.) M. Abramowitz and I.A. Stegun, National
    Mathematical   Bur. of Standards, App. Math. Ser. 55, 1964,
    Functions   pp. 371.

17. Heaps, N.S.   A Two-dimensional Numerical Sea Model, Phil.
                         Trans. 1969, A265, pp. 96.

18. Hoerner, S.F.   Fluid-Dynamic Drag, 3rd ed. Hoerner, Midland
                         Park, N.J., (1965), pp. (2-4).

19. Hough, S.S.   On the Influence of Viscosity on Waves and
                         Currents, Proc. London. Math. Soc., 1897, Vol.
                         28, pp. 264-288.

20. Hunt, J.N.   Viscous Damping of Waves over an Inclined Bed
                         in a Channel of Finite Width, La Houille Blanche,
                         1952, Vol. 7, pp. 836-842.

21. Hunt, J.N.   The Viscous Damping of Gravity Waves in Shallow
                         Water, La Houille Blanche, 1964, Vol. 19,
                         pp. 685-690.

22. Ippen, A.T. (ed.)   "Estuary and Coastline Hydrodynamics", McGraw-
                         Hill, Inc., New York, 1966, pp. 71-77.

23. Iwagaki, Y., Tsuchiya, Y. and Chen, H.

On the Mechanism of Laminar Damping of Oscillatory Waves due to Bottom Friction, Bull. of the Disaster Prevention Res. Inst., February 1967, Vol. 16, Part 3, No. 116, pp. 49-75.

24. Iwagaki, Y. and Kakinuma, T.

On the Bottom Friction Factors off five Japanese Coasts, Coastal Engineering of Japan, 1967, Vol. 10, pp. 13-22.

25. Johns, B.

A Boundary Layer Method for the Determination of the Viscous Damping of small amplitude gravity waves, Quart. Journal of Mech. and Applied Mathematics, Vo. 28, Part 1, 1968, pp. 93-103.

26. Kinsman, B.

Wind Waves, Prentice-Hall Inc., Englewood Cliffs, N.J., 1965, pp. 145-149.

27. Lamb, H.

Hydrodynamics, 6th Ed., Cambridge, 1932, pp. 262-263.

28. Le Me haute, B.

Periodic Gravity Waves at Discontinuity, Journal of the Hydraulics Division Proc. Am. Soc. of Civil Engineers, Nov. 1960, pp. 11-41.

29. Li, H.

Stability of Oscillatory Laminar Flow along a Wall, U.S.A. Beach Erosion Board, Tech. Memo. No. 47, 1954, pp. 1-48.

30. Longuet-Higgins, M.S.

On the Trapping of Wave Energy Round Islands, J. Fluid Mech., 1968, Vol. 29, pp. 781-821.

31. Lord Raleigh   On Progressive Waves, Proc. Lon. Math. Soc.

                           1877, pp. 21-26.

32. McLachlan, N.W.   Bessel Functions for Engineers, 2nd Ed. Oxford

                           University Press, London 1955, pp. 83, pp. 86.

33. Milne-Thompson, L.M. Theoretical Hydrodynamics, 4th Ed., Macmillan

                           and Co. Ltd., London, 1962, pp. 408-409.

34. Neumann, G.   Die Impedanz Mechanischen Schwingungs - Systime

                           und ihre Anwendung ouf die Theorie der Seiches,

                           Ann. Hydr. Mar. Met., Vol. 72, 1944, pp. 65-193.

35. Newman, J.N.   Propagation of Water Waves over an Infinite

                           Step, J. Fluid Mech. (1965) Vol. 23, Part 2,

                           pp. 399-415.

36. Proudman, J.   "Dynamic Oceanography", Methuen and Co. Ltd.,

                           London, 1952, pp. 302-333.

37. Putnam, J.A. and   The Dissipation of Wave Energy by Bottom Friction,
     Johnson, J.W.
                           Trans. Am. Geophysical Union, Vol. 30, No. 1,

                           February 1949, pp. 67-74.

38. Sommerfeld, A.   About the Propagation of Light in Dispersive Media,

                           Ann. Physic (4), 44, 1914, pp. 177.

39. Summerfield, W.C.   On the Trapping of Wave Energy by Bottom Topography, Horace Lamb Centre for Oceanographic Research, The Flinders University of South Australia, Res. Paper No. 30, pp. 3-12, pp. 89.

40. Steel Designers Manual   Crosby Lockwood and Sons Ltd., London, 1969, pp. 30.

41. Stokes, G.G.   On the Theory of Oscillatory Waves Mathematical and Physical Papers, Cambridge Unidersity Press, Vol. 1, 1880, pp. 197-229.

42. Van Doran, W.G.   Boundary Dissipation of Oscillatory Waves, J. Fluid Mechanics, 1966, Vol. 24, Part 4, pp. 769-779.

43. Voigt, W.   Ueber die Aenderung der Schwingungsform des Lichtes beim Fortschreiten in einem dispergirenden oder absorbirenden Mittel, Annalen der Physic und Chemie, 68, 1899, pp. 598-603.

44. Weenink, M.P.H.   Meded Verk. K. ned met. Inst., 73, 1958, pp. 111.

45. Wiegel, R.L.   Parallel Wire Resistance Wave Meter, Conference on Coastal Engineering Instruments, Proc. No. 1, 1955, pp. 39-43.

46. Wiegel, R.L.   Oceanographic Engineering, Prentice Hall Inc.,
                          Englewood Cliffs, N.J., 1964, pp. 33.

47. Williams, J.A.   Model Studies of Long-wave Amplification by
    and Krishna Kartha,   Circular Islands, Bulletin of the Seismic Soc.
        I.D.   of America, Vol. 59, No. 1, February 1969,
                          pp. 299-316.

48. Wong, K.K., Ippen,   Interaction of Tsunami with Oceanic Islands and
    A.T. and Harleman,   Submarine Topographies, M.I.T. Hydrodynamics
        D.R.F.   Lab., T.R. No. 62, August 1963, pp. 52-55.

This work has not been submitted to any other
University or Institution for a higher degree.

H. D. PITE